Analysis of Simply-Supported Single Cell Prismatic Box Sections

Sk Amjad Hossain

A Thesis

in

The Department

of

Building, Civil and Environmental Engineering

Presented in Partial Fulfillment of the Requirements
for the Degree of Master of Applied Science in Civil Engineering at
Concordia University
Montreal, Quebec, Canada

March 2006

© Sk Amjad Hossain, 2006

Library and Archives Canada

Published Heritage Branch

395 Wellington Street
Ottawa ON K1A 0N4
Canada

Bibliothèque et Archives Canada

Direction du Patrimoine de l'édition

395, rue Wellington
Ottawa ON K1A 0N4
Canada

Your file Votre référence
ISBN: 0-494-14248-0
Our file Notre référence
ISBN: 0-494-14248-0

NOTICE:
The author has granted a non-exclusive license allowing Library and Archives Canada to reproduce, publish, archive, preserve, conserve, communicate to the public by telecommunication or on the Internet, loan, distribute and sell theses worldwide, for commercial or non-commercial purposes, in microform, paper, electronic and/or any other formats.

The author retains copyright ownership and moral rights in this thesis. Neither the thesis nor substantial extracts from it may be printed or otherwise reproduced without the author's permission.

AVIS:
L'auteur a accordé une licence non exclusive permettant à la Bibliothèque et Archives Canada de reproduire, publier, archiver, sauvegarder, conserver, transmettre au public par télécommunication ou par l'Internet, prêter, distribuer et vendre des thèses partout dans le monde, à des fins commerciales ou autres, sur support microforme, papier, électronique et/ou autres formats.

L'auteur conserve la propriété du droit d'auteur et des droits moraux qui protège cette thèse. Ni la thèse ni des extraits substantiels de celle-ci ne doivent être imprimés ou autrement reproduits sans son autorisation.

In compliance with the Canadian Privacy Act some supporting forms may have been removed from this thesis.

While these forms may be included in the document page count, their removal does not represent any loss of content from the thesis.

Conformément à la loi canadienne sur la protection de la vie privée, quelques formulaires secondaires ont été enlevés de cette thèse.

Bien que ces formulaires aient inclus dans la pagination, il n'y aura aucun contenu manquant.

Canada

ABSTRACT

Analysis of Simply-Supported Single Cell Prismatic Box Sections

Sk Amjad Hossain

This research extends Maisel's (1982) methodology, the generalization of Vlasov's, simple beam theory, and its extension to evaluate torsional, distortional and shear lag effects in simply-supported girder consisting of a single cell uniform box section. The computer program developed can analyse simply supported box sections with trapezoidal and rectangular sections, any material properties, for a unit eccentric loading at midspan, formulate the bending, shear, torsion, distortion and warping stress at different locations of the section. Two separate computer programs have been developed, the first dealing with shear flow, shear stresses, combined shearing stress, torsional warping stress, distortional warping stress, maximum transverse bending stress, etc. The second program includes shear lag only. Torsional warping is treated using the method of Kollbrunner and Hajdin and Heilig (1966), while Sedlacek's (1971) method is used to account for the distortional effects.

Acknowledgements

I would like to express my sincerest and profound gratitude to my supervisor, Professor M. Saeed Mirza of McGill University for his guidance and valuable advice at all stages of this study. His enthusiasm and great interest in this work were major sources of motivation for the author. Without his valuable direction and cordial assistance this work could never have been completed.

I am grateful to my supervisor Dr. Z. A. Zielinski and Concordia university for the financial support and his guidance at different stages of this study.

To my wife I am indebted for her constant support, inspiration, love, and understanding. Special thanks to my friend Masum Ahmed Jaigirdar for his continious inspiration for this research work.

Finally, I am thankful to the department of Civil Engineering, the engineering library of Concordia University, the engineering library of McGill University as well as the library of the British Cement and Concrete Association for the various papers and publications which were very useful in this research program.I like to acknoledge Wolfram Research's Mathematica version 5, which has been utilized extensively in this research program.

CHAPTER-1 1
INTRODUCTION 1
1.1 General: 1
1.2 Literature Review: 2
1.2.1 Elastic Analysis of Box Girder Bridges 2
1.2.2 Orthotropic Plate Theory Method 2
1.2.3 Grillage-Analogy Method 3
1.2.4 Folded-Plate Method 3
1.2.5 Finite-Strip Method 4
1.2.6 Finite-Element Method 6
1.3 Objectives of This Research: 10
CHAPTER 2 11
BEHAVIOUR OF THIN WALLED CROSS-SECTIONS 11
2.1General: 11
2.2.1: Co-ordinate Axes: 12
2.3:Displacements: 13
2.4: Positive directions of stresses and stress-resultants: 15
CHAPTER-3 17
ANALYSIS OF SIMPLE BENDING AND ST VENANT TORSION 17
3.1:Assumptions: 17
3.2:Simple Bending Without Twist: 17
3.3: Longitudinal Shearing Stress: 18
3.3.1: Multicell Sections: 18
3.3.2: Single Cell Section: 22
3.4: St.Venant Torsional Shearing Stress: 24
CHAPTER-4 28
ANALYSIS OF TORSIONAL WARPING 28
4.1: Assumptions: 28
4.2: Stress Pattern and the Physical Significance of Structural Actions: 28
4.3: Analysis of Torsional warping by the method of Kollbrunner,Hajdin and Heilig(1966)[Single cell]: 31
4.3.1 Loading: 31
4.3.2 Summary of Procedure for Analysis: 31
4.3.3 Bimoment B_{twr}: 31
4.3.4 Relation Between Applied Load, Internal Stress-Resultants and Twist: 36
4.4:Analysis of Torsional warping by the method of Kollbrunner,Hajdin and Heilig(1966)[multicell section]: 38
4.4.1:Summary of Procedure For Analysis: 38
4.4.2 Sectorial Co-Ordinate : 39
4.4.3 The Procedure for Determining the Position of the Shear Centre and the Diagram of the Normalized Sectorial Co-ordinate: 42
4.4.4Torsional Warping Stresses f_{twr} : 45
CHAPTER 5 47

ANALYSIS OF DISTORTIONAL EFFECTS 47
5.1 Introduction: 47
5.2Method of Distortional Analysis Developed by Sedlacek(1968) 49
5.2.1 Distortional Components, Warping Displacements and Shear Stresses 49
5.2.2 Relations Between Stresses, St. Venant Torsional Moments in Individual Walls, Transverse Bending Moments and Deformations of Cross-Section 54
5.2.3 Derivation of the Differential Equation 58
5.2.4 Orthogonalization of the Basic Co-Ordinates: 60
5.2.4.1 Orthogonalization of Non-Distotional Displacements : 60
5.2.4.2 Orthogonalization of Distortional Displacements: 63
CHAPTER-6 70
ANALYSIS OF SHEAR LAG EFFECT 70
6.1 Shear Lag Analysis of Box Girder 70
6.1.1 Introduction: 70
6.1.2 Definition of Shear Lag: 71
6.1.3 Method of Shear-Lag Analysis Developed by Roik,Sedlacek(1970) and Schmackpfe(1972): 72
6.1.3.1 Choice of Warping Displacement Functions for Shear Lag: 72
6.1.3.2 Derivation of Differential Equation: 73
6.1.3.3 Orthogonalization of the Basic Co-Ordinates: 78
6.1.3.4 Relation Between Stresses, Internal Forces and Deformations: 83
CHAPTER-7 87
ANALYSIS OF A SINGLE-CELL BOX SECTION BEAM 87
7.1General: 87
7.1.1 Analysis of simple bending and St. Venant torsional effects: 87
7.1.2 St.Venant torsional shear stresses due to live load: 92
7.1.3 Analysis of torsional warping by the method of Kollbrunner,Hajdin and Heilig: 93
7.1.4 Analysis of distortional effects: 101
7.1.5 Analysis of shear lag effects: 122
7.1.5.1 Assumption: 122
7.1.5.2 Basic shear lag warping function $\underline{w}_v$ and section properties $\underline{C}_v$ and $\underline{S}_v$: 123
7.1.5.3 Evaluation of $\underline{C}_v$: 126
7.1.5.4 Evaluation of $\underline{S}_v$: 127
7.1.5.5 Second stage of orthogonalization: 128
7.1.5.6 Orthogonalization of $\underline{w}_v$ and $\underline{r}_v$: 131
7.1.5.7 Solution of the analogous beam problem for shear lag effects. 135
7.1.5.7 Shear lag stresses in mode 5 due to live load: 136
7.1.5.8 Shear lag stresses in mode 5 due to dead load: 137
7.2 Computer Programs Developed for Analysis of Simply-Supported Single Cell Prismatic Box Sections: 138
7.2.1 User interface: 139
7.2.1(a)Input data for program –1 139

7.2.1.(b) Input data for program-2 140
CHAPTER-8 ..... **143**
RESULTS **143**
8.1 General: 143
8.2 Geometry studied : 143
8.3 Flexural stresses: 145
8.4: Statically Determinate Shear Flow vs live loading: 146
8.5 Statically determinate shear flow vs variable span: 147
8.6 Conventional Shearing Stresses: 148
8.7 :Shearing stresses due to St. Venant's torsion theory: 149
8.8: Maximum transverse Bending stress: 150
8.9:Maximum transverse bending stresses due to variable torsional moment: 151
8.10: Torsional warping shear stresses: 152
8.11:Distortional warping shear stresses: 154
8.12:Torsional warping stresses: 155
8.13:Distortional warping stresses: 156
8.14: Different stresses at A and C: 158
8.15: Effect of flange and web thickness on shear flow 160
8.16: Effect of top flange thickness on stresses of different location of the cross-section. 161
8.17: Effect of bottom flange thickness on stresses of different location of the cross-section. 162
8.18: Effect of L/B ratio ,web inclination by using different geometry[Rectangular section]: 164
8.19: Effect of L/B ratio ,web inclination by using different geometry[Trapezoidal section]: 167
8.21: Effect of flange thickness on different stresses 171
8.22: Effect of L/B ration on different stresses 175
8.23: Calculation of deflection 177
CHAPTER-9
9.1 Comparison of results 180
9.2: Conclusions 182
9.3: Limitations 184
9.4: Recommendation for future research 184

REFERENCES: **185**
Program-A: 191
`Output program-A:` 191
Program B 192
`Output Program-B` 196
Subroutine-C 201
Subroutine-D 201
Subroutine-E 202
Subroutine-F 202
Subroutine-G 203

APPENDIX-2 204
APPENDIX-3 206

LIST OF FIGURES

Figure 2. 1:Co-ordinate axes x,y and z 12
Figure 2. 2: Peripheral co-ordinate s_{per} ,showing origin and positive directions 13

Figure 3. 1: Dimensions of cross-section 17
Figure 3. 2: Perpferal co-ordinate s_{per} and cuts in the cross-section 18
Figure 3. 3: Positive directions of statically determinate shear flows. 19
Figure 3. 4: Evaluation of ($\overline{Ay}$), the first moment of area of the partial cross-section about the centroidal x-axis. 19
Figure 3. 5: Shear flows in cell M due to longitudinal bending. 21
Figure 3. 6: Dimensions of cross-sections and peripheral coordinate s_{per},showing origin and positive directions 22
Figure 3. 7: Zero bending shear stress v_{1bg} on axis of symmetry, for vertical loading 22
Figure 3. 8: Evaluation of $(\overline{Ay})_{1/2}$, the first moment of area of the partial half cross-section about the centridal x axis. 23
Figure 3. 9: St. Venant torsional shear flow 24

Figure 4. 1: Torsional loading of a simplys supported box beam. 30
Figure 4. 2: Distribution of the internal torsional moments due to St.Venant and torsional warping shear stresses along the beam. 30
Figure 4. 3:Warping force group and bimoment. 32
Figure 4. 4: Position of shear centre. 34
Figure 4. 5: Concentrated torsional moment applied to beam at midspan (Torsional restraint at supports but no warping restraint) 36
Figure 4. 6: Geometrical definition of sectorial co-ordinate 39
Figure 4. 7: Portion of diagram of $\int a_p ds_{perP}$ 42

Figure 5. 1: Modes of distortion (schematic) for various box-beam cross-sections 47
Figure 5. 2: Basic unit deformation in distortional analysis of closed section. 50
Figure 5. 3: Radial distance r_i for wall element experiencing tangential movement 53
Figure 5. 4: Distortion of statically determinate cut section 54
Figure 5. 5: Deflected shape in distortion and rotations of chords 56

Figure 6. 1:Basic warping displacement functions for shear-lag analysis 72
Figure 6. 2: Beam analogy for shear lag 83
Figure 6. 3: Element of analogous beam in shear lag mode i 85

Figure 7. 1: Loading and geometry 87
Figure 7. 2:Bending moment, shear force and torsional moment diagrams due to combined live and dead load 89

Figure 7. 3:Bending stress f_{1bg} at midspan section (N/mm^2) calculated by Engineer's bending theory 90
Figure 7. 4:Peripheral coordinate Sper and cut in cross-section 91
Figure 7. 5: Diagrams of shear stresses(N/mm^2) due to conventional bending theory at z=0 92
Figure 7. 6: Diagram of St.Venants shear stresses (N/mm2) at z=0 on positive face of cross-section 93
Figure 7. 7: Determination of shear centre position 95
Figure 7. 8: Shear center and normalized sectorial coordinate w_{twr} 96
Figure 7. 9: Diagrams of live load stresses f_{twr}, v_{twr} (N/mm^2), due to torsional loading 101
Figure 7. 10: Distortion of section 102
Figure 7. 11:Basic distortional warping function 104
Figure 7. 12: Values of $\tilde{w}_5$ in mm^2 108
Figure 7. 13: Distortional analysis of frame representing cross-section 109
Figure 7. 14: Transverse bending moments $\tilde{m}_5$ (kN/mm/mm) due to unit angular distortion on frame of unit "width" (Ordinates on tension face) 110
Figure 7. 15: Analogous beam on elastic foundation 111
Figure 7. 16: Non-distortional loading components 113
Figure 7. 17: Diagrams of live load stresses f_5, v_5 and f_{trb5} (N/mm^2) ,due to distortion calculated by the beam on elastic foundation analogy 119
Figure 7. 18:Diagrams of moments of area for evaluating distortional warping shear stress 120
Figure 7. 19:Basic shear lag warping functions w_{5v} and $\dot{w}_{5v}$ 123
Figure 7. 20: Basic shear lag functions w_{6v} and $\dot{w}_{6v}$ 124
Figure 7. 21: Basic shear lag warping functions w_{7v} and $\dot{w}_{7v}$ 125
Figure 7. 22: Parabolic function 125
Figure 7. 23:Orthogonalized shear lag warping functions ($\tilde{w}_{5v}$ and $\dot{\tilde{w}}_{5v}$) 133
Figure 7. 24:Orthogonalized shear lag warping functions $\tilde{w}_{6v}$ and $\dot{\tilde{w}}_{6v}$ 133
Figure 7. 25: Orthogonalized shear lag warping functions $\tilde{w}_{7v}$ and $\dot{\tilde{w}}_{7v}$ 134
Figure 7. 26: Analogous beam for shear lag analysis in mode 5 135
Figure 7. 27: Diagrams of shear lag stresses (N/mm^2) at midspan section due to live and dead load. 138

Figure 8. 1: Typical box sections. 144
Figure 8. 2: Bending stress at midspan by engineers bending theory 145
Figure 8. 3: Statically Determinate Shear Flow Vs Load 146
Figure 8. 4: Statically Determinate Shear Flow Vs Span Of Trapezoidal Section 147
Figure 8. 5: Shearing stress in bending calculated by engineers bending theory. 148
Figure 8. 6: Shearing stresses due to St. Venant torsion theory 149
Figure 8. 7: Max transverse bending stress at midspan with const. torsional moment 150
Figure 8. 8: Max transverse bending stress at midspan 151
Figure 8. 9: Torsional warping shear stress at midspan. 152
Figure 8. 10: Distortional warping shear stress at midspan 154

Figure 8. 11: Torsional warping stress at midspan section 155
Figure 8. 12: Distortional warping stress at midspan 156
Figure 8. 13: Different stresses at A 158
Figure 8. 14: Different stresses at C 159
Figure 8. 15: Shear lag stresses 170
Figure 8.16: Variation of shearing stresses with bottom flange thickness..... 171
Figure 8.17: Variation of torsional warping stresses with bottom flange thickness..... 172
Figure 8.18: Variation of distortional warping stresses with bottom flange thickness... 172
Figure 8.19: Variation of torsional warping stresses with top flange thickness..... 173
Figure 8.20: Variation of shearing stresses with top flange thickness 173
Figure 8.21: Variation of distortional warping stresses with top flange thickness 174
Figure 8.22: Stresses at A with different L/B ratio 175
Figure 8.23: Stresses at B with different L/B ratio 175
Figure 8.24: Stresses at C with different L/B ratio 176
Figure 9.1: Comparison of stresses (MPa) due to combined live and dead load calculated by the theory presented here and by finite strip model by Maisel's (1982)..... 180

LIST OF TABLES

Table 8.1: Comparison between Figure 8.13 and 8.14.....159
Table 8.2: Effect of flange and web thickness on shear flow.....160
Table 8.3: Effect of top flange thickness on stresses of different location of the cross-section.....161
Table 8.4: Effect of bottom flange thickness on stresses of different location of the cross-section.....163
Table 8.5: Effect of L/B ratio, web inclination by using different geometry[Rectangular section].....165

Table 8.6:Effect of L/B ratio, web inclination by using different geometry [Trapezoidal section].....167

LIST OF NOTATIONS

Note: A lower bar_ underneath a symbol denotes a matrix or vector.

a	resultant longitudinal displacement in shear lag analysis
$a, \overline{a}, \widetilde{a}$	basic , partially orthogonalized and fully orthogonalized displacement vectors respectively.
a_F	distance of concentrated load from left hand support
$a_i, \overline{a}_i, \widetilde{a}_i$	ith components of $a, \overline{a}, \widetilde{a}$ respectively
$a_{iv}, \overline{a}_{iv}, \widetilde{a}_{iv}$	ith components of $a_v, \overline{a}_v, \widetilde{a}_v$ respectively
a_P	perpendicular distance from pole P to tangent to midline of wall at point considered
a_Q	perpendicular distance from shear centre Q to tangent to midline of wall at point considered
a_r	vector of orthogonalized, non-distortional displacements
a_t	tangential transverse displacement in shear lag analysis
$a_v, \overline{a}_v, \widetilde{a}_v$	basic, partially orthogonalized and fully orthogonalized shear lag displacement vectors respectively
a_x	displacements in the direction of the x axis
a_y	displacements in the direction of the y axis
a_{y0}	a_y in beam on elastic foundation when $k_{fdn} = 0$
a_z	displacements in the direction of the z axis
a_{z0}	integration constant
A	total area of cross-section including side cantilevers
A_{enc}	area enclosed by mid-line of wall of closed portion of cross-section
A_{encM}	A_{enc} for cell M
$A_{enc1,2,3}$	A_{encM} for cells 1,2,3 respectively
$\overline{(Ay)}$	first moment about the centroidal x axis of the partial area of cross-section
b	flange breadth dimension
b_{cant}	breadth of side cantilever
b_{eff}	effective breadth of flange
b_m	breadth of wall element m
b_1, b_2	cell breadth dimensions
B	internal bimoment
$B, \overline{B}, \widetilde{B}$	basic, partially orthogonalized and fully orthogonalized matrices of section properties in distortion respectively
B_{ext}	concentrated applied bimoment
$B_{ij}, \overline{B}_{ij}, \widetilde{B}_{ij}$	ijth elementof $B, \overline{B}, \widetilde{B}$ respectively

B_{twr}	torsional warping bimoment
$C, \overline{C}, \widetilde{C}$	basic, partially orthogonalized and fully orthogonalized matrices of section properties in warping respectively
C_{cen}	central torsional moment of inertia of cross-section
$C_{ij}, \overline{C}_{ij}, \widetilde{C}_{ij}$	ijth elements of $C, \overline{C}, \widetilde{C}$ respectively
$C_{ijv}, \overline{C}_{ijv}, \widetilde{C}_{ijv}$	ijth elements of $C_v, \overline{C}_v, \widetilde{C}_v$ respectively
C_r	diagonal matrix of non-distortional section properties
C_{ri}	iith element of C_r
C_{svt}	torsional moment of inertia of a single cell cross-section in St Venant torsion
C_{twr}	torsional warping moment of inertia of cross-section
$\overline{C}_{twr}$	$K'_{19} C_{twr}$
$C_v, \overline{C}_v, \widetilde{C}_v$	basic, partially orthogonalized and fully orthogonalized matrices of section properties in shear-lag warping stiffness respectively
d	cell depth dimension
dwr	suffix denoting distortional warping
e	base of Napierian logarithms
f	normal stress
f_{dwr}	distortional warping stress
f_i	stress f in mode i
f_{iv}	stress f_v in mode i
f_{ibg}	bending stress, calculated by engineers' theory of bending
f_r	total longitudinal normal stress for non-distortional modes of displacement
f_{trb}	transverse bending stress at extreme fibre
f_{trbi}	f_{trb} in mode i
f_{twr}	torsional warping stress
f_v	longitudinal normal stress due to shear lag
f_{web}	longitudinal normal stress at web flange junction
F	concentrated loading
$F, \overline{F}, \widetilde{F}$	basic, partially orthogonalized and fully orthogonalized vectors of concentrated transverse loading respectively
$F_i, \overline{F}_i, \widetilde{F}_i$	ith components of $F, \overline{F}, \widetilde{F}$ respectively
$\widetilde{F}_{iv}$	fully orthogonalized concentrated load in shear-lag mode i
F_l	longitudinal concentrated load
F_{tr}	transverse concentrated load
F_x	concentrated applied load in the direction of x axis
F_y	concentrated applied load in the direction of y axis

F_z	concentrated applied load in the direction of z axis
G	shear modulus of elasticity
h	thickness of wall
h_{bot}	thickness of bottom slab
h_m	thickness of wall element m
h_{top}	thickness of top slab
$h_{web1,2}$	thickness of webs 1 and 2 respectively
i	mode of displacements
I	moment of inertia of cross-section of analogous beam
I	unit matrix
I_{trb}	moment of inertia of cross-section of frame member in transverse bending
I_x	moment of inertia of cross-section of box beam about centroidal or principal x axis
I_{xwP}	sectorial product of inertia with respect to x and ω_{twrP}
$I_{x\omega Q}$	sectorial product of inertia with respect to x and ω_{rwrQ}
I_y	moment of inertia of cross-section of box beam about centroidal or principal x axis
$I_{y\omega P}$	sectorial product of inertia with respect to y and ω_{twrP}
$I_{y\omega Q}$	sectorial product of inertia with respect to y and ω_{twrQ}
j	mode of displacement
$J, \bar{J}, \tilde{J}$	basic, partially orthogonalized and fully orthogonalized matrices of section properties in torsion respectively
J_m	St Venent torsional moment of inertia of wall element m
J_r	matrix of shear moments of inertia
J_1	diagonal matrix of torsional moment of inertia
k_{fdr}	foundation modulus
K, K_a, K_{av} K_b, K_{bv}	transformation matrix
K_{ija}	ijth element of K_a
K^*_{ija}	ijth element of K_a using K^*_{4a} instead of K_{4a}
K_{ijav}	ijth element of K_{av}
K_{ijb}	ijth element of K_b
K_{ja}	jth column vector of K_a
K_{jav}	jth column vector of K_{av}
K_M	constant arising in St Venant torsion analysis,corresponding to cell M
K_{svt}	torsional moment of inertia of a multi-cell cross-section in St.Venant torsion

K_t	frame stiffness matrix in distortional analysis
K_v	transformation matrix
K_1, K_2, K_3	for cells 1,2,3 respectively
K_M	
K_{18}, K_{19}, K'_{18}	constants arising in torsional analysis
K'_{19}, K_{20}, K_{21}	
l	span
l_{ijv}	ijth element of eigenvector in shear lag analysis
$\mathrm{I}_{qb}, \mathrm{I}_{sb}, \mathrm{I}_{tb}$	qth,sth and tth rows of K_b respectively
I_{qbv}	qth row of K_{bv}
L	dimension length or total length of beam
m	typical wall element
$m_{x,ext}$	distributed applied bending moment about the x axis
$m_{y,ext}$	distributed applied bending moment about the y axis
M	index of cell
$\widetilde{M}$	column vector of warping moments
$\widetilde{M}_i$	ith component of $\widetilde{M}$
$\widetilde{M}_{iv}$	ith component of $\widetilde{M}_v$
M_r	column vector of non-distortional warping moments
M_{ri}	ith component of M_r
M_x	internal bending moment about x axis
$M_{x,ext}$	concentrated applied bending moment about the x axis
M_y	internal bending moment about the y axis
$M_{y,ext}$	concentrated applied bending moment about the y axis
n	intensity of transverse distributed loading or total number of displacement modes of cross-section or number of Fourier harmonic
$n_i, \overline{n}_i, \widetilde{n}_i$	ith components of $n, \overline{n}, \widetilde{n}$ respectively
$\widetilde{n}_{iv}$	fully orthogonalized intensity of distributed load in shear lag mode i
n_l	intensity of longitudinal distributed load
n_r	column vector of distributed loading in the non-distortional modes
n_{tr}	intensity of transverse distributed loading
$\overline{n}_v, \widetilde{n}_v$	partially orthogonalized and fully orthogonalized vectors of distributed loading in shear lag respectively
n_x	intensity of distributed loading in the x direction
n_y	intensity of distributed loading in the y direction
N	internal axial force
p	node of frame

q	row of K_b
r	column vector of angles and distances in distortional analysis
r	suffix denoting non-distortional behaviour
$r^*, \bar{r}^*$	basic and partially orthogonalized column vectors associated with load positions in distortional analysis respectively
r_i	ith component of r
r^*_i	ith component of r^*
$\tilde{r}_{iv}$	ith component of $\tilde{r}_v$
$r_v, \bar{r}_v, \tilde{r}_v$	basic, partially orthogonalized and fully orthogonalized column vectors associated with load positions in shear lag analysis respectively row of K_b
S_{per}	peripheral coordinate along mid-line of wall
S_{perM}	S_{per} in cell M
S_{perP}	S_{per} in pole P
$S_{per1,2,3}$	S_{per} in cells or along side cantilevers respectively
$\tilde{S}_i$	first moment of area of the $\tilde{w}_i$ diagram at the point in question on the cross-section
$\tilde{S}_{i0}$	first moment of area $\int \tilde{w}_i dA$ for the statically determinate, cut section
$S_{ijv}, \bar{S}_{ijv}, \tilde{S}_{ijv}$	ith elements of $S_v, \bar{S}_v, \tilde{S}_v$ respectively
$S_v, \bar{S}_v, \tilde{S}_v$	basic, partially orthogonalized and fully orthogonalized matrices of section properties in shear-lag shear stiffness respectively
t	row of K_b
t_{ext}	distributed applied torsional moment
twr	suffix denoting torsional warping
T	superscript denoting transpose of matrix or vectors
T	internal torsional moment
T	transformation matrix
T_{ext}	concentrated applied torsional moment
$T_{ext,0}$	redundant applied torsional moment
T_{svt}	internal torsional moment in St. Venant torsion
$(T_{svt})_m$	T_{svt} in cell M
T_{twr}	internal torsional moment due to torsional warping shear stresses
T_1	J_1T
v	shear stress
v	suffix denoting shear lag
$\bar{v}$	column vector of basic shear lag distribution function
$\tilde{\bar{v}}$	column vector of fully orthogonalized shear stress distributions functions
v_{dwr}	distortional warping shear stress
v_i	shear stress in mode i

$\bar{v}_i$	v_i for $G(da_i/dz)=1$
$\tilde{v}_i$	fully orthogonalized shear stress functions required to restore continuity to cut section in mode i
$(v_i h)$	shear flow in mode i
$(\bar{v}_i h)$	$v_i h$ for $G(da_i/dz)=1$
v_{iv}	stress v_v in mode i
v_{ibg}	shear stress in longitudinal bending
$(v_{ibg} h)$	shear flow in longitudinal bending
v_r	total shear stress for non-distortional modes of displacements
v_{svt}	shear stress in St. Venant torsion
$\bar{v}_{svt}$	v_{svt} for $G(d\theta_z/dz)=1$
$(v_{svt} h)$	shear flow in St. Venant torsion
v_{twr}	torsional warping shear stress
v_v	shear stress due to shear lag
$\tilde{V}$	column vector of shear forces
$\tilde{V}_{iv}$	ith component of $\tilde{V}_{iv}$
V_r	column vector of non-distortional shear forces
$\tilde{V}_v$	column vector of shear lag shear forces
V_x	shear forces in x direction
V_Y	shear forces in y direction
$w, \bar{w}, \tilde{w}$	basic,partially orthogonalized and fully orthogonalized warping vectors respectively
$w_i, \bar{w}_i, \tilde{w}_i$	ith components of $w, \bar{w}, \tilde{w}$ respectively
$w_{iv}, \bar{w}_{iv}, \tilde{w}_{iv}$	ith components of $w_v, \bar{w}_v, \tilde{w}_v$ respectively
w_j	jth component of w
$w_r, \tilde{w}_r$	basic and partially orthogonalized vectors of non-distortional co-ordinates of a point on the cross-section respectively
$w_v, \bar{w}_v, \tilde{w}_v$	basic,partially orthogonalized and fully orthogonalized warping vectors respectively
x	horizontal coordinate reffered to centroidal axis
x_p	x co-ordinate of pole P
x_Q, x_{shc}	x co-ordinate of shear centre Q
y	vertical coordinate reffered to centroidal axis
y_p	y co-ordinate of pole P
y_Q, y_{shc}	x co-ordinate of shear centre Q

z	longitudinal co-ordinate
α	angle between x axis and tangent to mid-line of wall element or line of action of transverse loading
γ	shear strain
δ	variational symbol denoting virtual displacement, virtual strain or virtual work
δ_H	side-sway
δW_{ext}	external virtual work
δW_{int}	internal virtual work
ΔT	transformation matrix
$\Delta \widetilde{V}_{iv0}$	change in $\widetilde{V}_{iv0}$ when axial load is applied
Δw_i^0	warping incompatibility in w_i^0 at cut
Δx	$(x_1 - x_0) or (x_2 - x_1)$
$\Delta\theta$	column vector of relative rotations at nodes
$\Delta\theta_i$	$(\theta_{m+1} - \theta_m)$ in mode i
ε	normal strain
θ	relative rotation of chords meeting at nodes of frame
θ_m	twist of wall element m
θ_x	rotation about the x axis
θ_y	rotation about the y axis
θ_z	rotation about the z axis
λ	eigenvalue
λ_i	ith eigenvalue in distortional analysis
λ_{iv}	ith eigenvalue in shear lag analysis
ω_{dwr}	distortional warping co-ordinate
ω_{twr}	normalized sectorial co-ordinate in torsional warping

CHAPTER-1

INTRODUCTION

1.1 General:

Box girder bridges have a proven high structural efficiency and are therefore used in a wide variety of bridge applications. The use of concrete box beams in bridge deck construction has led to considerable economy in the use of materials. The advantage of the hollow section is that the material is efficiently used both in bending and in torsion comperative to bridge with concrete or steel I section. Lateral load-distribution characteristics are found to be good in this type of construction. The structural actions that need to be considered are the loading effects that cannot be predicted by the simple bending theory.It is revised to consider all structural actions such as shear lag effects, torsional and other shear stresses, warping stresses due to torsion and distorsion, transverse stress due to distorsion, bimoment, effect of creep ,relaxation and shrinkage and those of local stress concentrations.

The development of the curved beam theory by Saint-Venant (1843) and later the thin-walled beam theory by Vlasov (1965) marked the birth of all research efforts published to date on the analysis and design of straight and curved box-girder bridges.Since then, numerous technical papers, reports, and books have been published in the literature concerning the various applications and even modifications the two theories. A comprehensive review of analytical and experimental studies on box-girder bridges was undertaken by Maisel (1970). This comprehensive review was extended by Swann (1972), Maisel et al. (1973) , and Maisel (1982) .

This report extends Maisel's (1982) methodology for analysing single cell simply-supported box section.

1.2 Literature Review:

1.2.1 Elastic Analysis of Box Girder Bridges

Analysis is usually simplified by means of assumptions that establish the relationship between the behaviour of single elements in the integrated structure in the design of bridges. These single element's combined response is assumed to represent the response of the entire structure, and the accuracy of these solutions depends on the validity of the assumptions made.The Canadian Highway Bridge Design Code CHBDC 2000 as well as the American Association of State Highway Transportation Officials AASHTO 1996,AASHTO 1994 have recommended several methods of analysis for only straight box-girder bridges.These include: orthotropic plate theory, finite-difference technique, grillage analogy, folded plate method, finite strip method and the finite element method.These methods along with the thin-walled beam theory have been applied by several authors to the analysis of straight and curved box-girder bridges.

1.2.2 Orthotropic Plate Theory Method

In the orthotropic plate method, the stiffness of the flanges and girders are lumped into an orthotropic plate of equal stiffness, and the stiffness of diaphragms is distributed over the girder length.This method is suitable mainly for multigirder straight and curved bridges.However, this method has been recommended by CHBDC(2000) for the analysis of only straight box girder bridges of multispine cross-section but not multicell cross-section.The various methods of calculating the equivalent plate parameters, which are necessary for 2D analysis of straight cellular and voided slab bridges were presented by Bakht et al.(1981).The orthotropic method also used by Cheung et al (1982) to calculate the longitudinal moments and transverse shear in multispine box-girder bridges.The results were compared to those obtained from three dimensional analysis using the finite-strip method to establish the limits of validity of the orthotropic plate method. It was concluded that the orthotropic plate method gives accurate results provided that the number of spines is not less than three.Another method proposed by Kristek et al. (1990) for shear lag analysis of steel and composite single-cell box girders, using harmonic

analysis and simple calculations.This method was extended later to consider girders with more complex multicellular cross-sections by Evans et al. (1993)

1.2.3 Grillage-Analogy Method

In this method, the multicellular super structure was idealized as a grid assembly by Hambly and Pennells (1975). Kissane and Beal (1975) also applied similar idealization to curved multispine box-girder bridges. Cheung et al. (1982) dealt with the calculation of the longitudinal bending moment and transverse shear in multispine box-girder bridges using the grillage-analogy method.These results compared favourably with the results obtained from the three dimensional analysis using the finite-strip method.One difficulty in the grillage-analogy method lies in the representation of torsional stiffness of the closed cells.Satisfactory, but approximate representation can be achieved in modelling the torsional stiffness of a single closed cell by an equivalent I –beam torsional stiffness,Evans and Shanmugam,(1984). This method was used by Evans(1984) in the analysis of cellular bridge decks in the linear elastic and in the non-linear post buckling range.By using a simplified grillage technique Shan-mugam and Balendra (1986) described the dynamic analysis for free-vibration characteristics of multicell structures and the problems like adequate representation of the shear lag effects, and torsional stiffness of closed cells were discussed.Canadian Highway Bridge Design Code (CHBDC 2000) suggest that this method is only suitable for voided slab and box-girder bridges in which the number of cells or boxes is greater than two.

1.2.4 Folded-Plate Method

The folded plate method utilizes the plane-stress elasticity theory and the classical two-way plate bending theory to determine the membrane stresses and the slab moments in each folded plate member. The folded plate system consists of an assemblage of longitudinal annular plate elements interconnected at joints along their longitudinal edges and simply supported at the ends. No intermediate diaphragms are assumed.The solution of simply supported straight or curved box-girder bridges is obtained for any arbitrary longitudinal load function by using direct stiffness harmonic analysis. The method has

been applied to cellular structures by Meyer and Scordelis (1971) , Al-Rifaie and Evans (1979) , and Evans (1984) . However, it was evident that the method is complicated and time-consuming. Furthermore, the Canadian High-way Bridge Design Code (CHBDC, 2000) restricted this method to bridges with support conditions closely equivalent to line supports at both ends of the bridge. Marsh and Taylor (1990) developed a method that incorporates a classical folded plate analysis of an assemblage of orthotropic or isotropic plates to form box girders. Beam elements were included in the assembly, and the compatibility of actions and displacements at element junctions was established by a stiffness analysis under the effect of the applied loads, including the effect of settlement.

1.2.5 Finite-Strip Method

The finite-strip method may be regarded as a special formulation of the finite-element method. In principle, it employs the minimum total potential energy theorem to develop the relationship between the unknown nodal displacement parameters and the applied load. In this method, the box girders and the plates are discretized into annular finite strips running from one end support to the other and connected transversely along their edges by longitudinal nodal lines. The displacement functions of the finite strips are assumed to be combination of harmonics varying longitudinally with polynomials varying in the transverse direction. Cheung and Cheung (1971) applied the finite-strip method for curved box-girder bridges. Buragohain and Agrawal (1973) presented a method based on a harmonic analysis in the circumferential direction and a modified finite difference technique in the transverse direction of a curved box-girder bridge. Cusens and Loo (1974) presented a general finite-strip technique to single and multispan box bridges with an extension to the consideration of prestressing forces. At the same time, Kabir and Scordelis (1974) developed a finite-strip computer program to analyze curved continuous span cellular bridges with interior radial diaphragms on supporting planar frame bents. Cheung and Chan (1978) used the finite-strip method to determine the effective width of the compression flange of straight multispine and multicell box-girder bridges. Using the finite-strip method, Branco and Green (1984) investigated the effect of a cross- bracing system, as well as that of the transverse web stiffeners, in resisting

distortion and twist of straight composite twin-spine box girder bridges during service. Cheung (1984) used a numerical technique based on the finite-strip method and the force method for the analysis of continuous curved multicell box-girder bridges. Scordelis et al. (1985) extended the applicability of the available computer program, Kabir and Scordelis (1974) accounted the effect of post tensioned prestressing tendons. Li et al. (1988) presented the application of the spline finite-strip method to the elasto-static analysis of circular, and on circular multicell box-girder bridges. Arizumi et al. (1988) studied the distortional and slip behavior of simply supported curved composite box- girder bridges using the finite-strip method with spring elements representing the shear connectors. The results from the proposed finite-strip method were compared to those obtained from curved beam theory, distortional theory, and static tests. At the same time, Gambhir and Singla (1988) presented an optimization study, using the finite-strip method of prismatic multicellular bridge decks for minimum cost. Cheung and Li (1989) extended the applicability of finite-strip method to analyze continuous haunched box-girder bridges with variable depth web strip . Later, Cheung and Jaeger (1992) applied the spline finite-strip method to the same bridge configuration. Chang and Gang (1990) presented a spline finite-strip approach to analyze the cantilever deck of single-cell box-girder bridge. The effects of distortion of a thin-walled box section are taken into account by treating the cantilever deck as a cantilever slab with horizontally distributed spring support along the cantilever root. Abdullah and Abdul Razzak (1990) applied the finite-strip method for the analysis of a prestressed concrete box-girder bridge using higher order bending and in-plane strips and an auxiliary nodal line technique. Maleki (1991) further expanded the compound strip method for plates to analyze box girders. Shimizu and Yoshida (1991) utilized the finite-strip method to evaluate the reaction forces to be used in the design of load-bearing diaphragms at the intermediate support of two-span continuous curved box-girder bridges. Cheung and Li (1991) extended the spline finite-strip method for free-vibration analysis of curved box-girder bridges. Bradford and Wong (1992) used the finite-strip method to study the local buckling of straight composite concrete deck-steel box section in negative bending. Cheung and Au (1992) presented a spline finite-strip procedure using computed shape functions in the transverse direction for the analysis of right box-girder bridges. This procedure results in a relatively narrow band matrix that

requires only a nominal computational effort to solve. Lounis and Cohn (1995) illustrated the application of an effective optimization procedure for the design of prestressed concrete cellular bridge decks consisting of single-and two-cell box girders or voided slab systems. Using nonlinear programming for optimum design, using the finite-strip method and finite-difference techniques, an approximate live load moment analysis that determines moment sensitivities to change in the deck depth and flange thickness was proposed. Senthilvasan et al. (1996) developed stiffness and mass matrices of curved single- and multicell bridges by combining the spline finite-strip method and a horizontally curved folded-plate model of the bridge. Compared to the finite-element method, the finite-strip method yields considerable savings in both computer time and effort, because only a small number of unknowns are generally required in the analysis. However, the drawback of the finite-strip method is that the method is limited to simply supported prismatic structures with simple line support (CHBDC 2000) .

1.2.6 Finite-Element Method

During the past two decades, finite-element structural analysis has rapidly become a very popular technique for the computer solution of complex problems in engineering. In structural analysis, the method can be regarded as an extension of the earlier established analytical techniques, in which a structure is represented as an assemblage of discrete elements interconnected at a finite number of nodal points. Chapman et al. (1971) conducted a finite-element analysis on steel and concrete box-girder bridges to investigate the effect of intermediate diaphragms on the warping and distortional stresses. Lim et al. (1971) developed an element that has a beam-like-in-plane displacement field. The element is trapezoidal in shape, and it, can be used to analyze right, skew, or curved box-girder bridges with constant depth and width. Sisodiya et al. (1970) approximated the curvilinear boundaries of finite elements used to model the curved box-girder bridges by a series of straight boundaries using parallelogram elements. This approximation would require a large number of elements to achieve a satisfactory solution. Such an approach is impractical, especially for highly curved box section bridges. Bazant and El Nimeiri (1974) attributed the problems associated with the neglect of curvilinear boundaries in

elements used to model curved box beams to the loss of continuity at the end cross sections of two adjunct elements meeting at an angle. They developed a skew-ended finite element with shear deformation using straight elements and adopted a more accurate formulation to account theory that allows for transverse shear deformations. Chu and Pinjarkar (1971) developed a finite element formulation of curved box-girder bridges, consisting of horizontal sector plates and vertical cylindrical shell elements. The method can be applied only to simply supported bridges without intermediate diaphragms. William and Scordelis (1972) presented an elastic analysis of cellular structures of constant depth with arbitrary geometry in plan using quadrilateral elements. Fam and Turkstra (1975) developed a finite-element scheme for static and free-vibration analysis of box girders with orthogonal boundaries and arbitrary combinations of straight and horizontally curved sections using a four-node plate bending annular element with two straight radial boundaries, for the top and bottom flanges, and conical elements for the inclined web members. Ramesh et al. (1976) uncoupled in-plane and out-of-plane forces and neglected shear deformation to introduce a curved element with 6 degrees of freedom at each node. Their method is applicable to single and multicell sections. Moffat and Lim (1976) presented a finite-element technique to analyze straight composite box-girder bridges will complete or incomplete interaction with respect to the distribution of the shear connectors. Malcolm and Redwood (1970) and Moffatt and Dowling (1975) investigated the shear lag phenomena in steel box-girder bridges. Later on, Turkstra and Fam (1978) demonstrated the importance of warping and distortional stresses in a single-cell curved bridge, in relation to the longitudinal normal bending stresses obtained from curved beam theory. Sargious et al. (1979) studied the behavior of end diaphragm with opening in single-cell concrete box-girder bridges supported by a central pier. At the same time, Daniels et al. (1979) presented the results of a finite-element study concerning the effect of spacing of the rigid interior diaphragms on the fatigue strength of curved steel box girders. The results showed that reducing the interior diaphragms spacing effectively controls the distortional normal and bending stresses and increases the fatigue strength of curved steel box girders. Jirousek and Bouberguig (1979) presented an efficient macro-element formulation for static analysis of curved box-girder bridges with variable cross sections. Templeman and Winterbottom (1979) used the finite-element

method to investigate the minimum cost design of concrete spine box beam bridge decks. Dezi (1985) examined the influence of some parameters on the deformation of the cross section in curved single-cell box beams over those in straight single-cell box beams. The parameters considered in this study were transverse and longitudinal locations of external loads, span-to-radius ratio, width-to-depth of the cell, and number of cross diaphragms. Ishac and Smith (1985) presented simple design approximations for determining the transverse moments in single-span single-cell concrete box-girder bridges. Chang and Zheng (1987) used the finite-element method to analyze the shear lag effects in cantilever box girders. Expressions were derived to determine the region of negative shear lag effect with the interrelation of span and width parameters. Dilger et al. (1988) studied the effect of presence and orientation of diaphragms on the reaction, internal forces, and the behavior of skew, single cell, concrete box-girder bridges. Shushkewich (1988) showed that the actual 3D behavior of a straight box-girder bridge, as predicted by a folded-plate, finite-strip, or finite-element analysis, can be approximated by using some simple membrane equations in conjunction with a plane frame analysis. In particular, the proposed method allows the reinforcing and prestressing to be proportional for transverse flexure, as well as the stirrups to be proportioned for longitudinal shear and torsion in single-cell, precast concrete, segmental box-girder bridges. Mishra et al. (1992) presented an investigation into the use of closely associated finite-difference technique for the analysis of right box-girder bridges as a feasible alternative to the finite-element method. The method discritizes the total energy of the structure into energy due to extension and bending and that due to shear and twisting contributed by two separate sets of rectangular elements formed by a suitable finite-difference network.

Galuta and Cheung (1995) developed a hybrid analytical solution that combines the boundary element method with the finite-element method to analyze box-girder bridges. The finite-element method was used to model the webs and bottom slab of the bridge, while the boundary element method was employed to model the top slab. Jeon et al. (1995) presented a procedure for static and dynamic analysis of composite box beams using a large deflection beam theory. The finite-element equations of motion for beams undergoing arbitrary large displacements and rotations, but small strains, were obtained

from Hamilton's principle. Fafitis and Rong (1995) presented a substructuring analysis method for thin-walled box girders. In this method, instead of solving the condensed equilibrium equations in the traditional substructuring method, a mix of compatibility and equilibrium equations are employed with shear forces at the interfaces of thin walls as major unknowns. The proposed method can be performed using any commercial finite-element analysis software. Abdelfattah (1997) utilized three dimensional finite-element modelling to study the efficiency of different systems for stiffening steel box girders against shear lag.

Recently, few authors have dealt with temperature effects in box-girder bridges. Branco and Martins (1984) studied the temperature distribution in straight concrete box bridges based on a finite-element solution of the Fourier equation. This study gives the temperature gradient that should be considered in the design of such bridges. Chan et al.(1990) presented temperature data collected continuously in three composite box-girder bridges over a one-to-two year period. The first bridge was the Portage Bridge spanning the Ottawa River between Hull, Quebec, and Ottawa, Ontario. This bridge is a three-lane, three-span, continuous, composite concrete deck-five-box steel structure with a total length of 158.5 m. The second bridge was the St. Leonard International Bridge over the St. John River connecting St. Leonard, New Brunswick, and Van Buren, Maine. This bridge is a continuous, five-span, composite concrete, deck-steel, two-box girder bridge with a total length of 222.5 m. The third bridge was the Robert Campbell Bridge that spans the Yukon River in the city of White-horse. It is a continuous, two-span, composite concrete, deck, three-box section steel bridge with a total span of 109.7 m. Thermal stresses induced in these bridges were determined using the finite-element method with input being the measured extreme temperature profiles. Mirambell and Aguado (1990) presented an analytical model, based on a mathematical technique and the finite-difference method, to predict temperature and stress distributions in concrete box-girder bridges. Elbadry and Ibrahim (1996) determined the time-dependent temperature variations within the cross section and along the length of curved concrete single-cell box-girder bridges using a three dimensional finite-element model used in heat transfer. A similar study was presented by Gilliland and Dilger (1998).

Elbadry and Debaiky (1998) presented a numerical procedure and a computer program for the analysis of the time-dependent stresses and deformations induced in curved, prestressed, concrete cellular bridges due to changes in geometry, in the statical system, and in the loading conditions during construction. The effects of creep and shrinkage in concrete and relaxation of prestressed steel during and after construction were considered. The procedure was based on the displacement formulation of the finite-element method in which multi-node, variable, cross-section curved beam elements were used to model prestressed concrete bridges of an arbitrary geometry in plan. A similar study was presented by Luoxi et al. (1993) .

1.3 Objectives of This Research:

- To develop computer program for analysing a simply-supported single cell box section considering all structural actions.

- To study the load deformation behaviour of a single cell box beam with different loading and geometric condition.

- To develop a complete stress analysis chart considering all structural action, flexure, shear, torsion, distortion, warping, and shear lag in calibrated form for different loading and geometric condition, so that one designer could get some reasonable help for designing a single cell simply supported box section .

CHAPTER 2

BEHAVIOUR OF THIN WALLED CROSS-SECTIONS

2.1 General:

An appropriate sign convension for the analysis of thin-walled box sections can be defined by following the work of Maisel (1982) .The sign convension of all stresses, co-ordinate axes, displacements patterns, positive and negative sections for analysis of all structural actions are shown for a multicell section.

2.2 Definition of Thin-Walled Beam:

Vlasov (1961) defines a thin-walled beams as a structure having the form of a long, prismatic shell. The shell thickness is small compared with any characteristic dimension of the cross-section, and the cross-sectional dimensions are small compared with the length of the shell. He gives as criteria the following:

$$\frac{\text{shell thickness}}{\text{width or depth of cross-section}} \leq 0.1$$

and

$$\frac{\text{width or depth of cross-section}}{\text{length of shell}} \leq 0.1$$

The first criterion is frequently not satisfied for concrete boxbeams, but Vlasov's theory has nevertheless been used for analysis. Dabrowski (1972) epresses the view that the theory of beam-type members applies if the span is more than 3 or 4 times the breadth of the cross-section measured between the outer webs of a (multicell girder). Kollbrunner and Basler (1969), in discussing St. Venant torsion, state the following criterion for classifying a section as thin-walled, by specifying a certain accuracy of calculation.

There is less than 10% error in calculating the shear stresses for hollow cross-section with a constant wall thickness, if the effective area of cross-section is less than one-fifth of the area enclosed by the wall centre line. Concrete structures do not usually satisfy this

geometrical condition. There is less than 10% error in the calculated internal torsional moment if the effective area of cross-section does not exceed the area enclosed by the wall centre line. Concrete structures usually do satisfy this geometrical condition.

2.2.1: Co-ordinate Axes:

To obtain a right-handed system of co-ordinates, the arrangement shown in Figure-2.1 is adopted.

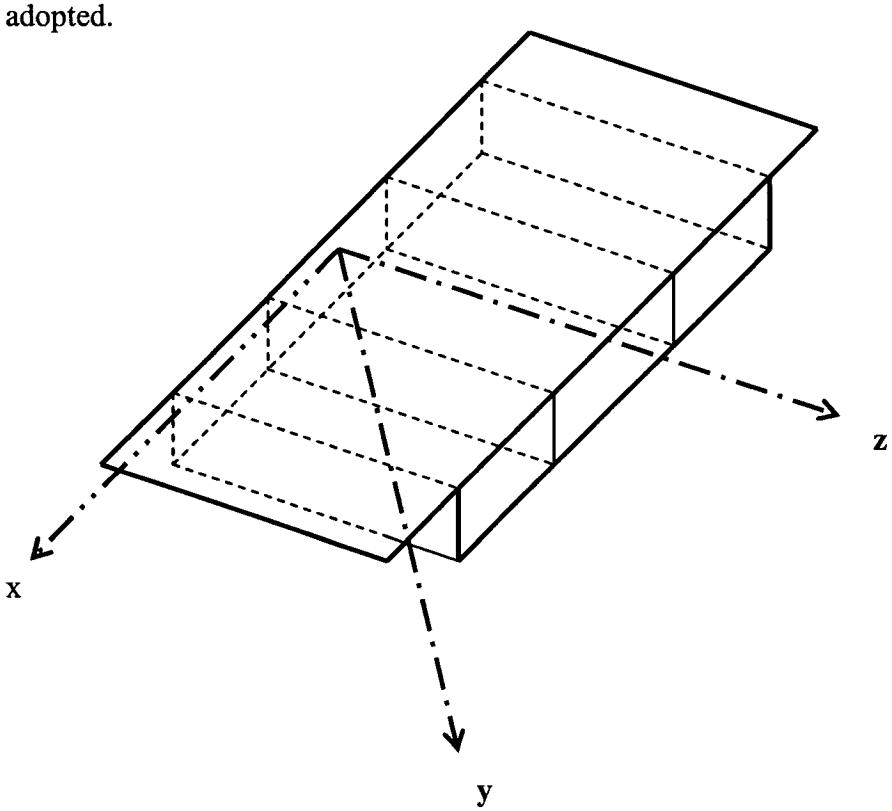

Figure 2. 1:Co-ordinate axes x,y and z

The position of the origin within the cross-section is usually taken as the centroid for a longitudinal bending analysis and as the shear centre for a torsional warping analysis. For a distortional analysis, this origin could be taken arbitrary as the midpoint of the central cell, or centre web, but it is more important to refer such an analysis to the peripheral co-ordinate, s_{per}. Figure 2,2(a), 2.2(b) and 3.2 show the arrangements of origin and positive directions considered appropriate for s_{per} in the treatment of longitudinal bending and torsional warping, respectively.

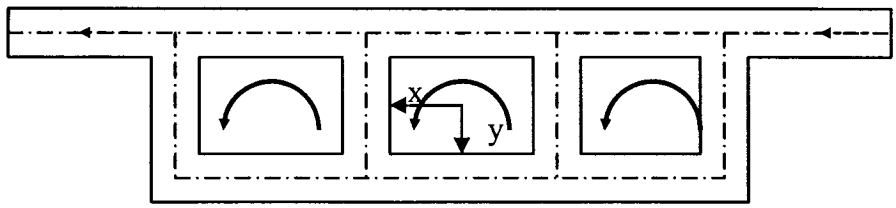

(a) For longitudinal bending (without torsion)

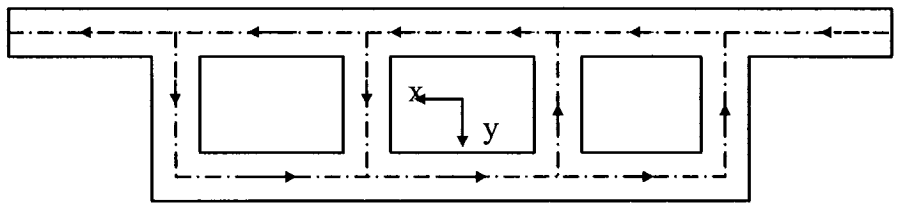

(b) For torsional warping

Figure 2. 2: Peripheral co-ordinate s_{per}, showing origin and positive directions (Maisel,1982)

2.3: Displacements:

Displacements in the directions of the x, y, z axes are positive when in the positive directions of these axes , and are denoted by a_x, a_y, a_z respectively, as shown in Figure 2.3. Rotations θ_x and θ_y, and twist θ_z, are also shown, and are positive when they occur in the directions indicated.

Face of cross-section:

A positive face of cross-section is one whose external normal points are in the positive directions of the z axis. A negative face of cross-section is one whose external normal points are in the negative direction of the z axis.

Stresss:

All stresses discussed in this report are internal resistive stresses caused by applied external loading.

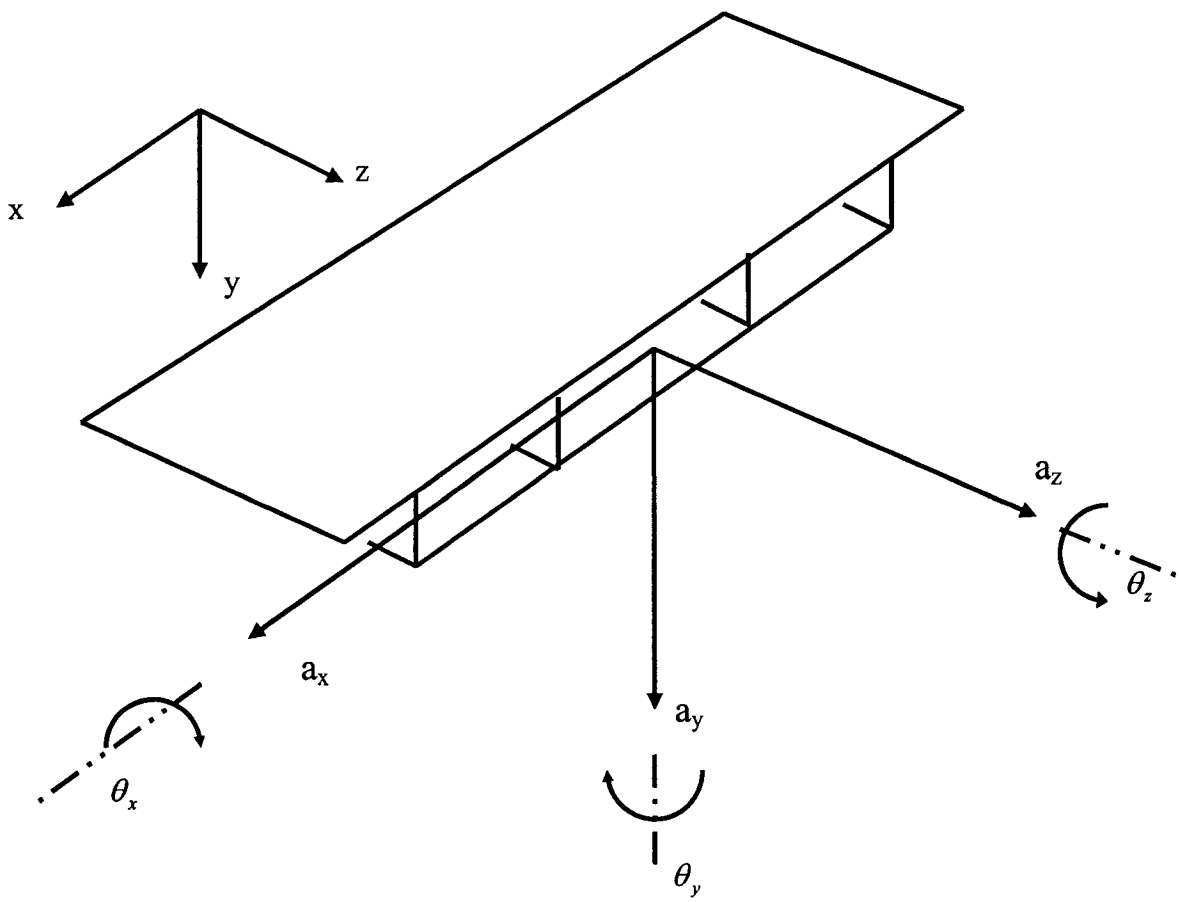

Figure 2. 3: Positive directions of displacements, rotation and twist (Maisel, 1982)

2.4: Positive directions of stresses and stress-resultants:

The following sign convention applies for normal stresses f and shear stresses v.

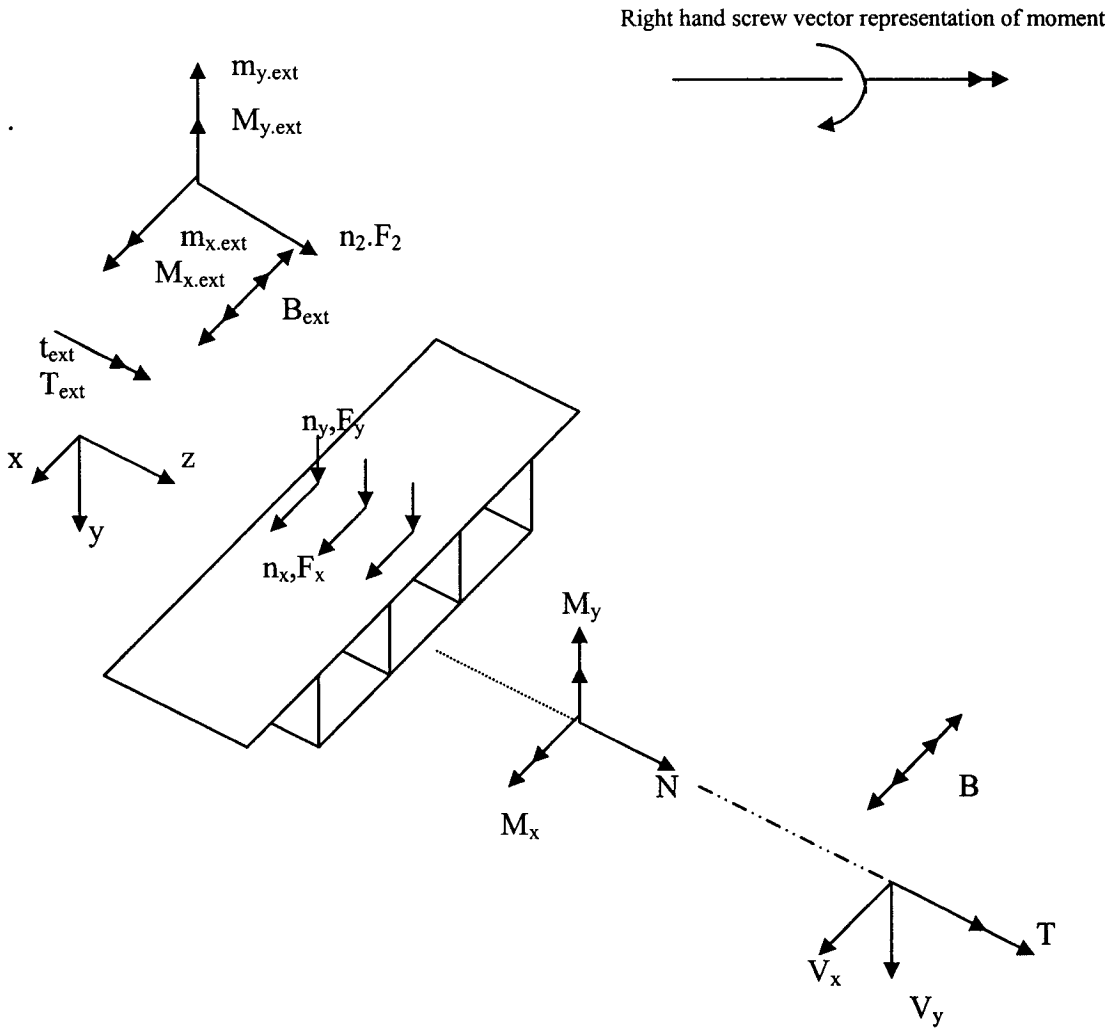

Figure 2. 4: Positive directions of internal stress-resultants and external loading (Maisel, 1982)

For a positive direction of an axis; a stress component is to be regarded as positive if it acts in the positive direction of an axis, otherwise it is negative. For a negative face of the cross-section, a stress components acting in the negative direction of an axis is positive. Hence, tensile stresses on a cross-section are always positive quantities, and compressive stresses are negative.

Shear stresses acting in the positive direction of the s_{per} co-ordinate are positive, otherwise they are negative (for the positive face of cross-section). Where as in Figure

2.2, the positive direction of s_{per} varies accordingly to the type of structural action being considered, each type of analysis must be performed separately. This leads to a knowledge of the physical directions of the component shear stress in all parts of the cross-section. Only then, these component shear stresses can be superimposed for thpese cases in which two or more types of structural action occur simultaneously.

Since internal forces or stress-resultants are the resultants of internal stresses, they follow the same rule of signs. The positive directions of the internal stress-resultants acting on a posive face of a cross-section are shown in Figure 2.4 . Note that the shear forces V_x and V_y and the axial force N are positive when in the positive directions of the x, y and z axes, respectively. The bending moments M_x, M_y and twisting moments T are shown using the right-hand rotational vector representing of moment. M_x and M_y are positive when in the negative senses of rotation of θx and θy, respectively, because of the definition adopted for positive bending; Kollbrunner and Basler (1964). T is positive when in the positive sence of twist, θz, and B is the internal bimoment, shown acting positively accordingly to the convention . Maisel and Roll, F. (1974)).

Figure 2.4 also shows the positive directions of applied loading on the beam element: n_x, n_y and n_z are distributed loadings in the x,y and z directions, respectively, and F_x, F_y and F_z are concentrated loads acting in these directions; t_{ext} and T_{ext} are, respectively, the distributed and concentrated applied torsional moments $m_{x,ext}$ and $m_{y,ext}$ are distributed applied bending moments about the x and y axes, respectively, and $M_{x,ext}$ and $M_{y,ext}$ are the corresponding concentrated applied bending moments; B_{ext} is the concentrated applied bimoment.It will be noted, from Figure 2.4, that the positive directions of the internal resistive stress-resultants acting on the positive face of the cross-section shown are the same as those of the external applied loads acting on the beam element shown.

CHAPTER-3

ANALYSIS OF SIMPLE BENDING AND ST VENANT TORSION

3.1: Assumptions:

The structural effects neglected here are torsional and distortional warping, shear lag and distortion.

3.2: Simple Bending Without Twist:

The following expression is obtained for the normal stresses in longitudinal bending, using engineer's theory of bending, in which plane cross-sections are assumed to remain plane before and after the bending of a thin –walled beam whose cross-section has a vertical axis of symmetry (Figure 3.1)

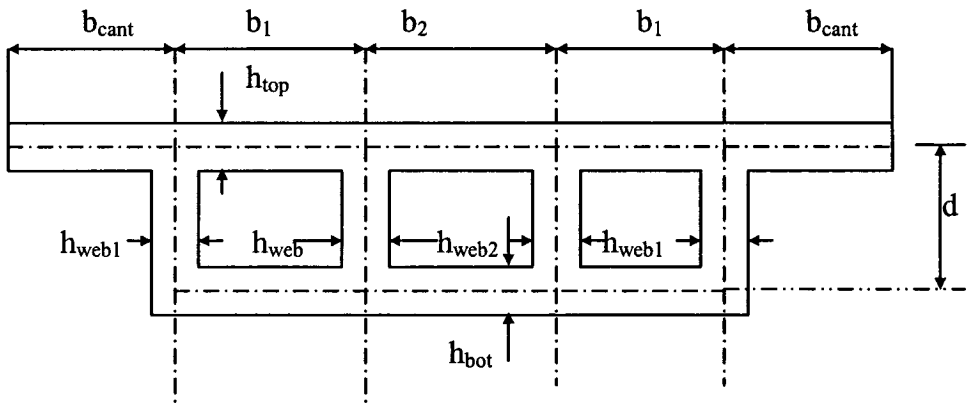

Figure 3. 1: Dimensions of cross-section (Maisel, 1982)

$$f_{1bg} = \frac{M_x y}{I_x} + \frac{M_Y x}{I_y} \qquad (3.1)$$

where f_{1bg} = normal stress in longitudinal bending (positive tensile)

x,y = co-ordinates of a point on the mid-line of the wall of cross-section,referred to centroidal axes (see Figure 2.1)

M_x= bending moment about x axis (see Figure 2.4);

M_y= bending moment about y axis (see Figure 2.4)

I_x= second moment of entire cross-section about centroidal x axis;

I_y= second moment of entire cross-section about centroidal y axis;

3.3: Longitudinal Shearing Stress:

3.3.1: Multicell Sections:

For the shear stresses arising due to the longitudinal bending, Venkatraman and Petel (1970) developed an analysis for the general multicell, thin walled section, and the results of this are given here in the form appropriate to vertical loading on a three-cell section of the type shown in Figures-3.1.

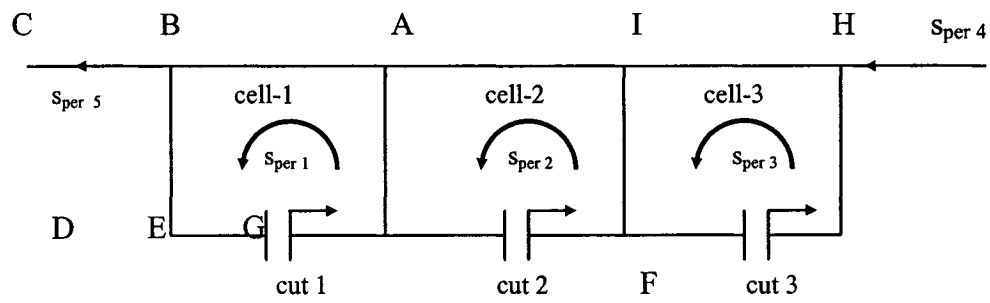

Figure 3. 2: Peripheral co-ordinate s_{per} and cuts in the cross-section (Maisel ,1982)

Let v_{1bg} be the shear stress in longitudinal bending and h be the wall thickness. The positive directions of the peripheral co-ordinate, s_{per}, are defined as shown in Figure 2.2(a) and shown as s_{per1} to s_{per5} in Figure 3.2.

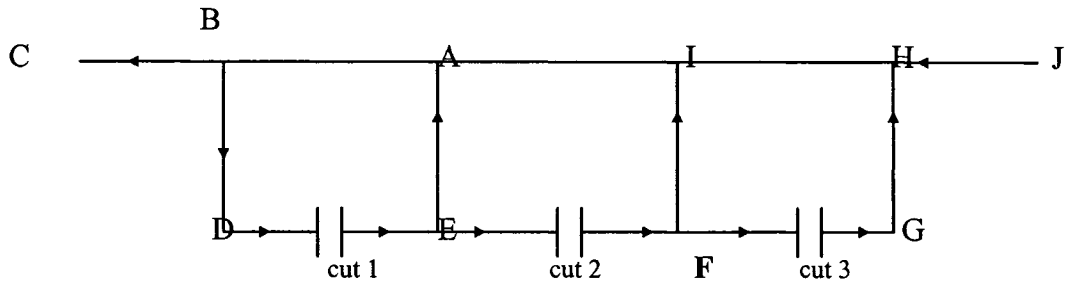

Figure 3. 3: Positive directions of statically determinate shear flows

Insert imaginary cuts 1, 2, 3 at the points indicated, thus transforming the open-closed cross-section into a fully open section.Megson (1974) states that there are arithmetic advantages in placing the cut midway between adjacent webs. Let the origins of s_{per1}, s_{per2}, s_{per3}, be at cut 1, cut 2 and cut 3, rspectively, as shown in Figure-3.2.

Define $(v_{1bg}\,h)_1$,$(v_{1bg}\,h)_2$,$(v_{1bg}\,h)_3$ and $(v_{1bg}\,h)_{cant}$ as the shear flows in longitudinal bending of the open section, in cells 1,2 and 3, and along the cantilevers, respectively.They are positive in the directions shown in Figure-3.3

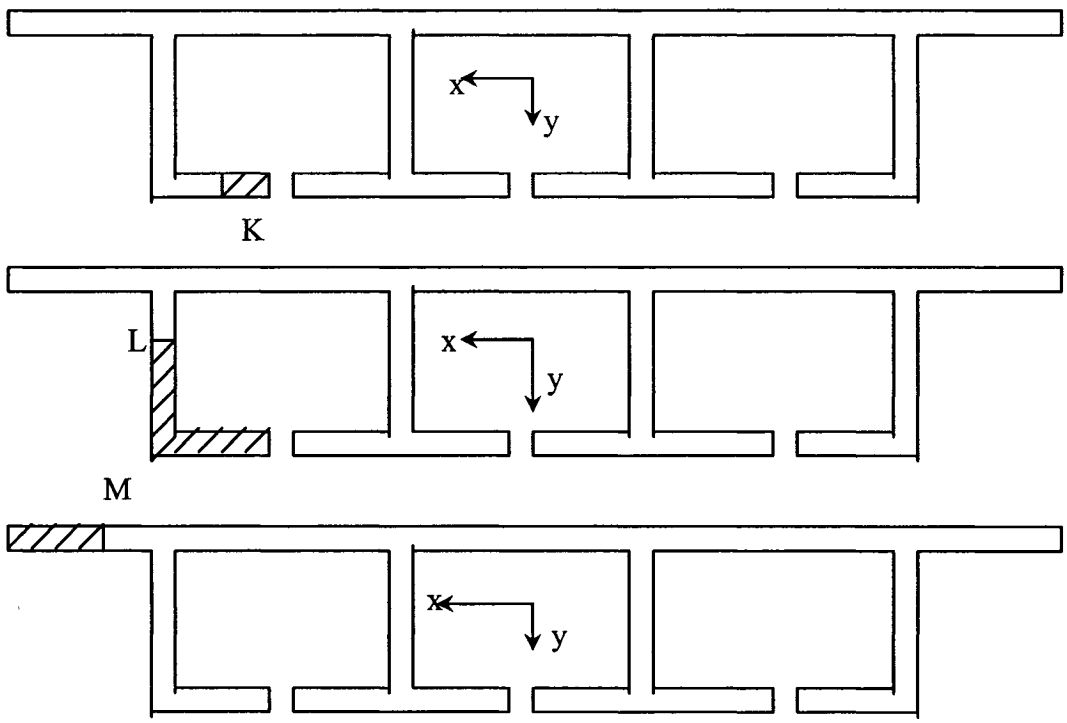

Figure 3. 4: Evaluation of ($\overline{Ay}$), the first moment of area of the partial cross-section about the centroidal x-axis (Maisel, 1982)

Let $(v_{1bg}\ h)_{01}$, $(v_{1bg}\ h)_{02}$, $(v_{1bg}\ h)_{03}$ be the statically indeterminate shear flows required to restore compatibility at cuts 1,2 and 3, respectively.These shear flows are positive in the same directions as s_{per1},s_{per2} and s_{per3} respectively.

Let V_y=shear force on the cross-section in the y direction (see Figure 2.4). Then, for the fully open section (i,e with the imaginary cuts)

$$(v_{1bg}\ h)_{1,etc} = -\frac{V_y(\overline{Ay})}{I_x} \tag{3.2}$$

where $(\overline{Ay})$ is the first moment of the partial area of cross-section about the centroidal x axis [see Figure 3.4:($\overline{Ay}$) at K,L or M is the first moment of the shaded area about the X axis].

To obtain $(v_{1bg}\ h)_{01}$ in each cell, the following system of simultaneous equations is set up, corresponding to the condition that there is no twist of the section.

$$(v_{1bg}h)_{01}\int_{ABDE}\frac{ds_{per1}}{h} - (v_{1bg}h)_{02}\int_{EA}\frac{ds_{per1}}{h} = -\int_{ABDE}\frac{(v_{1bg}h)_1}{h}ds_{per1} \tag{3.3}$$

$$-(v_{1bg}h)_{01}\int_{AE}\frac{ds_{per2}}{h} + (v_{1bg}h)_{02}\int_{AEFI}\frac{ds_{per2}}{h} - (v_{1bg}h)_{03}\int_{FI}\frac{ds_{per2}}{h} = -\int_{AEFI}\frac{(v_{1bg}h)_2}{h}ds_{per2} \tag{3.4}$$

$$-(v_{1bg}h)_{02}\int_{IF}\frac{ds_{per3}}{h} + (v_{1bg}h)_{03}\int_{FGHI}\frac{ds_{per3}}{h} = -\int_{FGHI}\frac{(v_{1bg}h)_3}{h}ds_{per3} \tag{3.5}$$

In evaluating the right-hand sides, the sign of the statically determinate shear flow $(v_{1bg}h)_{1,2,3}$ must be changed whenever its positive direction,as shown in Figure3.3;

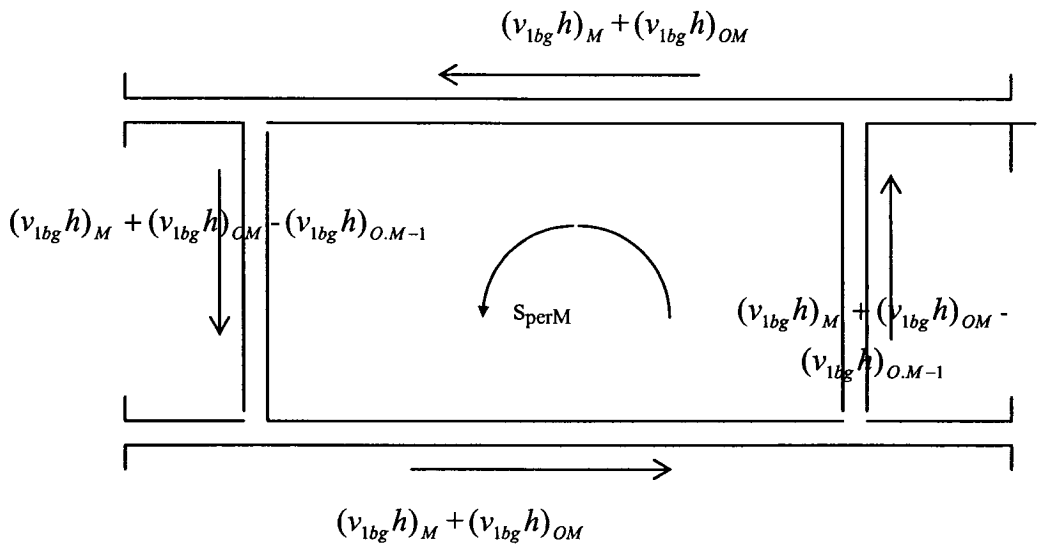

Figure 3. 5: Shear flows in cell M due to longitudinal bending (Maisel 1982)

This conflicts with the positive direction of s_{per} as shown in Figure 3.2.This will be the case in webs EA and FI.

Solving for $(v_{1bg}h)_{01}$, $(v_{1bg}h)_{02}$ and $(v_{1bg}h)_{03}$, the final values of shear flow for the actual section are given by

$$(v_{1bg}h) = (v_{1bg}h)_1 + (v_{1bg}h)_{01} \quad \text{in walls AB,BD and DE of cell 1}$$
$$(v_{1bg}h) = (v_{1bg}h)_1 + (v_{1bg}h)_{01} - (v_{1bg}h)_{02} \quad \text{in wall EA of cell 1} \qquad (3.6)$$

and similarly for the other cells. Figure 3.5 shows the general situation for cell M of a multi-cell cross-section. In the cantilevers, the statically indeterminate shear flows $(v_{1bg}h)_0$ do not act. The positive directions of all shear flows in equations 3.6 are the same as those of s_{per} in Figure 3.2.

To evaluate the shear stresses in bending due to the horizontal loading,the analyses given by Venkatraman and Patel (1970) are used for the bending of unsymmetrical sections.

In summary, the above procedure for vetical loading consists of the following steps.

(1) Insert imaginary cuts in the section to make it statically determinate.

(2) From equation 3.2, determine the shear flows $(v_{1bg}h)_1$, etc. in the resulting open sections.

(3) Insert results of (2) on the right hand sides of equations 3.3,3.4 and 3.5 and solve for statically indeterminate shear flows $(v_{1bg}h)_{01}$, etc.

(4) Evaluate the resultant shear flows $(v_{1bg}h)$ from equation 3.6.

3.3.2: Single Cell Section:

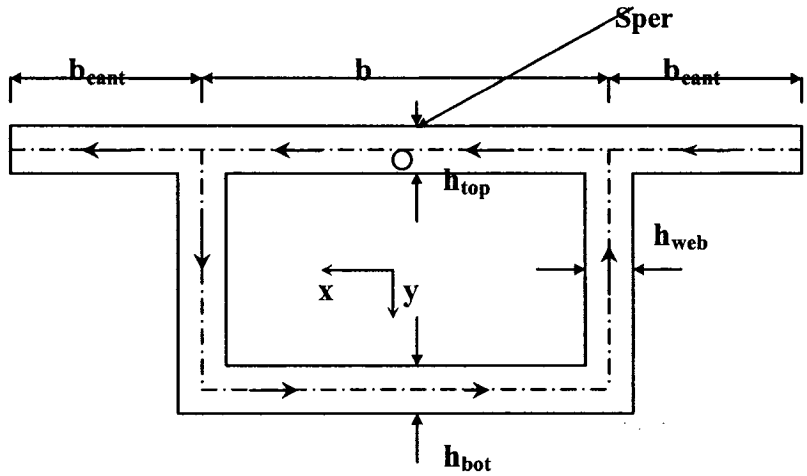

Figure 3. 6: Dimensions of cross-sections and peripheral coordinate s_{per},showing origin and positive directions (Maisel and Roll 1974)

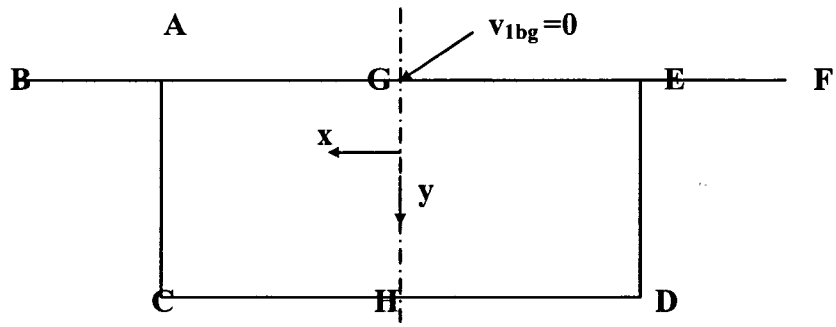

Figure 3. 7: Zero bending shear stress v_{1bg} on the axis of symmetry for vertical loading

For shear stresses arising in longitudinal bending due to the vertical loading only, note that because of the symmetry about the vertical axis of the cross-section, the longitudinal shear stress is zero at this axis, hence the complementary shear stress v_{1bg} in the plane of cross-section is also zero at x=0, as shown in Figure 3.7.

Therefore half of the open-closed section (BACHG in Figure 3.7) can therefore be analysed as an open section, since the boundary conditions for the open sections are now satisfied, i.e there are zero longitudinal shear stress in bending at the ends of the cross-section (G,B and H). Kollbrunner and Basler (1964) developed the following equation which can be applied here:

$$(v_{1bg}h) = -\frac{V_y(\bar{A}y)_{1/2}}{I_x} \tag{3.7}$$

where $(v_{1bg}h)$ = shear flow in longitudinal bending

v_{1bg}= shear stress in longitudinal bending

h=thickness of the wall

Vy=shear force on the cross-section in the y direction

$(\bar{A}y)_{1/2}$ = first moment of area of the partial half-cross section about the centridal x axis.(See Figure 3.8). $(\bar{A}y)_{1/2}$ at J, K or L is the first moment of the shaded area about the x axis.

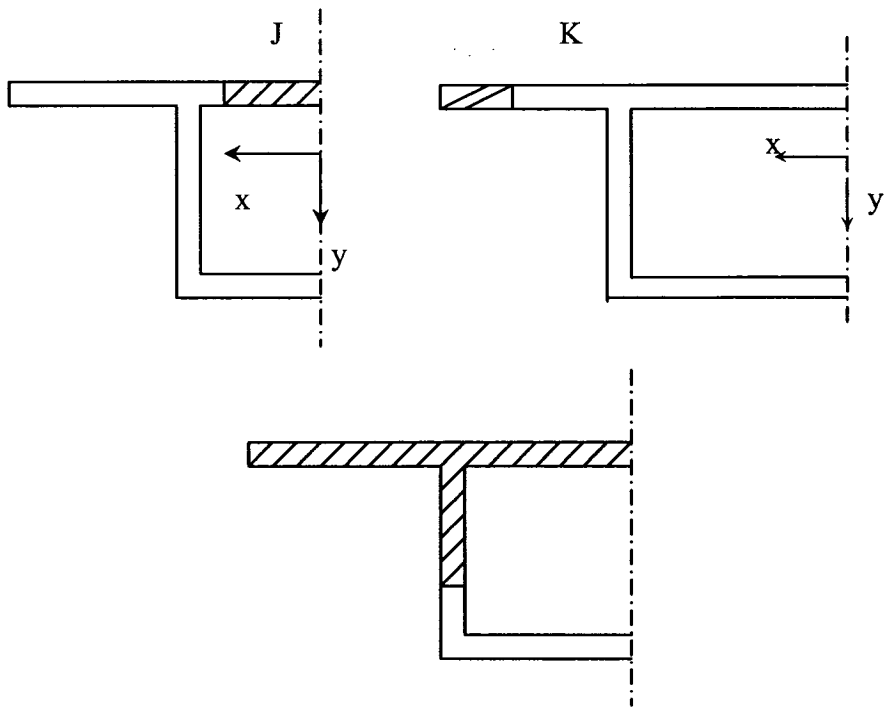

Figure 3. 8: Evaluation of $(\bar{A}y)_{1/2}$, the first moment of area of the partial half cross-section about the centridal x axis (Maisel and Roll , 1974)

I_x = second moment of entire cross-section about the centroidal x axis.

I_y = second moment of entire cross-section about the centroidal y axis.

To find the statically ndeterminate shear flows in a single-cell section (Figure3.7), equations 3.3, 3.4, 3.5 get reduces to:

$$(v_{1bg}h)_0 \oint_{ACDE} \frac{ds_{per}}{h} = -\oint_{ACDE} \frac{(v_{1bg}h)_1}{h} ds_{per} \qquad (3.8)$$

3.4: St.Venant Torsional Shearing Stress:

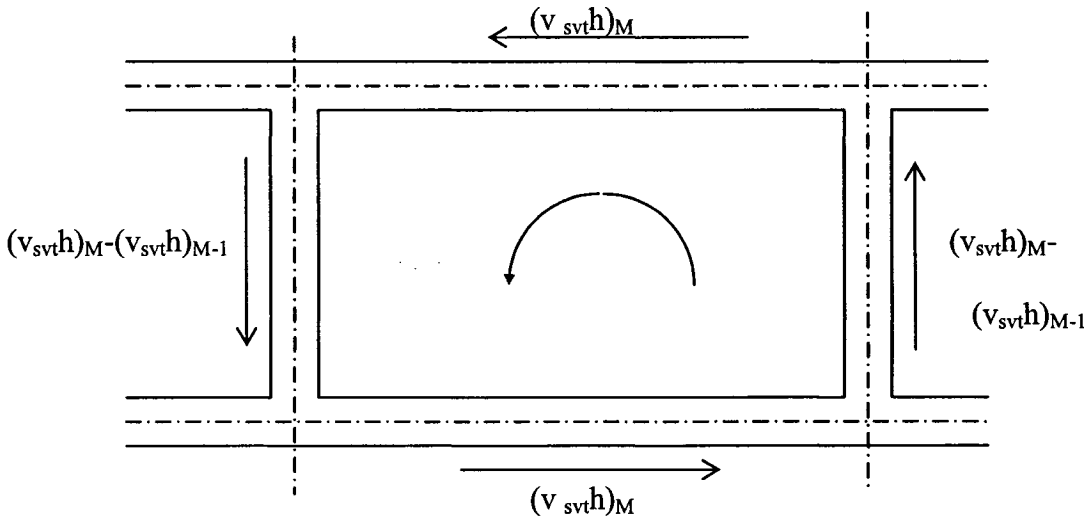

(a): St. venant torsional shear flows in cell M

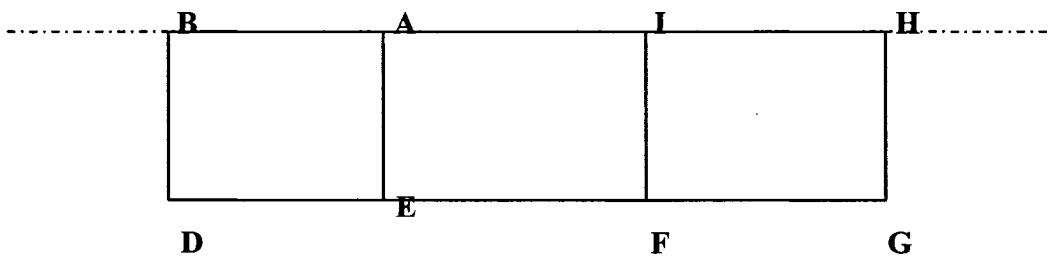

(b): Three –cell section for St. Venant torsion analysis

Figure 3. 9: St. Venant torsional shear flow (Maisel,1982)

For the St. Venant torsion of thin-walled multi-cell box beams of open-closed section, the analysis given by Venkatraman and Patel (1970) may be expressed in the following form. Kelsey (1961).

Consider a torsional moment, $T_{svt,}$to act on a section in St. Venant torsion. Let v_{svt} be the shear stress in St. Venant torsion and h be the wall thickness.Then (v_{svt}h) is the corresponding shear flow.

As the torsional strength of the cantilevers is small in comparison with that of the closed portion of cross-section, neglect the cantilevers and define the positive directions of the peripheral co-ordinate, s_{per} ,as shown in Figure 3.2. for cells 1,2 and 3.

Define $(v_{svt}h)_1$, $(v_{svt}h)_2$, $(v_{svt}h)_3$ as the shear flows in St. Venant torsion in cells1,2and 3, respectively.They are positive in the same directions as s_{per} for the respective cells.If each cell is considered individually, as indicated in Figure 3.9(a), the St. Venant torsion theory gives the following equation:

$$\frac{d\theta_z}{dz} = \frac{(v_{svt}h)_M}{2A_{encM}G}\oint_M \frac{ds_{perM}}{h} \tag{3.9}$$

where θ_z =angle of twist of cell M;

z= longitudinal co-ordinate

v_{svt}h)M= shear flow in cell M;

A_{enc}M=area enclosed by mid-line of wall of cell M;

s_{perM}= s_{per} in cell M

G= shear modulus of elasticity.

The symbol $\oint$ denotes integration along the mid-line of the wall of a closed portion of the cross-section.

Note that in the common walls between the adjacents cells, the positive directions of shear flow, as defined above, oppose one another.This is shown in Figure 3.9(a).

An equation similar to (3.9) can be set up for each cell of a multi-cell section.The condition that there is no distortion of the entire cross-section implies that $d\theta_z / dz$ is the same for each cell.

In addition,on taking moment about any point in the plane of cross-section, the theory yields the result that

$$T_{svt} = \sum_{M} 2A_{encM} (v_{svt} h)_M \tag{3.10}$$

where Tsvt =Total torsional moment at the cross-section in St. Venant torsion, and the summation extends over all the cells.

For the case of a three-cell section, as shown in Figure 3.9(b), the set of simultaneous equations corresponding to equation 3.9 has the following form:

$$(v_{svt} h)_1 \int_{ABDE} \frac{ds_{per1}}{h} - (v_{svt} h)_2 \int_{EA} \frac{ds_{per1}}{h} = 2A_{enc1} G \frac{d\theta_z}{dz} \tag{3.11a}$$

$$-(v_{svt} h)_1 \int_{AE} \frac{ds_{per2}}{h} + (v_{svt} h)_2 \int_{AEFI} \frac{ds_{per2}}{h} - (v_{svt} h)_3 \int_{FI} \frac{ds_{per2}}{h} = 2A_{enc2} G \frac{d\theta_z}{dz} \tag{3.11b}$$

$$-(v_{svt} h)_2 \int_{IF} \frac{ds_{per3}}{h} + (v_{svt} h)_3 \int_{FGHI} \frac{ds_{per3}}{h} = 2A_{enc3} G \frac{d\theta_z}{dz} \tag{3.11c}$$

The solution of equations 3.11a,b,c is of the type

$$(v_{svt} h)_M = K_M G \frac{d\theta_z}{dz} \tag{3.12}$$

where K_M is a known numerical constant corresponding to cell M.

From equation 3.10,

$$T_{svt} = \sum_M 2A_{encM} K_M G \frac{d\theta_z}{dz}$$

$$= G \frac{d\theta_z}{dz} \sum_M 2A_{encM} K_M$$

Therefore,

$$G \frac{d\theta_z}{dz} = \frac{T_{svt}}{\sum_M 2A_{encM} K_M}$$

Hence, in equation 3.12,

$$(v_{svt} h)_M = \frac{T_{svt} K_M}{\sum_M 2A_{encM} K_M} \tag{3.13}$$

As all the quantities on the right hand side of equation 3.13 are known, this completes the solution for the St. Venant torsion shear flows

For single cell section: For a single-cell section, equation 3.13 reduces to

$$(v_{svt} h) = \frac{T_{svt}}{2A_{enc}} \tag{3.14}$$

CHAPTER-4

ANALYSIS OF TORSIONAL WARPING

4.1: Assumptions:

- In torsional warping analysis, it is assumed ,by definition, that there is no distortion of the cross-section.
- The only other structural effect neglected is a minor one, giving rise to transverse normal stresses constant through the wall thickness.

4.2: Stress Pattern and the Physical Significance of Structural Actions:

When the cross-section of a beam does not remain plane and it is free to warp under a torsional load, it is considered being subjected to St.Venant or uniform torsion.If however,one or more cross-sections are forced to remain plane, or not free to warp then "warping stresses" would arise and such torsion is termed warping or non uniform torsion.The simply-supported beam of Figure 4.1 is subjected to a torsional load at its midspan.This midspan cross-section remains plane because of symmetry considerations.The longitudinal out-of-plane displacements (or warping displacements) are also shown in the same Figure 4.1.

The pattern of these displacements is such that the longitudinal torsional warping stresses vary both around the perimeter of the cross-section and along the axis of the beam. Hence longitudinal shear stresses arise which cause complementary shear stresses in the cross-section of the beam; these are called warping shear stresses.

Assuming that the cross-section does not distort in its own plane, as in Figure 4.1(c) and thus distortional warping displacements are neglected.

A box beam whose cross-section is not permitted to distort, develops its resistive torsional moment as a combination of the torsional moment caused by the St. Venant shear stresses

and that caused by the torsional warping shear stresses. It is shown in Figure 4.2 that the moment due to the torsional warping shear stresses are maximum near the section where

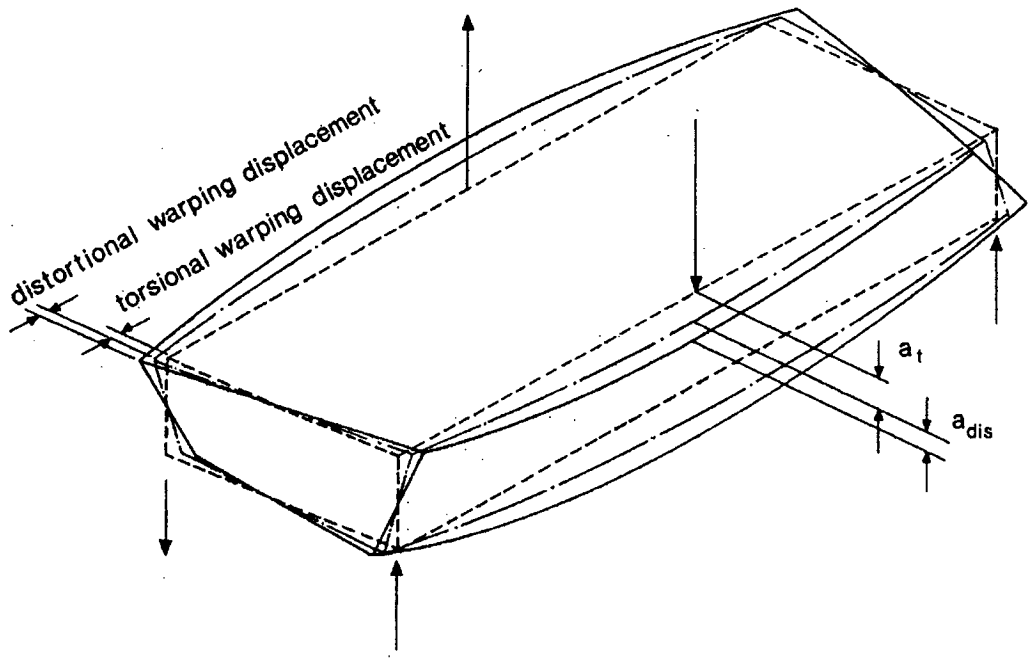

(a) Torsional and distorsional warping

---------- undeflected form of structure

— - — deflected form of structure with rigid transverse diaphragms all along the span

_____ deflected form of structure after removal of diaphragms between supports

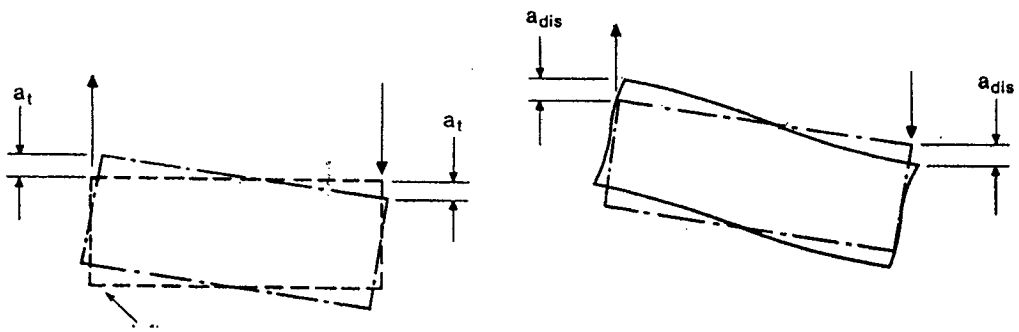

(b) Twisting of midspan cross-section without distortion

(c) Additional twisting of midspan cross-section when distortion is permitted

Figure 4. 1: Torsional loading of a simply supported box beam. (Maisel ,1982)

warping is restrained and it gradually decrease toward the region where the cross-section is free to warp. Note that the sum of the magnitudes of the two above torques is always equal to the total resistive torque caused by the external loading ($T_{ext}/2$ in the case of Figure 4.2)

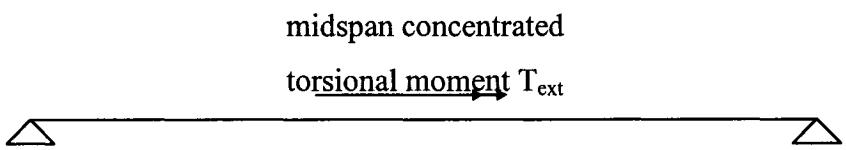

(a) Elevation of the beam (Torsional restraint at the supports but no warping restraint)

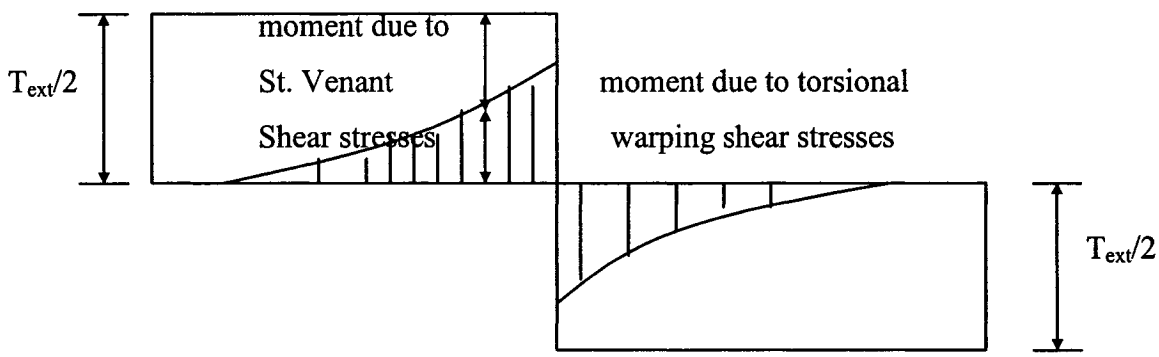

(b) Variation of component internal torsional moments along the beam.

Figure 4. 2: Distribution of the internal torsional moments due to St.Venant and torsional warping shear stresses along the beam (Maisel , 1982)

The warping stresses, as mentioned above, give rise to shear deformations. These deformations are normally neglected in the case of open thin walled cross-sections (Kollbrunner and Basler(1966)) and Oden, J.T. and Ripperger(1981). However, it has been shown by a number of authors, Godden and Aslam (1974), Maisel and Roll (1974) and Scordelis, Bouwkamp and Wasti (1971) that the influence of this deformation must be considered in any torsional warping analysis of closed cross-sections.

4.3: Analysis of Torsional warping by the method of Kollbrunner,Hajdin and Heilig(1966)[Single cell]:

4.3.1 Loading:

The analysis considers only the torsional system of Figure 4.1(b) .The torsional component of the actual loading is used, and not its Fourier representation .

4.3.2 Summary of Procedure for Analysis:

Following Vlasov (1961), Kollbrunner and Hajdin (1966) have developed the theory of warping torsion of thin walled beams of closed or open-closed, undeformable cross-section. The torsional warping (longitudinal) stresses, $f_{twr,}$ and torsional warping shear stresses, $v_{twr,}$ are obtained in terms of the applied torsional moment, the bimoment B_{twr} and the section properties known as the sectorial coordinate, $w_{twr,}$ and the torsional warping moment of inertia, $C_{twr.}$ The algebraic expressions required for obtaining the above quantities, as well as the St.Venant torsional shear stresses, $v_{svt,}$ are given, for a number of load cases and end conditions.

4.3.3 Bimoment B_{twr}:

Instead of working with a group of four forces,it is usual to represent them by a pair of equal and opposite moments in parallel planes, as shown in Figure 4.3 (b) where the moments are taken about a horizontal axis(Figure 4.3(c))where the axis of the moments as vertical. Such a pair of moments is called a bimoment, and has zero force resultant and zero moment resultant.

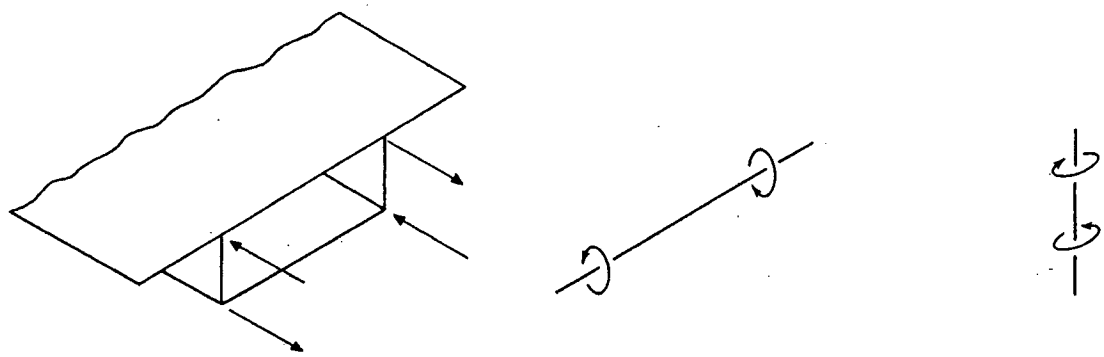

(a) Warping force group (Four forces equal in magnitude) (b) Positive bimoment (Shown using horizontal axis) (c) Positive bimoment (Shown using verticalaxis)

Figure 4. 3: Warping force group and bimoment (Maisel B.I and Roll. F, 1974)

The idea of representing warping stress system by a pair of equal and opposite moments in parallel planes was developed by Vlasov (1967).The magnitude of the bimoment is measured by one component moment multiplied by the distance between the planes. This gives dimension of (force*length^2). A bimoment is the simplest possible physical representation of the longitudinal normal stress system associated with warping. It satisfies the following conditions, which arose in Vlasovs analysis of a thin-walled beam.

(1) There must be zero force resultant and zero moment resultant of the longitudinal normal stress system, which is therefore self-equilibrating at a cross-section.

(2) In general, there must exist longitudinal displacements of cross-section, varying around the perimeter.

(3) The quantity which enters into the analysis must be of dimension (force*length^2)

There is fundamental difference between the bimoment on one hand, and the usual six quantities axial force,longitudinal bending moment (vertical and horizontal transverse shear forces (vertical and horizontal), and torsional moments, on the other.The latter six generalized forces can be found at any cross-section from the equilibrium conditions for external and internal forces acting on the beam, if the forces and moments acting at one end of the beam are known. However the bimoments (of torsional and distortional warping) cannot be found from from the equilibrium equations for the beam, since a self

equilibrating quantity does not affect equilibrium.It can therefore always be said that an individual thin walled beam in a system of such beams is internally statically indeterminate when considered by itself (Kollbrunner. and Hajdin,1966).Only when the deformation is known,in particular the angle of twist(Kollbrunner and Hajdin, 1966) and the distortional deflection(Steinle, 1970), and their second derivatives with respect to the longitudinal coordinate, the bimoments of torsional and distortional warping ,respectively can be obtained.

In the torsional warping analysis of systems of two or more interconnected beams, the loading condition cannot usually be divided into warping torsion, axial loading and bending (Kollbrunner and Hajdin, 1966). Only in particular cases it possible to separate warping torsion from the other loadings.With straight beams, the bimoment are independent of the bending moments, however this is not true of curved beams.

For purpose of numerical calculations, a quantitative definition of the torsional warping bimoment is:

$$B_{twr} = \int_A f_{twr}\,\omega_{twr}\,dA \qquad (4.1)$$

where,

A= total area of cross-section including side cantilevers.

f_{twr} =torsional warping stress.

ω_{twr} =sectorial coordinate in torsional warping, referred to the shear centre.

Note that the integral $\int_A$ is summed over the entire cross-sectional area.

Sectorial coordinate:

The sectorial coordinate w_{twr} is defined as

$$\omega_{twr} = \int_0^{s_{per}} (a_8 - \frac{C_{svt}}{2A_{enc}h}) ds_{per} \tag{4.2}$$

where,

a_8= the perpendicular distance from the shear centre to the tangent to the mid-line of wall at the point considered, and

C_{svt}=torsional second moment of cross-sectional area in St. Venant torsion

$$= \frac{4A_{enc}^2}{\oint \frac{ds_{per}}{h}} \tag{4.3}$$

$$\oint \frac{ds_{per}}{h} = \frac{b}{h_{top}} + \frac{b}{h_{bot}} + \frac{2d}{h_{web}}$$

where,

b=breadth, the distance between mid-lines of webs

d=depth, the distance between mid-lines of top and bottom slabs

h_{top}=thickness of top slab

h_{bot}=thickness of bottom slab

h_{web}=thickness of web

s_{per}=peripheral coordinate along the mid-line of the wall

All of these dimensions are shown in Figure 3.6;

$\oint$ =integral along the mid-line of wall of the closed portion of cross-section.

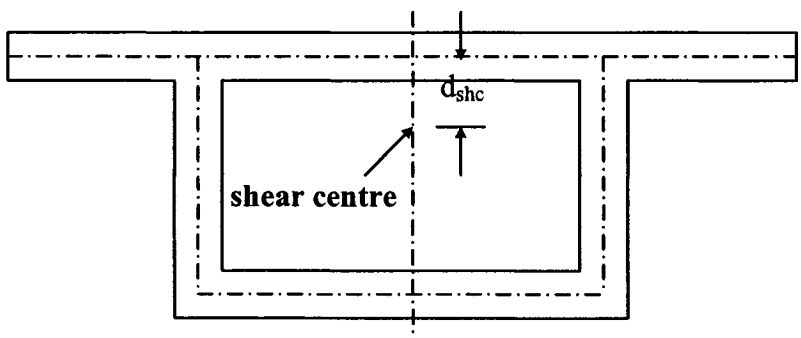

Figure 4. 4: Position of shear centre (Maisel and Roll 1974)

It should be noted that the term ($C_{svt}/2A_{enc}h$) is included only for integration round the wall of the closed portion of the cross-section. It is not included for integration along the side cantilevers.

To find a_8, the following expression is used for the position of shear centre Kollbrunner.and Hajdin, (1965).

$$d_{shc} = \frac{b^2 d}{I_y}[\frac{K_{13}+K_{14}+K_{15}+K_{16}}{K_{17}} \tag{4.4}$$

where

d_{shc}= depth of shear centre below the mid-line of top slab (Figure 4.4)

I_y = second moment of entire cross-section about the centroidal y axis.

$$K_{13} = \frac{1}{4} b h_{bot} h_{web} (\frac{1}{3} b h_{bot} + 3 d h_{web})$$

$$K_{14} = b d h_{top} (\frac{1}{6} h_{bot}^{\ 2} - \frac{1}{4} h_{web}^{\ 2})$$

$$K_{15} = \frac{1}{2} h_{top} h_{bot} h_{web} (\frac{1}{6} b^2 + d^2)$$

$$K_{16} = b_{cant} h_{top} h_{bot} h_{web} (b_{cant} + b)$$

$$K_{17} = b h_{web} (h_{top} + h_{bot}) + 2 d h_{top} h_{bot}$$

The following sign convention is adopted for ω_{twr}, Kollbrunner.and Hajdin,(1965):

Regard the element of mid-line ds_{per} as a vector whose direction is the same as that of the direction of integration.If this vector causes an anticlockwise rotation about the shear centre, then the increment $a_8\, ds_{per}$ is considered positive.Conversely, a negative increment corresponds to a clockwise rotaion of the vector ds_{per} about the shear centre. Figure 3.6 shows the origin and the positive directions of the peripheral coordinate, S_{per}. The term ($C_{svt}/2A_{enc}h$) in equation (4.2) is always positive for a single-cell section.

Hence, by the above convention, the magnitude and sign of ω_{twr} can be determined for all points on the mid-line of the cross-section.The dimensions of ω_{twr} are (length^2)

Torsional warping moment of inertia of cross-section ,C_{TWT}:

$$C_{twr} = \int_A \omega_{twr}{}^2 dA \tag{4.5}$$

This quantity is of dimension (length^6)

4.3.4 Relation Between Applied Load, Internal Stress-Resultants and Twist:

Kollbrunner and Hajdin (1965) and Heilig (1971) give the following expressions for the torsional warping of a single single-span thin walled beam of closed or open-closed cross-section, torsionally restrained at each end but without restraint at the ends, and subject to a midspan concentrated torsional moment T_{ext}, as shown in following Figure.

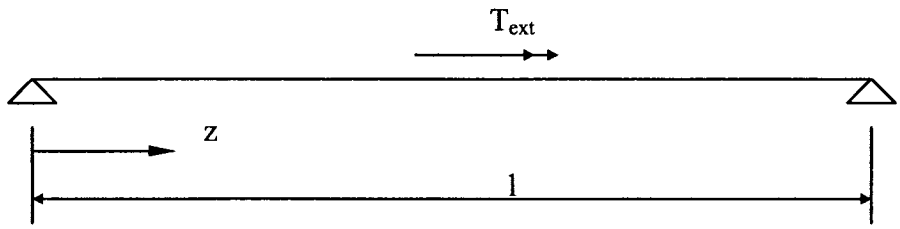

Figure 4. 5: Concentrated torsional moment applied to the beam at midspan (Torsional restraint at supports but no warping restraint)

when

$0 \le z \le l/2$:

$$B_{twr}(z) = \frac{T_{ext}}{2K_{18}K_{19}} \frac{\sinh K_{18} z}{\cosh \frac{K_{18} l}{2}} \tag{4.6}$$

$$T_{svt}(z) = \frac{T_{ext}}{2}(1 - \frac{\cosh K_{18} z}{K_{19} \cosh \frac{K_{18} l}{2}}) \tag{4.7}$$

$$T_{twr}(z) = \frac{T_{ext}}{2K_{19}} \frac{\cosh K_{18} z}{\cosh \frac{K_{18} l}{2}} \tag{4.8}$$

$$\theta_z(z) = \frac{T_{ext}}{2GC_{svt} K_{18} K_{19}} (K_{18} K_{19} z - \frac{\sinh K_{18} z}{\cosh \frac{K_{18} l}{2}} \tag{4.9}$$

when

$l/2 \le z \le l$:

$$B_{twr}(z) = \frac{T_{ext}}{2K_{18} K_{19}} \frac{\sinh K_{18}(l-z)}{\cosh \frac{K_{18} l}{2}} \tag{4.10}$$

$$T_{svt}(z) = \frac{T_{ext}}{2}[-1 + \frac{\cosh K_{18}(l-z)}{K_{19} \cosh \frac{K_{18} l}{2}}] \tag{4.11}$$

$$T_{twr}(z) = -\frac{T_{ext}}{2K_{19}} \frac{\cosh K_{18}(l-z)}{\cosh \frac{K_{18} l}{2}} \tag{4.12}$$

$$\theta_z(z) = \frac{T_{ext}}{2GC_{svt} K_{18} K_{19}} [K_{18} K_{19}(l-z) - \frac{\sinh K_{18}(l-z)}{\cosh \frac{K_{18} l}{2}}] \tag{4.13}$$

where

$B_{twr}(z)$ = bimoment of torsional warping at section z.

$T_{svt}(z)$ = torsional moment due to St.Venant shear stresses at section z.

$T_{twr}(z)$ = torsional moment due to torsional warping shear stresses at section z.

$\theta_z(z)$ = twist about shear axis at section z

$$K_{18} = \sqrt{\frac{GC_{svt}}{E\overline{C}_{twr}}} \tag{4.14}$$

$$K_{19} = \frac{C_{cen}}{C_{cen} - C_{svt}} \tag{4.15}$$

$$\overline{C}_{twr} = K_{19} C_{twr} \tag{4.16}$$

C_{cen} = central torsional moment of inertia of cross-section

$$= \int_A a^2 {}_8 dA \tag{4.17}$$

Note that $(T_{svt} + T_{twr})$ equals ½ T_{ext} in magnitude for all sections z , as is required for equilibrium(Figure 4.2(b))

Torsional warping stresses f_{twr}:

The tortional warping stresses are given by the following expression:

$$f_{twr} = \frac{B_{twr}\,\omega_{twr}}{C_{twr}} \tag{4.18}$$

The form of this expression is the same as that of equation 1.1, since M_x, M_y, B_{twr} are all stress-resultants at section z; x,y and ω_{twr} are all coordinates of the point considered on the cross-section; and I_x, I_y and C_{twr} are all geometrical properties of the entire cross-section

Under eccentric loading, the longitudinal stresses f_{1bg} of equation 1.1 and f_{twr} of equation 4.18 are superimposed, with due regard to sign.

Torsional warping shear stresses , v_{twr} these are given by the following expression:

$$v_{twr} = T_{twr} \frac{\dfrac{d\omega_{twr}}{ds_{per}}}{C_{cen} - C_{svt}} \tag{4.19}$$

where $\dfrac{d\omega_{twr}}{ds_{per}} = a_8 - \dfrac{C_{svt}}{2A_{enc}h}$ for a single cell cross-section

4.4: Analysis of Torsional warping by the method of Kollbrunner, Hajdin and Heilig (1966) [multicell section]:

4.4.1: Summary of Procedure For Analysis:

The above analytical treatment to cover multicell box-beams, as originally presented by Kollbrunner and Hajdin (1965) and Heilig (1971). The method is applicable to thin-waled

beams of closed or open closed cross-section.The torsional warping(longitudinal) stresses, $f_{twr,}$ and torsional warping shear stresses, v_{twr} ,are obtained in terms of the applied torsional moment,the bimoment B_{twr} and the section properties known the sectorial coordinate, $w_{twr,}$ and the torsional warping second moment of area, C_{twr} .The algebric expressions for obtaining these section properties and stresses, and also the St.Venant torsional shear stresses v_{svt} are given. St. Venant shear stresses are important because part of the torsional moment is resisted by these stresses and the rest is resisted by the torsional warping shear stresses , $v_{twr.}$

4.4.2 Sectorial Co-ordinate :

It has been found convenient to refer to points on the cross-section using a sectorial co-ordinate ω_{twr} .The physical , definition of this quantity has been shown by Kollbrunner and Hajdin(1964) to correspond to the warping displacements of the point per unit rate of twist, $d\theta_z / dz$, of the cross-section, and it has therefore also been called the unit warping.The dimensions are accordingly

$$L/(1/L)=L^2$$

where L denotes length.There is also a geometrical definition of ω_{twr} ,which is illustrated in Figure 4.6 for an open thin walled cross-sections.

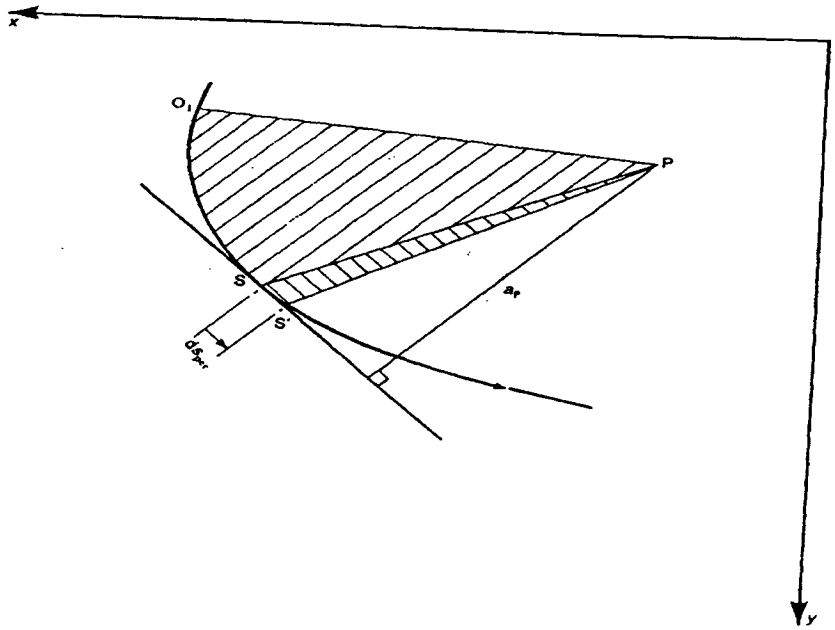

Figure 4. 6: Geometrical definition of sectorial co-ordinate (Maisel, 1982)

Let S be any point on the mid-line of the wall of cross-section.Let P be an arbitrary point in the cross-sectional plane, taken as the origin (or pole) of a radial vector running to S, and let O1 be an arbitrary origin for the peripheral co-ordinate s_{per}, as used in torsional warping analysis. The unit warping, ω_{twrP} is given by twice where the suffix P refers to the use of P as the radial vector origin and of the lever arm a_p extending from P to the tangent at S.The doubled incremental area PSS' is given by

$$a_p ds_{per} = d\omega_{twrP}$$

which leads to the analytical definition

$$\omega_{twrP} = \int a_p ds_{per} \qquad (4.20)$$

This is consistent with the above statement that the sectorial co-ordinate is of dimension $(\text{length})^2$

A modification is necessary for closed thin walled sections such as box beams or open-closed sections such as box beams with side cantilevers.

The analytical definition of ω_{twrP} in equation 4.20 now becomes:

$$\omega_{twrP} = \int_0^{s_{per}} (a_p - \bar{v}_{svt}) ds_{per} \qquad (4.21)$$

where $\bar{v}_{svt}$, which is a function of s_{per}, is the value of St. Venant torsional shear stress, v_{svt} , for $G(d\theta_z / dz) = 1$. The term $\bar{v}_{svt}$ is the shear stress distribution function of the cross-section for the case of pure torsion.It follows that

$$v_{svt} = G\frac{d\theta_z}{dz}\bar{v}_{svt} \qquad (4.22)$$

Here, $\bar{v}_{svt}$ is determined from the analysis of St. Venant torsion in the previous chapter.By putting $G(d\theta_z / dz) = 1$ in equations 3.11 a,b and c, the equations are solved for the quantities

$$\overline{(v_{svt}h)}_M = \frac{1}{G\dfrac{d\theta_z}{dz}}(v_{svt}h)_M \tag{4.23}$$

where $\overline{(v_{svt}h)}_M$ is the St. Venant torsional shear flow in a typical cell M of a multicell section for $G(d\theta_z/dz)=1$.It is constant for cell M and is positive anticlockwise direction; it is identical to K_M in equation 3.12.

Once $\overline{(v_{svt}h)}$ is known for all points on the closed portion of a cross-section, division by the wall thickness h gives the function $\bar{v}_{svt}$. Hence ω_{twrP} can be determined from equation 4.21.

It should be noted that The integration in equation 4.21 is performed over the entire area of cross-section, but the second term, $\bar{v}_{svt}$, is included in the integrand only for integration round the wall of the closed portion of the cross-section.It is not included for integration along the side cantilevers, since the action of these cantilevers in St. Venant torsion is neglected.

For a single cell section,

$$\bar{v}_{svt} = \frac{C_{svt}}{2A_{enc}h} \tag{4.24}$$

where C_{svt}=torsional second moment of a single-cell cross-section in St. Venant torsion, and is given by:

$$C_{svt} = \frac{4A^2{}_{enc}}{\oint\dfrac{ds_{per}}{h}} \tag{4.25}$$

The symbol $\oint$ denotes integration over the closed portion of the cross-section only.

The value of ω_{twrP} depends upon the co-ordinates x_p anf y_p of the point P and upon the value of s_{per} at point S, i,e., upon the position chosen for the origin O1. The theory is simplified by a suitable choice of the points P and O1,with P at the shear centre Q and O1 such that

$$\int_A \omega_{twrP} dA = \int \omega_{twrP} h ds_{per} = 0 \qquad (4.26)$$

where h denotes the wall thickness and the integration is performed over the entire cross-section .The shear centre is chractised by the fact that, when the resultant transverse shear on the section acts through it, there is no torsion on the section. The above choices result in the uncoupling of the equations of flexure and torsional warping. The sectorial coordinate referred to these specific positions of P and O1 is called the normalized sectorial coordinate.

4.4.3 The Procedure for Determining the Position of the Shear Centre and the Diagram of the Normalized Sectorial Co-ordinate:

As in Figures 4.6 and 4.7, select an arbitrary pole P (x_p,y_p) and an arbitrary origin O1 for the peripheral coordinate s_{perP}.

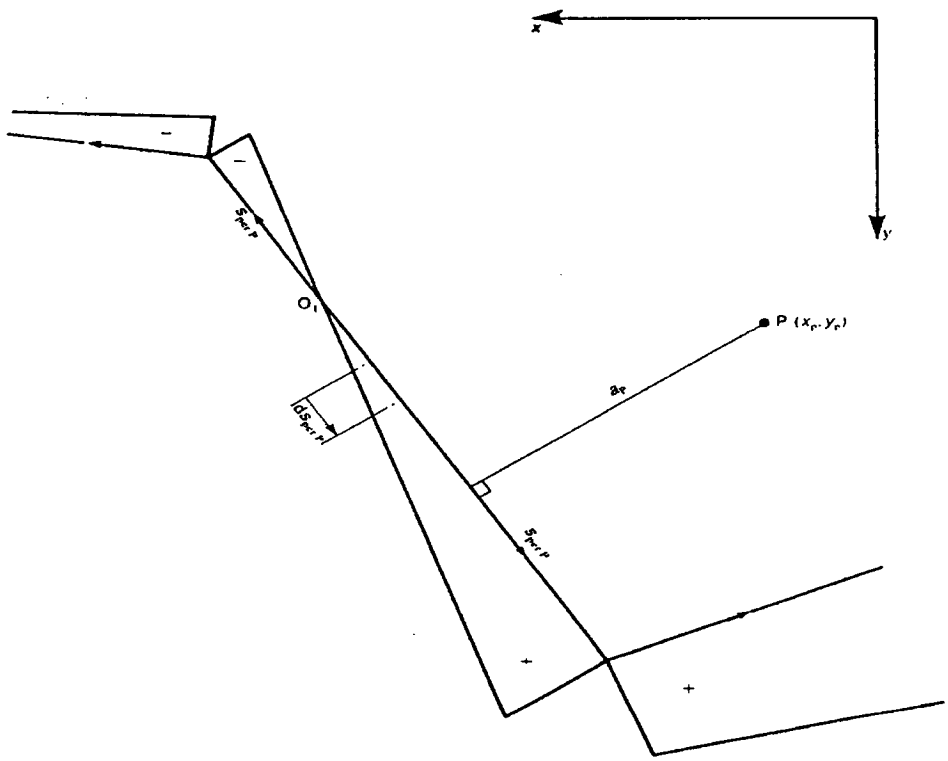

Figure 4. 7: Portion of diagram of $\int a_p ds_{perP}$ (Maisel, 1982)

For the numerical determination of the sectorial coordinate, ω_{twrP} , which depends upon P, O1 and S_{perP}, the following sign convensions is adopted for the first term only in the integrand of equation 4.21 .Consider s_{perP} to be increasing in both directions from O1.The increament, $a_p ds_{perP}$, is regarded as positive if the directed element ds_{perP} on the positive face of cross-section has an anticlockwise sence of rotation relative to pole P.If the sense is clockwise, the increament is negative. With regard to the second term $\bar{v}_{svt}$ in the integrand of equation 4.21, this is obtained as a shear stress vector in accordance with the St. Venant torsion analysis of Chapter 3. If the physical direction of $\bar{v}_{svt}$ in a particular problem agrees with that of ds_{perP} in integration, then the increament $\bar{v}_{svt}$ ds_{perP} is positive;otherwise, it is negative.

The diagram of the sectorial coordinate ω_{twrP} as defined in equation 4.21 is drawn by plotting this quantity as an ordinate from the mid-line of cross-section, the value at O1 being taken as zero.The coordinate of the shear centre Q, reffered to the principal axes of the cross-section ,are then given by:

$$x_{shc} = \frac{I_{y\omega P}}{Ix} + x_P \qquad (4.27)$$

$$y_{shc} = -\frac{I_{x\omega P}}{I_y} + y_P$$

where

$$I_{y\omega P} = \int_A y\omega_{twrP} dA$$

$$I_{x\omega P} = \int_A x\omega_{twrP} dA$$

are the sectorial products of the cross-sectional area, obtained by numerical integration from the diagram for ω_{twrP} and the known values of x and y for all points on the cross-section, referred to the principal axes, and

I_x = second moment of the cross-sectional area about the principal x-axis.

I_y= second moment of the cross-sectional area about the principal y axis.

Once the position of the shear centre Q is known, the diagram of ω_{twrP} is now redrawn, using Q and not P as the pole.This gives ω_{twrQ}, which can be checked using the equation:

$$I_{xwQ} = 0 = I_{ywQ}$$

This follows from equations 4.27 uppon substituting

$$x_p=x_Q=x_{shc} \text{ and } yp=y_Q=y_{shc}$$

To obtain the specific position Os of the arbitrary origin O1, giving the normalized sectorial coordinate , ω_{twr} , the equation

$$\int_A \omega_{twr}\, dA = 0 \tag{4.28}$$

is satisfied by substituting

$$\omega_{twr} = \omega_{twrQ} + \omega_0 \tag{4.29}$$

where $\omega_0 = -\frac{1}{A}\int_A \omega_{twrQ}\, dA$ (4.30)

with the integrating performed over the entire cross-sectional area.
This defines the distance between the origins as

$$O_1O_s = \frac{\omega_0}{a_{010S}} \tag{4.31}$$

Here O1 and Os lie on a straight-line portion of the midline of section at a distance a_{O1OS} from the shear centre.

The quantity , ω_{twr} , is evaluated using equation 4.29, and the diagram for ω_{twr} is drawn .An arithmetic check can be made,using the condition in equation in equation 4.28.

The torsional warping moment of the cross-sectional area C_{twr} is also required, and is defined as

$$C_{twr} = \int_A \omega_{twr}^2 dA \tag{4.32}$$

This quantity has the dimension of (length)^6 and is evaluated from the diagram of ω_{twr} by numerical integration

The torsional second moment of the cross-sectional area of a multicell section in St. Venant torsion, K_{svt}, and is given by

$$K_{svt} = 2\sum_M A_{encM} (\overline{v_{svt} h})_M \tag{4.33}$$

where the summation extends over all cells of a multicell section.The suffix M refers to a typical cell in such a section .A_{encM} is the area enclosed by the midline of the walls of the cell M and $(\overline{v_{svt} h})_M$ has been defined by equation 4.23.

For a single cell section, $K_{svt} = C_{svt}$, as can be seen from equation 4.24.

This procedure for determining the section properties described above is applicable in the case of general, asymmetrical, thin walled cross section.

4.4.4 Torsional Warping Stresses f_{twr} :

The rorsional warping stress, f_{twr}, is given by:

$$f_{twr} = \frac{B_{twr}\omega_{twr}}{C_{twr}} \tag{4.34}$$

The form of this equation is the same as that of equation 1.1,since M_x, M_y and B_{twr} are all stress resultants at that section z; x, y and ω_{twr} are all coordinates of the point considered on the cross-section; and I_x, I_y, and C_{twr} are all geometrical properties of the entire cross-section.

Under eccentric loading the longitudinal stresses f_{1bg}, of equation 1.1 and f_{twr} of equation 4.34 are superimposed, with due regard to sign.

The Torsional warping shear stresses v_{twr} is given by:

$$v_{twr} = T_{twr} \frac{\frac{d\omega_{twr}}{ds_{per}}}{C_{cen} - K_{svt}} \tag{4.35}$$

where $d\omega_{twr} / ds_{per}$ is the slope of the ω_{twr} diagram, obtained by numerical differentiation The positive direction s_{per} is as shown in Figure 2.2(b).

CHAPTER 5

ANALYSIS OF DISTORTIONAL EFFECTS

5.1 Introduction:

Distortional effects comprise distortional warping and transverse bending, and arise in concrete box beam construction as a result of the usual practice of inserting diaphragms only at the supports, or at specific spacings within the span. They are superimposed upon the effects of longitudinal bending and torsional warping.

Figure 5.1 shows schematically the modes of distortion possible in the various types of singly symmetric cross-sections. These are the linearly independent basic modes, i.e., none of them can be expressed as a linear combination of any, or all of the others, for a given form of cross-section. The analysis to follow is formulated in terms of these modes.

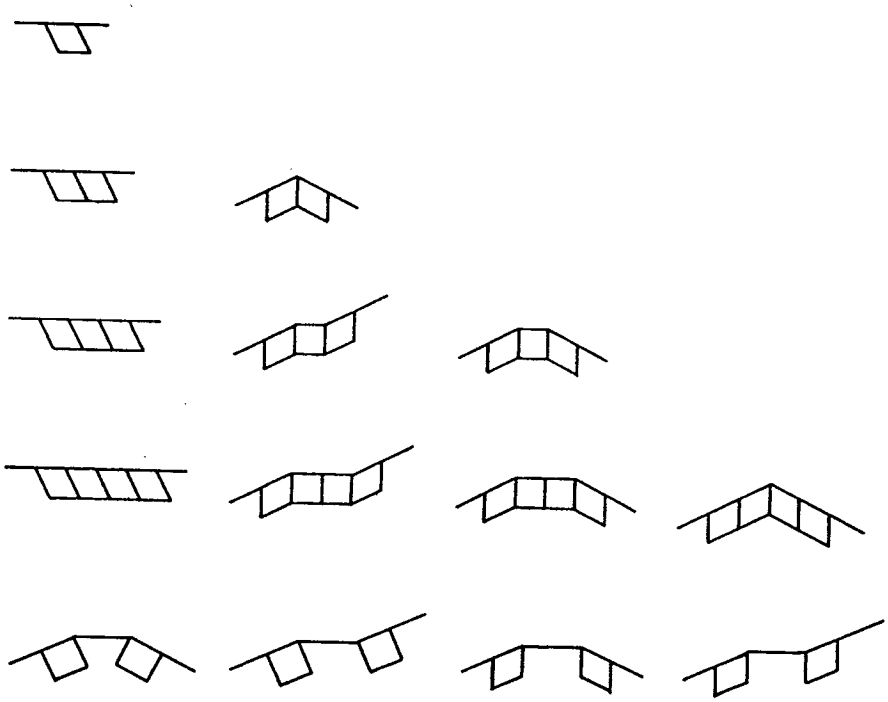

Figure 5. 1: Modes of distortion (schematic) for various box-beam cross-sections (Maisel,1982)

The redistribution of stress caused by distortion of cross-section is a measure of the deterioration of transverse load distribution towards that obtaining in a grillage structure.

Distortion can be regarded as a differential torsional deformation of the individual portions of the cross-section, as indicated by the schematic deflected shapes in Figure 5.1. The elastic resistances with which the structure opposes these deformations can be subdivided into warping resistance and torsional resistance (as in torsional warping) and, in addition, an elastic transverse bending resistance of a 'frame' of the same configuration as the cross-section; this resistance is proportional to the amount of distortion occurring.

Sedlacek's (1968) procedure uses warping functions defined to be associated with the physical behavior through the independent sway modes of the 'frame', representing the cross-sectional distortion. The warping functions are linear over each individual wall element, as in Vlasov's generalized co-ordinate method, but they are associated with the kinematics degrees of freedoms of the cross-section selected to define the distortional behavior. A virtual work approach yields the following fourth-order matrix differential equation below:

$$E\tilde{C}\tilde{a}'''' - G\tilde{J}\tilde{a}'' + \tilde{B}\tilde{a} = \tilde{n} \tag{5.1}$$

where $\tilde{a}$ is a displacement vector including distortional displacements at section z;

$\tilde{n}$ is a load vector including distortional loading

$\tilde{C}$ is a matrix of the section properties in warping including distortional warping;

$\tilde{J}$ is a matrix of the section properties in torsion;

$\tilde{B}$ is a matrix of the section properties in transverse bending.

Sedlacek(1968) separately considered the non-distortional modes (axial extension, longitudinal bending about the two principal axes of the cross-section, and torsional warping).Equation 5.1 refers in its orthogonalized form to the distortional modes only. The process of orthogonalization, denoted by the symbol ~, yields an uncoupled system of fourth-order differential equations, and the equation for each mode of distortion (in a multi-cell box beam) is of the same form as that for a beam on elastic foundation.

For the prismatic thin-walled beams considered, the analysis does not require discretization of the structure in the longitudinal direction, so that the matrices arising are of a much lower order than those in a finite element treatment. The use of the methods of calculus (via beam statics) to solve the governing quation gives an analytical solution for the sharply peaking, longitudinally localized stress distributions near concentrated loads, or the supports of a continuous thin-walled beam. Local effects near the loads not applied at web-flange junctions, and similar effects must be considered separately. The global analysis in these cases uses statically equivalent loading at the web-junctions.

5.2 Method of Distortional Analysis Developed by Sedlacek (1968)

5.2.1 Distortional Components, Warping Displacements and Shear Stresses

Consider a general polygonal cell of a prismatic box beam, as shown in Figure 5.2. Distortional movement may be regarded as leading to the relative inclinations between the individual plates at the nodes, the angle of inclination θ_m being referred to the line joining the node points. The total deformation of the cross-section can be represented by a linear combination of the independent basic deformations a_i for each mode i. To determine these latter deformations, the periphery is treated as a hinged system, with hinges at all nodes, and the various systems with only one degree of freedom are considered successively. Thus, the basic unit relative deformation, $a_i = 1$, is defined as the basic rotation, $\theta_m = 1$ of a movable plate m, as shown in Figure 5.2, where only a three-bar link mechanism is allowed to move, and the nodes of the other members of the 'frame' are constrained. Such a three-bar mechanism is kinematically determinate, i.e., all its movements are known when θ_m is known. Figure 5.1 illustrates the way in which this general concept is applied to the types of the cross-section considered here.

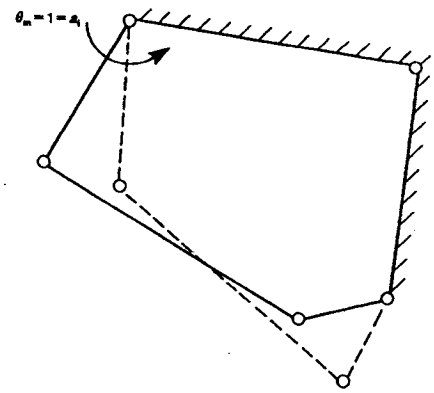

Figure 5. 2: Basic unit deformation in distortional analysi s of aclosed section (Maisel, 1982)

Sedlacek (1968) and Roik, Carl and Linder (1972) developed the matrix differential equation for the non-distortional behaviour of a prismatic thin-walled beam as:

$$EC_r a_r'''' - GJ_r a_r'' = n_r + \int^{s_{per}} n_z' w_r ds_{per}$$

where a_r is a vector of orthogonalized, non-distortional displacements at section z.

$$a_r = \begin{bmatrix} -\int_{s_{per}=0}^{s_{per}} a_{z0}(z)dz \\ a_x \\ a_y \\ \theta_z \end{bmatrix}$$

in which $a_{z0}(z)$ is an integration constant, giving the initial value of $a_z(z, s_{per})$ at the point, $s_{per} = 0$. The components a_z, a_x, a_y, θ_z are shown in Figure 2.3. C_r is a diagonal matrix of the sectional properties. J_r is a matrix of the shear second moments of the cross-sectional areas.

If the definition of vector a_r described above is extended to include the distortional components, the column vector

$$a = \{a_i\} = \{a_r\} \vdots a_5 a_6 \ldots\ldots\ldots a_n\} \qquad (5.2)$$

represents all n possible modes of displacement of the cross-section. Here, a_r is the column vector of the four orthogonalized, non-distortional displacements, and a_5 to a_n are the components of distortion. The total number of linearly independent distortional modes is (n-4).

In the distortional analysis of single-cell box beams performed by Maisel and Roll (1974), it was found from the parametric studies that conservative values of maximum distortional warping stress are obtained, If the shear deformations in the planes of the walls are neglected in the distortional analysis; this justifies the uncoupling of torsional warping and distortional warping analyses, as a safe approximation. Accordingly, to simplify the calculation, it is assumed that individual walls of the box beam behave as simple beams longitudinally when they undergo distorsional warping. Likewise, for the twisting of individual walls occurring in distortion, St Venant torsion theory is applied. This leads to the following expression for the warping vector, w:

$$w = \{w_i\} = \int \{r - \bar{v}\} ds_{per} \tag{5.3}$$

where

$$w = \begin{bmatrix} 1 \\ x \\ y \\ \omega_{twr} \\ w_5 \\ w_6 \\ . \\ . \\ . \\ w_n \end{bmatrix} \text{ and } r = \begin{bmatrix} 0 \\ \cos\alpha \\ \sin\alpha \\ a_Q \\ r_5 \\ r_6 \\ . \\ . \\ . \\ r_n \end{bmatrix} \text{ and } \bar{v} = \begin{bmatrix} 0 \\ 0 \\ 0 \\ \bar{v}_{svt} \\ \bar{v}_5 \\ \bar{v}_6 \\ . \\ . \\ . \\ \bar{v}_n \end{bmatrix}$$

The first four components of each vector relate to the non-distortional behaviour. Here w_5 to w_n are the components of distortional warping arising from the various basic modes of distorsion.

The second, third and fourth components of r are defined in Figure 5.3, where α is the angle between the tangent to the wall element and the principal x-axis; a_Q is the distance from the shear centre to this tangent.The variables r_5 to r_n are of the same nature as a_Q and are illustrated typically, for distortional mode i in Figure 5.3, as the distance from the centre of rotation defining a_i to the tangent to a wall element experiencing the tangential movement. Thus the distortional components of r are radial distances.

The component $\bar{v}_{svt}$ of $\bar{v}$ was defined in equation 4.21 as the St Venant torsional shear stress for $G(d\theta_z / dz) = 1$. Simultaneous equations need to be solved to obtain $\bar{v}_{svt}$ for a multicell section.The components $\bar{v}_5$ to $\bar{v}_n$ are the corresponding statically indeterminate St Venant shear stress functions associated with the distortional behavior. Thus $\bar{v}_i$ is the distortional warping shear stress in mode i for $G(da_i / dz) = 1$ .For a multi-cell section, the corresponding shear flows $(\overline{v_i h})$ are obtained from a set of simultaneous equations, formed as follows.

For a typical cell M in distortional mode i, where i runs from 5 to n,

$$-(\overline{v_i h})_{M-1} \int_{M-1,M} \frac{ds_{perM}}{h} + (\overline{v_i h})_M \oint_M \frac{ds_{perM}}{h} - (\overline{v_i h})_{M+1} \int_{M,M+1} \frac{ds_{perM}}{h} = \int_M r_i ds_{perM} \qquad (5.4)$$

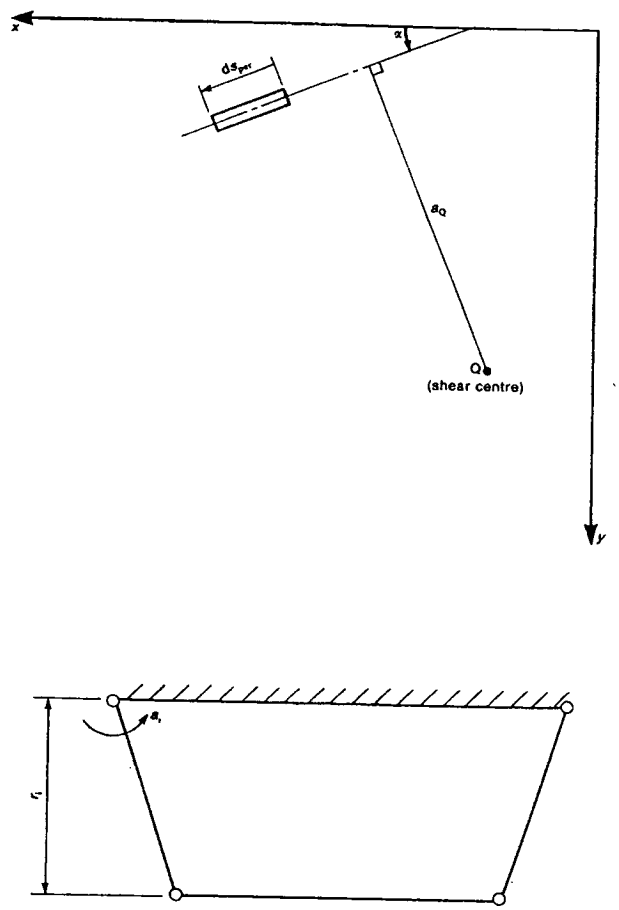

Figure 5. 3: Radial distance r_i for wall element experiencing tangential movement (Maisel, 1982)

The left hand side is constructed in the same fashion as that of equations 3.11(a),(b) and (c) in the analysis of St Venant torsion, presented in chapter-3. Here, $\overline{(v_i h)_M}$ is the value of distortional warping shear flow $(v_i h)$ in cell M for $G(da_i/dz)=1$, h is the wall thickness and s_{perM} is the peripheral coordinate in cell M.

The integral on the right-hand side is a measure of warping incompatibility related to the tangential movements of the statically determinate, cut section, illustrated in Figure 3.2 for a three-cell section. The tangential movements are those indicated in Figure 5.4, where for unit anticlockwise rotation of A, only the portion ABC moves. Such

movements are positive if in the positive directions of s_{per} and they generate warping incompatibility at a cut, and represent the shear deformation associated with the particular mode of distortion.

There is one equation of the above type for each cell, and the solution of the simultaneous equations gives the distribution of shear flow over the entire cross-section, such that compatibility is restored at each cut.

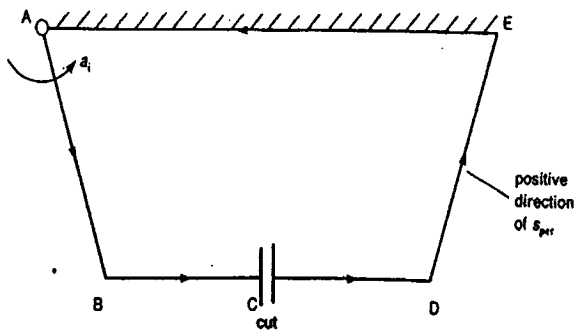

Figure 5. 4: Distortion of statically determinate cut section (Maisel,1982)

5.2.2 Relations Between Stresses, St. Venant Torsional Moments in Individual Walls, Transverse Bending Moments and Deformations of Cross-Section.

Sedlacek(1971) showed that the resultant longitudinal normal stress, f, is given by

$$f = -Ew^T a'' \tag{5.5}$$

where T denotes the transpose of a vector or matrix and $''$ denotes d^2/dz^2. E is Youngs modulus of elasticity.

In addition, the superimposed torsional and distortional shear stresses give

$$v = G\bar{v}^T a' \tag{5.6}$$

where the operator $'$ denotes d/dz and G is the shear modulus.

For each wall element m, St. Venant torsion theory states that

$$(T_{svt})_m = GJ_m\theta'_m$$

where

$(T_{svt})_m$ = St. Venant torsional moment on wall m;

$$J_m = \frac{1}{3}b_m h^3{}_m \tag{5.7}$$

=St. Venant torsional moment of inertia of plate of breadth b_m and thickness h_m;

and θ'_m = rate of twist of wall element m.

The individual rates of twist, θ'_m, of the m wall elements are collected together as a column vector $\theta' = \{\theta'_m\}$, and this is related to the deformation vector, a', by the equation

$$\theta' = Ta' \tag{5.8}$$

where the transformation matrix T, of order $m \times n$, is

$$T = \begin{bmatrix} 0 & 0 & 0 & 1 & . & . & . \\ 0 & 0 & 0 & 1 & . & . & . \\ . & . & . & . & . & . & . \\ 0 & 0 & 0 & 1 & . & . & . \end{bmatrix}$$

Columns of T beyond the fourth contain non-zero terms which reflect the rotations of the individual wall elements m set up in the various basic distortional modes i. In Figure 5.5, the

θ values are the changes in slope of chords AB, BD, DE and EA due to the relative rotation a_i between EA and AB, imposed at A, as shown. These values form the ith column of T.

The diagonal matrix $\mathbf{J_1}$ of torsional moments of inertia can be defined as:

$$J_1 = \begin{bmatrix} J_1 & 0 & 0 & . & . & . & 0 \\ 0 & J_2 & 0 & . & . & . & 0 \\ 0 & 0 & . & & & & . \\ . & . & . & & & & . \\ . & . & & . & & & \\ . & . & & & & & 0 \\ 0 & 0 & . & . & . & . & J_m \end{bmatrix} \tag{5.9}$$

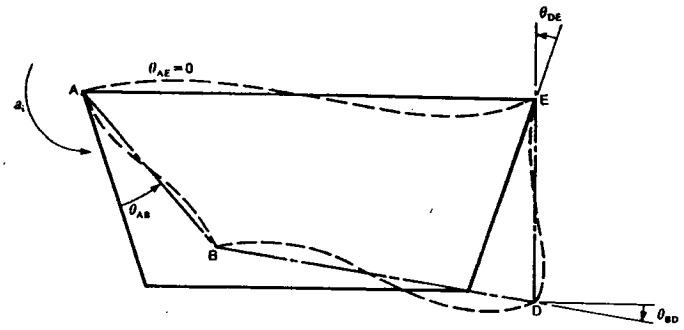

Figure 5. 5: Deflected shape in distortion and rotations of chords (Maisel,1982)

The following relation is obtained between the vector of the St Venant torsional moments T_{svt}, on individual walls and the deformation vector, a':

$$T_{svt} = GJ_1\theta' = GJ_1Ta' = GT_1a' \tag{5.10}$$

where

$$T_1 = J_1T \tag{5.11}$$

To derive the relationship between the transverse bending moments in the walls, and the deformation vector, a, it is assumed that the torsional moments and longitudinal moments occurring within the plates can be neglected, and that the transverse bending strength arises as if there were infinitely many cross-sectional 'frames' of infinitesimal breadth positioned next to one another along the box beam. It is required to evaluate the transverse bending moments at all nodes of the 'frame' of unit breadth (along the beam) when subjected to unit relative rotation of two adjacent members in distortional mode i as

in Figure 5.5 ($a_i = 1$). These moments can be found by conventional frame analysis. The internal work done is then given by:

$$\sum_p M_{tpi} \Delta\theta_{pi} \tag{5.12}$$

where M_{tpi} is the transverse bending moment at node p due to unit a_i and $\Delta\theta_{pi}$ is the relative rotation of chords meeting at node p, due to unit a_i.Thus, at B in Figure 5.5,

$$\Delta\theta_{Bi} = \theta_{BD} - \theta_{AB}$$

In general, $\Delta\theta_i = \theta_{m+1} - \theta_m$ for adjacent walls (m+1) and (m) in mode i, with θ_m measured positively anticlockwise, and m increasing anticlockwise round the periphery of a cell.

By considering each distortional mode i separately, and the nodal transverse moments occurring in each mode, the following equation is obtained.

$$M_t = K_t \Delta\theta \tag{5.13}$$

where K_t is the symmetrical square stiffness matrix giving the transverse moments at nodes, generated by unit relative rotations , $\Delta\theta$, at nodes (the typical element , K_{tpi} , of this matrix is the transverse moment at node p due to the unit relative rotation defining mode i);

$\Delta\theta$ is a column vector of relative rotations at nodes;

M_t is a column vector of transverse moments at nodes.

Now equation 5.8 gives:

$$\Delta\theta = \Delta T a \tag{5.14}$$

where ΔT is obtained from the differences between the appropriate T values to give $\Delta\theta$ for each distortional mode i.

Therefore,

$$M_t = K_t \Delta T a$$

$$= \Delta T_1 a \tag{5.15}$$

where $\Delta T_1 = K_t \Delta T$ (5.16)

5.2.3 Derivation of the Differential Equation

If the beam undergoes a virtual displacement δa from its equilibrium position, there is no change in its potential energy, i.e. the virtual work δW_{ext} done by the external loads is equal to the virtual work δW_{int} done by the internal forces.The differential equation of the problem can be found by equating δW_{ext} to. δW_{int}

$$\delta W_{\text{int}} = \int_0^L \{ \int_A (f \partial \varepsilon + v \partial \gamma) dA + T_{svt}^T \delta \theta' + M_t^T \delta \Delta \theta \} dz \tag{5.17}$$

where

f =normal stress in z direction;

ε =normal strain corresponding to f;

v =shear stress in the plane of cross-section;

γ =shear strain corresponding to v;

δ =a variation symbol denoting virtual displacement,virtual strain or virtual work;

L=total length of beam;

A= cross-sectional of beam.

If the stresses, strains, moments and rotations are expressed in terms of the displacements, the equation becomes

$$\delta W_{\text{int}} = \int_0^L \{E \int_A ((a'')^T w)(w^T \delta a'')dA + G \int_A (a')^T \bar{v}(\bar{v}^T \partial a')dA + G(a')^T (T_1^T T)\delta a'$$
$$+ a^T (\Delta T_1)^T \Delta T \delta a\} dz$$

$$= \int_0^L \{E(a'')^T \int_A ww^T dA \delta a'' + G(a')^T (\int_A \bar{v}\bar{v}^T dA + T_1^T T)\delta a' + a^T (\Delta T_1)^T \Delta T \delta a\} dz \tag{5.18}$$

Sedlacek (1968) derived the following equation for δW_{ext}

$$\partial W_{ext} = \int_0^L \{n_{tr} r^{*T} \partial a - \int_{sper} n_l w^T ds_{per} \partial a'\} dz + \sum_F [F_{tr} r^{*T} \partial a - F_l w^T \partial a'] \tag{5.19}$$

where

n_{tr} =transverse distributed load;

n_l =longitudinal distributed load, varying generally around the perimeter of cross-section;

F_{tr} =transverse concentrated load;

F_l = longitudinal concentrated load;

r^* =a vector associated with loading positions.

$\sum_F$ =summation over all concentrated loads.

W_{int} to W_{ext} are equal, and integrated by parts and the following summarized notation is introduced.

$$C = [C_{ij}] = \int_A ww^T dA \tag{5.20}$$

$$J = [J_{ij}] = \int_A \bar{v}\bar{v}^T dA + T_1^T T \tag{5.21}$$

$$B = [B_{ij}] = (\Delta T_1)^T \Delta T \tag{5.22}$$

where C,J and B are matrices of section properties in warping, torsion and distortion, respectively, the following differential equation is obtained:

$$ECa'''' - GJa'' + Ba = n_{tr}r^* + \int_{s_{per}} n_l' w ds_{per} \tag{5.23}$$

This is the generalized differential equation representing combined bending, torsional and distortional behavior. Shear lag is not considered.

5.2.4 Orthogonalization of the Basic Co-Ordinates:

The matrix differential equation 5.23 expressed in terms of the displacement vector a, represents a system of coupled, simultaneous differential equations in the basic displacements components a_i. To simplify the solution, the displacements or deformations , a_i, are to be orthogonalized in such a way that matrices C,J and B attain diagonal form simultaneously, as much as possible.

5.2.4.1 Orthogonalization of Non-Distotional Displacements :

Sedlacek(1968) and Roik, Carl and Linder(1972) developed the following matrix differential equation(as described before) for non-distortional behaviour of a prismatic, thin-walled beam:

$$EC_r a_r''' - GJ_r a_r'' = n_r + \int^{s_{per}} n_z' w_r ds_{per} \tag{5.24}$$

where a_r is a vector of orthogonalized displacements at section z , given by

$$a_r = \begin{bmatrix} -\int_{s_{per}=0}^{s_{per}} a_{z0}(z)dz \\ a_x \\ a_y \\ \theta_z \end{bmatrix}$$

in which $a_{z0}(z)$ is an integration constant, giving the initial value of $a_z(z, s_{per})$ at the point $s_{per} = 0$.

The components a_z, a_x, a_y, θ_z are shown in Figure 2.3. The longitudinal displacements, a_z,are measured along the centroidal axis of the beam; a_x and a_y are the flexural displacements of the points on the shear axis of the beam. θ_z is the rotation about the shear centre.The suffix r in a_r denotes "rigid" i,e undistored, form of all cross-sections on the application of load to the structure.

C_r is a diagonal matrix of section properties, given by:

$$C_r = \begin{bmatrix} A & 0 & 0 & 0 \\ 0 & I_y & 0 & 0 \\ 0 & 0 & I_x & 0 \\ 0 & 0 & 0 & C_{twr} \end{bmatrix}$$

where

A= area of cross-section;

I_x = second moment of cross-sectional area about principal x axis;

I_y = second moment of cross-sectional area about principal y axis;

C_{twr} = torsional warping second moment of the cross-sectional area refer to the shear centre.

The matrix is diagonal because the displacements have been referred to principal axes and the shear centre, i.e. they have been orthogonalized.

J_r is a matrix of shear second moments of cross-sectional area, populated only by the St. Venant torsional second moment of area, K_{svt}, given by:

$$J_r = \begin{bmatrix} 0 & 0 & 0 & 0 \\ 0 & 0 & 0 & 0 \\ 0 & 0 & 0 & 0 \\ 0 & 0 & 0 & K_{svt} \end{bmatrix}$$

E=Young's modulus of elasticity

G=shear modulus of elasticity

n_r=is a vector of loading defined as

$$n_r = \begin{bmatrix} n_z \\ n_x \\ n_y \\ t_{ext} \end{bmatrix}$$

the components of this vector are shown in Figure 2.4.

$\int_{s_{per}} n_z' w_r ds_{per}$ is a vector of loading associated with the variable longitudinal load intensity and is defined by Roik, Carl and Linder(1972) as:

$$\int_{s_{per}} n_z' w_r ds_{per} = \int_{s_{per}} \begin{bmatrix} 0 \\ (\partial n_z / \partial z).x \\ (\partial n_z / \partial z).y \\ (\partial n_z / \partial z).\omega_{twr} \end{bmatrix} ds_{per}$$

w_r is a vector of orthogonalized co-ordinates of a point on the cross-section, given by:

$$w_r = \begin{bmatrix} 1 \\ x \\ y \\ \omega_{twr} \end{bmatrix}$$

where x and y are referred to the principal axes as before and ω_{twr} is the normalized sectorial co-ordinate discussed previously.

The operators '," and"" ,respectively denote the first,second and fourth derivatives with respect to the axial coordinate z.

The solution of equation 5.24 yields the following expression for longitudinal normal stress f_r at section z;

$$f_r = \sum_{i=1}^{4} \frac{M_{ri}}{C_{ri}} w_{ri} \tag{5.25}$$

where i denotes a non-distortional mode of displacement; there are four such modes.

M_{ri} is the ith component of the warping moment vector M_r at section z

$$M_r = \begin{bmatrix} N \\ M_y \\ M_x \\ B_{twr} \end{bmatrix} \tag{5.26}$$

with the components as defined in Figure 2.4

C_{ri} is the element C_{ii} of matrix C_r

w_{ri} is the ith element of vector w_r

5.2.4.2 Orthogonalization of Distortional Displacements:

The non-distortional displacements have already been orthogonalized, so that the first four rows of equation 5.23 correspond to equation 5.24. The remaining rows represent the distortional modes of behaviour.

Further orthogonalization required is performed in two stages. Firstly, the elements matrices of C,J and B showing coupling with the non-distortional elements are eliminated using the transformation matrix K_a. This gives matrices $\overline{C}, \overline{J}$ and $\overline{B}$, respectively.In the second stage, any remaining non-zero off-diagonal elements of two of these matrices are eliminated by a transformation matrix, K_b, obtained in general by solution of an eigenvalue problem. Any off-diagonal terms in the third matrix which still remain after the use of K_b are neglected. The diagonalized forms of matrices C,J and B are denoted by $\widetilde{C}, \widetilde{J}$ and $\widetilde{B}$ respectively.

First stage: Orthogonalization with respect to the non-distortional displacements :

Transformation matrix ,K_a, is defined as follows:

$$\overline{w} = K_a w = \begin{bmatrix} 1 & 0 & 0 & 0 & 0 & 0 & . & . & . & 0 \\ 0 & 1 & 0 & 0 & 0 & 0 & . & . & . & 0 \\ 0 & 0 & 1 & 0 & 0 & 0 & . & . & . & 0 \\ 0 & 0 & 0 & 1 & 0 & 0 & . & . & . & 0 \\ K_{51a} & K_{52a} & K_{53a} & K_{54a} & 1 & 0 & . & . & . & 0 \\ K_{61a} & K_{62a} & K_{63a} & K_{64a} & 0 & 1 & . & . & . & 0 \\ . & . & . & . & . & . & . & & . & . \\ . & . & . & . & . & . & & . & . & . \\ . & . & . & . & . & . & & . & . & . \\ K_{n1a} & K_{n2a} & K_{n3a} & K_{n4a} & 0 & 0 & . & . & . & 1 \end{bmatrix} \begin{bmatrix} 1 \\ \tilde{x} \\ \tilde{y} \\ \tilde{\omega}_{twr} \\ w_5 \\ w_6 \\ . \\ . \\ . \\ w_n \end{bmatrix} \tag{5.27}$$

$$= w + K_{1a}.1 + K_{2a}\tilde{x} + K_{3a}\tilde{y} + K_{4a}\tilde{\omega}_{twr} \tag{5.28}$$

The symbol ~ denotes full orthogonalization. For values of j from 1 to 4,

$$K_{ja} = \begin{bmatrix} 0 \\ 0 \\ 0 \\ 0 \\ K_{5ja} \\ K_{6ja} \\ . \\ . \\ . \\ K_{nja} \end{bmatrix} \tag{5.29}$$

K_{ja} is a vector of unknown terms forming the jth column of the matrix K_a. The matrix K_{ja} is calculated from equations 5.30 and 5.31 below, which correspond to the condition that the off-diagonal submatrices of $\overline{C}$ are zero.

$$\int_A \overline{w}\tilde{w}_r^T dA = \int_A w\tilde{w}_r^T dA + K_{ja}\int_A \tilde{w}_{ri}\tilde{w}_r^T dA = 0 \tag{5.30}$$

for i and j from 1 to 4 and only for distortional modes of $\overline{w}$ and w. $\tilde{w}_{ri}$ is the ith component of the orthogonalized non-distortional vector $\tilde{w}_r$ (equation 5.25)

Written more fully, equation 5.30 becomes

$$\begin{bmatrix} C_{5j} \\ C_{6j} \\ \cdot \\ \cdot \\ \cdot \\ C_{nj} \end{bmatrix} + \begin{bmatrix} K_{5ja} \\ K_{6ja} \\ \cdot \\ \cdot \\ \cdot \\ K_{nja} \end{bmatrix} C_{ii} = 0 \text{ for values of i and j from 1 to 4} \tag{5.31}$$

Each of the four column vectors K_{ja} is obtained from equation 5.31 for the appropriate value of j. The transformation matrix K_a is now known, giving

$$\overline{C} = [\overline{C}_{ij}] = K_a C K_a^T = \begin{bmatrix} A & 0 & 0 & 0 & & & & & \\ 0 & I_y & 0 & 0 & & & & 0 & \\ 0 & 0 & I_x & 0 & & & & & \\ 0 & 0 & 0 & C_{twr} & 0 & 0 & \cdots & 0 & \\ & & & 0 & \overline{C}_{55} & \overline{C}_{56} & & \overline{C}_{5n} & \\ & 0 & & 0 & \overline{C}_{65} & \overline{C}_{66} & & \overline{C}_{6n} & \\ & & & \cdot & & & & & \\ & & & \cdot & & & & & \\ & & & \cdot & & & & & \\ & & & 0 & \overline{C}_{n5} & \overline{C}_{N6} & & \overline{C}_{nn} & \end{bmatrix} \tag{5.32}$$

In addition, Sedlacek(1968) used the transformation

$$\bar{J} = K_a J K_a^T = \begin{bmatrix} 0 & 0 & 0 & 0 & & & & & \\ 0 & 0 & 0 & 0 & & & 0 & & \\ 0 & 0 & 0 & 0 & & & & & \\ 0 & 0 & 0 & \bar{J}_{44} & \bar{J}_{45} & . & . & . & \bar{J}_{4n} \\ & & & \bar{J}_{54} & \bar{J}_{55} & . & . & . & \bar{J}_{5n} \\ & & & . & . & . & . & . & . \\ & & 0 & . & . & . & . & . & . \\ & & & . & . & . & . & . & . \\ & & & \bar{J}_{n4} & \bar{J}_{n5} & . & . & . & \bar{J}_{nn} \end{bmatrix} \tag{5.33}$$

As the matrix B refers only to distortional behaviour, it follows that

$$\bar{B} = B = \begin{bmatrix} 0 & 0 & 0 & 0 & & & & & \\ 0 & 0 & 0 & 0 & & & 0 & & \\ 0 & 0 & 0 & 0 & & & & & \\ 0 & 0 & 0 & 0 & 0 & 0 & . & . & . & 0 \\ & & & 0 & \bar{B}_{55} & \bar{B}_{56} & . & . & . & \bar{B}_{5n} \\ & & & 0 & \bar{B}_{65} & \bar{B}_{66} & . & . & . & \bar{B}_{5n} \\ & & & . & . & . & . & . & . & . \\ & 0 & & . & . & . & . & . & . & . \\ & & & . & . & . & . & . & . & . \\ & & & 0 & \bar{B}_{n5} & \bar{B}_{n6} & . & . & . & \bar{B}_{nn} \end{bmatrix} \tag{5.34}$$

For a closed box sections, it is known from thin-walled beam theory that the St.Venant torsional second moment of the cross-sectional area, J_{44} is significant for such sections, whereas the torsional warping moment of inertia C_{44} or (C_{twr}), is relatively insignificant. Sedlacek(1971) therefore suggested that, when $\bar{C}$ and $\bar{J}$ are evaluated in the first stage of orthogonalization, only three non-distortional displacements a_1,a_2 and a_3(or a_x,a_y and a_z) be orthogonalized with respect to the distortional displacements using the above procedure involving warping displacements as in equations 5.27 to 5.31, and that the fourth non-distortional displacements a4 (twist) be orthogonalized using shear functions $\bar{v}_i$ defined in equations 5.3 and 5.4, because the shear stress is a more sensitive measure of the stress state in torsion than in torsional warping stress, for a closed box section. If

orthogonalization is viewed as the selection of mutually independent components of the total stress or deformation state, the best selection is the one in which the components are the most sensitive possible measures of that state.

This gives the following equation as a substitute for equation 5.31:

$$\begin{bmatrix} J_{54} \\ J_{64} \\ . \\ . \\ . \\ J_{n4} \end{bmatrix} + \begin{bmatrix} K^{*}_{54a} \\ K^{*}_{64a} \\ . \\ . \\ . \\ K^{*}_{n4a} \end{bmatrix} J_{44} = 0 \qquad (5.35)$$

where the second column vector K^{*}_{4a} is used instead of K_{44} in equation 5.28.
In general matrices of the following form are then obtained.where × denotes a non-zero element.

$$\overline{C} = \begin{bmatrix} \times & & & & & & & & \\ & \times & & & 0 & & & 0 & \\ & & \times & & & & & & \\ 0 & & & \times & \times & \times & . & . & . & \times \\ & & & \times & \times & \times & . & . & . & \times \\ & & & \times & \times & \times & . & . & . & \times \\ 0 & & & . & . & . & . & . & . & . \\ & & & . & . & . & . & . & . & . \\ & & & . & . & . & . & . & . & . \\ & & & \times & \times & \times & . & . & . & \times \end{bmatrix} \qquad (5.36)$$

Any non-zero warping stiffness among the terms $\overline{C}_{54}, \overline{C}_{64}, \ldots\ldots\ldots \overline{C}_{n4}$ are neglected as being of relatively low structural significance in closed box sections.

$$\bar{J} = \begin{bmatrix} 0 & & & & & & & & \\ & 0 & & 0 & & & 0 & & \\ & & 0 & & & & & & \\ & & & \times & 0 & 0 & . & . & . & 0 \\ & & & 0 & \times & \times & . & . & . & \times \\ & & & 0 & \times & \times & . & . & . & \times \\ & 0 & & . & . & . & . & . & . & . \\ & & & . & . & . & . & . & . & . \\ & & & . & . & . & . & . & . & . \\ & & & 0 & \times & \times & . & . & . & \times \end{bmatrix} \tag{5.37}$$

$$\bar{B} = \begin{bmatrix} 0 & & & & & & & & \\ & 0 & & 0 & & & 0 & & \\ & & 0 & & & & & & \\ & 0 & & 0 & & & 0 & & \\ & & & & \times & \times & . & . & . & \times \\ & & & & \times & \times & . & . & . & \times \\ & & & & . & . & . & & & . \\ & 0 & & & . & . & & . & & . \\ & & & & . & . & & & . & . \\ & & & & \times & \times & . & . & . & \times \end{bmatrix} \tag{5.38}$$

The first stage of orthogonalization thus yields the following differential equation for the partially orthogonalized displacement vector $\bar{a}$.

$$E\bar{C}a''' - G\bar{J}a'' + \bar{B}\bar{a} = n_{tr}\bar{r}^* + \int_{s_{per}} n_l' \bar{w} ds_{per} = \bar{n} \tag{5.39}$$

where $\bar{a} = (K_a^T)^{-1} a$, and $\bar{r}^*$ and $\bar{n}$ are the appropriate transformed versions of r^* and the load vectors.

Second stage: Orthogonalization with respect to deformations which are still coupled after the first stage

The transformation matrices K and K_b are now defined such that

$$K = K_b K_a \tag{5.40}$$

The use of K_b transform at most two of the three stiffness matrices $\overline{C}, \overline{J}$ and $\overline{B}$ into the diagonal form.Sedlacek(1968) analysed single cell, two-cell and three-cell box beams whose sections were symmetrical about a vertical axis, and found that the second stage of orthogonalization is necessary only for the three-cell section.He chose $\overline{C}$ and $\overline{B}$ as the two matrices to be orthogonalized, pointing out that the off-diagonal terms of $\overline{J}$ in his example were small enough and could be to neglected.

The matrix K_b is required to be such that

$$\widetilde{C} = K_b \overline{C} K^T{}_b$$

$$\widetilde{B} = K_b \overline{B} K_b^T$$

$$\widetilde{J} = K_b \overline{J} K^T{}_b$$

where $\widetilde{C}$ and $\widetilde{B}$ are diagonal matrices and the non-zero off-diagonal elements of $\widetilde{J}$ are neglected.

CHAPTER-6

ANALYSIS OF SHEAR LAG EFFECT

6.1 Shear Lag Analysis of Box Girder

6.1.1 Introduction:

The theory presented is general enough to handle loadings causing both longitudinal bending and torsion, but only longitudinal bending with shear lag will be considered here, as torsional warping and distortional effects were discussed in Chapter-5.
Roik and Sedlacek (1970) extended the engineers bending theory for thin walled sections by allowing for shear deformation in the plane of the walls, by introducing additional internal forces chosen in such a way that their distribution over the section is related the shear deformation, leading to the definition of a warping function associated with the shear lag.The capacity of shear deformation can either be considered at discrete points on the cross-section (such as those at which longitudinal slip might occur elastically at joints in composite construction), or taken to vary continiously around the perimeter of the cross-section, reflecting the deformability of plate elements in shear.Suitable warping functions can be chosen for either case , and the choice can be based on the results of simple bending theory. or its refinement.

The governing differential equations developed for the shear lag mode of deformation are uncoupled and are of the same form that for the simple beam subjected to combined transverse loading and axial tension.The additional internal forces mentioned above can thus be obtained using statics. It is not necessary to assume an "effective flange width" in the analysis, but such a quantity can be evaluated latter, once the variation of the stress over the cross-section has been obtained from the completed shear lag calculation.

At the junctions between flanges and webs, Kuper and Ewald (1977) found that the stress state can be one of combined shear and transverse tensile stress. They have developed design proposals for reinforcement to resist these stresses, but these are not considered in the work by Roik and Sedlacek (1968) .

6.1.2 Definition of Shear Lag:

Accoring to the basic assumptions of the simple beam theory, where the cross sections are assumed to remain plane before and after bending , the stress distribution across the top flange of a beam is constant. In a wide flanged T or I or Box section , this assumption is not true except for sections which are far from the point of contraflexure. At the point of contraflexure the section is subjected to shearing force, but no bending moment. The zero moment implies that there is no direct stress in the flanges, while transverse shear on the section indicates that there are horizontal shearing stress reducing in intencity towards the extremities of the section . For the case of wide flanged I or Box section, this implies that the horizontal shear flow diminishes to zero at the outer edges of the flanges. Away from the point of contraflexure, direct stresses are present because of the moment on the section and therefore the shearing stress gets modified. As for the case of the simple beam bending theory for beam the horizontal shear flow and direct stresses are inter-related and they can be visualized as the shear flow injecting direct stresses into the flange. The build up of these direct stresses resulting from the shear flow is not uniform across the width of the wide flange, but it produces stresses which tail off towards the extremities, until a distance is attained that is far enough from the point of contraflexure for the pattern of stresses to have reached a balance which produces uniform direct stress. This phenomenon of the change of distribution of direct stress are known as shear lag and it consequently reduces the effectiveness of the area of compression flange.In the design, consideration of effective flange width is the indirect representation of shear lag phenomenon.

Positive shear lag: The bending stress in the regions close to webs are necessarily greater than those in the flange remote from the web as a consequences of shear deformation of the thin flange plate. This phenomenon is called positive shear lag.

Ref: Lee; Yoo, and Yoon: Analysis of Shear Lag Anomaly in Box Girders, Journal of Structural Engineering, Vol.128, No. 11, November 1, 2002. ASCE

Negative shear lag: Where the centre line stress exceeds the edge stress in the flange. This unusual stress distribution is sometimes called negative shear lag.

Ref: Lee; Yoo, and Yoon: Analysis of Shear Lag Anomaly in Box Girders, Journal of Structural Engineering, Vol.128, No. 11 , November 1, 2002. ASCE

6.1.3 Method of Shear-Lag Analysis Developed by Roik,Sedlacek(1970) and Schmackpfe(1972):

6.1.3.1 Choice of Warping Displacement Functions for Shear Lag:

These are chosen for each portion of the cross-section for which a shear lag analysis is required. Figure 6.1 shows qualitatively the kind of functions that might be selected for flange stress variation in single symmetrical one,two and three cell cross-sections acting in longitudinal bending without torsion.If shear lag were considered to be significant in the webs (as might occur with very thin webs, possibly having longitudinal prestressing) functions similar to the ones defined in this region could represent shear lag effects in the webs near the points of introduction of the prestressing forces.The magnitudes of the various ordinates can be made arbitrary, as they are automatically adjusted in the analysis when combined with simple bending effects. The units of the warping functions are defined so as to give the correct stress in the numerical work.

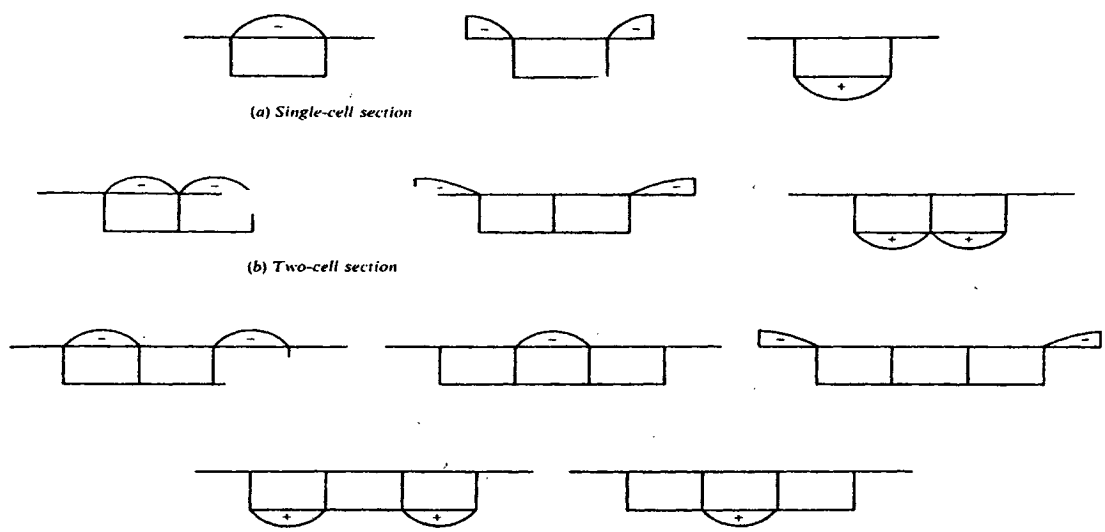

Figure 6. 1: Basic warping displacement functions for shear-lag analysis (Maisel, 1982)

In the program summarized in the appendices, parabolic warping functions are used, as these have been found to give good agreement with the folded plate theory for the

concrete cross-section investigated by Turner,Rawnsley and Salter (1977).However, Moffat and Dowling(1976) noted that for steel box girders with stiffened flanges, the flange stress variation is approximately to a fourth –order curve.As more experimental evidence becomes available for concrete, the choice of warping functions in shear lag can be modified, if desired.

6.1.3.2 Derivation of Differential Equation:

Define the basic shear lag warping function w_v as

$$w_v = \{w_{iv}\} = \begin{bmatrix} 1 \\ x \\ y \\ \omega_{twr} \\ w_{5v} \\ w_{6v} \\ . \\ . \\ . \\ w_{nv} \end{bmatrix} \tag{6.1}$$

where the suffix v refers to shear lag behaviour.The first four components of w_v are the same as those of w in equation 5.3, and relate to simple beam behaviour and torsional warping terms. w_{5v} to w_{nv} are (n-4) functions illustrated typically in Figure 6.1. Here n denotes the total number of deformation modes appropriate to non-distortional and shear lag behaviour.

Define the basic deformation vector a_v as:

$$a_v = \{a_{iv}\} = \begin{bmatrix} a_r \\ .... \\ a_{5v} \\ a_{6v} \\ . \\ . \\ . \\ a_{nv} \end{bmatrix} \tag{6.2}$$

where a_v is the vector of orthogonalized non-distortional displacements as in equation 5.24, and a_{5v} to a_{nv} are (n-4) components of displacement, each of which characterizes the mode of shear lag behaviour corresponding to components w_{5v} to w_{nv} ,respectively.

At any point on the cross-section, the resultant longitudinal displacement is (Roik and Sedlacek (1970):

$$a(z, s_{per}) = -w_v^T a_V' \tag{6.3}$$

The resultant longitudinal strain is

$$\varepsilon(z, s_{per}) = -w_v^T a_v'' \tag{6.4}$$

and the corresponding longitudinal normal stress is

$$f(z, s_{per}) = -E w_v^T a_v'' \tag{6.5}$$

If consider the continious shear deformation is considered in plate elements(and not the possible slip at the joints in composite construction), the continuity condition for shear strain γ is:

$$\frac{\partial a(z, s_{per})}{\partial s_{per}} + \frac{a_t(z, s_{per})}{\partial z} = \gamma$$

where $a_t(z,s_{per})$ is the transverse displacement in the plate element, along the tangent to the cross-sectional periphery at the point (z,s_{per}).

Schmackpfeffer (1972) quotes Schmidt's work(1970) as justifying the neglect of Poisson's ratio effects, and accordingly $a_t(z,s_{per})$ will beneglected here.Hence

$$\frac{\partial a(z,s_{per})}{\partial s_{per}} = \gamma = \frac{v}{G} \tag{6.6}$$

where v is the resultant shear stress in the plane of the cross-section due to combined non-distortional and shear lag behaviour.

Equations 6.3,6.4 and 6.5 result in the variation of f being proportional to that of w_v; Equations 6.6 and 6.3 lead to the variation of v over the cross-section for shear lag effects only being proportional to that of $\partial a/\partial s_{per}$ and therefore to that of $\partial w_v/\partial s_{per} = \dot{w}_v$, where the dot denots partial differentiation with respect to the peripheral co-ordinate s_{per}. Thus for shear lag only:

$$v = -G\dot{w}_v^T a_v' \tag{6.7}$$

In the virtual work analysis to follow, there will be a need for the vector r_v of order (nx1), where,

$$r_v = \begin{bmatrix} 0 \\ \cos\alpha \\ \sin\alpha \\ a_Q \\ 0 \\ . \\ . \\ . \\ 0 \end{bmatrix} \tag{6.8}$$

The first four components of r_v are the same as those for r in equation 5.3 , and they refer here to the position and direction of the resultant applied loading.

Now consider the beam to undergo a virtual displacement ∂a_v from its equilibrium position. There is no change in the potential energy, i,e the virtual work ∂W_{ext} done by the external loads is equal to the virtual work ∂W_{int} done by the internal forces.By equating these two quantities, the differential equation of the problem can be obtained.

The virtual work is found for ∂W_{int}.

$$\partial W_{\text{int}} = \int_0^L \{ \int_A (f\partial\varepsilon + v\partial\gamma) dA \} dz \tag{6.9}$$

where

f = normal stress in the z direction;

ε = normal strain corresponding to f ;

v = shear stress in the plane of cross-section;

γ = shear strain corresponding to v;

δ = a variational symbol denoting virtual displacement, virtual strain or virtual work;

L= total length of beam;

A = cross-sectional area of beam;

If the stresses and strains are expressed in terms of displacements, the equation becomes

$$\partial W_{\text{int}} = \int_0^L \{E \int_A ((a_v'')^T w_v)(w_v^T \delta a_v'')dA + G \int_A ((a_v')^T \dot{w}_v)(\dot{w}_v^T \delta a_v')dA\}dz$$

$$= \int_0^L \{E(a_v'')^T \int_A w_v w_v^T dA \delta a_v'' + G(a_v')^T \int_A \dot{w}_v \dot{w}_v^T dA \delta a_v'\}dz \tag{6.10}$$

Roik and Sedlacek(1970) derived the following equation for δW_{ext};

$$\delta W_{ext} = \int_0^L \{n_{tr} r_v^T \partial a_v - \int_{s_{per}} n_l w_v^T ds_{per} \partial a'_v\}dz + \sum_F [F_{tr} r_v^T \partial a_v - F_l w_v^T \partial a_v'] \tag{6.11}$$

where

n_{tr} = transverse distributed load;

n_l = longitudinal distributed load, in general varying around the periphery of the cross-section;

F_{tr} = transverse comcentrated load;

F_l = longitudinal concentrated load;

r_v = a vector associated with loading positions;

$\sum_F$ = summation over all concentrated loads;

Equating δW_{int} to δW_{ext} and integrating by parts and introducing the summarized notation

$$C_v = [C_{ijv}] = \int_A w_v w_v^T dA \tag{6.12}$$

$$S_v = [S_{ijv}] = \int_A \dot{w}_v \dot{w}_v^T dA \tag{6.13}$$

where C_v and S_v are matrices of section properties in shear lag warping and shear stiffness, respectively, the following differential equation is obtained:

$$EC_v a_v''' - GS_v a_v'' = n_{tr} r_v + \int_{s_{per}} n_l' w_v ds_{per} \qquad (6.14)$$

This is the generalized differential equation representing the shear lag behaviour.

6.1.3.3 Orthogonalization of the Basic Co-Ordinates:

The matrix differential equation 6.14, expressed in terms of the displacement vector , a_v , represents a system of coupled, simultaneous differential equations in the basic displacement components , $a_{iv.}$

As the first four displacement components have already been orthogonalized, the first four rows of equation 6.14 correspond to equation 5.24. The remaining rows represents the shear lag modes of behaviour.

Further orthogonalization is performed in two stages.Firstly , the elements of C_v showing coupling with the shear lag elements are eliminated by using of a transformation matrix K_{av}. (Such coupling will not occur in S_v if only the flange shear lag is considered.)This results in matrices $\widetilde{C}_v$ and $\widetilde{S}_v$, respectfully.In the second stage, any remaining non-zero off –diagonal elements of these matrices are eliminated by a transformation matrix, $K_{bv,}$ obtained by solution of an eigenvalue problem.The diagonalized form of C_v and S_v , are denoted by $\widetilde{C}_v$ and S_v, respectfully.

First stage: Orthoganalization with respect to the first four displacement components:

Define transformation matrix, K_{av} as indicated in the following equations:

$$\overline{w}_v = K_{av} w_v = \begin{bmatrix} 1 & 0 & 0 & 0 & 0 & 0 & \cdots & 0 \\ 0 & 1 & 0 & 0 & 0 & 0 & \cdots & 0 \\ 0 & 0 & 1 & 0 & 0 & 0 & \cdots & 0 \\ 0 & 0 & 0 & 1 & 0 & 0 & \cdots & 0 \\ K_{51av} & K_{52av} & K_{53av} & K_{54av} & 1 & 0 & \cdots & 0 \\ K_{61av} & K_{62av} & K_{63av} & K_{64av} & 0 & 1 & \cdots & 0 \\ \cdot & \cdot & \cdot & \cdot & \cdot & \cdot & \cdots & \cdot \\ \cdot & \cdot & \cdot & \cdot & \cdot & \cdot & \cdots & \cdot \\ \cdot & \cdot & \cdot & \cdot & \cdot & \cdot & \cdots & \cdot \\ K_{n1av} & K_{n2av} & K_{n3av} & K_{n4av} & 0 & 0 & \cdots & 0 \end{bmatrix} \begin{bmatrix} 1 \\ \tilde{x} \\ \tilde{y} \\ \tilde{\omega}_{twr} \\ w_{5v} \\ w_{6v} \\ \cdot \\ \cdot \\ \cdot \\ w_{nv} \end{bmatrix} \tag{6.15}$$

$$= w_{av} + K_{1av}.1 + K_{2av}\tilde{x} + K_{3av}\tilde{y} + K_{4av}\tilde{\omega}_{twr} \tag{6.16}$$

For values of j from 1 to 4,

$$K_{jav} = \begin{bmatrix} 0 \\ 0 \\ 0 \\ 0 \\ K_{5jav} \\ K_{6jav} \\ \cdot \\ \cdot \\ \cdot \\ K_{njav} \end{bmatrix} \tag{6.17}$$

where K_{jav} is a vector of unknown terms forming the jth column of matrix $K_{av}.K_{jav}$ is calculated using the following equations 6.18 and 6.19, below, which correspond to the condition that the off-diagonal submatrices of $\overline{C}_v$ are zero.

$$\int_A \overline{w}_v \tilde{w}_r^T dA = \int_A w_v \tilde{w}_r^T dA + K_{jav} \int_A \tilde{w}_{ri} \tilde{w}_r^T dA = 0 \tag{6.18}$$

For values of i and j from 1 to 4 and only for shear lag modes of $\overline{w}_v$ and w_v. $\widetilde{w}_{ri}$ is the ith component of the orthogonalized vector $\widetilde{w}_r$ (equation5.25).

Written more fully, equation 6.18 becomes

$$\begin{bmatrix} C_{5jv} \\ C_{6jv} \\ \cdot \\ \cdot \\ \cdot \\ C_{njv} \end{bmatrix} + \begin{bmatrix} K_{5jav} \\ K_{6jav} \\ \cdot \\ \cdot \\ \cdot \\ K_{njav} \end{bmatrix} C_{ii} = 0 \quad \text{for values of i and j from 1 to 4} \tag{6.19}$$

Each of the four column vectors K_{jav} is obtained from equation 6.19 for the appropriate value of j. The transformation matrix K_{av} is now known, giving

$$\overline{C}_v = [\overline{C}_{ijv}] = K_{av} C_v K_{av}^T = \begin{bmatrix} A & 0 & 0 & 0 & & & & & & \\ 0 & I_y & 0 & 0 & & & 0 & & & \\ 0 & 0 & I_x & 0 & & & & & & \\ 0 & 0 & 0 & C_{twr} & 0 & 0 & . & . & . & 0 \\ & & & 0 & \overline{C}_{55v} & \overline{C}_{56v} & . & . & . & \overline{C}_{5nv} \\ & & & 0 & \overline{C}_{65v} & \overline{C}_{66v} & . & . & . & \overline{C}_{6nv} \\ & & & . & . & . & . & . & . & . \\ & 0 & & . & . & . & . & . & . & . \\ & & & . & . & . & . & . & . & . \\ & & & 0 & \overline{C}_{n5v} & \overline{C}_{n6v} & . & . & . & \overline{C}_{nnv} \end{bmatrix} \tag{6.20}$$

In addition,

$$\bar{S}_v = K_{av} S_v K_{av}^T = \begin{bmatrix} 0 & 0 & 0 & 0 & & & & & \\ 0 & 0 & 0 & 0 & & & & 0 & \\ 0 & 0 & 0 & 0 & & & & & \\ 0 & 0 & 0 & 0 & & & & & \\ & & & & \bar{S}_{55v} & \bar{S}_{56v} & . \; . \; . & & \bar{S}_{5nv} \\ & & & & \bar{S}_{65v} & \bar{S}_{66v} & . \; . \; . & & \bar{S}_{6nv} \\ & & 0 & & & & & & \\ & & & & & & & & \\ & & & & \bar{S}_{n5v} & \bar{S}_{n6v} & . \; . \; . & & \bar{S}_{nnv} \end{bmatrix} \tag{6.21}$$

The first stage of orthogonalization thus yields the following differential equation for the partially orthogonalized displacement vector $\bar{a}_v$:

$$E\bar{C}_v \bar{a}_v''' - G\bar{S}_v \bar{a}_v'' = n_{tr} \bar{r}_v + \int_{s_{per}} n_l' \bar{w}_v ds_{per} = \bar{n}_v \tag{6.22}$$

where

$$\bar{a}_v = (K_{av}^T)^{-1} a_v$$

and $\bar{r}_v = K_{av} r_v$

Second stage: Orthogonalization with respect to deformations which are still coupled after the first stage.

Transformation matrices K_v and K_{bv} are now defined such that

$$K_v = K_{bv} K_{av} \tag{6.23}$$

Use of K_{bv} transforms $\bar{C}_v$ and $\bar{S}_v$ into the diagonal form. K_{bv} is required to be such that

$$\tilde{C}_v = K_{bv} \bar{C}_v K_{bv}^T \tag{6.24}$$

and

$$\tilde{S}_v = K_{bv} \bar{S}_v K_{bv}^T \tag{6.25}$$

where $\widetilde{C}_v$ and $\widetilde{S}_v$ are diagonal matrices.

As in the distortional analysis, the requirements in equations 6.24 and 6.25 are met if the rows I_{qbv} of matrix K_{bv} satisfy the eigenvalue equation

$$[\overline{C}_v - \lambda_{qv}\overline{S}_v]I_{qbv}^T = 0 \tag{6.26}$$

for a typical row q, where λ_{qv} are the eigenvalues obtained from the condition for a non-trival solution.

$$\left|\overline{C}_v - \lambda\overline{S}_v\right| = 0 \tag{6.27}$$

The governing equation now has the form

$$E\widetilde{C}_v\widetilde{a}_v''' - G\widetilde{S}_v a_v'' = n_{tr}\widetilde{r}_v + \int_{s_{per}} n_l'\widetilde{w}_v ds_{per} = \widetilde{n}_v \tag{6.28}$$

where

$$\widetilde{a}_v = (K_v^T)^{-1}a_v \tag{6.29}$$

$$\widetilde{r}_v = K_v r_v \tag{6.30}$$

and

$$\widetilde{w}_v = K_v w_v \tag{6.31}$$

Hetenyi(1946) derived the following equation for an ordinary beam on elastic foundation,subjected to vertical loading n_y and axial tension N;

$$EI_x\frac{d^4}{dz^4}(a_y) - N\frac{d^2}{dz^2}(a_y) + k_{fdn}a_y = n_y$$

Substituting $k_{fdn} = 0$ gives the following equation :

$$EI_x\frac{d^4}{dz^4}(a_y) - N\frac{d^2}{dz^2}(a_y) = n_y \tag{6.32}$$

Equations 6.28 and 6.32 are of the same mathematical form, and since equation 6.28 now represents an uncoupled system, each member of this system can be solved independently by analogy with equation 6.32, using ordinary beam statics. Figure 6.2 illustrates this, with each shear lag mode having a separate equivalent beam.

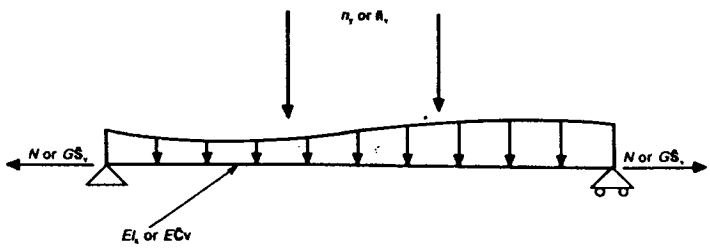

Figure 6. 2: Beam analogy for shear lag (Maisel, 1982)

6.1.3.4 Relation Between Stresses, Internal Forces and Deformations:

Considering only the shear lag effects, and not the first four mode of simple beam action and torsional warping, equation 6.28 is solved using the analogy of the beam on the elastic foundation .

Here the following quantities are required.

Column vector of "shear lag moments" $\tilde{M}_v$

$$= \{\tilde{M}_{iv}\} \text{ where i>4}$$

$$= \{\tilde{M}_{5v}\tilde{M}_{6v}.....\tilde{M}_{nv}\}$$

$$= -E\tilde{C}_v\tilde{a}_v'' \qquad (6.33)$$

Longitudinal normal stress at section z

$$= f_v$$

$$= \sum_{i=5}^{n} f_{iv}$$

$$= \sum_{i=5}^{n} \frac{\tilde{M}_{iv}}{\tilde{C}_{iiv}} \tilde{w}_{iv} \tag{6.34}$$

where f_{iv} is the value of f_v in mode i ;

$\tilde{w}_{iv}$ is the ith component of the vector $\tilde{w}_{iv}$;

$\tilde{C}_{iiv}$ is the iith element of matrix $\tilde{C}_v$.

The column vector of shear lag shear force, $\tilde{V}_v$ is given by

$$\tilde{V}_v = \{\tilde{V}_{iv}\} = \tilde{M}'_v = -E\tilde{C}_v \tilde{a}'''_v \tag{6.35}$$

The shear lag shear stress , v_v ,can be obtained by transforming equation 6.7, using equations 6.29 and 6.31. Thus

$$v_v = -G\dot{w}_v^T a'_v = -G\dot{\tilde{w}}_v^T (K_v^{-1})^T K_v^T \tilde{a}'_v = -G\dot{\tilde{w}}_v^T \tilde{a}'_v$$

i.e., $$\sum_{i=5}^{n} v_{iv} = -G \sum_{i=5}^{n} \dot{\tilde{w}}_{iv} \tilde{a}'_{iv} \tag{6.36}$$

where v_{iv} is the value of v_v in mode i ;

$$\dot{\tilde{w}}_{iv} = \frac{d}{ds_{per}} \tilde{w}_{iv};$$

$$\tilde{a}'_{iv} = \frac{d}{dz} \tilde{a}_{iv}$$

as obtained from the analogous beam calculation.

In equation 6.36, the quantity $G\tilde{a}'_{iv}$ can be specified more explicitly in terms of the loads on the analogous beam in mode i .

Consider an element of this beam, as shown in Figure 6.3.

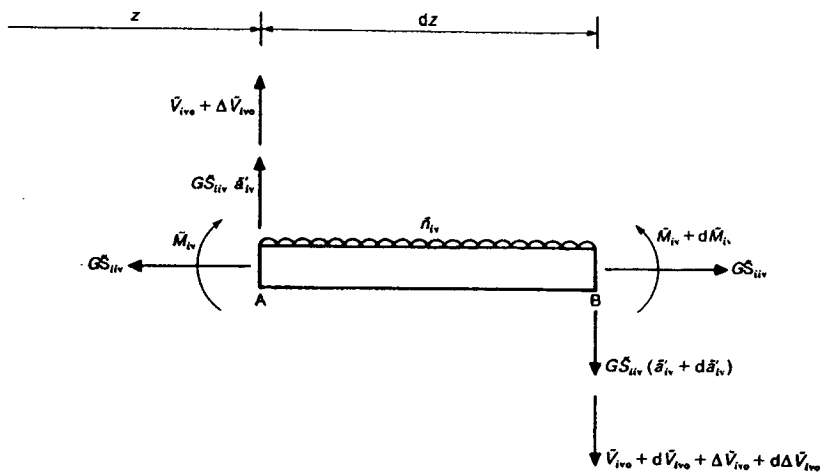

Figure 6. 3: Element of analogous beam in shear lag mode i (Maisel,1982)

Small deflection theory is assumed to be valid, and the transverse shear force at section z is composed partly of $G\widetilde{S}_{iiv}\widetilde{a}_{iv}$, which is the transverse component of axial force, $G\widetilde{S}_{iiv}$, and $\widetilde{V}_{iv0}+\Delta\widetilde{V}_{iv0}$, where $\widetilde{V}_{iv0}$ is the shear force on the analogous beam when the axial force is zero and $\Delta\widetilde{V}_{iv0}$ is the change in $\widetilde{V}_{iv0}$ when the axial load is applied.The distributed load of intensity $\widetilde{n}_{iv}$ also acts on the element.

Taking moments about A in Figure 6.3 gives

$$\widetilde{M}_{iv}+d\widetilde{M}_{iv}-\frac{\widetilde{n}_{iv}(dz)^2}{2}-G\widetilde{S}_{iiv}(\widetilde{a}'_{iv}+d\widetilde{a}'_{iv})dz-(\widetilde{V}_{iv0}+d\widetilde{V}_{iv0})dz-(\Delta\widetilde{V}_{iv0}+d\Delta\widetilde{V}_{iv0})dz-\widetilde{M}_{iv}$$

$$=0$$

Neglecting quantities of second order this goves

$$d\widetilde{M}_{iv}-G\widetilde{S}_{iiv}\widetilde{a}'_{iv}dz-\widetilde{V}_{iv0}dz-\Delta\widetilde{V}_{iv0}dz=0$$

therefore, $$\frac{d\widetilde{M}_{iv}}{dz}=G\widetilde{S}_{iiv}\widetilde{a}'_{iv}+\widetilde{V}_{iv0}+\Delta\widetilde{V}_{iv0}$$

$$G\widetilde{a}_{iv} = \frac{1}{\widetilde{S}_{iiv}}(\widetilde{M}'_{iv} - \widetilde{V}_{iv0} - \Delta\widetilde{V}_{iv0})$$

Therefore, in equation 6.36

$$v_v = \sum_{i=5}^{n} v_{iv} = \sum_{i=5}^{n} \frac{\dot{\widetilde{w}}_{iv}}{\widetilde{S}_{iiv}}(\widetilde{V}_{iv0} + \Delta\widetilde{V}_{iv0} - \widetilde{M}'_{iv}) \qquad (6.37)$$

CHAPTER-7

ANALYSIS OF A SINGLE-CELL BOX SECTION BEAM

7.1 General:

The analysis procedure described in the previous chapters has been applied a numerical example in this Chapter. Consider a simply-supported single cell box beam over a span of 32 m, which has diaphragms only at the supports, where there is full torsional and distorsional restraint, but no resistance to warping.At midspan there is a live concentrated load of 1000 kN over the web as shown in Figure 7.1

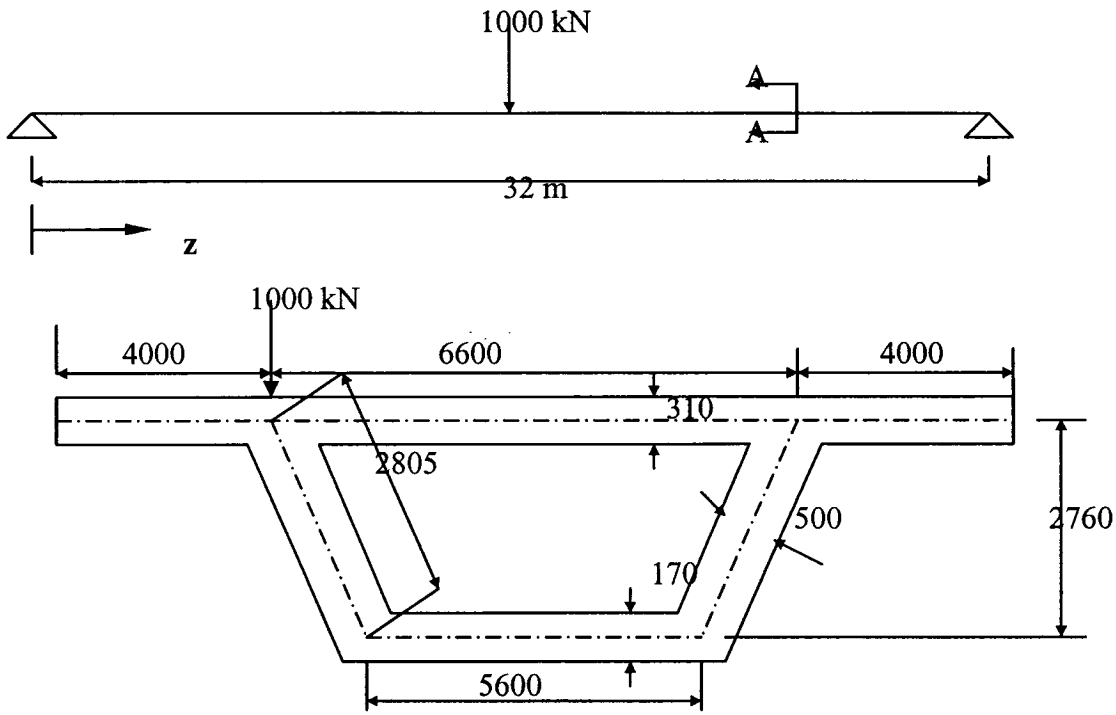

Section A-A

Dimensions in mm

Figure 7. 1: Loading and geometry

7.1.1 Analysis of simple bending and St. Venant torsional effects:

(a) **Calculation of dead and live load moment and section properties:**

Assume that the density of concrete=25 kN/m^3

Area of cross-section $= 8.283\ m^2$

Total dead load =32*8.283*25

=6626 kN

At midspan, the bending moment M_x =6626*32/8+1000*32/4

=34504 kN.m

At z=0, shear force V_y = (6626+1000)/2

=3813 kN

The depth of centroid below the mid-line of the top slab: =

((5600*170*2760)+(2*2805*500*1380))/8.283*10^6

=785 mm

The second moment of area of the cross-section about the centroidal x axis, I_x =

(14600*310^3/12)+(14600*310*785^2)+(2*2805*500*2760^2/12)+(2*2805*500*(1380-785)^2)+(5600*170^3/12)+(5600*170*1975^2)

I_x =9.3146*10^{12} mm^4

Similarly therefore the second moment of the area of cross-section about centroidal y axis, I_y

I_y =1.093*10^{14} mm^4

The bending moment, shearing force and the twisting moment diagrams are shown in Figure 7.2

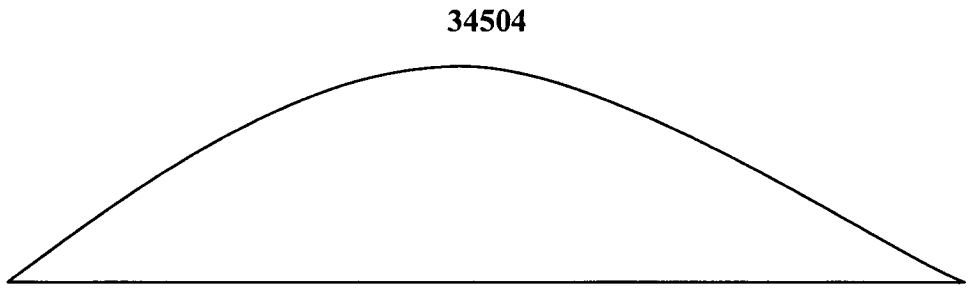

(a) Bending moment diagram(kN.m)

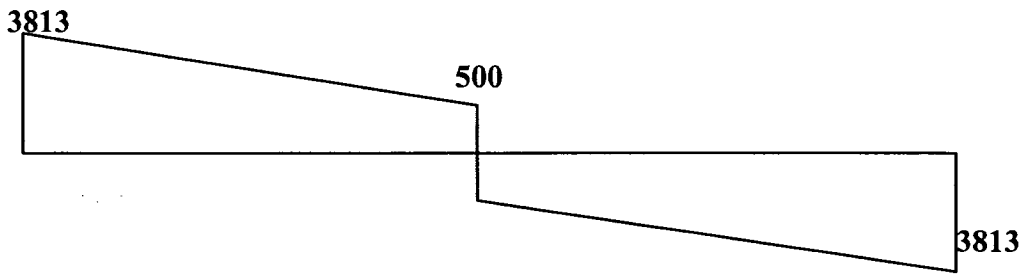

(b) shear force diagram(kN)

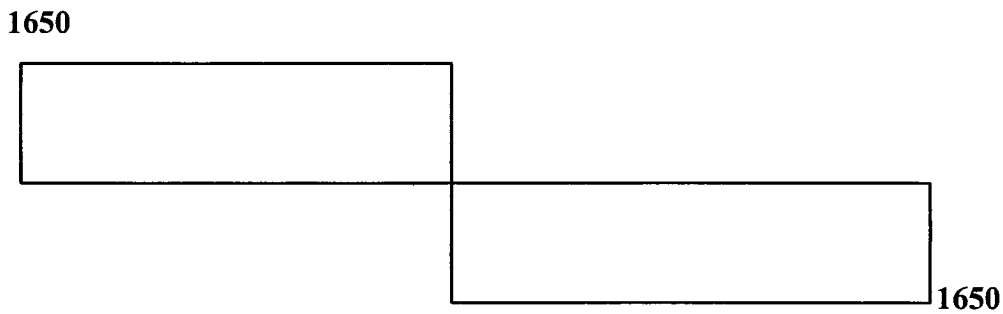

(c) Twisting moment diagram (kN.m)

Figure 7. 2:Bending moment, shear force and twisting moment diagrams due to combined dead and live load

(b) **Bending stress due to dead and live load:**

By Equation 1.1 gives:

$$f_{1bg} = \frac{M_x y}{I_x} + \frac{M_y x}{I_y}$$

At midspan, M_x=34504 kN.m ; M_y=0

Hence, at the mid-line of the top slab

$$f_{1bg} = -2.907 \quad \text{MPa}$$

and at mid-line of the bottom slab

$$f_{1bg} = 7.3159 \text{ MPa}$$

These stresses are shown in Figure 7.3

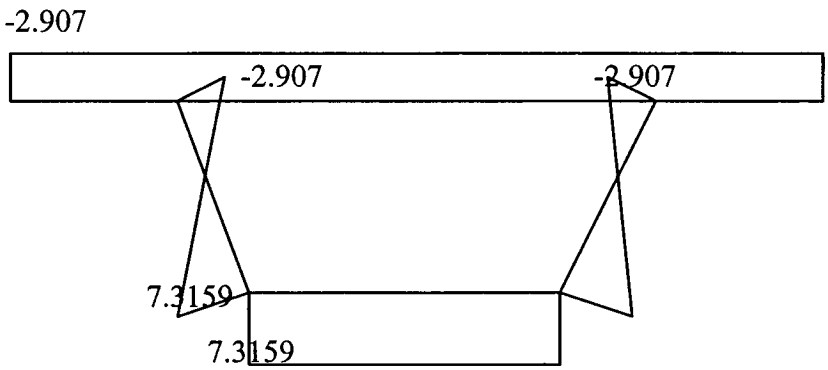

Figure 7. 3: Bending stress f_{1bg} at midspan section (MPa) from the beam bending theory

(c) Shear stresses v_{1bg} at the left-hand support:

Insert an imaginary cut in middle of the bottom flange to make it determinate as shown in Figure 7.4.

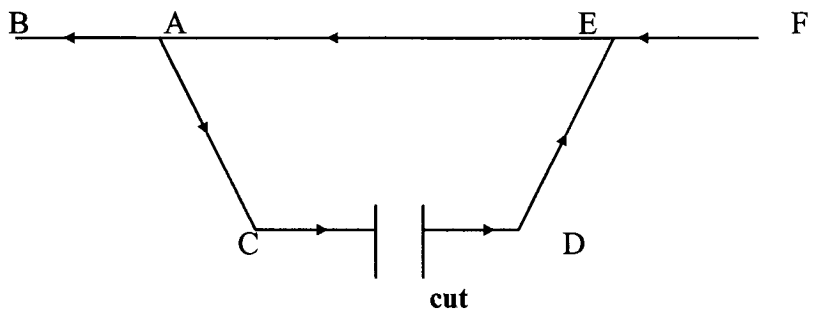

Figure 7. 4: Peripheral coordinate Sper and cut in cross-section

The statically determinate shear flows are now determined from equation 3.2 as:

$$v_{1bg}h = -\frac{V_y(\overline{Ay})}{I_x}$$

Calculation of $\overline{Ay}$ at different locations of the cross-section:

The positive directions must be the same as those of S_{per}(Figure 7.4)

At cut, $\overline{Ay} \rightarrow 0$ since statically determinate shear flow=0

At C, $\overline{Ay} \rightarrow$ = -(2800*170*1975)= -940100000 mm^3 since positive direction in Figure 7.4 runs from C towards cut.

Similarly, at the mid-depth of web AC , $\overline{Ay}$ = (-940100000-(2805*0.5*500*(1975-1380/2))= -1841206250 mm^3

The values of $\overline{Ay}$ can be determined similarly for the rest of the cross-sections.The above moments of area are converted to shear flow in accordance with equation 3.2 and then divided by the thickness to calculate the shear stresses.

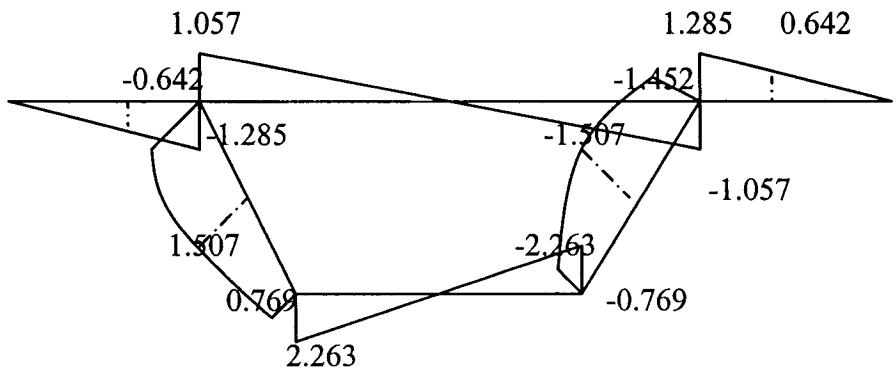

Figure 7. 5: Diagrams of shear stresses(MPa) derived using the beam bending theory at z=0

Statically indeterminate shear flows: To find the statically indeterminate shear flows in a single cell section, equations 3.3,3.4 and 3.5 reduces to

$$(v_{1bg}h)_0 \oint_{ACDE} \frac{ds_{per}}{h} = -\oint_{ACDE} \frac{(v_{1bg}h)_1}{h} ds_{per} \tag{7.1}$$

The integral on the right-hand side extends round the periphery of the closed cell, and as the integrand in antisymmetric about the vertical centre-line, the integral is zero. The integral on the left-hand side is not equal to zero, hence the statically indeterminate shear flow in the cell is equal to zero.

7.1.2 St.Venant torsional shear stresses due to live load:

From equation 3.14,

$$(v_{svt}h) = \frac{T_{svt}}{2A_{enc}}$$

At z=0, T_{svt}=1650 kN.m (Figure 7.2)

The area enclosed with the midlines of the sides,

A_{enc}=2760/2*(6600+5600)=16836000 mm^2

Therefore from equation 3.14, St.Venant shear stresses can be calculated at different location of the section. Figure 7.6 shows the St.Venant shear stresses at z=0 on the positive face of the section.

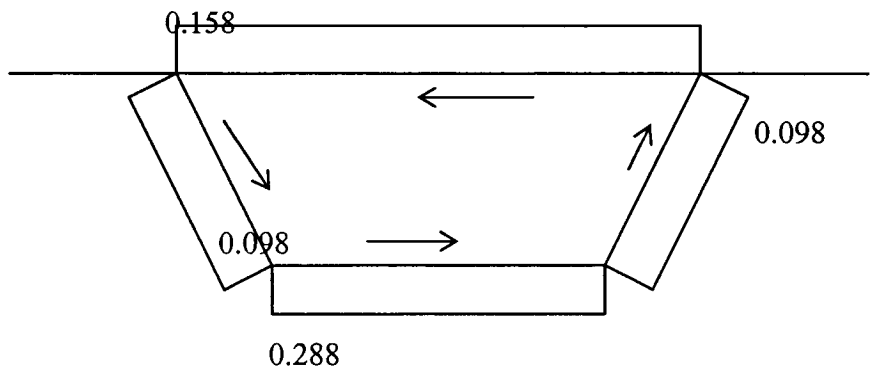

Figure 7. 6: Diagram for St.Venants shear stresses (MPa) at z=0 on the positive face of cross-section

7.1.3 Analysis of torsional warping by the method of Kollbrunner,Hajdin and Heilig:

The required section properties are first evaluated:

Sectorial coordinate ω_{twr} :

As shown in Figure 7.7(a), choose the midpoint of the top flange as the position for pole P and and origin O1 of coordinate s_{perP} .To evaluate ω_{twrP} from equation 4.21, use s_{perP} as a temporary coordinate instead of s_{per}. The value of $\bar{v}_{svt}$ is obtained from equations 4.24 and 4.25, as :

$$C_{svt} = \frac{4A^2_{enc}}{\oint \frac{ds_{per}}{h}}$$

By substituting the above value = $4*(16836000)^2/(6600/310+2*2805/500+5600/170)$

$=1.732*10^{13}$ mm^4

and $\bar{v}_{svt} = \dfrac{C_{svt}}{2A_{enc}h}$

$=514457.277/h$ mm

The positive directions of $\bar{v}_{svt}$ are shown in Figure7.6. On the left hand side of the centre-line of the section, the positive directions coincide with those of s_{perP} in Figure 7.7(a) and on the right hand side, they are oppose.Hence by the sign convension stated in connection with equation 4.21, the increment $\bar{v}_{svt} ds_{perP}$ is positive on the left-hand side of the section, and negative on the right-hand side.

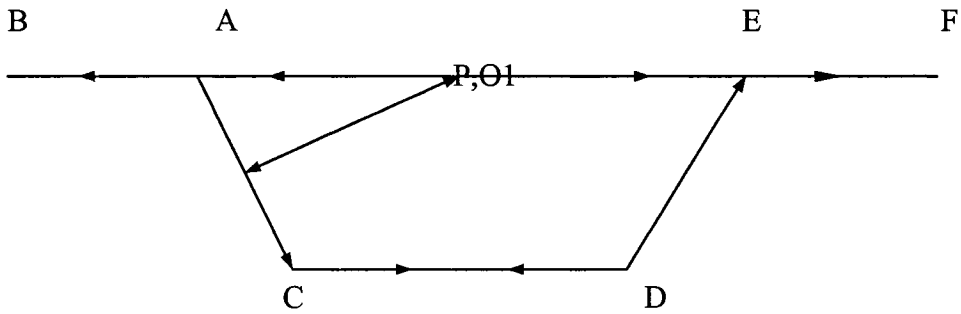

(a) Coordinate s_{perP}

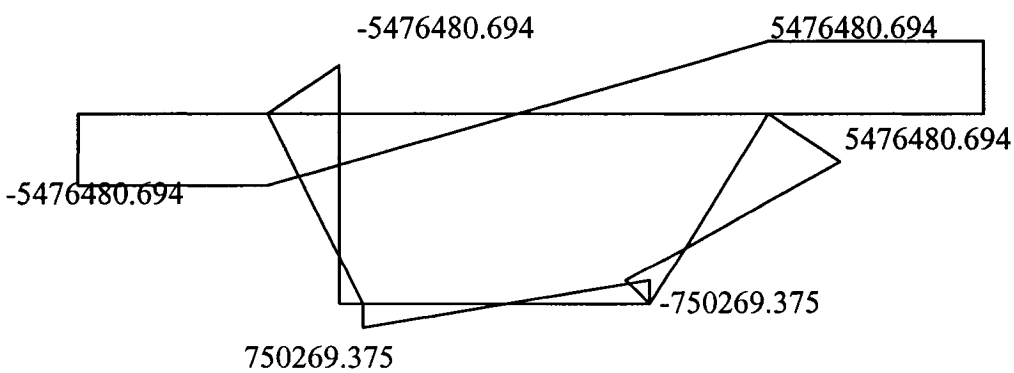

(b) Values of ω_{twrP} in mm^2

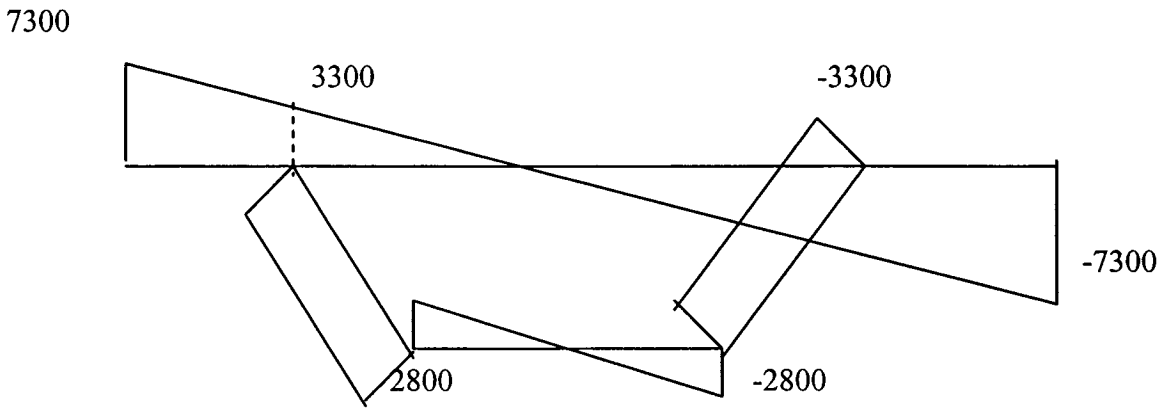

(c) Values of x in mm

Figure 7. 7: Determination of shear centre position

From geometry of Figure7.7(a), perpendicular distance of P from AC=3248.789 mm

The integration for ω_{twrP} will now be performed, using equation 4.21

At 01, ω_{twrP}=0

At A, $\omega_{twrP} = \int_0^{3300} (0 - \frac{514457.277}{310}) ds_{perP}$ =-5476480.694 mm^2

The values of the sectorial co-ordinate, θ_{twr} can be similarly evaluated for other sections.

The variations of ω_{twrP} around the section are plotted in Figure7.7(b)

Location of the shear centre:

From equation 4.27 ,

$$y_{shc} = -\frac{I_{x\omega P}}{I_y} + y_P$$

From Figure 7.7 and using Simpson's integration formula gives:

$$I_{x\omega P} = \int_A x\omega_{twrP} dA$$

$=2*4000*310/6*(7300+4*5300+3300)*(5476480.694)+$ ---------

$= -1.045*10^{17}\ mm^5$

Hence, the position of shear centre: $=-(-1.045*10^{17}/1.093*10^{14})+(-785)$

$=172$ mm

Hence, the shear centre Q lies at a distance of 172 mm below the centroid or 957 mm below the midline of the top flange.

Now the sectorial coordinate must be orthogonalised. Using Q as a pole in the θ_{twrP} diagram, and with O1 as the origin of the peripheral coordinate, the following values are calculated.

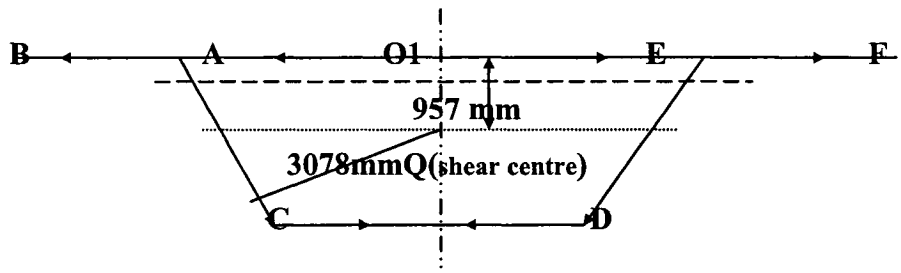

Figure 7.8(a) Shear centre position and s_{perP}

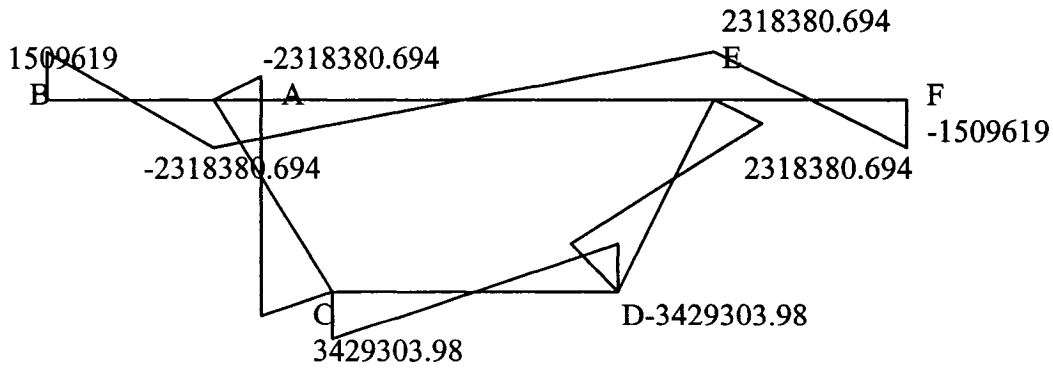

Figure7.8 (b) Values of ω_{twrQ} and ω_{twr} in mm^2

Figure 7. 8: Shear center and normalized sectorial coordinate w_{twr}

Figure 7.8(a) indicates the dimensions to be used in the integration for ω_{twrQ}. Hence by equation 4.21

At O1, ω_{twrQ}.=0

At A, $\omega_{twrQ} = \int_0^{3300} (957 - \frac{514457.277}{310}) ds_{perP} =$ -2318380.694 mm^2

Similarly, the values of ω_{twrQ} can be derived for the rest of the cross-section.

Figure 7.8(b) shows the variation of ω_{twrQ} around the section

The arithmatic check $I_{x\omega Q} = 0$ is now applied. From Figure 7.8(b) and 7.7(c), using the Simpson's integration method

$I_{x\omega Q}$= 2*4000*310/6*((7300)*(1509619)+4*(5300)*((1509619-2318380.694)/2)+(3300)*(-2318380.694))=0

To normalize ω_{twrQ}, obtain ω_0 from equation 4.30.Since the diagram of ω_{twrQ} is antisymmetric (Figure 7.8(b))

$\omega_0 = -\frac{1}{A}\int_A \omega_{twrQ} dA$ is equal to zero. Hence, from equation 4.29

$\omega_{twr} = \omega_{twrQ}$

i,e., Figure 7.8(b) is also the diagram of the normalized sectorial coordinate, ω_{twr} .

Torsional warping second moment of area, C_{twr} :

Torsional warping second moment of area is obtained from equation 4.32 and Figure 7.8(b), using Simpson's integration method

$C_{twr} = \int_A \omega^2{}_{twr} dA$ =1.941*10^{19} mm^6

Internal stress-resultants B_{twr}, T_{svt} and T_{twr} :

For the given loading and support conditions, the expressions for the above internal stress-resultants at midspan are obtained from equations 4.6,4.7 and 4.8.

By substituting z=l/2

The equation 4.6,4.7 gives:

$$B_{twr}(l/2) = \frac{T_{ext}}{2K_{18}K_{19}} \tanh \frac{K_{18}l}{2}$$

$T_{svt}(l/2) = \frac{T_{ext}}{2}(1 - \frac{1}{K_{19}})$ just to left of midspan section

From equation 4.15,

$$K_{19} = \frac{C_{cen}}{C_{cen} - C_{svt}}$$

where C_{cen} = central torsional second moment of area of cross-section

$$= \int_A a^2 Q \, dA$$

Where a_Q is the perpendicular distance from the shear centre at the tangent to the midline of wall at the point considered.(Figure 4.7 when Q is replaced by P)

From Figure, 7.1 and 7.8(a),

C_{cen}= (14600*310*(957)^2)+(2*2805*500*(3078)^2)+(5600*170*(2760-957)^2)
=3.194*10^{13}

Hence from equation 4.15

K_{19}= 2.185

Using equation 4.16 gives:

$\overline{C}_{twr} = K_{19}C_{twr}$ =4.243*10^{19} mm^6

From equation 4.14

$$K_{18} = \sqrt{\frac{GC_{svt}}{E\bar{C}_{twr}}} = \ 0.000421\text{mm}^{-1}$$

(Assume the Poisson's ratio to be 0.15
Therefore G/E=1/2(1+0.15)=0.435)

From equations 4.6 and 4.7

$$B_{twr}(l/2) = \frac{T_{ext}}{2K_{18}K_{19}} \tanh\frac{K_{18}l}{2} \quad = 1.791*10^{12}\ \text{N.mm}^2$$

$$T_{svt}(l/2) = \frac{T_{ext}}{2}(1 - \frac{1}{K_{19}}) \quad = \ 894860373.4\ \text{N.mm}$$

$$T_{svt}(0) = T_{ext}[\frac{1}{2} - \frac{\sinh K_{18}l/2}{K_{19}\sinh K_{18}l} \quad = 1648350000\ \text{N.mm}$$

From equation 4.8,

$$T_{twr}(z) = \frac{T_{ext}}{2K_{19}} \frac{\cosh K_{18}z}{\cosh\frac{K_{18}l}{2}}$$

$T_{twr}(l/2) =$ 755139626.6 N.mm [here T_{ext}=3300 kN.m]
$T_{twr}(0) =$ 1,650,000 N.mm

Torsional equilibrium:

Here $T_{svt} + T_{twr} = T_{ext}/2$

Hence, torsional equilibrium is satisfied.

Torsional warping stresses f_{twr} at midspan:

From equation 4.34,

$$f_{twr} = \frac{B_{twr}\omega_{twr}}{C_{twr}}$$

$$= 9.227*10^{-8}*\omega_{twr}\ \text{MPa}$$

The diagram for ω_{twr} is presented in Figure 7.8(b).

Hence at A

f_{twr} = -0.213 N/mm^2

The values of f_{twr} for the rest of the cross-sections can be similarly evaluated. Figure 7.9(a) shows the torsional warping stresses at different location of the section.

Torsional warping shear stresses v_{twr} at z=l.

From equation 4.19,

$$v_{twr} = T_{twr} \frac{\frac{d\omega_{twr}}{ds_{per}}}{C_{cen} - C_{svt}}$$

Substituting the values of T_{twr}, C_{cen} and C_{svt} gives,

$$v_{twr} = 5.165*10^{-5} * \frac{d\omega_{twr}}{ds_{per}} \text{ MPa}$$

and at z=0, $v_{twr} = 1.128*10^{-7} * d\omega_{twr} / ds_{per}$

The term $d\omega_{twr} / ds_{per}$ is equal to the slope of the ω_{twr} diagram (Figure 7.8(b)) in each segment of the cross-section.The positive directions of s_{per} are shown in Figure 7.4.

Hence, in segment EA(Figure 7.8b)

$d\omega_{twr} / ds_{per}$ =((-2318380.694)-(2318380.694))/6600=-703 mm
In segment AB, $d\omega_{twr} / ds_{per}$ =957 mm
In segment AC, $d\omega_{twr} / ds_{per}$ =2049 mm
In segment CD, $d\omega_{twr} / ds_{per}$ =-1225mm

Hence, using equation 4.19, torsional warping shear stresses (v_{twr}) can be evaluated.

at segment EA and it is -0.0363 MPa

Similarly, the values of v_{twr} can be calculated at different sections along the rest of the segment.

At z=0, v_{twr} is negligible.
Figure 7.9(b) shows the variation of v_{twr} around the cross-section.

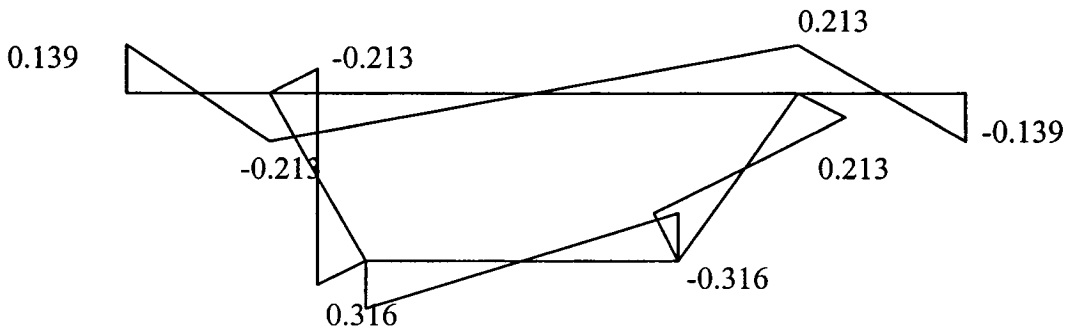

Figure 7.9 (a) Torsional warping stress(MPa) f_{twr} at midspan section

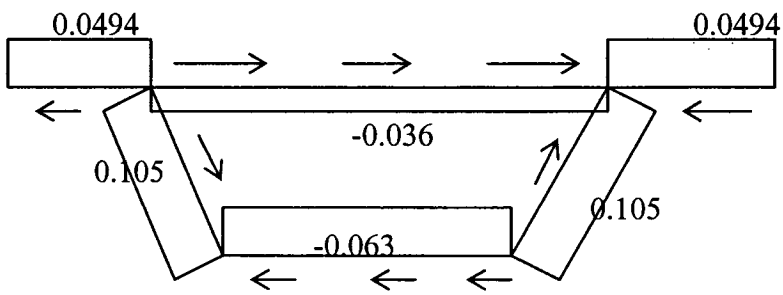

Figure 7.9(b) Torsional warping shear stress v_{twr} (MPa) on the positive face of cross-section z=16000mm.

Figure 7. 9: Diagrams of live load stresses f_{twr}, v_{twr} (MPa), due to torsional loading

7.1.4 Analysis of distortional effects:

In the single-cell cross-section, there is only one mode of global distortion as shown in Figure 5.1, and is called mode 5 in the notation of equation 5.2.

Unit warping function $\widetilde{w}_5$ and section properties $\widetilde{C}_{55}$ and $\widetilde{J}_{55}$:

To determine the basic distortion function a_5, the box section is regarded as a hinged quadrilateral mechanism, with one side held fixed, one plate is twisted through a unit angle. Thus the remaining members of the kinematic chain move as well, as shown in Figure 7.10(a), which represents the single antisymmetric mode of distortion arising in the symmetric single-cell box section.

In equation 5.3, define the basic distortional function w_5^0 as

$$w_5^0 = \int r_5 ds_{per} \tag{7.2}$$

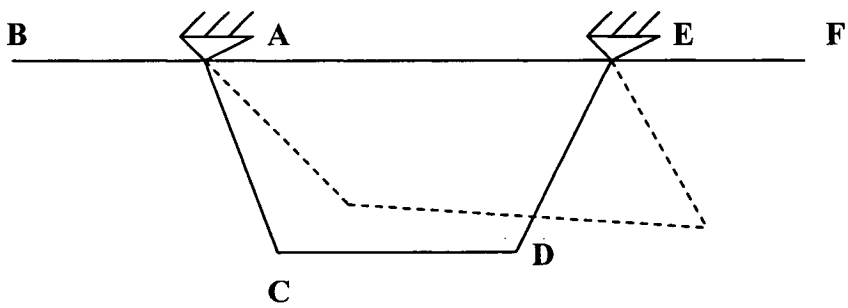

(a) Hinged quadrilateral mechanism.

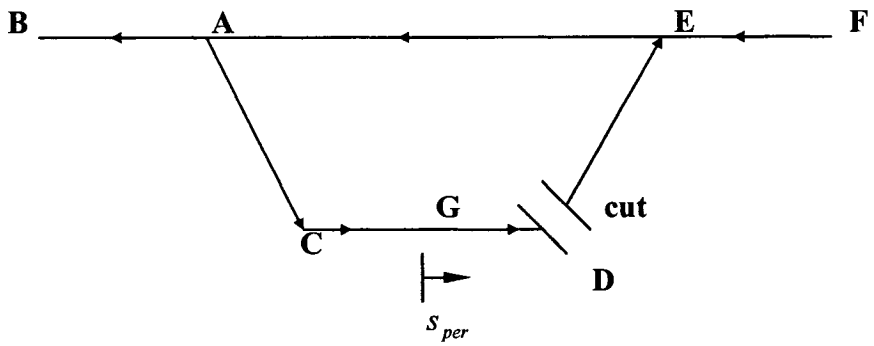

(b) Open section

Figure 7. 10: Distortion of section

The function can be determined by reducing the closed box section to an open section by introducing a cut, (Figure 7.10b). Placing the origin of coordinat e, s_{per}, positive anticlockwise, and r_5 defined as the radial distance from hinge A to the tangent at the point under consideration, the right hand side of equation 7.2 is evaluated for the segment ACD only,

as the remainder of the periphery of the cut section is not caused to move tangentially by substituting $\theta_{AC} = 1$. The tangential movements considered positive in the positive direction of $s_{per.}$

For AC, $r_5 = 0$.

At G, the origin of s_{per}, $\int r_5 ds_{per} = 0 = w_5^0$

At D, $w_5^0 = \int_0^{2800} 2760 ds_{per}$ from Figure 7.1

$=7728000 \text{ mm}^2$

At C, integration from G to C against the positive direction of s_{per} gives

$$w_5^0 = -7728000 \text{ mm}^2$$

For AC, w_5^0 retains this value, as r_5 is zero in this member, and in the stationary portions of the periphery there is also no increment in w_5^0.

The values of w_5^0 over the entire cross-section are shown in Figure 7.11(a)

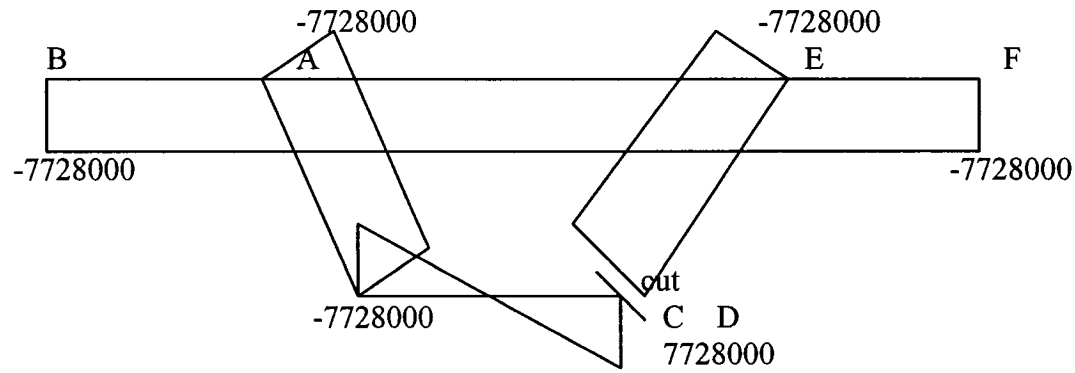

(a) Values of w_5^0 in mm^2

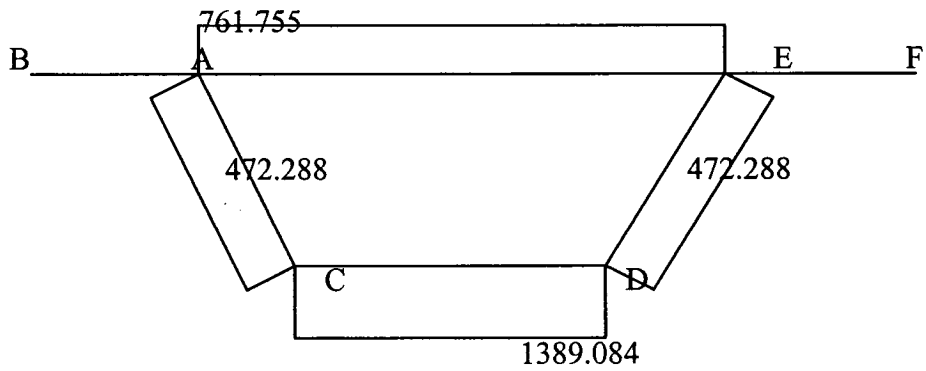

(c) Values of $\bar{v}_5$ in mm

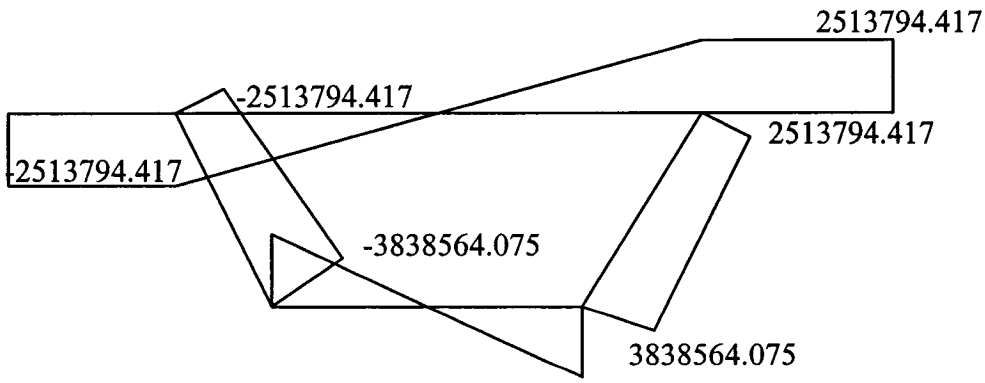

(c) Values of w_5 in mm^2

Figure 7. 11:Basic distortional warping function

At the cut, there is a discontinuity , Δw_5^0 = 7728000+7728000=15,456,000 mm^2

This represents a warping incompatibility, and is removed by calculating the unit shear stress function $\bar{v}_5$ in equation 5.4 and substituting it in equation 5.3 to obtain the compatible warping function w_5. For the single cell section, equation 5.4 becomes:

$$(\overline{v_5 h})\oint \frac{ds_{per}}{h} = \Delta w_5^0 \tag{7.3}$$

therefore substituting the value of Δw_5^0 in equation 7.3, gives:

$(\overline{v_5 h})$=15456000/(5600/170+2*2805/500+6600/310)=236144.324 mm^2

For CD , $\bar{v}_5$ = 1,389.084 mm

Similarly, the values of $\bar{v}_5$ can be evaluated for the rest of the sections.
These values of $\bar{v}_5$ are plotted in Figure 7.11(b).

From equation 5.3,

$$w_5 = w_5^0 - \int \bar{v}_5 ds_{per}$$

At G, (Figure 7.10b)

$$w_5 = 0 - 1389.084 * 0 = 0$$

At D in CD,

$$w_5 = -(7728000)-(1389.084)*(-2800)$$
$$=3838564.075 \text{ mm}^2$$

Similarly, the values of w_5 can be calculated for the remainder of the sections.

Figure 7.11(c) shows the diagram of w_5 regarded as antisymmetrical about the vertical centre line of cross-section.

The orthogonalization associated with equations 5.28,5.31 and 5.35 is now performed. Equation 5.31 has only one row with terms C_{51}, C_{52}, C_{53}, C_{11}, C_{22}, C_{33}, K_{51a}, K_{52a} and K_{53a}. Instead of C_{54}, C_{44} and K_{54a}, the terms J_{54}, J_{44} and K^*_{54a} are considered for the closed box sections as discussed in connection with equation 5.35.

Beginning with the latter group,

$$J_{44} = \int_A \bar{v}_{svt}^2 dA \tag{7.4}$$

using only the first term on the right-hand side of equation 5.21.

Substituting the value of $\bar{v}_{svt}$ fron equation 4.25 in equation 7.4

Hence, for the top flange AE, $\bar{v}_{svt}$ = 1659.539 mm

For the web AC and DE, $\bar{v}_{svt}$ = 1028.914 mm

For the bottom flange CD, $\bar{v}_{svt}$ = 3026.219 mm

Using Simpson's integration formula, for the closed portion of the section gives,

J_{44}= (6600*310/6)*[6*(1659.539)^2+----------]

=1.732*10^{13} mm^4, as found previously for C_{svt}

Again, using the first term on the right-side of equation 5.21, and referring to Figure 7.11b

$$J_{54} = \int_A \bar{v}_5 \bar{v}_{svt} dA \tag{7.5}$$

=6600*310/6*[6*761.755*1659.539]+--------

=7.951*10^{12} mm^4

Hence, from equation 5.35,

$$K_{54a}^* = -\frac{J_{54}}{J_{44}} = -0.459$$

Substituting the values of j=1,2 and 3 in equation 5.31 gives:

$C_{5j} = \int_A w_5 w_j dA$ as in equation 5.20, and the w_5 diagram is antisymmetric about the vertical centre line of cross-section, as shown in Figure 7.11(c). The w_1 and w_3 diagrams are a constant ordinate of unity and the $\tilde{y}$ coordinatly, respectively and are

symmetrical about the vertical centre line, hence $C_{51} = C_{53} = 0$ .The $w_2 (= \tilde{x})$ diagram, shown in Figure 7.7(c), is antisymmetric about the vertical centre line, hence by Simpson's integration formula,

$$C_{52} = \int_A w_5 w_2 dA$$

$$= -6.912 * 10^{16} \text{ mm}^5$$

$$C_{22} = I_y = 1.093 * 10^{14} \text{ mm}^4$$

Hence, from equation 5.31, substituting i=j=2,

$$K_{52a} = -\frac{C_{52}}{C_{22}} = 632 \text{ mm}$$

Equation 5.28 now becomes,

$$\overline{w}_5 = w_5 + K_{52a} * \tilde{x} - K^*_{54a} * \tilde{w}_{twr}$$

As the right hand lower submatrices in equations 5.32,5.33 and 5.34 are of order (1×1), there is no second stage of orthogonalization, and

$$\overline{w}_5 = \tilde{w}_5 = w_5 + 632 * \tilde{x} - 0.459 * \tilde{w}_{twr} \qquad (7.6)$$

where $w_5, \tilde{x}$ and $\tilde{w}_{twr}$ are obtained from Figures 7.11(c),7.7(c)and 7.8(b)respectively.

From equation 7.6 , $\tilde{w}_5$ can be calculated at different points of the cross-section.

The antisymmetric diagram for $\tilde{w}_5$ is shown in Figure 7.12.

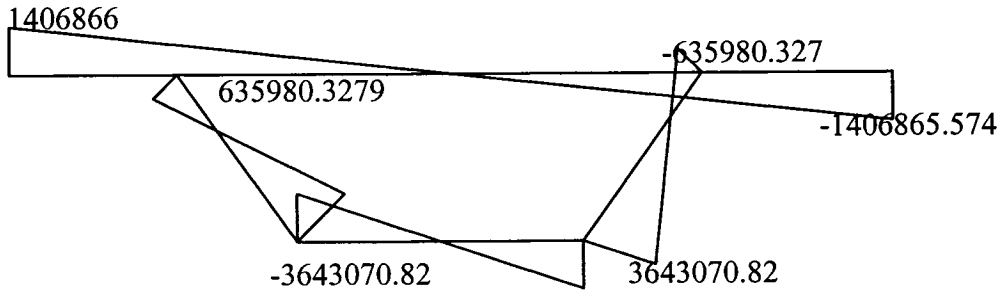

Figure 7. 12: Values of $\widetilde{w}_5$ in mm^2

The distortional warping second moment of cross-sectional area $\widetilde{C}_{55}$ will be required for the calculation of distortional warping stress. Using Simpson's rule:

$$\widetilde{C}_{55} = \int_A \widetilde{w}_5 \widetilde{w}_5 dA$$

$$= 1.781 * 10^{19} \text{ mm}^6$$

Unit transverse bending moment distribution function $\widetilde{m}_5$:

This function is determined for a frame comprising a transverse slice of the box beam, 1mm "wide" measured along the span. To represent the assumed cross-sectional distortion $\widetilde{a}_5$, a unit angular deformation is applied as shown in Figure 7.13(a), and the corresponding transverse bending moment values $\widetilde{m}_5$ are calculated, assuming that the small deflection theory is applicable.

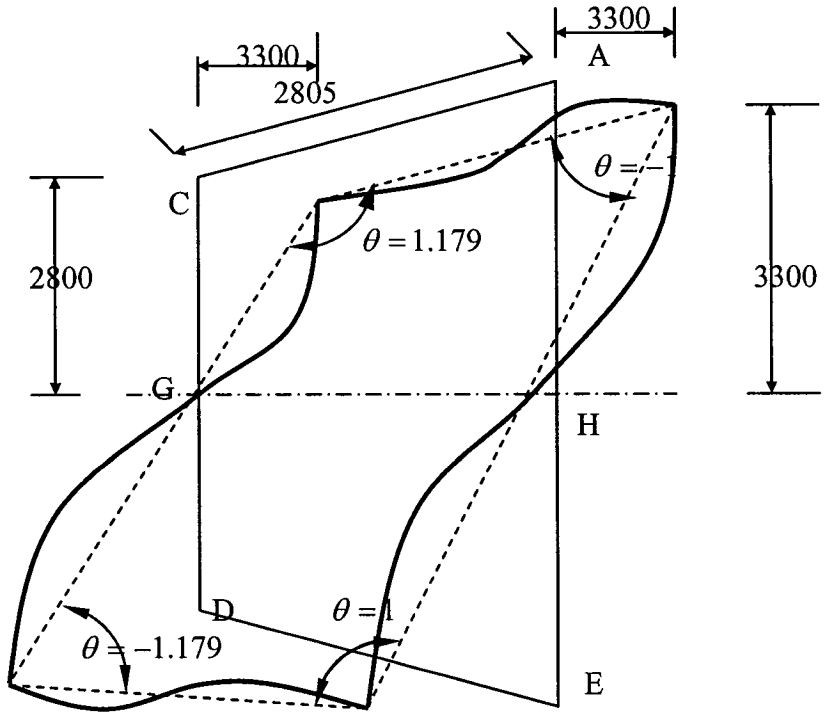

(a) **Deflected shape of frame due to imposed unit angular deformation. Dimensions in mm (not to scale)**

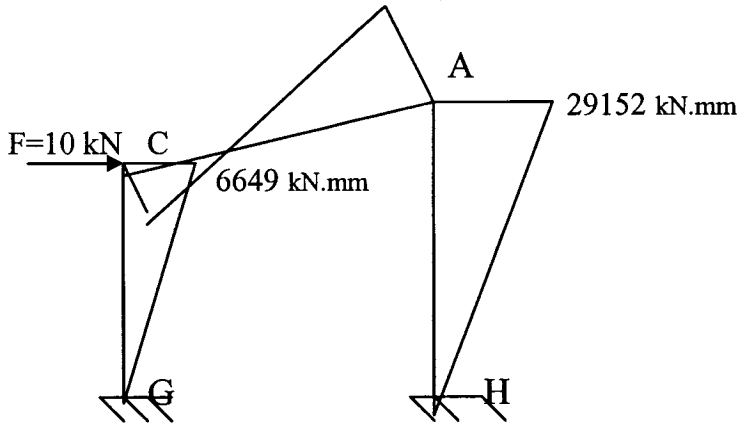

(b) Bending moment diagram and reactions for frame loaded by F=10 kN at C. ordinates plotted on tension face.

Figure 7. 13: Distortional analysis of cross-sectional frame.

Due to symmentry of the frame, the deflected shape is antisymmetric, and half the frame can be analysed , as indicated in Figure 7.13b. A dummy load F=10 kN is applied at the

corner (Figure 7.13(b), and the resulting deflections and moments are scaled to correspond with the unit angular deformation of the Figure 7.13(a). The relative angular deformations θ are taken as positive when the resulting transverse bending causes tension on the inner face of the corner angle where the members meet.

Sideway at the level of the load is calculated from Program-A [See appendix-1]

The sideway $\delta_H = 1237.97$ [Computed using the computer program-A,matrix B, element $_{11}$] for F=10 kN.

Therefore, F=26.676 kN , considering E=34.5 GPa.

Using this scaled value of F, the bending moments $\tilde{m}_5$ are plotted in Figure 7.14.

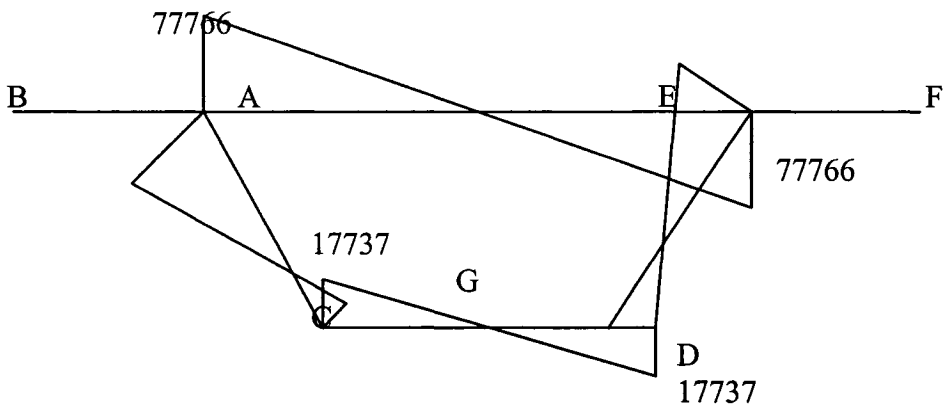

Figure 7. 14: Transverse bending moments $\tilde{m}_5$ (kN/mm/mm) due to a unit angular distortion on frame of unit "width" (Ordinates on tension face)

Transverse bending stiffness, $\tilde{B}_{55}$:

This is the only term of matrix $\underline{B}$, which is defined in equation 5.22. It acts as a spring stiffness in resisting distortion and corresponds to the foundation modulus in the beam-on-elastic foundation analogy, illustrated in Figure 7.15

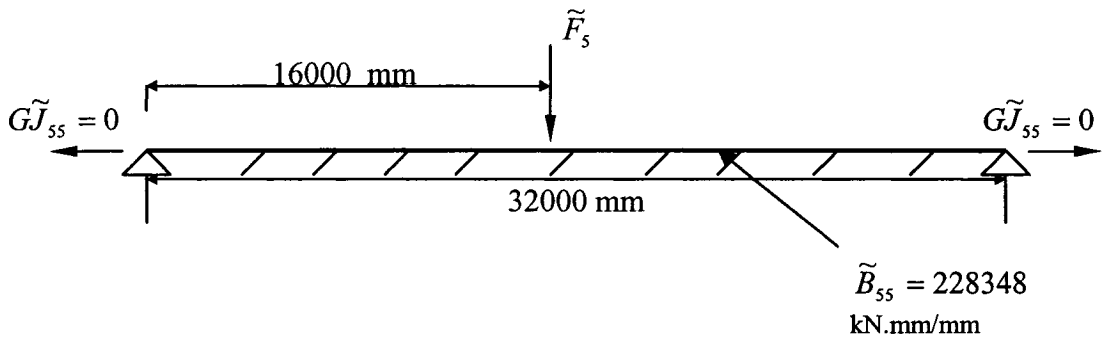

Figure 7. 15: Analogous beam on elastic foundation

From equations 5.22 and 5.16,

$$\underline{B} = (\Delta \underline{T}_1)^T \Delta \underline{T}$$

$$= (\Delta \underline{T})^T \underline{K}_t \underline{T}$$

By equation 5.14,

$$\Delta \underline{\theta} = \Delta \underline{T} \quad \text{for unit} \quad \underline{a}$$

Therefore

$$\underline{B} = (\Delta \underline{\theta})^T \underline{K}_t \Delta \underline{\theta}$$
$$= (\Delta \underline{\theta})^T \underline{M}_t$$

from equation 5.13, where $\underline{M}_t$ refers only to mode 5.

i.e., $\tilde{B}_{55} = \sum_p \tilde{m}_{p5} \Delta \theta_{p5}$ summed over nodes p.

where $\tilde{m}_{p5}$ is the transverse bending moment at node p due to a unit angular distortion $\tilde{a}_5$

and $\Delta\theta_{p5}$ is the relative rotation of the cords meeting at the node p due to a unit $\tilde{a}_5$.

As stated in equation 5.12, $\tilde{B}_{55}$ is the internal work done when unit $\tilde{a}_5$ is imposed on the frame, and is therefore also given by

$$\tilde{B}_{55} = \int (\tilde{m}_5)^2 \frac{ds_{per}}{EI_{trb}} \tag{7.7}$$

where $\tilde{m}_5$ has been defined previously as the transverse bending moment (within a member) due to a unit $\tilde{a}_5$ and I_{trb} is the second moment of the cross-sectional area of the frame member in transverse bending.

To evaluate $\tilde{B}_{55}$ numerically, use Figure 7.14 and Simpson's integration method.

$E\tilde{B}_{55}$ = [5600/(6*4.094*10^5)]*{2*(17737)^2+----------

=7878019

Therefore, $\tilde{B}_{55}$ =228,348 kN.mm/mm"width " of frame with E=34.5 GPa.

Orthogonalization of loading terms:

Consider the general transverse loading vector, $\underline{n}$,with nondistortional components, n_x and n_y. These components can be interpreted, respectively, as the product of the load and the displacement under the load and in its direction, due to the respective unit displacements $a_x = 1$ and $a_y = 1$. This is indicated in Figure 7.16a and b for n_x and n_y.

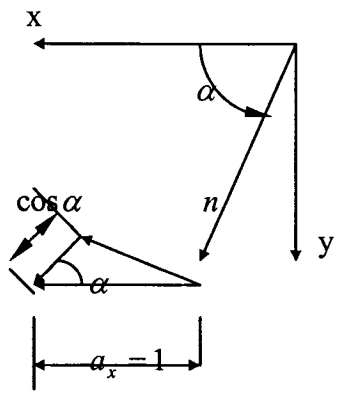

(a) $n_x = n\cos\alpha$

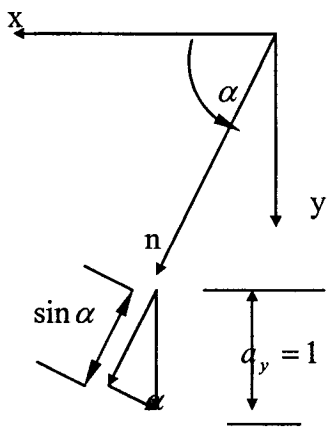

(b) $n_y = n\sin\alpha$

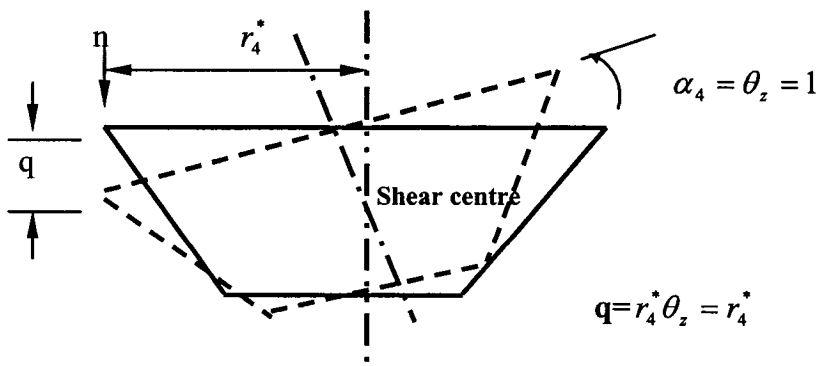

(c) Applied torque= $n_4 = nr_4^*$

Figure 7. 16: Non-distortional loading components

For warping torsion, the applied torque is the product of the transverse loading and the lever arm to the shear centre. This can also be interpreted as the product of the transverse loading and the displacement under the load and in its direction due to the unit displacement $a_4 (= \theta_4) = 1$, as shown in Figure 7.16(c) for vertical loading.

Thus, for transverse loading n, the non-distortional load components are:

$n_x = n\cos\alpha = n_2$,

$n_y = n\sin\alpha = n_3$ and

$n_4 = nr_4^*$ (for vertical loading) can be expressed as $\underline{n} = n\underline{r^*}$

where $\underline{r^*}$ is defined by analogy with equation 5.3, and r_4^* is the distance from the shear centre to the line of action of the load. The components n_2,n_3 and n_4 are already orthogonalized, as they refer to the principal axes of the cross-section and the shear centre. Hence $n_2 = \bar{n}_2$, $n_3 = \bar{n}_3$ and $n_4 = \bar{n}_4$.

Extending the above interpretation of the load components to the loading in distortional modes, the loading $\bar{n}_5$ in the single cell box beam requires consideration of the displacements in mode 5, using the vector $\underline{\bar{r}^*} = \underline{K}_a \underline{r}^*$.

Thus, as in equations 5.28 and 5.35 for $\underline{\bar{w}}$,

$$\bar{r}_5^* = r_5^* + K_{51a} r_1^* + K_{52a} r_2^* + K_{53a} r_3^* + K_{54a}^* r_4^*$$

This shows that $\bar{r}_5^*$ is composed of the basic quantity r_5^* and the components added to it by orthogonalization. Similarly, the orthogonalized distortional loading $\bar{n}_5$ can be put together as a sum of the components, arising from the displacements under the load n and its direction due to the unit deformations , $a_5 = 1 = a_x = a_y = a_z = \theta_z$. Thus

$$\bar{n}_5 = n(r_5^* + K_{51a}r_1^* + K_{52a}r_2^* + K_{53a}^*r_3^* + K_{54a}^*r_4^*$$

$$= n_5 + K_{51a}\bar{n}_1 + K_{52a}\bar{n}_2 + K_{53a}\bar{n}_3 + K_{54a}^*\bar{n}_4$$

Now $r_1^* = 0$ from equation 5.3 , so that $\bar{n}_1 = 0$ for transverse loading. Also, for vertical loading, $n_x = 0 = \bar{n}_2$.

As the w_5 diagram (Figure 7.11c) is antisymmetric and the $w_3 (= \tilde{y})$ diagram is symmetric about the vertical centre line of the cross-section; C_{53} in equation 5.31 is zero and K_{53a} is also zero.Hence, for vertical loading,

$$\bar{n}_5 = n_5 + K_{54a}^*\bar{n}_4 \tag{7.8}$$

The component n_5 arises from the displacements due to distortion of the cross-sectional frame, which give rise to moments $\tilde{m}_5$ .These displacements r_5^* are represented in Figure 7.13(a) by the differences between the deflected shape drawn as the solid curve and the deflected hinged polygon drawn as the dased lines, plus the deflection of the hinged polygon in Figure 7.10(a).

From this expression, Sedlacek(1971) constructed an influence line for $\bar{n}_5$ laterally moving the vertical load and this can be used to design for distortional effects. As noted previously, the symbol - may be replaced by ~ , as there is no second stage of orthogonalization needed.

For the concentrated live loading shown in Figure 7.1, n is replaced by $F_y = 1000$ kN.Also, $\bar{n}_4$ is now $T_{ext} = 1000 * 3300 = 3.3 * 10^6$ kN.mm. K_{54a}^* has previously been found to be -0.459. For the mode of distortion, $a_5 = 1$, shown in Figure 7.13a, r_5^* is zero at A, since the solid and dased deflection shapes coincide at this point, there is no deflection at point A (Figure 7.10a). Hence, in equation 7.8, using $\underline{F}$ to represent a vector of concentrated transverse loading, the component of $\underline{F}$ in mode 5 is,

$$\text{of } \overline{F}_5 = \widetilde{F}_5 = F_5 + K^*_{54a} T_{ext} \tag{7.9}$$

Substituting the values in equation 7.9 gives:

$$\overline{F}_5 = \text{-}1514754 \quad \text{kN.mm}$$

Use of the beam-on-elastic-foundation analogy to evaluate distortional effects:

The beam and the loading to be considered are shown in Figure 7.15.

The following quantities are required:

Concentrated load: $\widetilde{F}_5$ = -1514754 kN.mm

Axial load, $= G\widetilde{J}_{55} = 0$

The foundation modulus,

$$= \widetilde{B}_{55} = 228348 \text{ kN.mm/mm}$$

The flexural rigidity,

$$E\widetilde{C}_{55} = 6.147 * 10^{20} \text{ kN.mm}^4$$

The end conditions are simply supports, as the end diaphragms are assumed to prevent distortion but not warping.

Hetenyi (1946) developed the following expressions for deflection a_y, moment M_x and shear V_y at midspan, for a beam on elastic foundation, loaded and supported as shown in Figure 7.15.

$$a_y = \frac{F_y \lambda^*}{2k_{fdn}} \frac{\sinh \lambda^* 1 - \sin \lambda^* 1}{\cosh \lambda^* 1 + \cos \lambda^* 1} \tag{7.10}$$

$$M_x = \frac{F_y}{4\lambda^*} \frac{\sinh \lambda^* 1 + \sin \lambda^* 1}{\cosh \lambda^* 1 + \cos \lambda^* 1} \tag{7.11}$$

$$V_y = \frac{F_y}{2} \text{ just to the left at midspan} \tag{7.12}$$

where

F_y= concentrated load at midspan

l= span

k_{fdn} = foundation modulus

$$\lambda^* = \sqrt[4]{\frac{k_{fdn}}{4EI}}$$

EI= flexural rigidity of beam

Applying equations 7.10-7.12 to the box beam problem, at the section just to the left of midspan,

Substituting the values of $\widetilde{B}_{55}$ and $\widetilde{C}_{55}$, gives:

$$\lambda^* = \sqrt[4]{\widetilde{B}_{55} / 4E\widetilde{C}_{55}} = 9.816*10^{-5} \text{ mm}^{-1}$$

$\lambda^* l$ = 3.141

From equation 7.10, $a_y = -0.0004$, it is dimensionless, and represents an angle of cross-sectional distortion in the box beam, corresponding to $\widetilde{a}_5$ in equation 5.15.

From equation 7.11,

M_x = -4206325770 kN.mm^2 , M_x correpond to $\widetilde{M}_5$

Again $V_y = F_5 / 2$ =-757377.049 kN.mm, V_y represents the derivative with respect to z of the bimoment, (Maisel and Roll1974) on distortional warping shear stresses. It correspond to $\widetilde{V}_5$.

Distortional warping stresses due to live load:

Connection to previous text as f_5

$$f_5 = \frac{\widetilde{M}_5}{\widetilde{C}_{55}} \widetilde{w}_5 \tag{7.13}$$

Using the values of $\widetilde{w}_5$ given in Figure 7.12 and substituting the values of $\widetilde{M}_5$ and $\widetilde{C}_{55}$, the distortional warping stresses are calculated at different points of the cross-section.

These stresses are plotted in Figure 7.17(a).

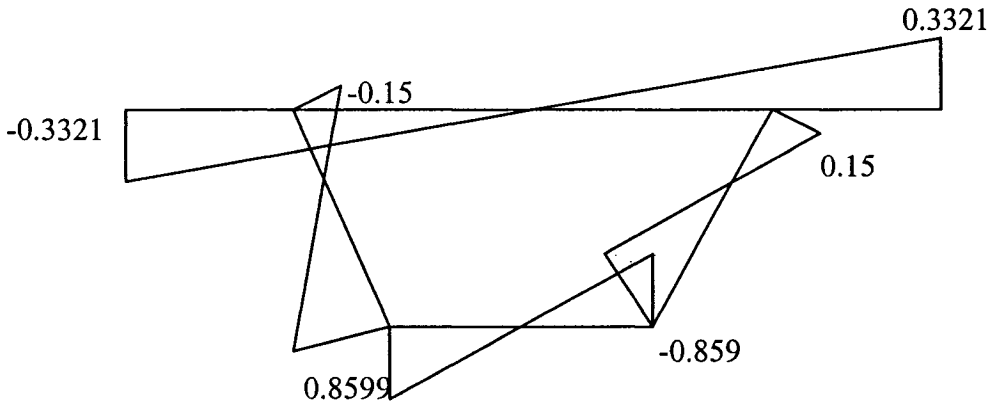

(a) Distortional warping stress f_5 at midspan section(MPa)

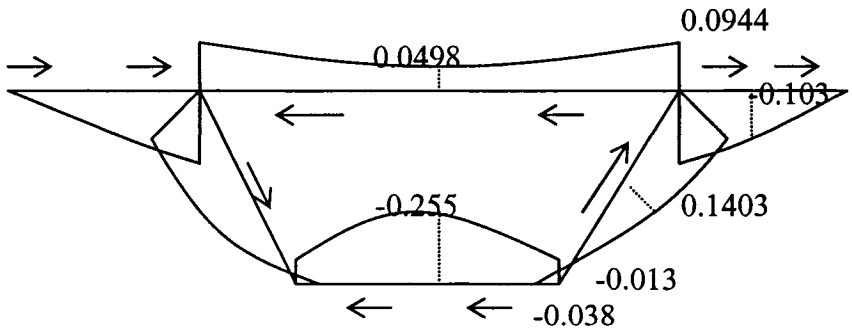

(b) Distortional warping shear stress v_5 on positive face section z=16000 mm

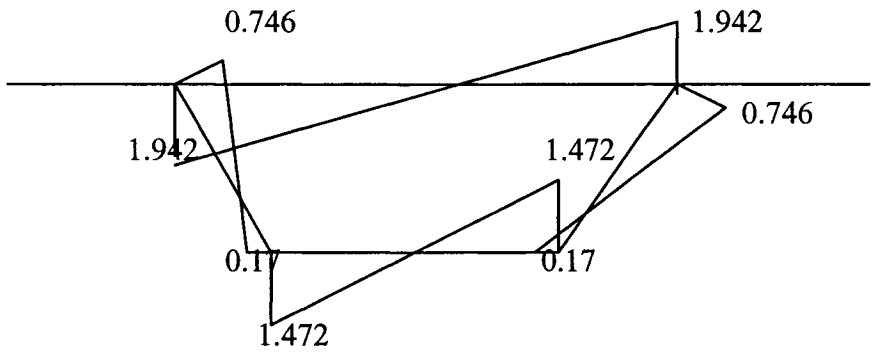

(c) Maximum transverse bending stress f_{trb5} at midspan section(extreme fibre stress) ordinates drawn on the tension face.

Figure 7. 17: Diagrams of live load stresses f_5, v_5 and f_{trb5} (MPa) ,due to distortion calculated using the beam on elastic foundation analogy

Distortional warping shear stress:

Consider the positive face of the cross-section at z=16000 mm, i.e just to the left of the midspan applied load.

The following equations due to Maisel (1982) are used for the evaluation of the distortional warping stresses.

$$v_5 = -\frac{\tilde{v}_5}{\tilde{C}_{55}}\frac{\tilde{S}_5}{h} \tag{7.14}$$

$$\tilde{S}_5 = \tilde{S}_{50} - \tilde{v}_5 \tag{7.15}$$

$$\tilde{v}_5 \oint \frac{ds_{per}}{h} = \oint \frac{\tilde{S}_{50}}{h} ds_{per} \tag{7.16}$$

Where $\widetilde{S}_{50}$ is the moment of area $\int \widetilde{w}_5 dA$ for the statically determinate, section, and will now be evaluated with the cut at the centre of the bottom flange, as shown in Figure 7.18a.

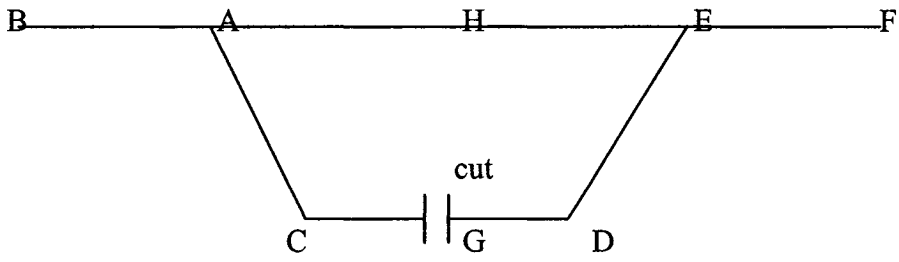

(a) **Statically determinate section**

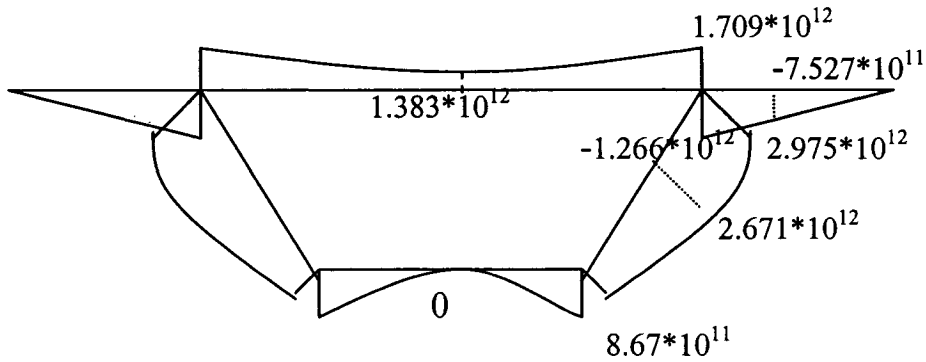

(b) Values of $\widetilde{S}_{50}$ in mm^4

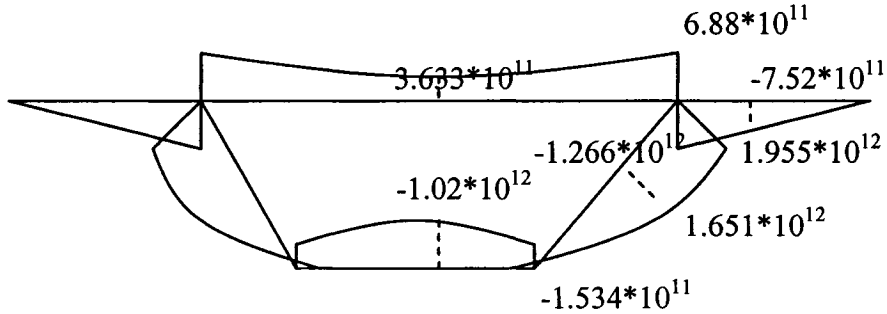

(c) Values of $\widetilde{S}_5$ in mm^4

Figure 7. 18:Diagrams of moments of area for evaluating distortional warping shear stress

Taking the origin of s_{per} at the cut, the values of $\widetilde{S}_{50}$ Iis calculated.

At G, $\widetilde{S}_{50} = 0$

At D, $\widetilde{S}_{50}$ = 170*2800*0.5*-3643070.82=$8.67*10^{11}$ mm^4 (from Figure 7.1 and 7.12)

Similarly, the values of $\widetilde{S}_{50}$ can be calculated for the remainder of the section

Figure 7.18b shows the values of $\widetilde{S}_{50}$ plotted round the periphery of the cross-section.

From equation 7.16,

$\oint \frac{\widetilde{S}_{50}}{h} ds_{per}$ =(5600/6*170)[2*$8.67*10^{11}$]+----------[from Figures 7.1 and 7.18b]

=$6.679*10^{13}$ mm^4

and $\oint \frac{ds_{per}}{h}$ =6600/310+2*2805/500+5600/170=65.45 [from Figure 7.1]

Therefore, $\widetilde{v}_5 = 1.02*10^{12}$ (from equation 7.16).
Now $\widetilde{S}_5$ can be calculated from equation 7.15 and the values are plotted in Figure 7.18(c).

The, distortional warping shear stress are calculated from equation 7.14 and are plotted in Figure 7.17(b) together with the physical directions in which they act on the positive face of cross-section at mispan.

Transverse bending stresses due to live load:

The transverse bending moments M_t in each distortional mode are given by equations 5.13,5.14 and 5.15 once $\tilde{a}$ is known. Hence, the transverse bending stress f_{trbi} ate i at the extreme fibres are

$$f_{trbi} = \frac{6}{h^2} M_t \tag{7.17}$$

In equation 7.17 , the extreme fibre stresses, f_{trb5}, require a knowledge of the transverse bending moments, M_t, at the nodes of the cross-section in the deflected shape corresponding to mode 5, under the given midspan concentrated load of 1000 kN over one web. Figure 7.14 shows the bending moments $\tilde{m}_5$ (kN.mm/mm) due to unit angular distortion $\tilde{a}_5$ (Figure 7.13a). Application of the beam-on-elastic foundation analogy has already given the value of $\tilde{a}_5$ at midspan as –0.0004. Hence, from equation 7.17

$$f_{trb5} = \frac{6}{h^2}(-0.0004)\tilde{m}_5. \tag{7.18}$$

The negative sign indicates that the sense of distortion under the given loading is opposite to that selected arbitrarily as positive in Figure 7.13(a)

Substituting the values of $\tilde{m}_5$ from Figure 7.14 in equation 7.18, the transverse bending stress is calculated at different points of the cross-section. Figure 7.17(c) shows the values of f_{trb5} plotted on the tension face.

7.1.5 Analysis of shear lag effects:

7.1.5.1 Assumption:

Since torsional and distortional effects are not being considered in the treatment of shear lag, the live loading of Figure 7.1 will be regarded as acting at the vertical centre-line of cross-section.

7.1.5.2 Basic shear lag warping function $\underline{w}_v$ and section properties $\underline{C}_v$ and $\underline{S}_v$:

Parabolic warping functions:

Three parabolic warping functions w_{5v}, w_{6v} and w_{7v} are chosen to represent shear lag displacements in the flanges under symmetric downward loading. These functions are shown in Figures 7.19(a), 7.20(a) and 7.21(a)

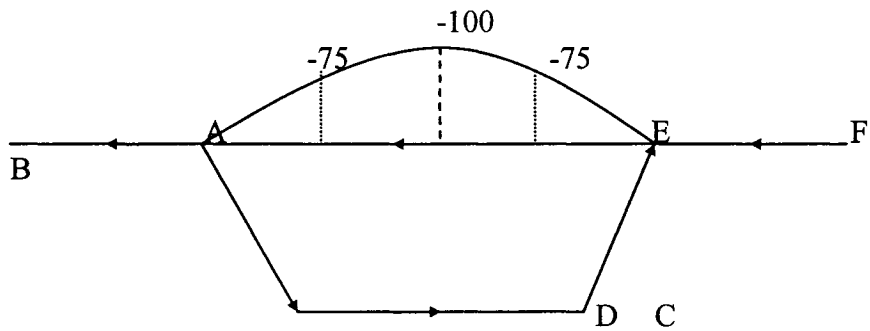

(a) Function w_{5v}

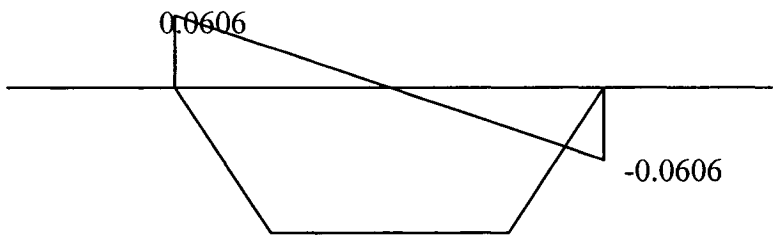

(b) Function $\dot{w}_{5v}$

Figure 7. 19: Basic shear lag warping functions w_{5v} and $\dot{w}_{5v}$

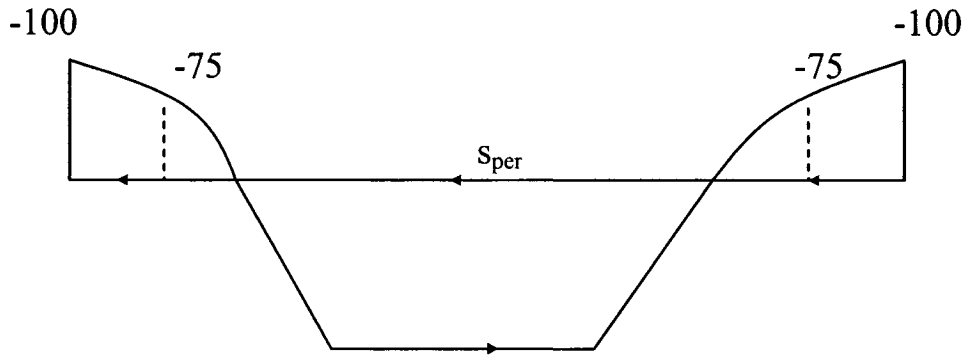

(a) Function w_{6v}

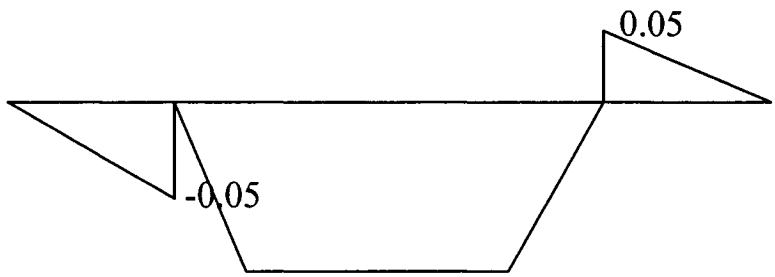

(b)Function $\dot{w}_{6v}$ (mm^{-1})

Figure 7. 20: Basic shear lag functions w_{6v} and $\dot{w}_{6v}$

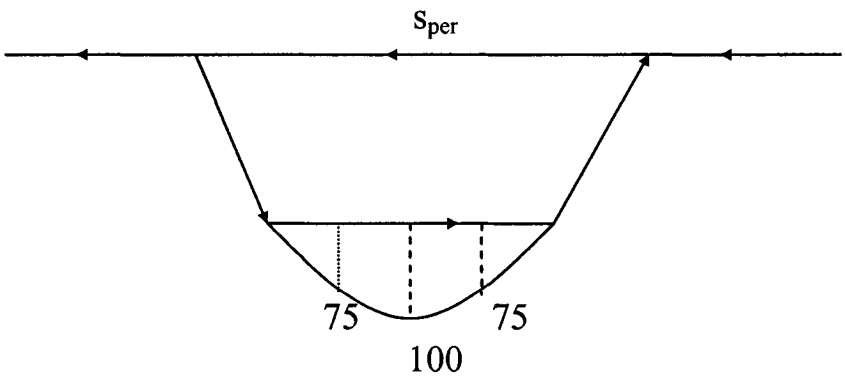

(a) Function w_{7v}

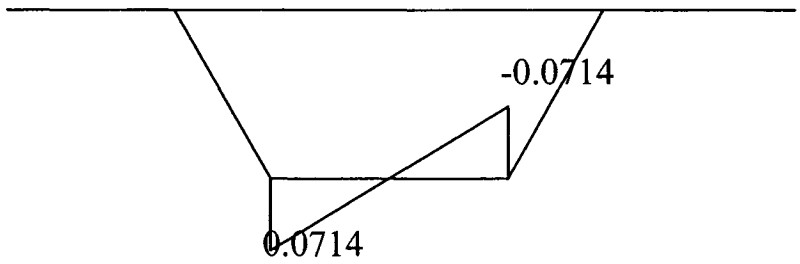

(a) Function $\dot{w}_{7v}$(mm^{-1})

Figure 7. 21: Basic shear lag warping functions w_{7v} and $\dot{w}_{7v}$

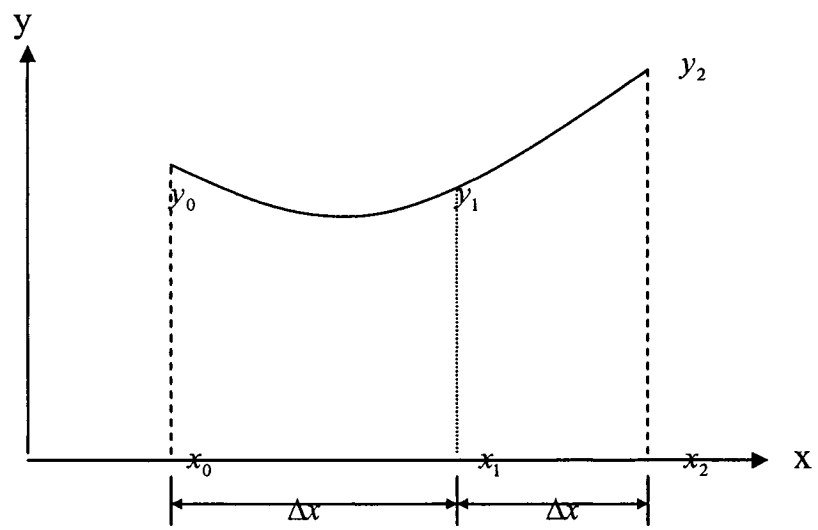

Figure 7. 22: Parabolic function

The ordinates of 100 are arbitrary, and the units are assumed to be dimensionless.

Equation 6.13 shows that $\dot{w}_v$ is required and the functions are calculated using the following equations .For the general parabolic function in Figure 7.22, with ordinates y_0, y_1 and y_2, the derivatives are:

$$\text{At } x_0,\ \frac{dy}{dx} = \frac{1}{\Delta x}(-\frac{3}{2}y_0 + 2y_1 - \frac{1}{2}y_1) \tag{7.19}$$

$$\text{At } x_1,\ \frac{dy}{dx} = \frac{1}{2\Delta x}(y_2 - y_0) \tag{7.20}$$

$$\text{At } x_2,\ \frac{dy}{dx} = \frac{1}{\Delta x}(\frac{1}{2}y_0 - 2y_1 + \frac{3}{2}y_2) \tag{7.21}$$

These functions are plotted in Figures 7.19(b),7.20(b) and 7.21(b)

7.1.5.3 Evaluation of $\underline{C}_v$:

Using equation 6.12, the elements of $\underline{C}_v$ involving w_{5v}, w_{6v} and w_{7v} will now be determined. Figures 7.19(a), 7.20(a) and 7.21(a) show that these three functions are symmetric about the vertical centre line of the cross-section, as are $w_1 (= 1)$ at all points of cross-sections and $w_3 (= \tilde{y})$. From Figures 7.7(c) and 7.8(b), $w_2 (= \tilde{x})$ and $w_4 (= \tilde{w}_{twr})$ are antisymmetric, so that

$$C_{52v} = 0 = C_{62v} = C_{72v} = C_{54v} = C_{64v} = C_{74v}$$

In addition, $C_{65v} = 0 = C_{75v} = C_{76v}$ can be noted, from the range of definition of w_{5v}, w_{6v} and w_{7v}

The non-zero elements are obtained using Simpson's integration formula.

$C_{51v} = \int_A w_{5v} w_1 dA$ =6600*310/6*[0+4*(-100)(1)+0]= -136,400,000 mm^2 [from Figure7.1]

Similarly, $C_{61v}.C_{71v}$ are calculated.

C_{53v}=6600*310/6*[0+4*(-100)(-785)+0]=1.070*10^{11} mm^3 [$\tilde{y} = 785$]

Similarly C_{63v} and C_{73v} are calculated as:

In evaluating C_{55v}, C_{66v} and C_{77v} the integrads are fourth order functions, since

w_{5v}, w_{6v} and w_{7v} are parabolic. For these three functions, the following equations are used:

$$\int_{x_0}^{x_2} y^2 dx = \frac{\Delta x}{3}(y_0^2 + 4y_1^2 + y_2^2) - \frac{4}{15}\Delta x(\frac{y_0 + y_2)}{2} - y_1)^2 \qquad (7.22)$$

The matrix $\underline{C}_v$ is now formed formed. These processes are included in the Mathematica.See Appendix-1, program-B.

7.1.5.4 Evaluation of $\underline{S}_v$:

Equation 6.13 will be used, and can be noted that $\dot{w}_{iv}$ in the flanges is either zero or symmetrical about the vertical centre line of the cross-section, for values of i from 1 to 4. Figures 7.19(b), 7.20(b) and 7.21(b) show that $\dot{w}_{iv}$ is antisymmetric for values of i from 5 to 7, so that the non-zero elements of $\underline{S}_v$ are $\underline{S_{55v}}, \underline{S_{66v}}$ and $\underline{S}_{77v}$,and

$\underline{S}_{55v} = 6600*310/6*[2*(0.0606)^2]$ [from Figure 7.1 and 7.19(b)]

Similarly, the other values of $\underline{S}_{55v}$ can be calculated for the different sections. This would lead to the formation of the $\underline{S}_v$ matrix.

Now $\underline{S}_v$ matrix is formed.

First stage of orthogonalization:

From equation 6.19,

$$K_{51av} = -\frac{C_{51v}}{C_{11}} = 16.467$$

Similarly, the values of the K_{61av}, K_{71av} are calculated.

Here, $K_{52av} = 0 = K_{62av} = K_{72av}$

$$K_{53av} = -\frac{C_{53v}}{C_{33}} = -0.01149$$

Similarly, the values of K_{63av}, K_{73av} are calculated.

Again, $K_{54av} = 0 = K_{64av} = K_{74av}$

Now from equation 6.15, $\underline{K}_{av}$ matrix is formed. These process are included in the Mathematica.See Appendix-1,Program-B.

Evaluation of $\overline{\underline{C}}_v$ matrix:

From equation 6.20

$$\overline{\underline{C}}_v = K_{av}\underline{C}_v K_{av}^T$$

Now $\overline{\underline{C}}_v$ matrix is formed using Mathematica (See Appendix-1, program-B)

Evaluation of $\overline{\underline{S}}_v$ matrix:

From equation 6.21

$$\overline{\underline{S}}_v = \underline{K}_{av}\underline{S}_v\underline{K}_{av}^T = \underline{S}_v$$

Using Mathematica Program B, find the $\overline{\underline{S}}_v$ matrix.

7.1.5.5 Second stage of orthogonalization:

Considering only the right-hand lower submatrices, $\overline{\underline{C}}_v$ and $\overline{\underline{S}}_v$
equation 6.27 gives:

$$\left|\overline{\underline{C}}_v - \lambda\overline{\underline{S}}_v\right| = 0$$

Using the Mmathematica subroutine-C , the eigenvalues are calculated to be:

$$\{\{\lambda \to 1.3298\times10^6\}, \{\lambda \to 1.9036\times10^6\}, \{\lambda \to 5.35916\times10^6\}\}$$

Evaluation of vectors:

Subroutines D,E and F [Appendix-1] help evaluate the first,second and the third eigenvectors.The eigenvectors are as follows:

First eigenvector is [-0.555099,-0.488713,-0.673071]=[1, 0.88, 1.21]=[1_{11v} 1_{12v} 1_{13v}]

[from subroutine-D,Appendix-1]

The second eigenvector is [-0.431985, -0.34487, 0.833339]=[1.25, 1 , -2.42]=[1_{21v} 1_{22v} 1_{23v}]

[from subroutine-E,Appendix-1]

The third eigenvector is [0.573315, -0.81886 , 0.02789]=[20.55, -29.36 ,1]=[1_{31v} 1_{32v} 1_{33v}]

[from subroutine –F,Appendix-1]

Hence matrix $\underline{K}_{bv}$ is formed. [Program-B, Output B13]

$$\begin{pmatrix} 1 & 0 & 0 & 0 & 0 & 0 & 0 \\ 0 & 1 & 0 & 0 & 0 & 0 & 0 \\ 0 & 0 & 1 & 0 & 0 & 0 & 0 \\ 0 & 0 & 0 & 1 & 0 & 0 & 0 \\ 0 & 0 & 0 & 0 & 1 & 0.88 & 1.21 \\ 0 & 0 & 0 & 0 & 1.25 & 1 & -2.42 \\ 0 & 0 & 0 & 0 & 20.55 & -29.36 & 1 \end{pmatrix}$$

From equation 6.23 ,

$$\underline{K}_v = \underline{K}_{bv}\underline{K}_{av}$$

From Program-B[Output- B14],Appendix –1, establish the $\underline{K}_v$ matrix as:

$$\begin{pmatrix} 1. & 0. & 0. & 0. & 0. & 0. & 0. \\ 0. & 1. & 0. & 0. & 0. & 0. & 0. \\ 0. & 0. & 1. & 0. & 0. & 0. & 0. \\ 0. & 0. & 0. & 1. & 0. & 0. & 0. \\ 16.4675 & 0. & -0.0114953 & 0. & 1. & 0.88 & 1.21 \\ 19.9606 & 0. & -0.0139337 & 0. & 1.25 & 1. & -2.42 \\ -7.66228 & 0. & -0.013457 & 0. & 20.55 & -29.36 & 1. \end{pmatrix}$$

From equation 6.24,

$$\underline{\tilde{C}}_v = \underline{K}_{bv}\,\underline{\bar{C}}_v\,\underline{K}_{bv}^T$$

From Program-B[Output- B16], Appendix –1, establish the $\underline{\tilde{C}}_v$ matrix as:

$$\begin{pmatrix} 8.283\times10^{6} & 0. & 0. & 0. & 1.74092 & -3.44798 & 1.33657 \\ 0. & 1.09037\times10^{14} & 0. & 0. & 0. & 0. & 0. \\ 0. & 0. & 9.315\times10^{12} & 0. & -1.45109\times10^{7} & 1.14682\times10^{6} & 5.11085\times10^{7} \\ 0. & 0. & 0. & 1.93915\times10^{19} & 0. & 0. & 0. \\ 1.74092 & 0. & -1.45109\times10^{7} & 0. & 8.34509\times10^{9} & 3.47766\times10^{8} & 2.69685\times10^{8} \\ -3.44798 & 0. & 1.14682\times10^{6} & 0. & 3.47766\times10^{8} & 2.99942\times10^{10} & -1.31737\times10^{9} \\ 1.33657 & 0. & 5.11085\times10^{7} & 0. & 2.69685\times10^{8} & -1.31737\times10^{9} & 1.52381\times10^{13} \end{pmatrix}$$

From equation 6.25,

$$\underline{\tilde{S}}_v = \underline{K}_{bv}\,\underline{\bar{S}}_v\,\underline{K}_{bv}^T$$

$\underline{\tilde{S}}_v$ matrix [from Program-B,Output B17,Apendix-1] can be formulated as:

$$\begin{pmatrix} 0. & 0. & 0. & 0. & 0. & 0. & 0. \\ 0. & 0. & 0. & 0. & 0. & 0. & 0. \\ 0. & 0. & 0. & 0. & 0. & 0. & 0. \\ 0. & 0. & 0. & 0. & 0. & 0. & 0. \\ 0. & 0. & 0. & 0. & 6476.06 & 209.454 & 32.0744 \\ 0. & 0. & 0. & 0. & 209.454 & 15462.6 & -257.912 \\ 0. & 0. & 0. & 0. & 32.0744 & -257.912 & 2.84126\times10^{6} \end{pmatrix}$$

Neglecting the small off-diagonal terms, $\underline{\tilde{S}}_v$ is a diagonal matrix; the non-zero terms are dimensionless.

7.1.5.6 Orthogonalization of $\underline{w}_v$ and $\underline{r}_v$:

From equation 6.31,

$$\underline{\tilde{w}}_{5v} = \underline{K}_v \underline{w}_v$$

Using $\underline{K}_v$ [Program-B,Output B14,Appendix-1] matrix, the following three equations are formed.

$$\tilde{w}_{5v} = 16.4675 - 0.01149\tilde{y} + w_{5v} + 0.88w_{6v} + 1.21w_{7v} \quad (7.23)$$

$$\tilde{w}_{6v} = 19.96 - 0.01393\tilde{y} + 1.25w_{5v} + w_{6v} - 2.42w_{7v} \quad (7.24)$$

$$\tilde{w}_{7v} = -7.66 - 0.0134\tilde{y} + 20.55w_{5v} - 29.36w_{6v} + w_{7v} \quad (7.25)$$

The inclusion of the $\tilde{w}(=1)$ and $\tilde{w}(=\tilde{y})$ terms in the above equations means that $\tilde{w}_{5v}, \tilde{w}_{6v}$ and $\tilde{w}_{7v}$ exist both in the flanges and in the webs.

For the vertical loading on the vertical centre-line of the cross-section, from equations 6.8 and 6.30 with $\alpha = \pi/2$,

$$\underline{r}_v = \begin{bmatrix} 0 \\ 0 \\ 1 \\ 0 \\ \cdots \\ 0 \\ 0 \\ 0 \end{bmatrix}$$

Therefore, $\underline{\tilde{r}}_v = \underline{K}_v \underline{r}_v$

From the Mathematica Program-B[Output B18], Appendix-1, establish the $\underline{\tilde{r}}_v$ matrix as follows:

$$\begin{pmatrix} 0. \\ 0. \\ 1. \\ 0. \\ -0.0114953 \\ -0.0139337 \\ -0.013457 \end{pmatrix}$$

Orthogonalization of $\underline{\dot{w}}_v$

The matrices $\underline{S}_v$ and $\underline{\bar{S}}_v$ are populated only in their right-hand lower submatrices in equations 6.13 and 6.21 .This will also be true of $\underline{\tilde{S}}_v$ in equation 6.25. Hence, the terms involving $\tilde{w}_1(=1)$ and $\tilde{w}_3(=\tilde{y})$ in equations 7.23,7.24 and 7.25 must be omitted when these equations are differentiated with respect to s_{per} to give $\underline{\dot{\tilde{w}}}_v$, which accordingly exists only in the flanges.Thus:

$$\dot{\tilde{w}}_{5v} = \dot{w}_{5v} + 0.88\dot{w}_{6v} + 1.21\dot{w}_{7v} \qquad 7.23(a)$$

$$\dot{\tilde{w}}_{6v} = 1.25\dot{w}_{5v} + \dot{w}_{6v} - 2.42\dot{w}_{7v} \qquad 7.24(a)$$

$$\dot{\tilde{w}}_{7v} = 20.55\dot{w}_{5v} - 29.36\dot{w}_{6v} + \dot{w}_{7v} \qquad 7.25(a)$$

The diagrams of $\tilde{w}_{5v}, \tilde{w}_{6v}$, $\tilde{w}_{7v}$ and $\dot{\tilde{w}}_{5v}, \dot{\tilde{w}}_{6v}$, $\dot{\tilde{w}}_{7v}$ obtained using equations 7.23-7.25 and 7.23(a)-7.25(a)are shown in Figures 7.23, 7.24 and 7.25 .

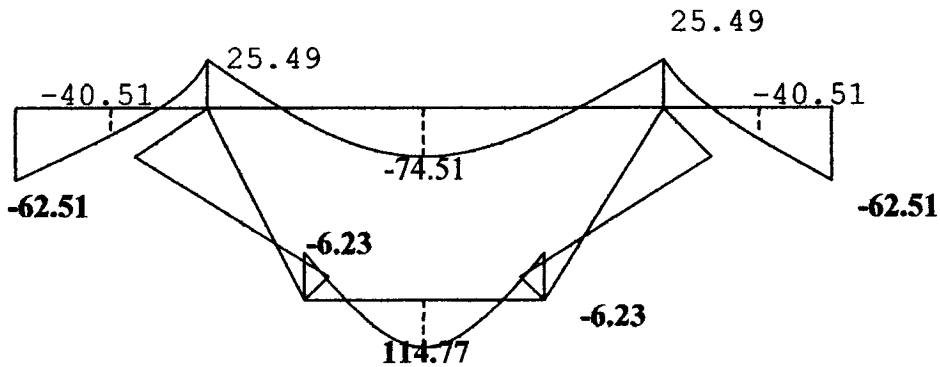

(a) Function $\tilde{w}_{5v}$

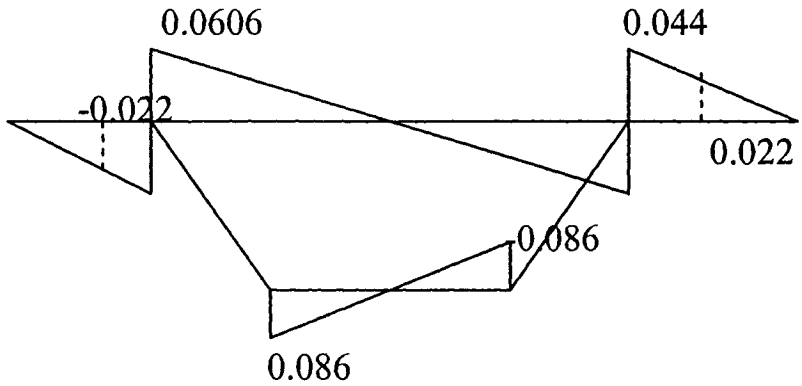

(b) Function $\dot{\tilde{w}}_v$ (mm^{-1})

Figure 7. 23:Orthogonalized shear lag warping functions ($\tilde{w}_{5v}$ and $\dot{\tilde{w}}_{5v}$)

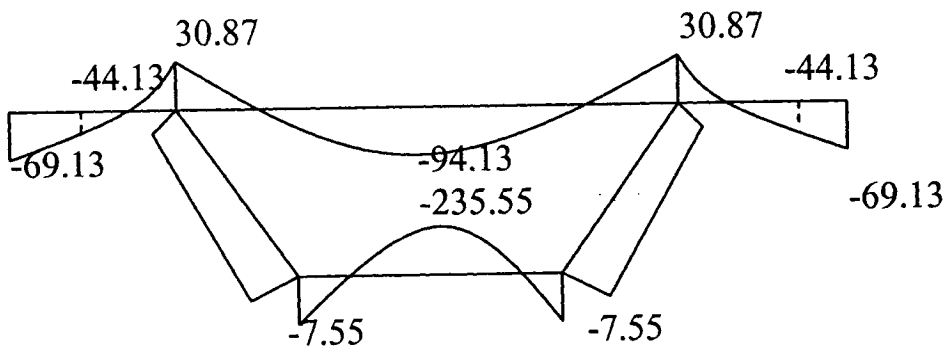

(a) **Function $\tilde{w}_{6v}$**

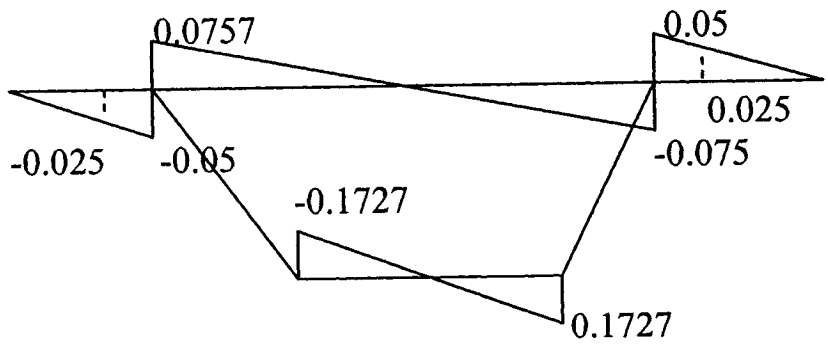

(b) Function $\dot{\tilde{w}}_{6v}$ (mm^{-1})

Figure 7. 24:Orthogonalized shear lag warping functions $\tilde{w}_{6v}$ and $\dot{\tilde{w}}_{6v}$

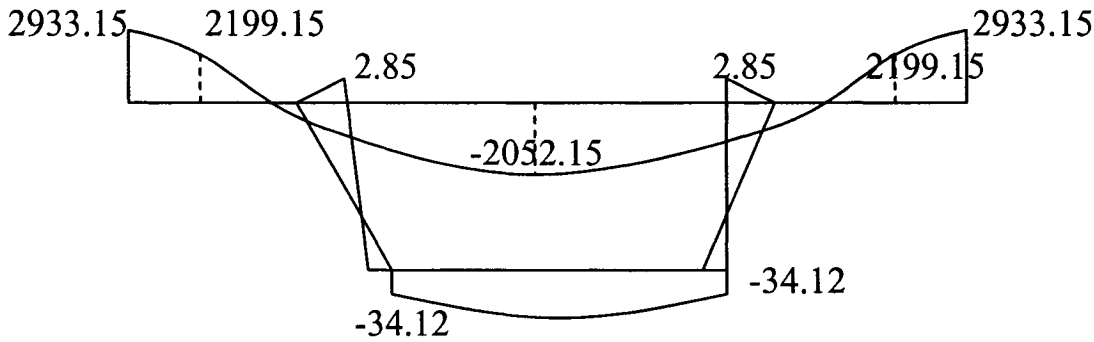

(a) Function $\tilde{w}_{7v}$

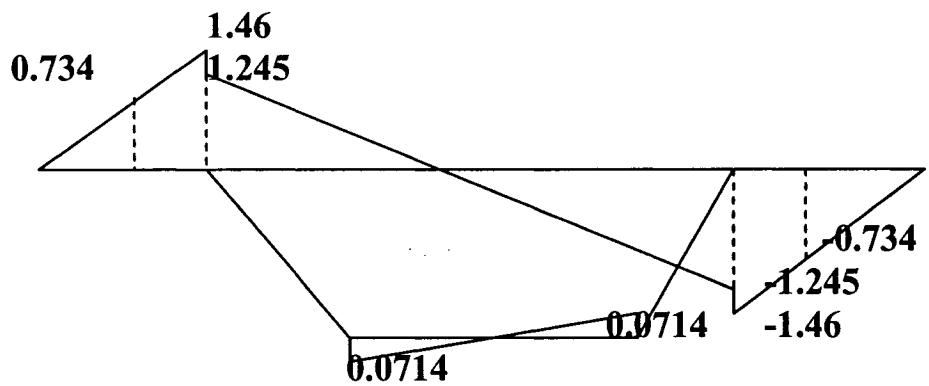

(b) Function $\dot{\tilde{w}}_{7v}$ (mm^{-1})

Figure 7. 25: Orthogonalized shear lag warping functions $\tilde{w}_{7v}$ and $\dot{\tilde{w}}_{7v}$

7.1.5.7 Solution of the analogous beam problem for shear lag effects. Mode-5 as defined by Maisel (1982)

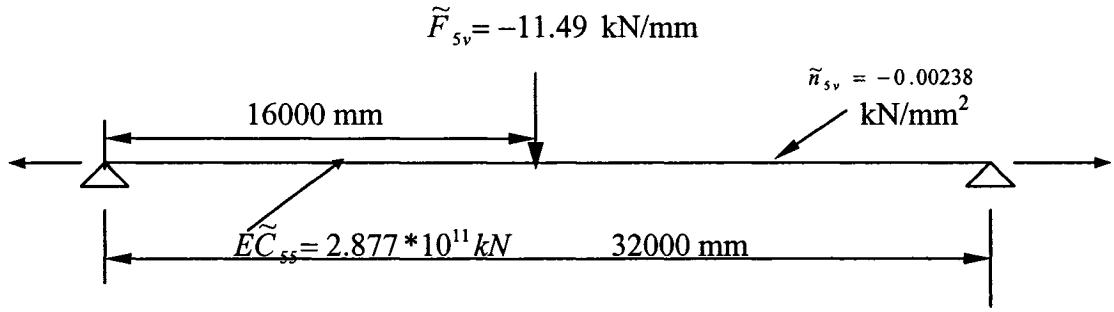

Figure 7. 26: Analogous beam for shear lag analysis in mode 5

Applying the analogy to shear lag mode 5 for the box beam behaviour, the beam and loading are shown in Figure 7.26. The following quantities are required.Figure 7.19(a) represents the mode 5 of shear lag behaviour of the box beam.

Concentrated live load	$= \tilde{F}_{5v}=F_y\tilde{r}_{5v}$	=-11.49 kN/mm
Distributed dead load	$=\tilde{n}_{5v}=n_y\tilde{r}_{5v}$	=-0.00238 kN/mm^2
Axial load	$=G\tilde{S}_{55v}$	= 97189.47 kN/mm^2
Flexural rigidity	$=E\tilde{C}_{55v}$	=2.877*10^{11} kN

Analysis for concentrated live loading:

For the beam of Figure 7.26, the bending moment M_x at midspan is given by

$$M_x = \frac{-11.49}{2\mu}\tanh\frac{\mu \times 32000}{2} = -9889.475 \text{ kN.M}$$

where $\mu = \sqrt{\frac{97189.47}{2.877*10^{11}}} = 0.00058 \text{ mm}^{-1}$

The values of M_x' at z=0 $= \frac{-11.49\sinh(0.00058*16000}{\sinh(0.00058*32000)} = -0.001 kN/mm$

From the simple beam theory, at z=0,

$$V_y = \tilde{V}_{5v0} = \frac{\tilde{F}_{5v}}{2} = -5.747 kN/mm$$

For the statically determinate single-span beam $\Delta\tilde{V}_{5v0} = 0$

Analysis for distributed dead load:

The bending moment M_x at midspan is given by $M_x = \frac{-0.00238}{(0.00058)^2}[1 - \frac{1}{\cosh(0.00058*16000)}] = -7045.44$ kN.m

$$M_x' \text{ at z=0} = \frac{-0.00238}{0.00058}\tanh\frac{0.00058*16000}{2} = -4.095 kN/mm$$

From the simple beam theory, at z=0

$V_y = \tilde{V}_{5v0} = \tilde{n}_{5v} * 16000 = -38.08$ kN/mm

At z=0, $\Delta\tilde{V}_{5v0} = 0$ for the single-span, statically determinate beam

7.1.5.7 Shear lag stresses in mode 5 due to live load:

From equation 6.34

$$f_{5v} = \frac{\tilde{M}_{5v}}{\tilde{C}_{55v}}\tilde{w}_{5v} = (-9889.475*1000/8.34*10^9) = -0.0011857*\tilde{w}_{5v} \text{ N/mm}^2 \qquad (7.26)$$

[$\tilde{C}_{55v}$ = from program-B,output B16]

7.1.5.8 Shear lag stresses in mode 5 due to dead load:

From equation 6.34

$$f_{5v}=\frac{-7045.44*1000}{\widetilde{C}_{55v}}*\widetilde{w}_{5v} \quad =-0.00085 * \widetilde{w}_{5v} \ \text{N/mm}^2 \tag{7.27}$$

Diagrams of $\widetilde{w}_{5v}$ are shown in Figure 7.23(a)

Substituting the values of $\widetilde{w}_{5v}$ in equations 7.26 and 7.27 , the shear lag stresses due to live load and daed loads at different points on the cross-section can be calculated.These stresses are plotted in the following Figures 7.27(a) and (b) .

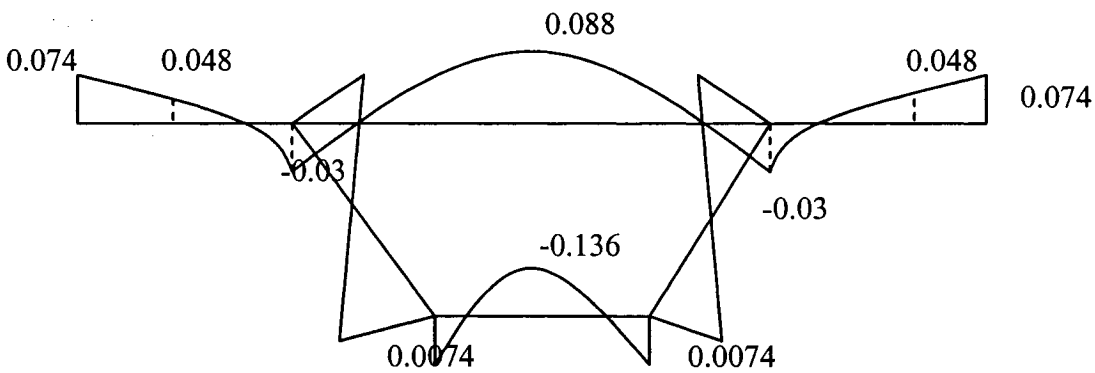

(a) Longitudinal stresses f_{5v} (MPa) at midspan section due to live load at mode 5

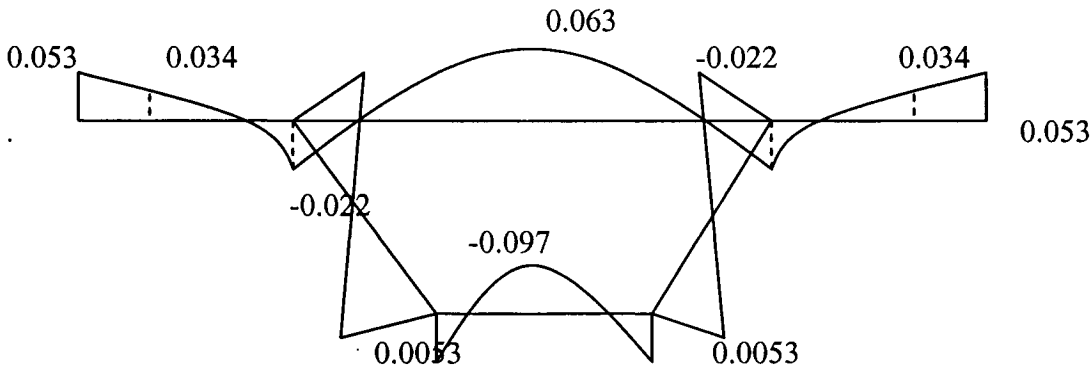

(b) Longitudinal stresses f_{5v} (MPa) at midspan section due to dead load at mode 5.

Figure 7. 27: Diagrams of shear lag stresses (MPa) at midspan section due to live and dead loads.

Similarly, the shear lag stresses due to mode 6 and 7 can be calculated. Detailed numerical calculation are shown in the spreadsheet programming sheet[Program-2],see Appendix-3.

7.2 Computer Programs Developed for Analysis of Simply-Supported Single Cell Prismatic Box Sections:

The above procedures have been formulated into two computer programs, the first dealing with shear flow, shear stresses, combined shearing stress, torsional warping stress, distortional warping stress, maximum transverse bending stress, etc. and the second program includes shear lag only. The computer programs developed can analyse simply supported box sections with trapezoidal and rectangular sections, any material properties, for a unit eccentric loading at midspan, formulate the bending, shear, torsion ,distortion and warping stresses at different location of the section.

The program has the following features:

(1) The programs can calculate the stresses concerning all structural actions at any location of the cross-section [Figure7.1]

(2) The programs can handle a single cell box section with both traphezoidal and rectangular geometry

(3) The programs handle the sections with side cantilever.

4) The programs handle the box sections with only simply-supported support condition.

The analysis consists of the following operations:

(1) Input geometriy , loading and material properties data.

(2)Calculation of flexural stresses by engineer's bending theory.

(3)Calculation of longitudinal bending and St. Venant torsional shear stresses.

(4) Calculation of torsional warping stresses using method of Kollbrunner,Hajdin and Heilig.

(5) Calculation of distortional warping stresses, distortional warping shear stresses, transverse bending stresses using method developed by Sedlacek.

(6) Analysis of shear lag stresses using method developed by Roik,Sedlacek and Schmackpfeffer.

7.2.1 User interface:

7.2.1(a)Input data for program –1

Input parameters or symbols	**Description**
Geometric data:	
Span length(m)	Geometry data from Figure 7.1
Top flange width(mm)	
Botton flange width(mm)	
Cantilever width(mm)	
Depth of web vertical (mm)	
Depth of web inclined (mm)	
Thickness of top flange with side cantilever (mm)	
Thickness of bottom flange (mm)	
Point load over a web at midspan (kN)	Load data

Torsional moment (kN.m)	From Figure 7.2(c)
Material properties data:	
Density of concrete (kN/m^3)	Given parameter
Poisson's ratio	
Modulus of Elasticity	
For distortional analysis:	
IGC (mm^4)	Second moment of area of member GC of Figure 7.13
ICA (mm^4)	Second moment of area of member CA of Figure 7.13
IAH (mm^4)	Second moment of area of member AH of Figure 7.13
Sidesway at level of load (δ) [Figure 7.13]	From Program-A , Output Matrix A2, element $_{11}$
Rotation at C from matrix analysis	From Program-A , Output Matrix A2, element $_{31}$
Rotation at A from matrix analysis	From Program-A , Output Matrix A2, element $_{41}$

7.2.1.(b) Input data for program-2

Input parameters or symbols	**Descriptions**
Geometric data:	From Figure 7.1
Span length (m)	
Top flange width (mm)	
Cantilever width (mm)	
Bottom flange width (mm)	
Top flange thickness (mm)	
Web thickness (mm)	
Bottom flange thickness (mm)	
Live load at flange web junction (kN)	
Material data:	
Shear modulus of elasticity	Given data for material properties.
Modulus of elasticity	
Ordinates of general parabolic function for shear lag:	
y_0	From Figure 7.19(a), 7.20(a) and 7.21(a)
y_1	
y_2	
Δx for top flange(1/4 th width)	
Δx for w_{6v} for cantilever(1/2 width)	
Δx for w_{7v} for bottom flange(1/2 width)	

Distance of the cntroid from top flange ($\tilde{y}$)	From program-1[Appendix-2]
Total dead load (kN)	
A(total cross-sectional area)	
I_x	
I_y	
C_{twr} (torsional warping moment of inertia)	
From Mathematica analysis:	
$\underline{\tilde{r}}_{5v}$	From Program-B Output matrices, Appendix 1
$\underline{\tilde{S}}_{55}$	
$\underline{\tilde{C}}_{55}$	
$\underline{\tilde{r}}_{6v}$	
$\underline{\tilde{S}}_{66v}$	
$\underline{\tilde{C}}_{66}$	
$\underline{\tilde{r}}_{7v}$	
$\underline{\tilde{C}}_{77}$	From Program-B Output Matrices, Appendix 1
$\underline{\tilde{S}}_{77v}$	
For orthogonalization of basic warping functions:	
$\tilde{w}_{5v}$ **at**	From equation 7.23
A and E	
C and D	
B and F	
Between B and A & between E and F	
Between A and E	
Between C and D	
$\tilde{w}_{6v}$ **at**	From equation 7.24
A and E	
C and D	
B and F	
Between B and A & between E and F	
Between A and E	
Between C and D	
$\tilde{w}_{7v}$ **at**	
A and E	
C and D	
B and F	

Between B and A & between E and F	From equation 7.25
Between A and E	
Between C and D	
$\dot{\tilde{w}}_{5v}$ **at**	From equation 7.23(a)
A (posi)	
A (neg)	
E (posi)	
E (neg)	
C	
D	
Between B and A	
Between E and F	
$\dot{\tilde{w}}_{6v}$ **at**	From equation 7.24(a)
A (posi)	
A (neg)	
E (posi)	
E (neg)	
C	
D	
Between B and A	
Between E and F	
$\dot{\tilde{w}}_{7v}$ **at**	From equation 7.25(a)
A (posi)	
A (neg)	
E (neg)	
E (neg)	
C	
D	
Between B and A	
Between E and F	

CHAPTER-8

RESULTS

8.1 General:

As mentioned earlier the main purpose of this invgstigation was to develop computer programs that would perform the stress calculations for box sections with different geometry and loading condition. In these programs it is assumed that diaphragms are used only at the supports where there is full torsional and distortional restraint, but no resistance to warping. Between the supports no diaphragms are considered to allow distortional effects. Live load is located eccentrically on only one web at midspan. The results were analyzed using the above two compouter programs (Program-1,Appendix 2 and Program-2 Appendix- 3) and the stress charts are developed and plotted as follows.

8.2 Geometry studied :

There are two types of geometry studied here.

(a) Box beam span

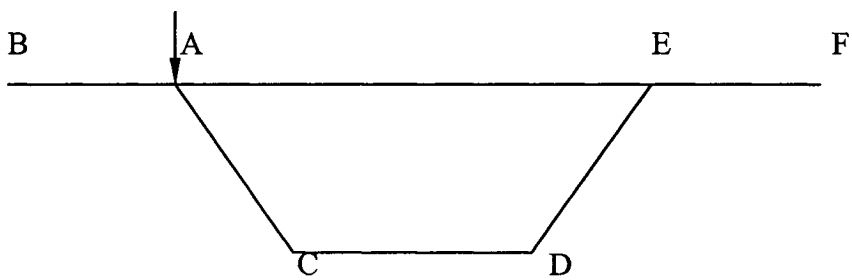

(b) Trapezoidal section

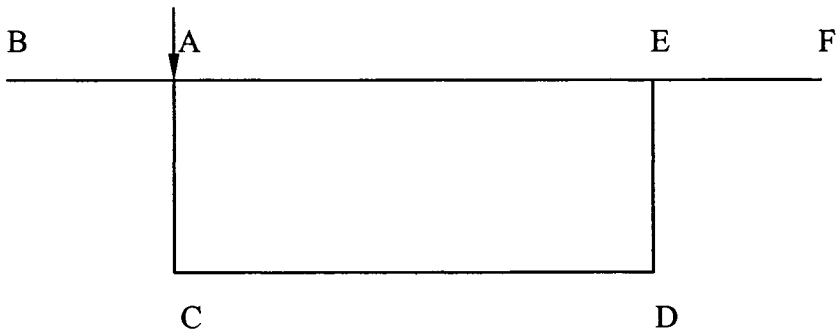

(c) Rectangular section

Figure 8. 1: Typical box sections.

8.3 Flexural stresses:

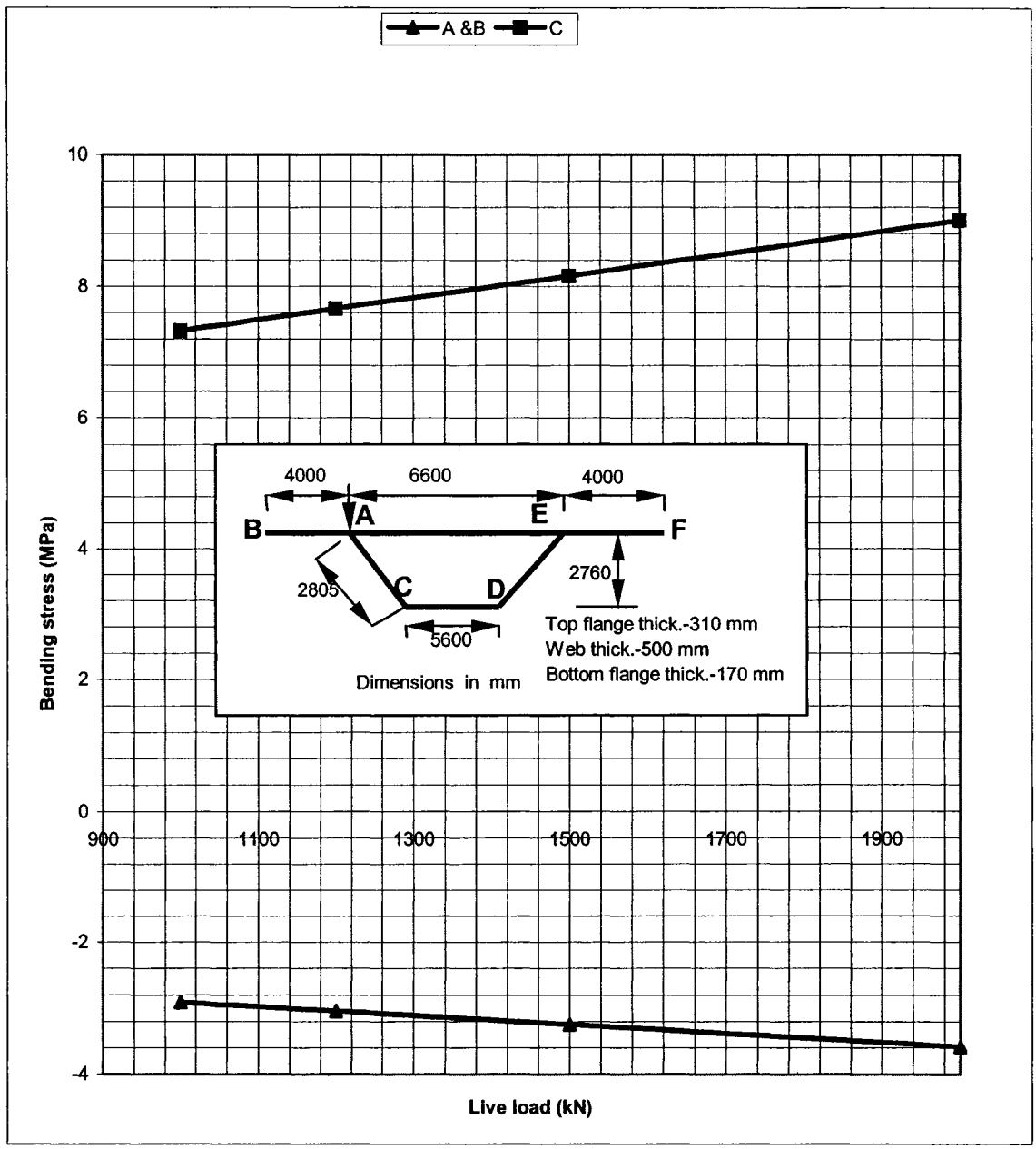

Figure 8. 2: Bending stress at midspan from engineers bending theory

From Figure 8.2: The flexural stresses are calculated considering the conventional bending theory.The results indicate that by increasing the live loading by 50 percent ,the bending stress increases by 11.6 percent at A & B and 11.47 percent at C.The shear deformation is not considered in this theory.

8.4: Statically Determinate Shear Flow vs live loading:

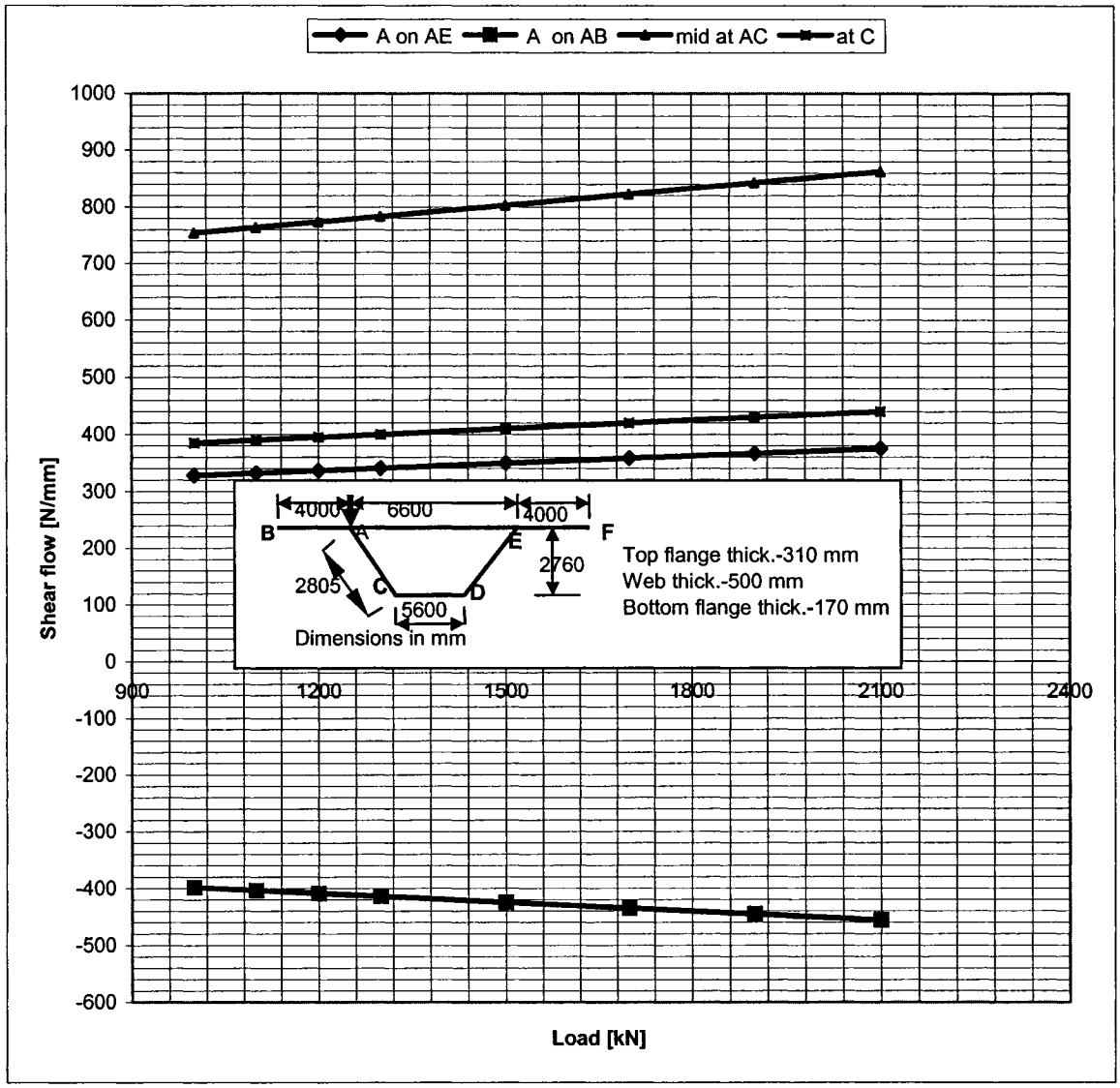

Figure 8. 3: Statically Determinate Shear Flow Vs Load Increament

From Figure 8.3, The statically determinate shear flows are plotted with increamental live loading at different locations of the section.The study shows that by increasing the live loading by 50 percent, the shear flow will increase 6.5 percent in all location of the cross-section (Figure 8.3)

8.5 Statically determinate shear flow vs variable span:

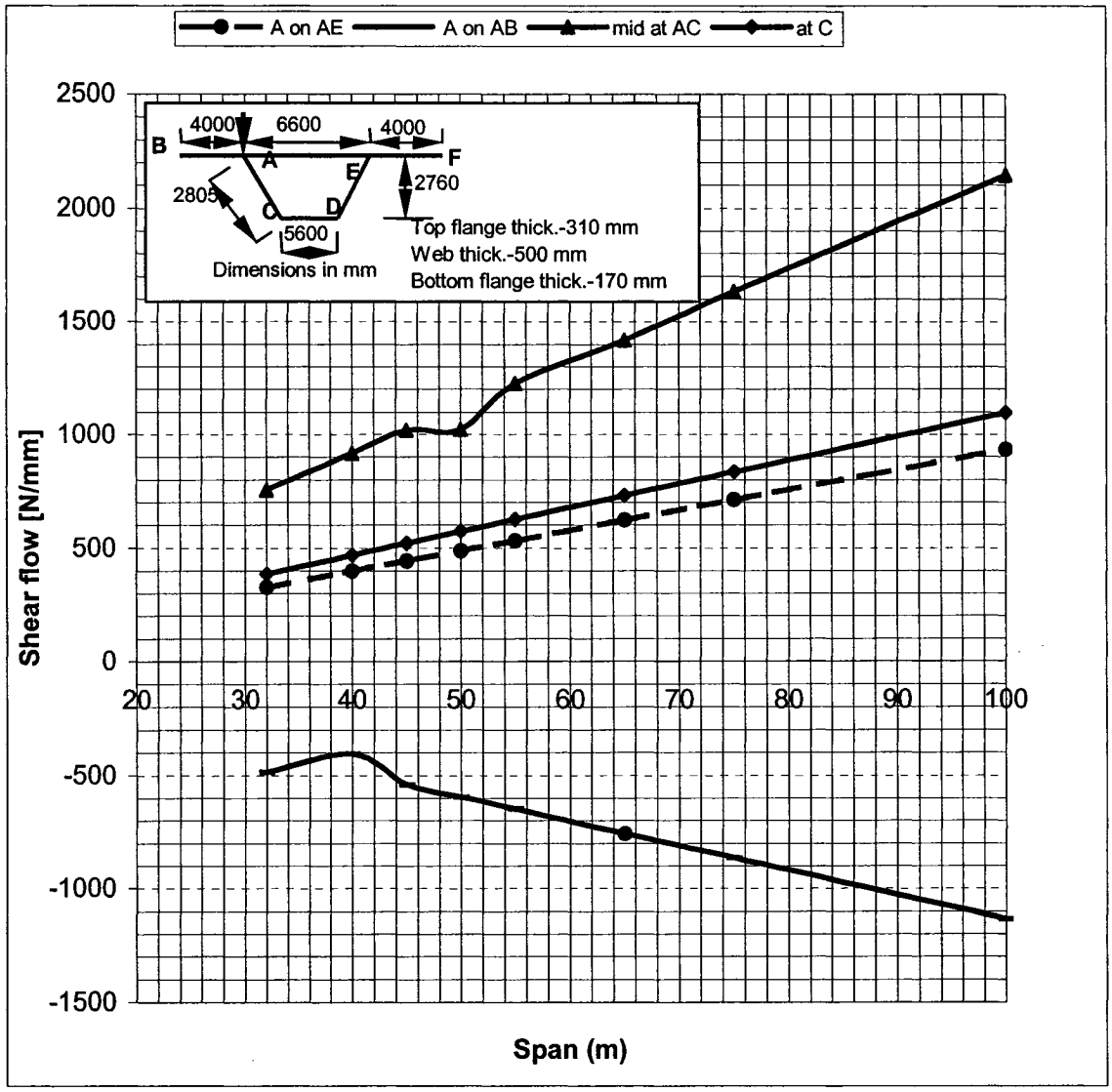

Figure 8. 4: Statically Determinate Shear Flow Vs Span Of Trapezoidal Section

From Figure 8.4 the statically determinate shear flows are plotted with variable span. In this case the results indicate non-uniform increaments of shear flows at different locations of the cross-section. The results show that by increasing live loading by 56.25 percent, the shear flow increases by 48.87 percent at A on AE, by 22.29 percent at A on AC, by 35.6 percent at the middle of AC and by 48.87 percent at C.

8.6 Conventional Shearing Stresses:

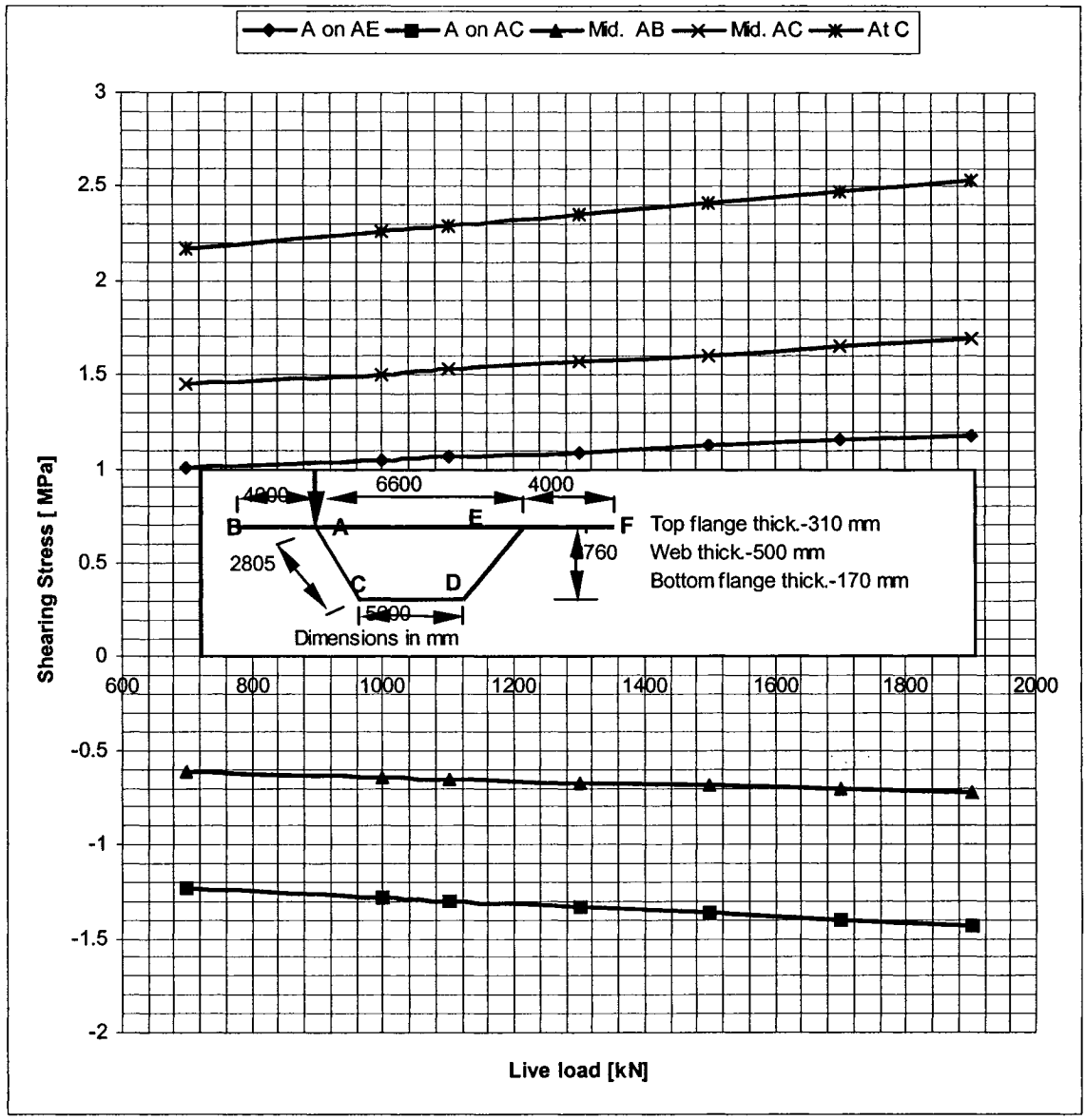

Figure **8. 5**: Shearing stress in bending calculated by engineers bending theory at z=0.

From Figure 8.5 The conventional shearing stresses are plotted with variable live loading.The study shows that by increasing live loading by 30 percent, the corresponding increamental shearing stresses are 7.9,8.13, 9.8, 8.27 and 8.29 percent at A on AE, A on AC, middle of AB, middle of AC and C, respectively.

8.7 :Shearing stresses due to St. Venant's torsion theory:

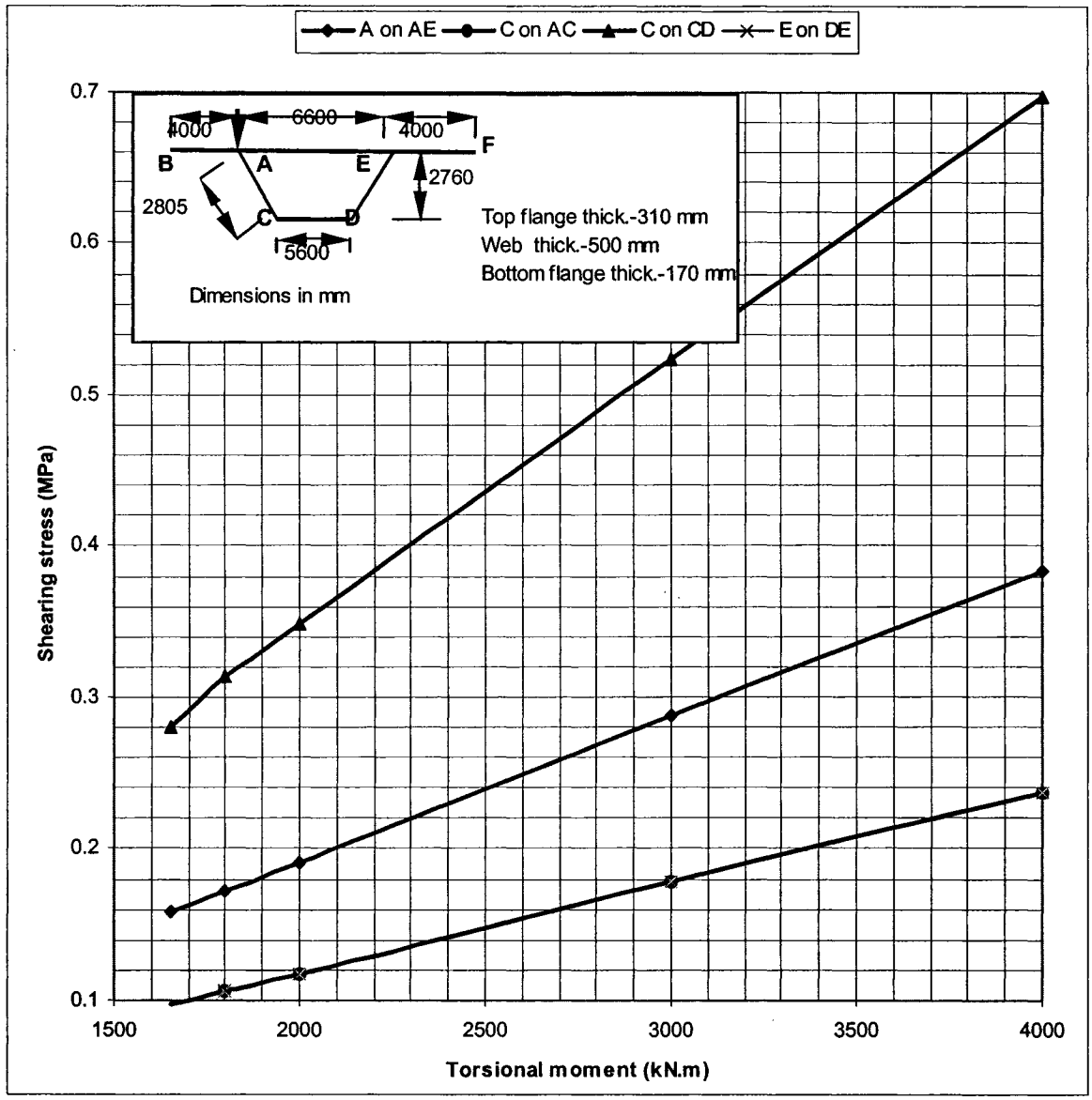

Figure **8. 6**: Shearing stresses due to St. Venant torsion theory at z=0.

From Figure 8.6**:** The theory of St. Venant torsion (pure torsion) assumes that there is no constraint on warping.Thus only shear stresses arise in the cross-section and there are no longitudinal warping stress as the torsional moments are considered as two equal and

opposite, one at each end. The St. Venant torsional stresses are usually taken as constant through the wall thickness of the closed box, although a more refined calculation, which considers a linear variation through the wall thickness.The St. Venants torsional shearing stresses at different locations of the cross-section are plotted (Figure 8.6).The results indicate that by increasing the torsional moment by 81.82 percent ,the corresponding increments of St. Venant's shearing torsional shearing stresses at A on AE, C on AC, C on CD and E on DE are 81.64, 81.64, 87.14 and 81.6 percent, respectively.

8.8: Maximum transverse bending stress:

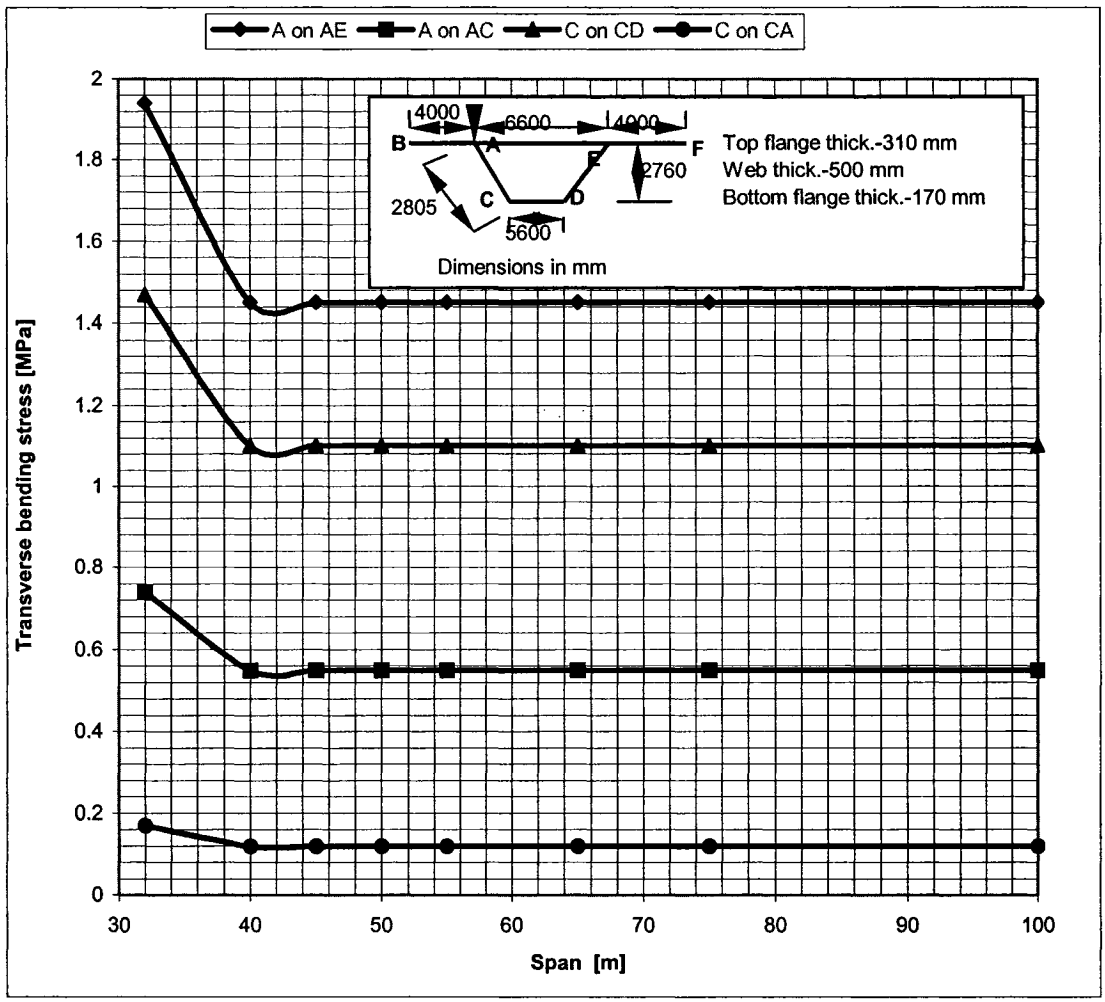

Figure **8. 7**: Maximum transverse bending stress at midspan with constant torsional moment.

From Figure 8.7:

The maximum transverse bending stresses are plotted for a variable span of a simply-supported box beam.The results indicate that if the box beam span is more than 40 m

there is no change of maximum transverse bending stresses at all location of the cross-section, i,e., it will remain constant .

8.9:Maximum transverse bending stresses due to variable torsional moment:

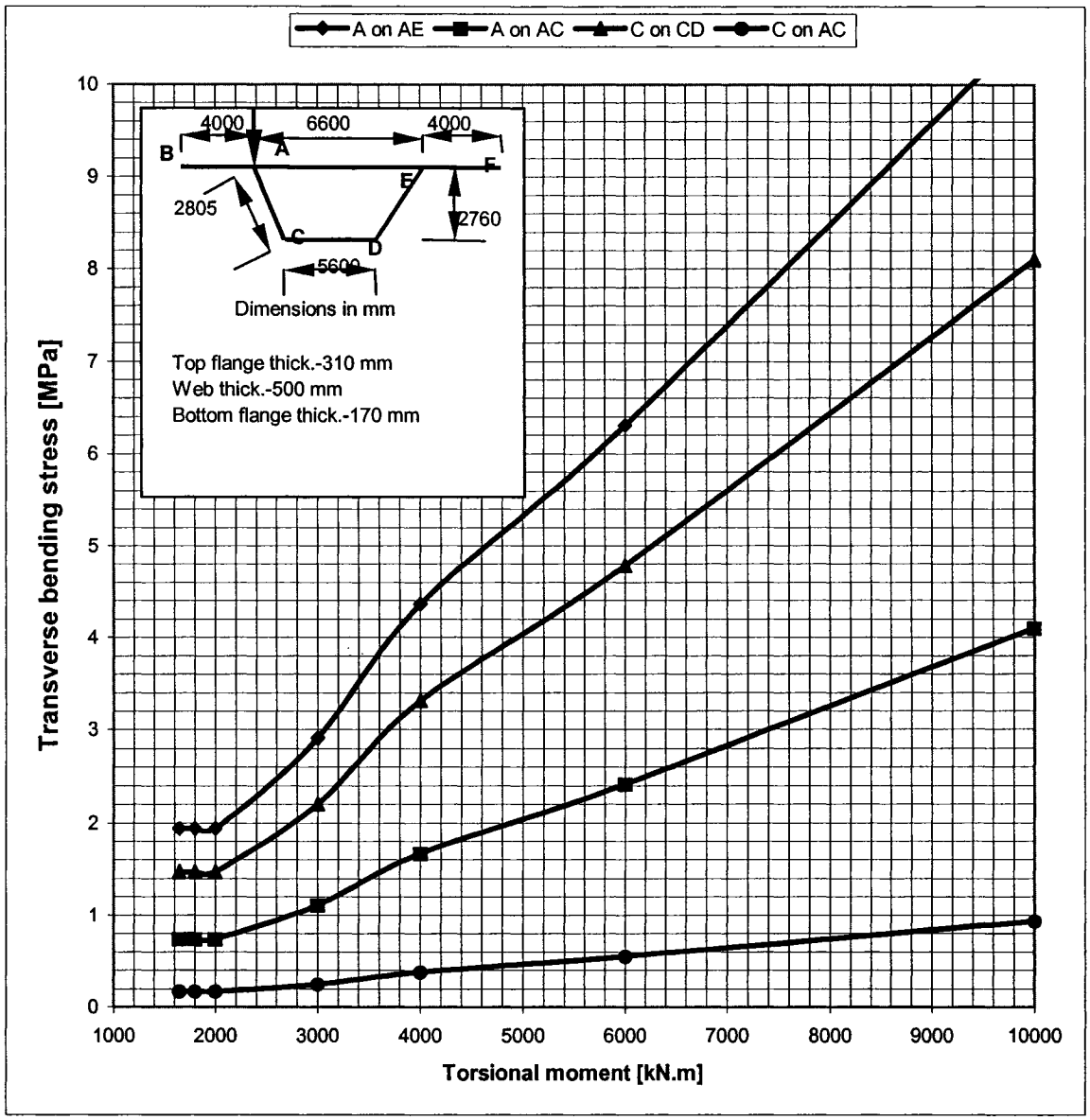

Figure **8. 8:** Max transverse bending stress at midspan

From Figure 8.8,The maximum transverse bending stresses due to the variable torsional moment at midspan are plotted.The transverse bending stresses are increased with increasing torsional moments.The study shows that by increasing of torsional moment by 81.8 percent, the corresponding transverse bending stress will increase at A on AE is 50

percent, at A on AC the increase is also 50 percent, C on CD (49.65 percent) and C on AC (47.05 percent.)

8.10: Torsional warping shear stresses:

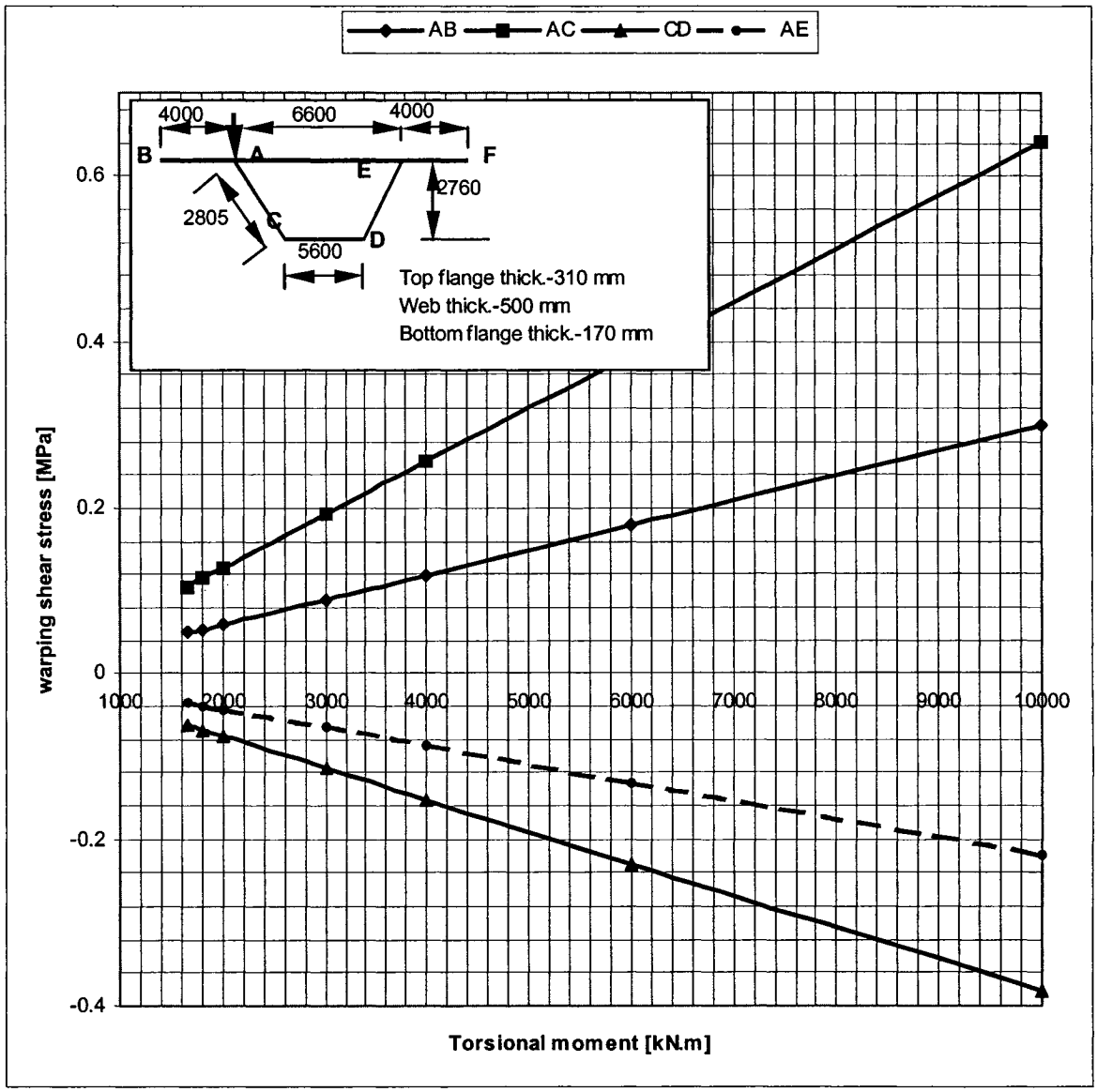

Figure 8. 9: Torsional warping shear stress at midspan.

When torsional warping arises, the pattern of warping displacements is such that the longitudinal torsional warping stresses vary both around the cross-sectional perimeter and

along the beam. Hence, longitudinal shear stress arise, and these cause complementary shear stresses to occur in the plane of the cross-section.These are called torsional warping shear stress.The torsional warping shear stresses are taken as constant through the wall thickness in the torsional warping theory. In the torsional warping of a closed section beam, the warping stress gives rise to shear deformations. It has been shown by Von Karman and Chein (1946), Heilig (1971), Benscoter (1954), Umansky (1948) and Dzhanelidze and Panovko (1948) that the influence of this warping shear deformation must be taken into account in the torsional warping analysis of a closed section beam. Stiissi (1965) pointed out that when warping shear deformation is considered in torsional warping analysis, the shear centre of the cross-section is no longer a fixed point and the shear axis or line joining the shear centres of the cross-sections is a curved line.Here it has been considered shear deformation.

The results indicate that by increasing the torsional moment by 81.8 percent, the torsional warping shear stresses increases on AB,AC,CD and AE by 80.16 ,81.47,82.53 and 83.33 percent, respectively.

8.11:Distortional warping shear stresses:

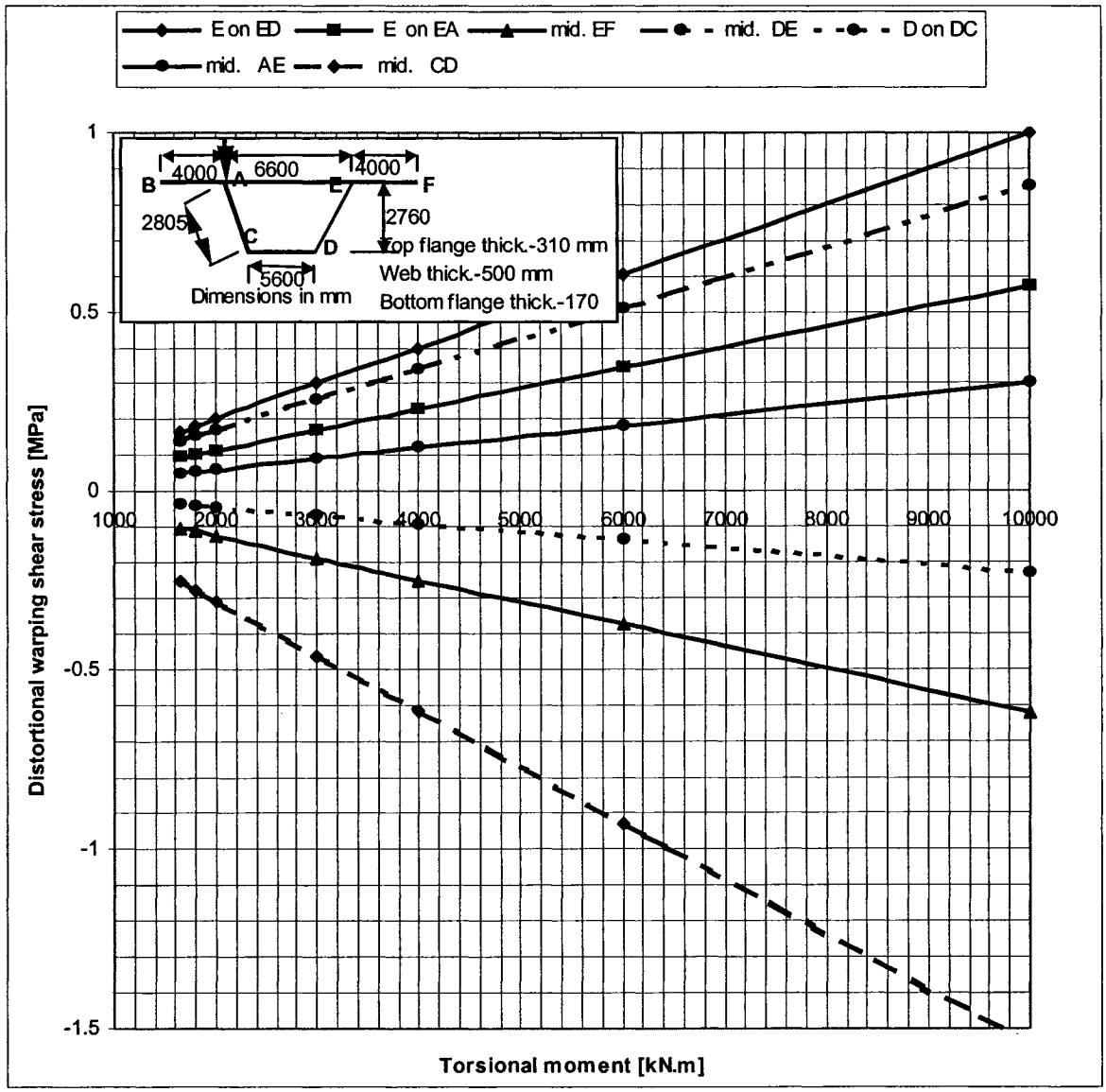

Figure **8. 10**: Distortional warping shear stress at midspan

As with torsional warping, the pattern of this displacement is such that the longitudinal distortional warping stresses which arise, vary both around the cross-sectional perimeter and along the beam. Hence, longitudinal shear stress arise, and these cause

complementary shear stresses to occur in the plane of the cross-section.These are called distortional warping shear stresses.

The distortional warping shear stresses are plotted with increamental torsional moment.The Study shows that by increasing torsional moment at midspan by81.8 percent at midspan, the distortional warping shear stresses will increase at E on ED, E on EA, middle of EF, middle of DE, D on CD, middle of AE and middle of CD by 80.72, 81.9, 81.5, 82.14, 81.57, 80.72 and 81.56 percent, respectively.

8.12:Torsional warping stresses:

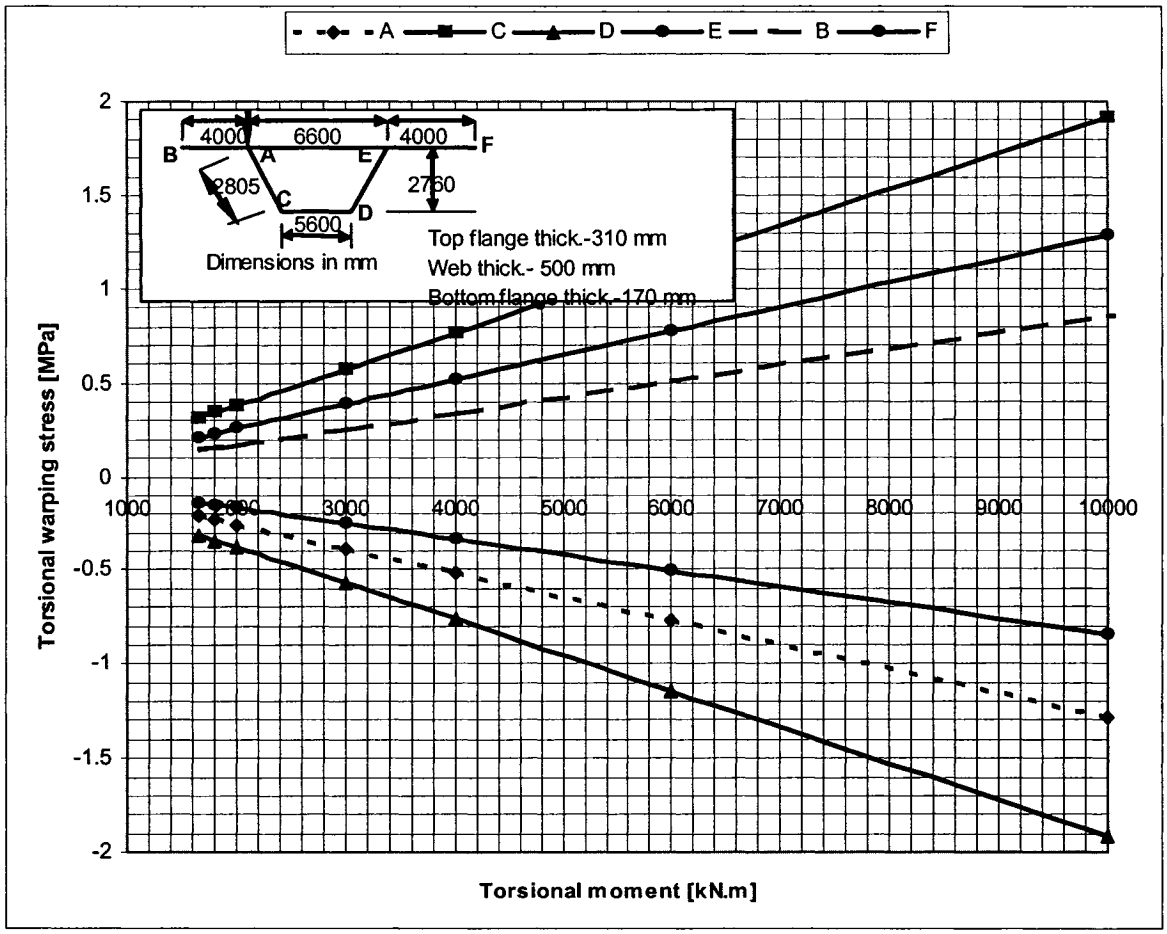

Figure **8. 11**: Torsional warping stress at midspan section

The elastic resistance with which the structure oppose the distortional deformation can be subdivided into warping resistance and torsional resistance;these known as torsional warping stress.The torsional warping stresses are plotted against variable torsional moments.The results indicate that by increasing the torsional warping by 81.8 percent, the torsional warping stress increases at A,C,D,E,B and F by 82.15, 81.9, 81.9, 82.15, 82.01 and 82.01 percent, respectively.

8.13:Distortional warping stresses:

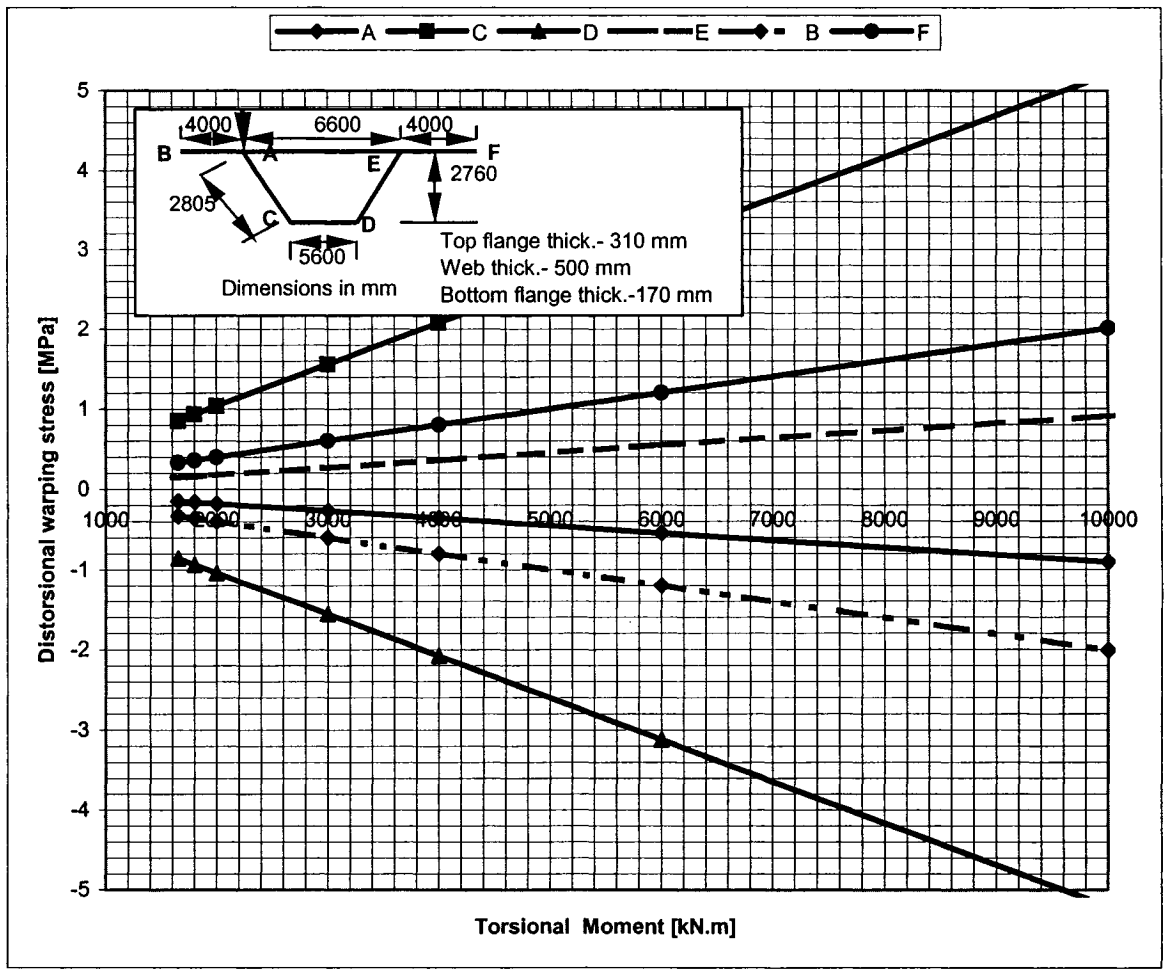

Figure 8. 12: Distortional warping stress at midspan

The distortional effects comprise distortional warping and transverse bending, and arise in concrete box beam construction as a result of the usual practice of inserting diaphragms

only at the supports, or at large spacing within the span. These effects need to be superimposed upon the effects of longitudinal bending and torsional warping.

If distortion is not prevented, distortional warping of a thin walled box beam always occurs under torsional load which arise in the bridge design practice,irrespective of the cross-sectional properties.In the distortional analysis of a box beam, Richmond (1969) shows that when the cross-section has a fairly low resistance to distortion, shear deformation is not important.He states that an increase in the distortional stiffness leads to shear deformation which is more important, and in the limiting case of a rigid cross-section, a solution can only be found by considering the shear deformation.

The distortional warping stresses are plotted against variable torsional moments.The results indicate that by increasing torsional moments at midspan by 81.8 percent, the distortional warping stresses increases at A,C,D,E,B and F are 80, 81.6, 81.6, 80, 81.6 and 81.6 percent ,respectively.

8.14: Different stresses at A and C:

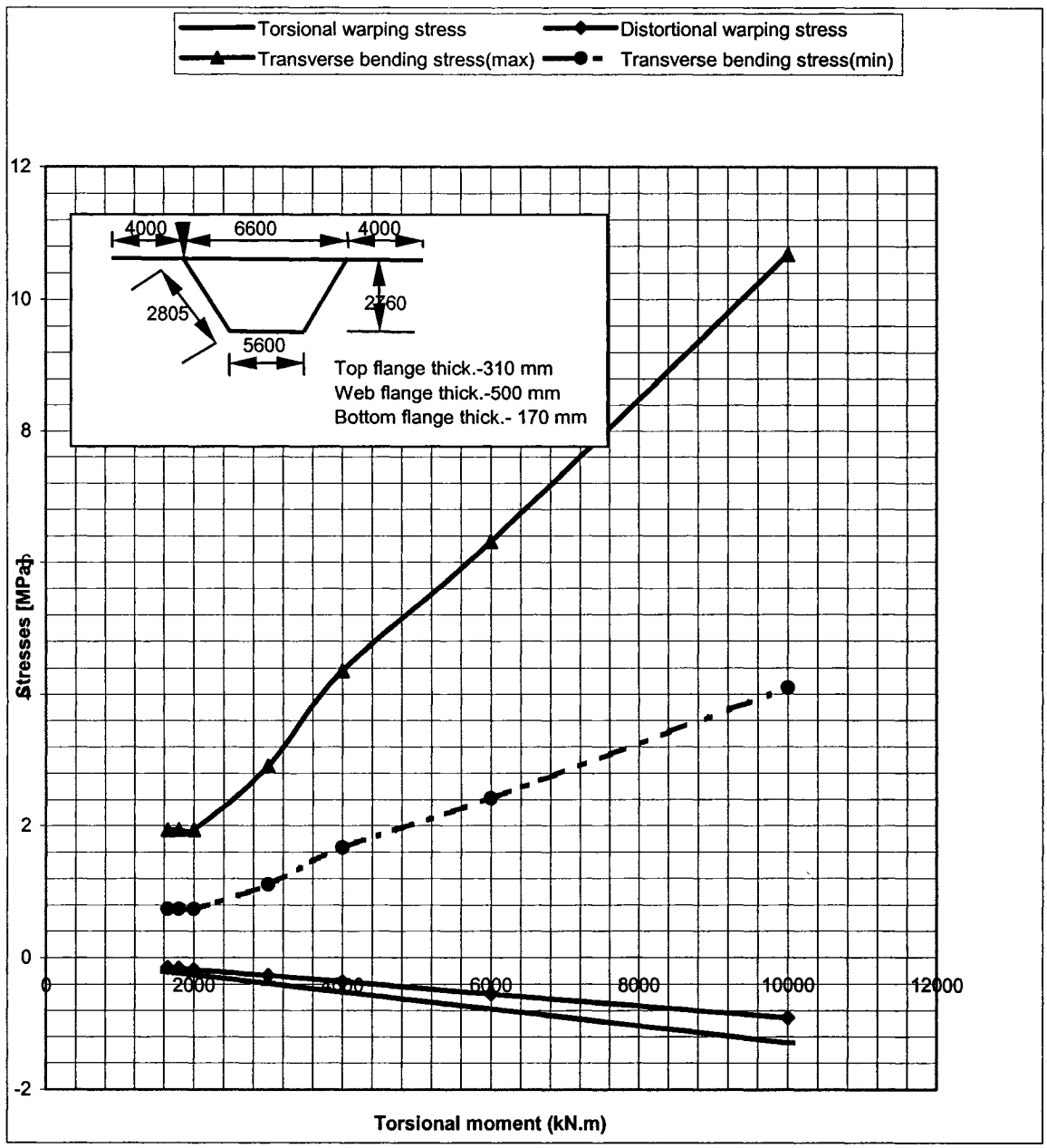

Figure 8. 13: Different stresses at A

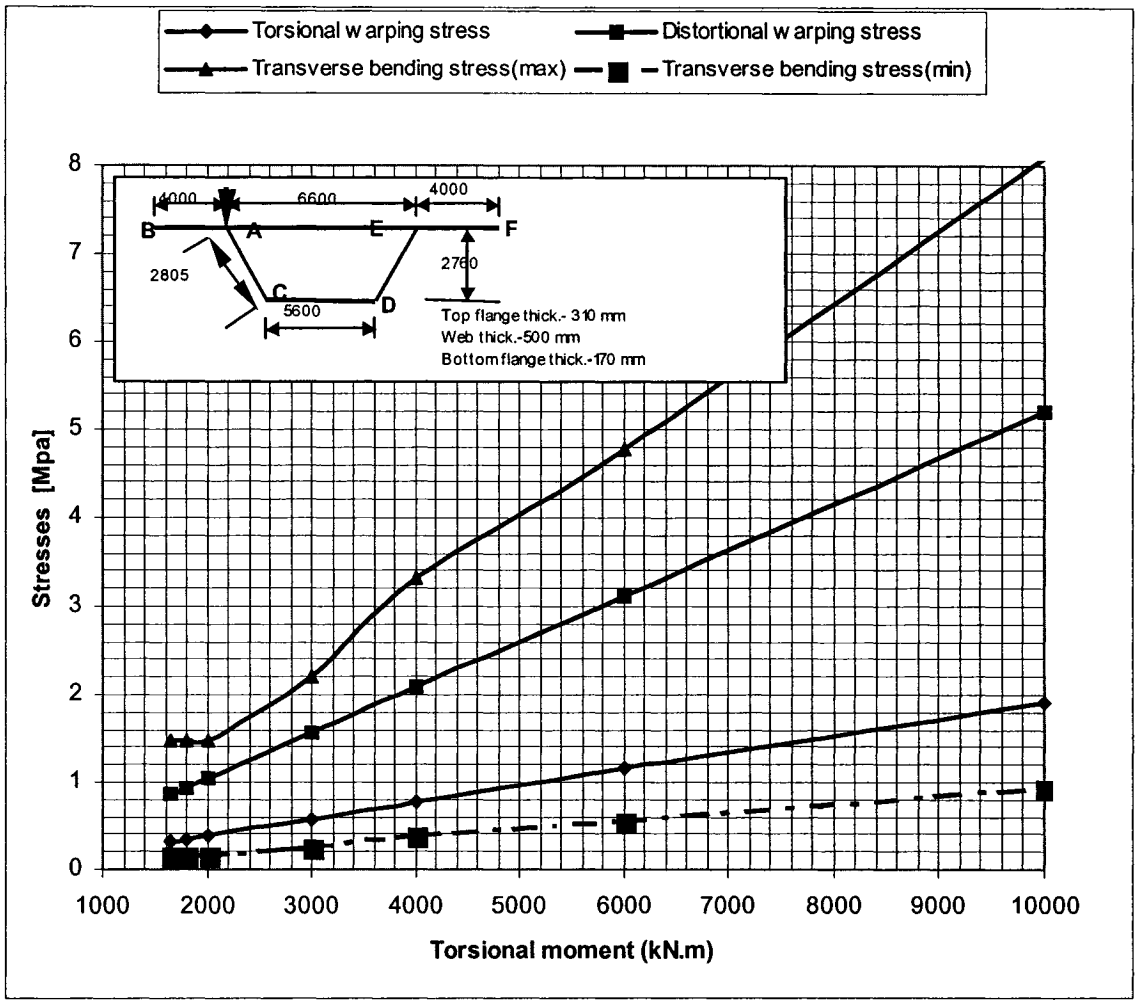

Figure 8. 14: Different stresses at C

Table 8.1 compares of all stresses at points A and C on the cross-section of Figure 8.1(a)

Table 8.1: Comparison between Figure 8.13 and 8.14

Stresses	% increase in Torsional Moment	Corresponding % increase at A	Corresponding % increase at C
Torsional warping stress	81.8	82.15	81.96
Distortional warping stress	81.8	80	81.6
Transverse bending stress at A on AE	81.8	50	49.65
Transverse bending stress at A on AC	81.8	50	47.05

8.15: Effect of flange and web thickness on shear flow

The shear flow at different locations of the cross-sections are calculated for different top flange and web thickness for the cross-section (Figure 7.1) using the computer Program – 1[Appendix-2].These stresses are summarized in Tables 8.2(a) and 8.2(b).

Table 8.2: Effect of flange and web thickness on shear flow

Table 8.2(a)

Position	Thickness 310 mm(top flange)	Thickness 350 (top flange)	Percentage increase(Flange thickness)	Percentage increase (Shear flow)
	Shear flow N/mm	Shear flow N/mm		
A	327.97	354.18	12.9	7.99
B	-199.23	-214.79	12.9	7.81
C	384.83	403.90	12.9	4.95
D	-384.83	-403.90	12.9	4.95

Table 8.2 (b)

Position	Thickness 170mm(Web)	Thickness 250 (Web)	Thickness 300 (Web)	Percentage increase(Web thickness)	Percentage increase (Shear flow)
	Shear flow N/mm	Shear flow N/mm	Shear flow		
A	327.97	329.44	332.26	76.47	1.3
B	-199.23	-199.74	-201.23		1.00
C	384.83	477.009	524.48		36.28

8.16: Effect of top flange thickness on stresses of different location of the cross-section.

The shearing stress,torsional warping stresses,distortional warping stresses and transverse bending stresses are calculated for different top flange thicknesses for the cross-section (Figure 7.1) using the computer Program –1[Appendix-2].These stresses are summarized in Tables 8.3(a) to 8.3(e).

Table 8.3: Effect of top flange thickness on stresses of different location of the cross-section.

Table 8.3 (a) stresses at A

Top flange thickness	Shearing stress		Torsional warping Stress	Distortional. Warping Stress	Transverse bending
mm	MPa		MPa	MPa	stress(MPa)
310	1.216	-1.28	-0.214	-0.15	1.94
350	1.15	-1.23	-0.19	-0.12	1.64
380	1.11	-1.19	-0.17	-0.10	1.18
400	1.08	-1.16	-0.169	-0.09	1.25

Table 8.3 (b) stresses at B

Top flange thickness	Shearing stress	Torsional warping Stress	Distortional Warping Stress	Transverse bending
mm	MPa	MPa	MPa	stress(MPa)
310	-0.64	0.139	-0.33	
350	-0.61	0.11	-0.26	
380	-0.59	0.1	-0.22	
400	-0.58	0.09	-0.20	

Table 8.3 (c) stresses at C

Top flange thickness	Shearing stress	Torsional warping Stress	Distortional. Warping Stress	Transverse bending
mm	MPa	MPa	MPa	stress(MPa)
310	2.55	0.316	0.86	1.47
350	2.66	0.311	0.749	1.10
380	2.74	0.308	0.68	0.73
400	2.8	0.306	0.64	0.73

Table 8.3 (d) stresses at D

Top flange thickness mm	Shearing stress MPa	Torsional warping Stress MPa	Distortional Warping stress MPa	Transverse bending stress(MPa)
310	-1.97	-0.316	-0.86	1.47
350	-2.08	-0.311	-0.749	1.10
380	-2.17	-0.308	-0.68	0.73
400	-2.22	-0.306	-0.64	0.73

Table 8.3 (e)stresses at E

Top flange thickness mm	Shearing stress MPa		Torsional warping Stress MPa	Distortional. Warping Stress MPa	Transverse bending stress(MPa)
310	1.28	-0.89	0.213	0.15	1.94
350	1.23	-0.87	0.191	0.12	1.64
380	1.19	-0.85	0.177	0.10	1.18
400	1.16	-0.84	0.169	0.09	1.25

8.17: Effect of bottom flange thickness on stresses of different location of the cross-section.

The shearing stress,torsional warping stresses,distortional warping stresses and transverse bending stresses are calculated for different bottom flange thicknesses for the cross-section (Figure 7.1) using the computer Program –1[Appendix-2].These stresses are summarized in Tables 8.4(a) to 8.4(e).

Table 8.4: Effect of bottom flange thickness on stresses of different location of the cross-section.

Table 8.4(a) stresses at A

Bottom flange thickness mm	Shearing stress MPa on AE	on AB	Torsional warping Stress MPa	Distortional Warping stress MPa	Transverse bending stress(MPa)
150	1.22	-1.28	-0.216	-0.15	1.94
170	1.216	-1.28	-0.213	-0.15	1.94
190	1.216	-1.28	-0.21	-0.15	1.45
250	1.22	-1.28	-0.198	-0.13	1.45

Table 8.4(b)stresses at B

Bottom flange thickness mm	Shearing stress MPa	Torsional warping Stress MPa	Distortional Warping stress MPa	Transverse bending stress(MPa)
150	-0.64	0.12	-0.34	
170	-0.64	0.139	-0.33	
190	-0.64	0.15	-0.32	
250	-0.64	0.18	-0.293	

Table 8.4(c) stresses at C

Bottom flange thickness mm	Shearing stress MPa	Torsional warping Stress MPa	Distortional Warping stress MPa	Transverse bending stress(MPa)
150	2.708	0.358	0.89	1.29
170	2.55	0.316	0.859	1.47
190	2.42	0.28	0.82	1.23
250	2.10	0.198	0.701	1.63

Table 8.4(d)stresses at D

Bottom flange thickness mm	Shearing stress MPa	Torsional warping Stress MPa	Distortional Warping stress MPa	Transverse bending stress(MPa)
150	-2.05	-0.358	-0.89	1.29
170	-1.97	-0.316	-0.859	1.47
190	-1.90	-0.28	-0.82	1.23
250	-1.71	-0.198	-0.701	1.63

Table 8.4(e)stresses at E

Bottom flange thickness mm	Shearing stress MPa		Torsional warping Stress MPa	Distortional Warping stress MPa	Transverse bending stress(MPa)
	EF	AE			
150	1.28	-0.90	0.216	0.15	1.939
170	1.28	-0.89	0.213	0.15	1.47
190	1.28	-0.90	0.210	0.15	1.45
250	1.28	-0.90	0.198	0.13	1.45

8.18: Effect of L/B ratio ,web inclination by using different geometry[Rectangular section]:

The shear flow, combined shearing stresses, torsional and distortional warping stresses and the maximum transverse bending stress values are calculated for different span-flange width (L/B) ratios for the rectangular section (Figure 8.1(b)) using the computer Program-1 (Appendix-1). These stresses are summarized in Tables 8.5(b) to 8.5(f).

Table 8.5: Effect of L/B ratio ,web inclination by using different geometry[Rectangular section]

Table-8.5 (a) Geometry for Rectangle section

Span (m)	Total width (mm)	Top and bottom flange width(mm)	Cantilever (mm)	Vertical web (mm)	L/B
27.4	16000	6000	4000	2760	1.71
32	14600	6600	4000	2760	2.19
35	15000	7000	4000	2760	2.33
27.4	10800	5640	2580	2760	2.53

Table-8.5 (b) stresses at A

L/B	Shear flow (N/mm)		Combined shearing stress (MPa)		Torsional warping stress (MPa)	Distortional Warping stress (MPa)	Maximum Transverse Bending Stress (MPa)
	AE	AC	AC	AE			
1.7125	264.21	-352.73	-1.13	1.01	-0.221	-0.18	2.139
2.19	327.47	-396.33	-1.27	1.20	-0.203	-0.18	1.94
2.33	371.41	-424.88	-1.37	1.33	-0.192	-0.18	1.83
2.53	276.51	-252.49	-0.81	1.06	-0.216	-0.3	2.27

Table-8.5 (c) stresses at B

L/B	Shear flow (N/mm)	Combined shearing stress (MPa)	Torsional warping stress (MPa)	Distortional Warping stress (MPa)	Maximum Transverse Bending Stress (MPa)
1.712	-176.36	-0.568	0.1215	-0.429	-
2.19	-198.16	-0.639	0.095	-0.403	-
2.33	-212.44	-0.68	0.08	-0.387	-
2.53	-126.24	-0.407	0.045	-0.581	-

Table-8.5 (d) stresses at E

L/B	Shear flow (N/mm)		Combined shearing stress (MPa)		Torsional warping stress (MPa)	Distortional Warping stress (MPa)	Maximum Transverse Bending Stress (MPa)
	AE	DE	DE	AE			
1.712	352.73	-264.21	-0.69	1.137	0.2215	0.429	2.139
2.19	396.33	-327.47	-0.91	1.27	0.203	0.403	1.94
2.33	424.88	-371.4	-1.06	1.37	0.192	0.387	1.83
2.53	252.49	-276.51	-0.72	0.814	0.216	0.58	2.276

Table-8.5 (e) stress at C

L/B	Shear flow (N/mm)	Combined shearing stress (MPa)	Torsional warping stress (MPa)	Distortional Warping stress (MPa)	Maximum Transverse Bending Stress (MPa)
1.712	345.62	2.326	0.3179	0.998	1.174
2.19	423.48	2.75	0.315	0.914	1.06
2.33	478.18	3.06	0.3115	0.87	1.007
2.53	306.16	2.11	0.3409	0.983	1.25

Table-8.5 (f) stresses at D

L/B	Shear flow (N/mm)	Combined shearing stress (MPa)	Torsional warping stress (MPa)	Distortional Warping stress (MPa)	Maximum Transverse Bending Stress (MPa)
1.712	-345.62	-1.74	-0.317	-0.998	1.174
2.19	-423.48	-2.22	-0.315	-0.914	1.06
2.33	-478.18	-2.56	-0.3115	-0.870	1.007
2.53	-306.16	-1.49	-0.3409	-0.983	1.25

8.19: Effect of L/B ratio ,web inclination by using different geometry[Trapezoidal section]:

The shear flow, combined shearing stresses, torsional and distortional warping stresses and the maximum transverse bending stress values are calculated for different span-flange width (L/B) ratio for the trapezoidal section (Figure 8.1(a)) using the computer Program-1 (Appendix-1). These stresses are summarized in Tables 8.6(b) to 8.6(f).

Table 8.6:Effect of L/B ratio , web inclination by using different geometry[Trapezoidal section]

Table-8.6 (a) Geometry for Trapezoidal section

Span (m)	Total width (mm)	Top flange width(mm)	Bottom flange width(mm)	Cantilever (mm)	Inclined Web (mm)	Vertical web (mm)	L/B
27.4	15000	7000	5600	4000	2847	2760	1.82
32	15000	7000	5600	4000	2847	2760	2.13
32	14600	6600	5600	4000	2804	2760	2.19
35	14600	6600	5600	4000	2804	2760	2.39
27.4	10800	5640	5600	2580	2760	2760	2.53

Table-8.6 (b) stresses at A

L/B	Shear flow (N/mm)		Combined shearing stress (MPa)		Torsional warping stress (MPa)	Distortional Warping stress (MPa)	Maximum Transverse Bending Stress (MPa)
	AE	AC	AC	AE			
1.82	302.91	-346.15	-1.11	1.13	-0.205	-0.16	1.83
2.13	346.30	-395.72	-1.27	1.27	-0.205	-0.15	1.83
2.19	327.97	-398.46	-1.28	1.216	-0.213	-0.15	1.94
2.39	354.67	-430.9	-1.39	1.30	-0.213	-0.14	1.456

Table 8.6 (c) stresses at B

L/B	Shear flow (N/mm)	Combined shearing stress (MPa)	Torsional warping stress (MPa)	Distortional Warping stress (MPa)	Maximum Transverse Bending Stress (MPa)
1.82	-173.07	-0.558	0.137	-0.344	
2.13	-197.86	-0.64	0.137	-0.314	
2.19	-199.23	-0.64	0.139	-0.33	
2.39	-215.45	-0.695	0.139	-0.317	
2.53	-126.36	-0.407	0.047	-0.57	

Table-8.6 (d) stresses at E

L/B	Shear flow (N/mm)		Combined shearing stress (MPa)		Torsional warping stress (MPa)	Distortional Warping stress (MPa)	Maximum Transverse Bending Stress (MPa)
	AE	DE	DE	AE			
1.82	346.15	-302.91	-0.82	1.11	0.205	0.344	1.83
2.13	395.72	-346.30	-0.96	1.27	0.205	0.314	1.83
2.19	398.46	-327.97	-0.89	1.28	0.2139	0.332	1.94
2.39	430.91	-354.67	-0.98	1.39	0.2139	0.317	1.456
2.53	252.73	-275.83	-0.71	0.815	0.2165	0.577	2.27

Table-8.6 (e) stresses at C

L/B	Shear flow (N/mm)	Combined shearing stress (MPa)	Torsional warping stress (MPa)	Distortional Warping stress (MPa)	Maximum Transverse Bending Stress (MPa)
1.82	339.73	2.27	0.313	0.914	1.56
2.13	388.38	2.56	0.313	0.8337	1.56
2.19	384.83	2.55	0.316	0.859	1.47
2.39	416.17	2.73	0.316	0.823	1.104
2.53	304.79	2.105	0.341	0.981	1.26

Table-8.6 (f) stresses at D

L/B	Shear flow (N/mm)	Combined shearing stress (MPa)	Torsional warping stress (MPa)	Distortional Warping stress (MPa)	Maximum Transverse Bending Stress (MPa)
1.82	-339.73	-1.72	-0.313	-0.914	1.56
2.13	-388.38	-2.005	-0.313	-0.833	1.56
2.19	-384.83	-1.975	-0.316	-0.859	1.47
2.39	-416.17	-2.159	-0.316	-0.823	1.104
2.53	-304.79	-1.48	-0.341	-0.981	1.26

8.20: Shear lag stresses:

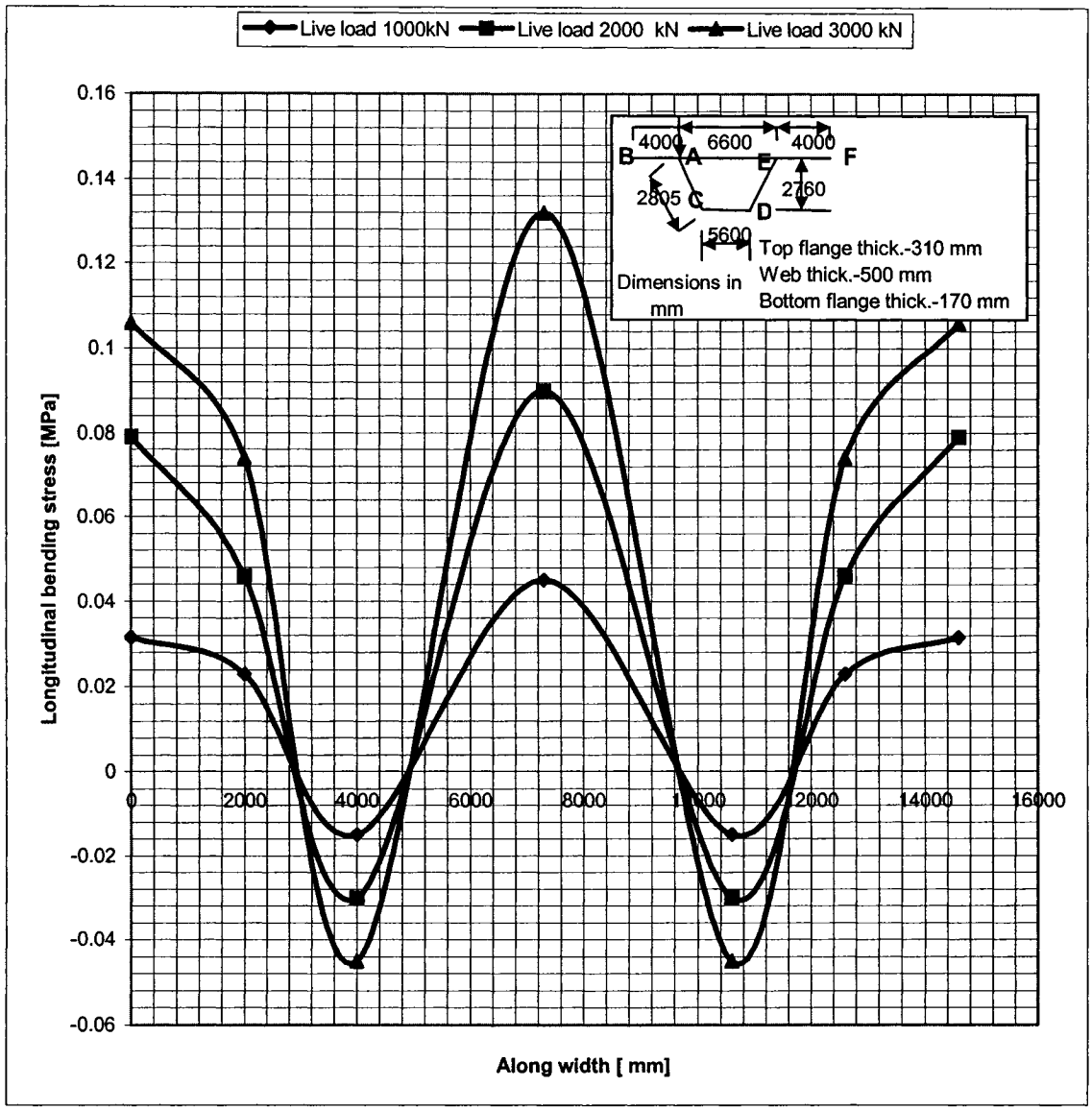

Figure **8. 15**: Shear lag stresses

Only shear lag stresses due to the live load along the width of the top flange are plotted.The study shows that for live load 1000 kN, the shear lag stresses is almost 2 percent for combined dead and live load stresses at the midspan section.

8.21 Effect of Flange Thickness on Different Stress:

8.21.1 Effect of top flange thickness:

Considering geometry (Figures 7.1) for an eccentric loading of 1000 kN at midspan, study shows that with increase of top flange thickness, the shearing stresses increase at A,B and E.Consequently the shearing stresses decreases at C and D as these locations are on the bottom flange. Torsional warping stresses and distortional warping stresses decrease at A,B,C ,D and E with increase of top flange thckness.The ratio of bottom flange thickness and top flange thickness varies between 0.54 to 0.425.

8.21.2 Effect of bottom flange thickness:

Considering the geometry described in Figure 7.1 with 1000kN eccentric loading an increase of bottom flange thickness does not affect the shearing stresses at A,B and E. Also, shearing stresses at on C and D decrease with an increasing of bottom flange thickness. The ratio of bottom flange thickness to top flange thickness varies 0.48 to 0.8

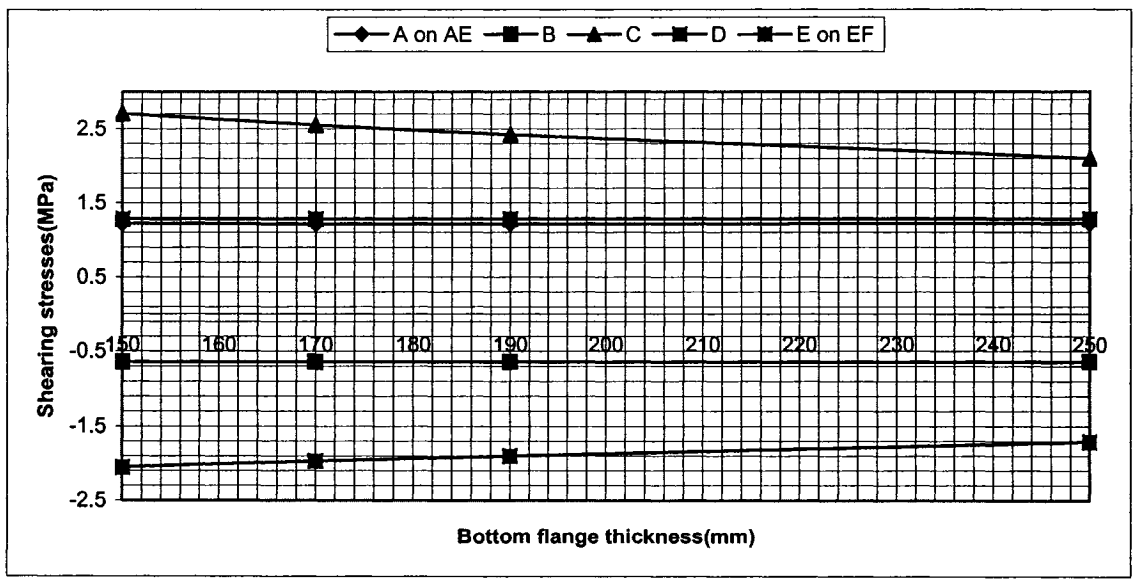

Figure 8.16:Variation of shearing stresses with bottom flange thickness (constant top flange thickness)

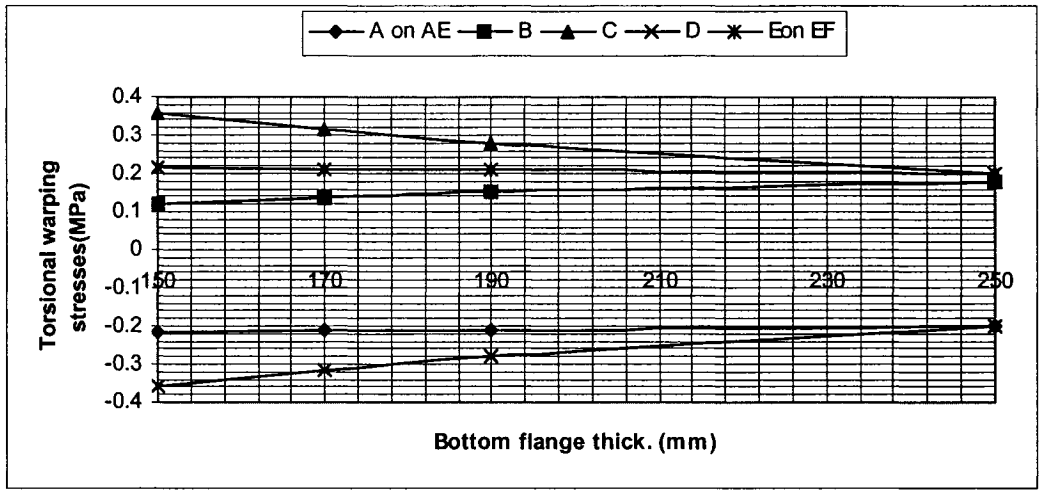

Figure 8.17: Variation of torsional warping stresses with bottom flange thickness (constant top flange thickness)

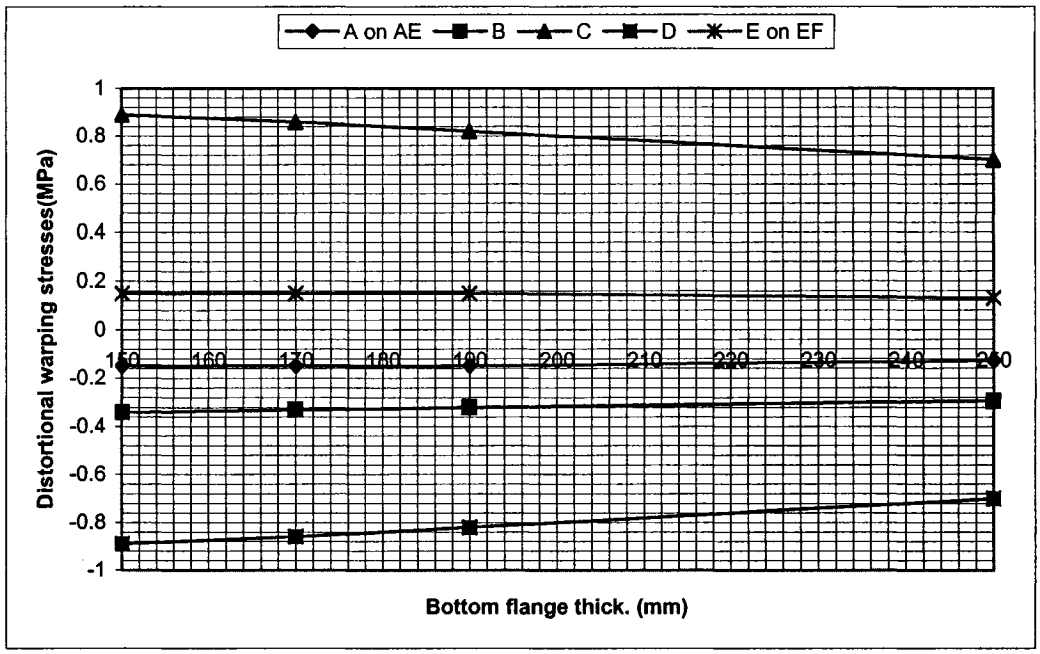

Figure 8.18: Variation of distortional warping stresses with bottom flange thicknesses (constant top flange thickness)

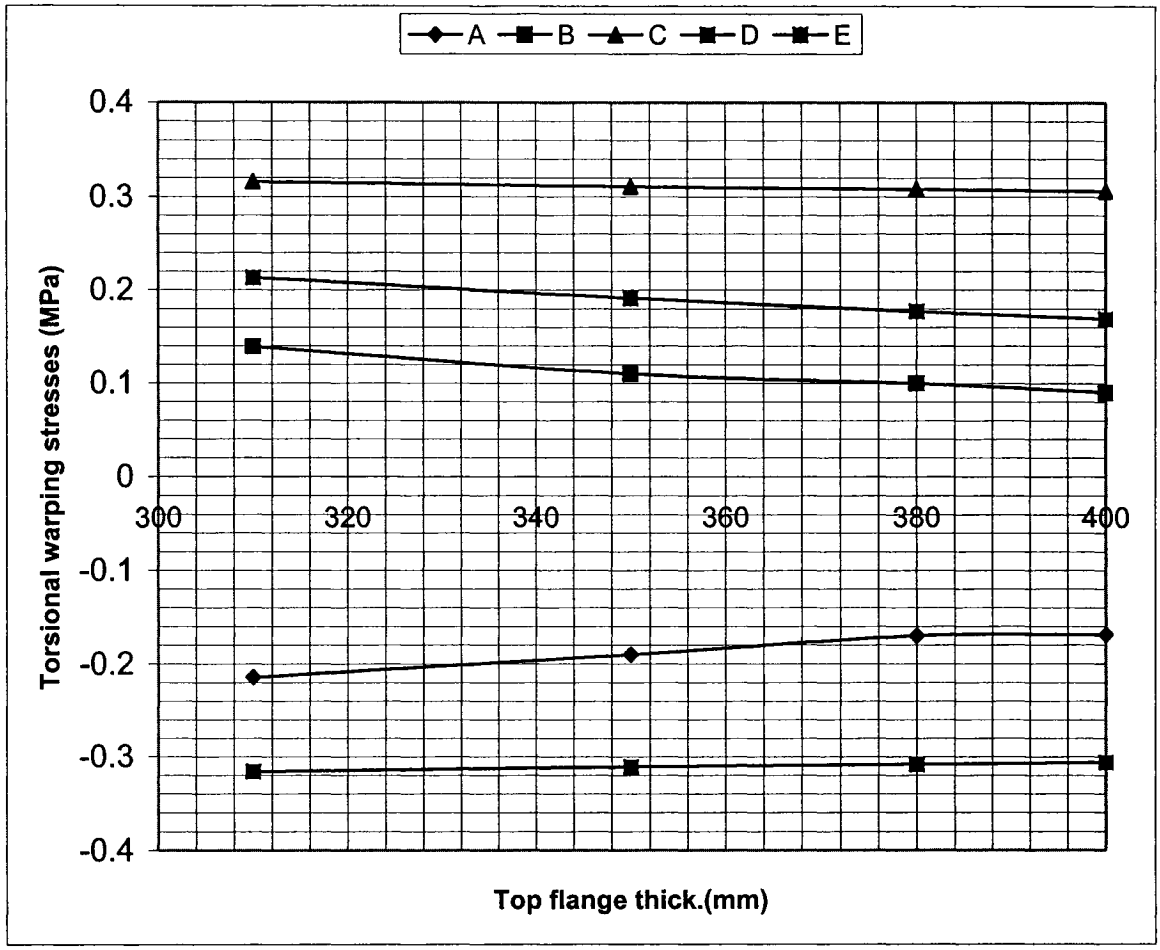

Figure 8.19: Variation of torsional warping stresses with top flange thicknesses (constant bottom flange thickness)

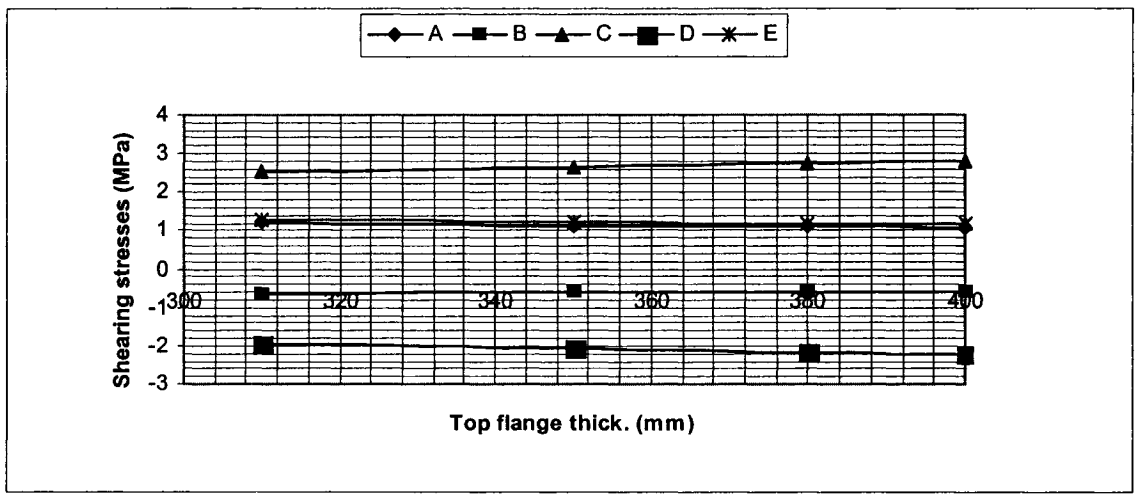

Figure 8.20: Variation of shearing stresses with top flange thickness (constant bottom Flange thickness)

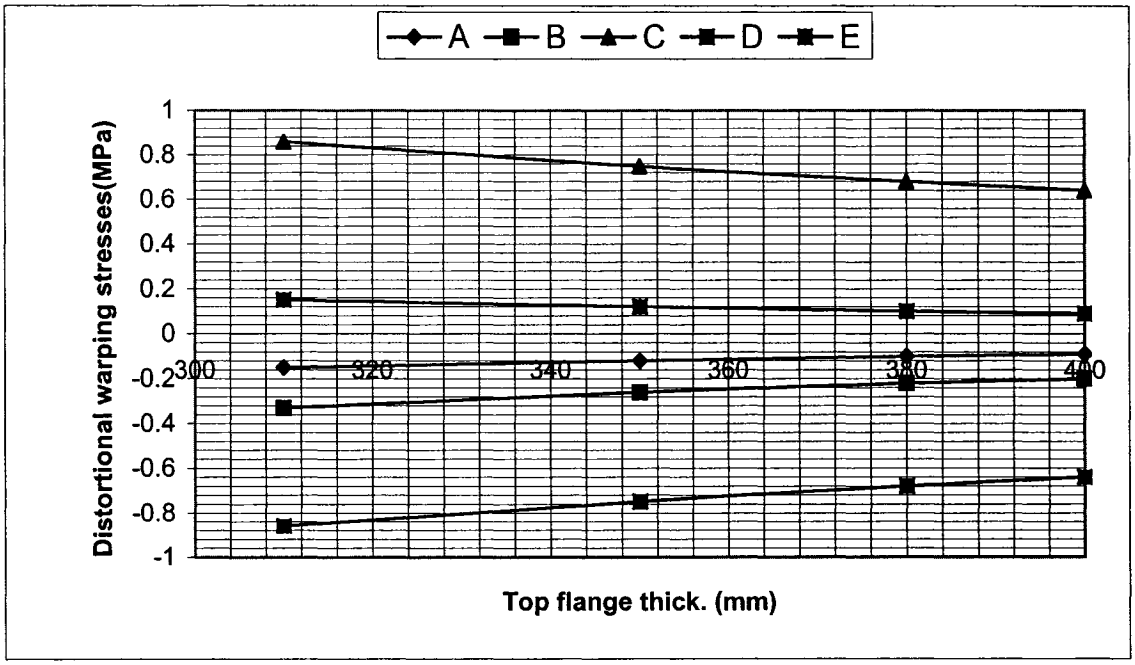

Figure 8.21: Variation of distortional warping stresses with top flange thicknesses (constant bottom flange thickness)

8.22 Effect of L/B ratio on Different Stresses:

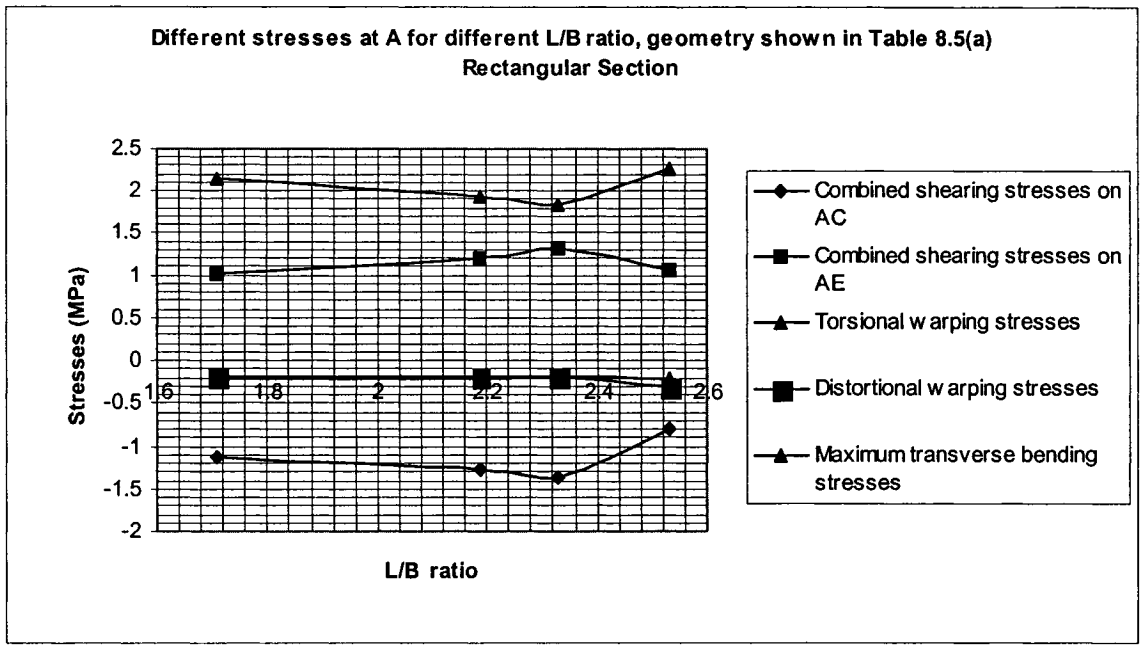

Figure 8.22: Stresses at A with different L/B ratio(Rectangular section)

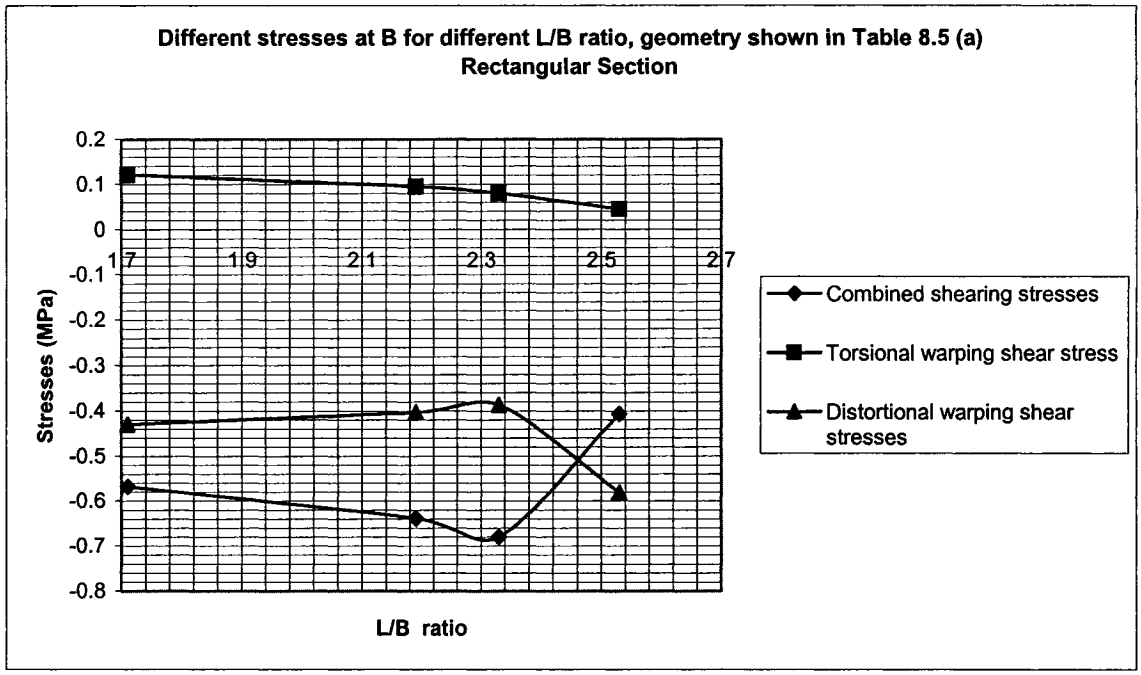

Figure 8.23: Stresses at B with different L/B ratio (Rectangular section)

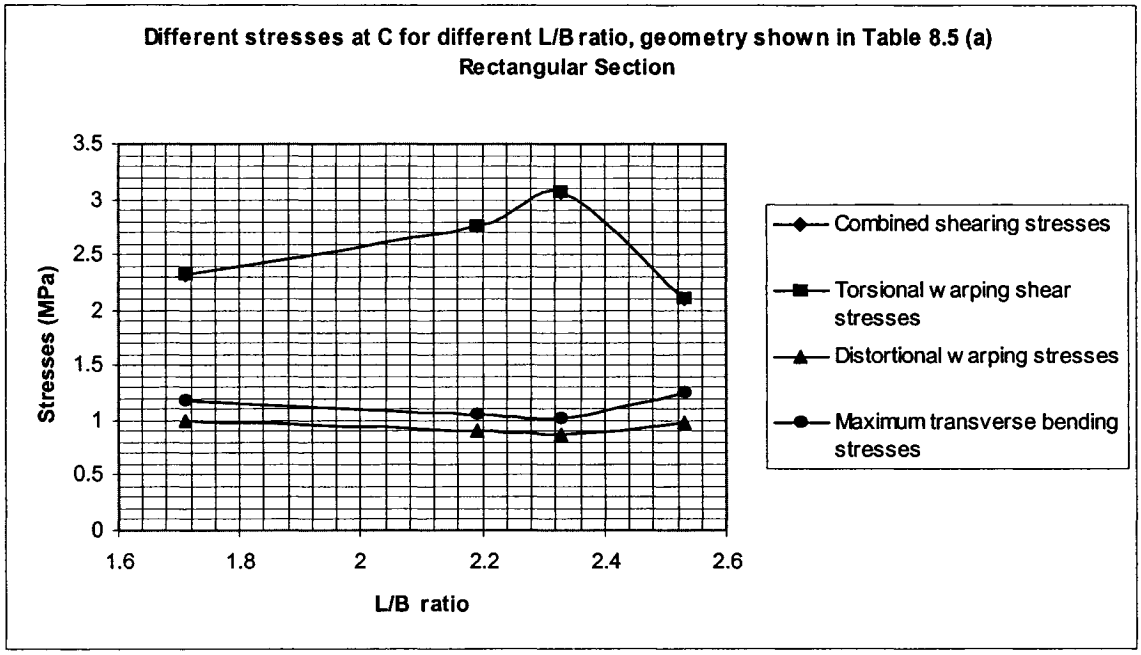

Figure 8.24: Stresses at C with different L/B ratios (Rectangular section)

From Figure 8.22-8.24, it can be noted that in the rectangular section at point B, combined shearing stresses and torsional warping shear stresses decrease with an increasing L/B ratio with a constant cantilever length. If the cantilever length decreases, the stresses start increasing.Distortional warping shear stresses increase with increasing L/B ratio with a constant cantilever length, similarly, if the cantilever length decreases, the stresses start decreasing.At point A, torsional warping stresses and combined shearing stresses decrease with an increasing L/B ratio with constant cantilever length.If the cantilever length decreases, the above stresses start increasing.At C, torsional warping shear stresses increase with an increase in the L/B ratio with constant cantilever length.If the cantilever length decreases, the stresses start decreasing.Also the distortional warping stresses, maximum transverse bending stresses decrease with an increasing L/B ratio.

8.23 Calculation of deflection:

For years, transverse flexure problem of box girders has been a subject of considerable research (Barker and Puckett, 1997; Schlaich and Scheef 1982) To summarize, there are several methods listed.

For an isotropic plate subjected to the transverse distributed load q, the equation governing the bending is given by (Reddy 1999)

$$D(\frac{\partial^4 w}{\partial x^4} + 2\frac{\partial^4 w}{\partial x^2 \partial y^2} + \frac{\partial^4 w}{\partial y^4}) = q \qquad 8.1$$

where $D = Et_u^{\ 3}/12(1-\mu^2)$

Navier's Method

The solution of equation 8.1 in the case where a rectangular plate with simply supported boundary conditions can be obtained using Navier's method (Reddy 1999). In Navier's method, the displacement and load are expanded in trigonometric series. The choice of these functions is restricted to those that satisfy the boundary conditions of the problem.

The simply supported boundary conditions are met by the following form of the transverse deflection;

$$w(x,y) = \sum_{n=1}^{\infty}\sum_{m=1}^{\infty} W_{mn} \sin\frac{m\pi x}{l}\sin\frac{n\pi y}{b} \qquad 8.2$$

where b= width of the top slab and l=span length.

Levy's Method:

The solution of equation 8.1 for a rectangular plate with simply supported edges along x=0, x=l, and the remaining two edges are free, simply supported, or clamped, can be obtained using Levy's method (Reddy 1999). The solution to the problem is represented as

$$w(x,y) = \sum_{n=1}^{\infty} W_n(y)\sin\frac{n\pi x}{l} \qquad 8.3$$

According to the codes and specifications (e.g., National Code and Specification 1985), the tire loads on pavement are distributed on the top slab with a rectangular configuration u x v .The intensity of the load on that area is q=P/uv.

The above two equations can be solved separately using Navier's method and Levy's method. The superposition of the two solutions will give us

$$w(x,y)=\frac{l^2}{2\pi^2 D}\sum_{n=1}^{\infty}\frac{1}{n^2}\{E_n(-\frac{\beta_n}{\sinh^2\beta_n}\sinh\frac{n\pi y}{l}-\frac{n\pi y}{l}\sinh\frac{n\pi y}{l}+\coth\beta_n\frac{n\pi y}{l}\cosh\frac{n\pi y}{l})$$
$$+F_n(\frac{\beta_n\cosh\beta_n}{\sinh^2\beta_n}\sinh\frac{n\pi y}{l}-\frac{1}{\sinh\beta_n}\frac{n\pi y}{l}\cosh\frac{n\pi y}{l})\}\sin\frac{n\pi x}{l}$$
$$+\frac{16P}{\pi^6 uvD}\sum_{n=1}^{\infty}\sum_{m=1}^{\infty}\frac{\sin\frac{n\pi\xi}{l}\sin\frac{m\pi\eta}{b}\sin\frac{n\pi u}{2l}\sin\frac{m\pi v}{2b}}{mn(\frac{n^2}{l^2}+\frac{m^2}{b^2})}\sin\frac{n\pi x}{l}\sin\frac{m\pi y}{b} \qquad 8.4$$

where $\beta_n=\frac{n\pi b}{l}$. b= width of the plate, l= length of the plate;

The first term is obtained using Levy's method for the elastic moments at y=0 and y=b, and the last term is the solution using Navier's method under load P.

For the elastically clamped boundary conditions, we get
When y=0

$$K(\frac{\partial w}{\partial y})_{y=0}=-\sum_{n=l}^{\infty}E_n\sin\frac{n\pi x}{l} \qquad 8.5$$

and when y=b

$$K(\frac{\partial w}{\partial y})_{y=b}=\sum_{n=l}^{\infty}F_n\sin\frac{n\pi x}{l} \qquad 8.6$$

where k=Kb/D. t_u = thickness of the top slab; E and μ = Young's modulas and Poissons ratio, respectively ; D= stiffness of flexure ; and k = rotational elastic coefficient.

Solving the above equations the constants En and Fn can be solved.

The moments in the plate in x and y directions can be calculated using the following formulas:

$$M_x = -D(\frac{\partial^2 w}{\partial x^2} + \mu \frac{\partial^2 w}{\partial y^2})$$

$$M_y = -D(\frac{\partial^2 w}{\partial y^2} + \mu \frac{\partial^2 w}{\partial x^2})$$

The above procedure for determining longitudinal bending stresses have been formulated in subroutine –G , Appendices-1.

Geometry considered :

A rectangular box beam of geometry as follows:

b=width of top flange=6600 mm

t_w= thickness of the web= 500mm

t_b=thickness of bottom flange=170 mm

t_u= thickness of top flange=310mm

h=height of the box beam=2760 mm

E= 2900 MPa

the rotational spring coefficient $K = \frac{3i_2 i_3 (2i_3 + 3i_2)(2i_3 + i_2)}{3i_3^{\,3} + 3i_3 i_2^{\,2} + 7i_2 i_3^{\,2}}$

where $i_2 = \frac{Et_w^{\,3}}{12h}, i_3 = \frac{Et_b^{\,3}}{12b}$

By using the above parameter , the longitudinal bending moment M_y has been calculated from subroutine G .M_y=5,500 kN.m

Now for linear elastic system, $\frac{\partial^2 v}{\partial x^2} = \frac{M}{EI}$

By solving the equation with the boundary conditions, at x=0, v=0 and x=l, v=0. The maximum deflection at x=l/2= 3.8 mm .

If the box beam is considered as a beam of equal EI value.

Maximum deflection at midspan $= \frac{Pl^3}{48EI}$ =2.8 mm.

CHAPTER 9

DISCUSSION AND CONCLUSIONS

9.1 Comparison of Results:

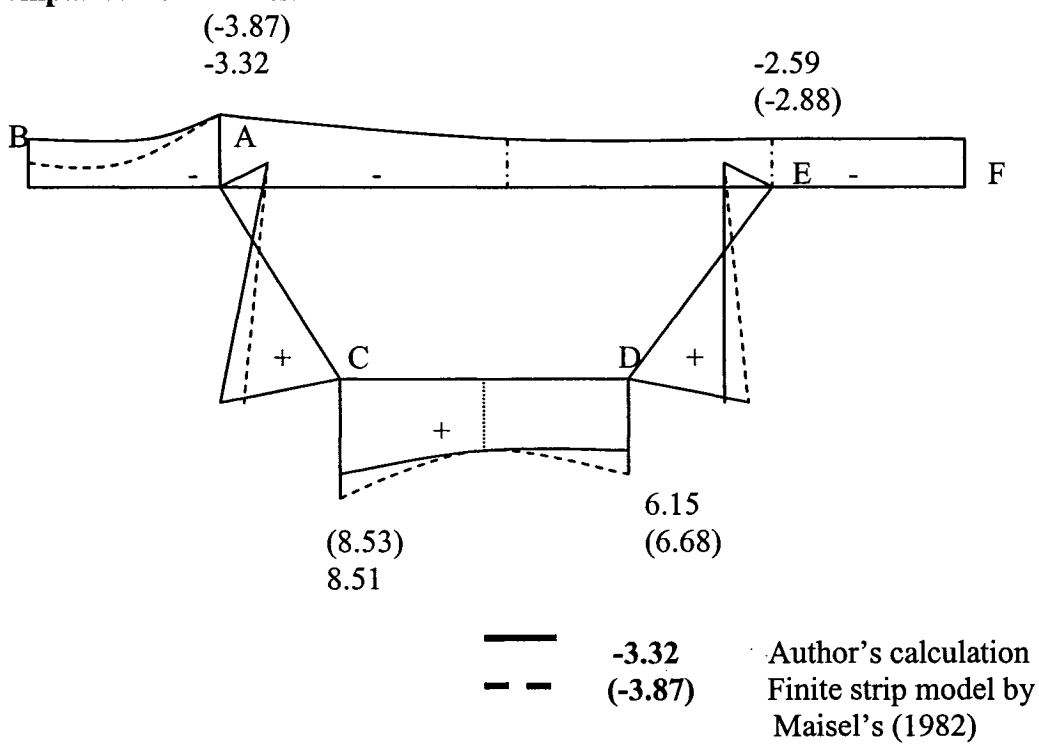

(a) Longitudinal stress at mid-span section

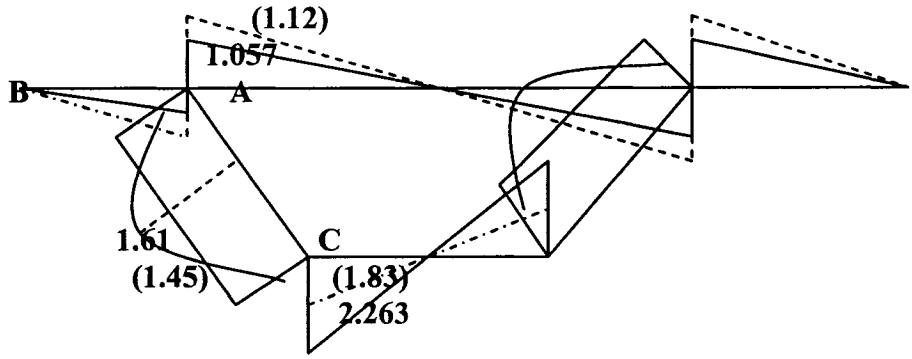

(b) Shear stress on positive face of section z=0

Figure 9.1: Comparison of stresses (MPa) due to combined live and dead load calculated by the theory presented here and by finite strip model by Maisel's (1982) Loading and geometry shown in Figure 7.1

Figure 9.1 summarizes the results obtained for longitudinal stress at mid span section and shear stress on positive face of the section at z=0 for eccentric live loading 1000 kN at

midspan, by the thin walled beam theory and the finite strip method.The results obtained from the computer program are also tabulated in Chapter 8.

There is good agreement between results from Maisel's finite strip model and author's calculations. Similarly there is good agreement for transverse bending stresses, except for the local regions near the concentrated loads.The use of thin plate theory in the finite strip method gives rise to a prediction of infinite local bending stresses in such areas, as the number of load harmonics is increased. This infinite local bending stress is avoided in the theory presented here in analysis of cross-sectional distortion.

The discrepancy between the values of shear stress obtained by the thin walled beam theory and the finite strip method appears to be significant. The finite strip theory considers shear lag effects both in the flanges and webs of a cross-section.The longitudinal stresses at midspan section calculated using the author's method (Figure 9.1) compare as follows with Maisel's finite strip model(1982)

At C, an increase of 0.23%

At D, an increase of 8%

At E, an increase of 10%

The shear stresses at z=0, calculated using author's method (Figure9.1) compare as follows with Maisel's(1982) finite strip model.

At middle of web AC, a 10% decrease

At A, an increase of 5%

9.2: Conclusions:

An in-depth study for analysis of simply supported, single cell prismatic box sections was conducted to evaluate all structural actions, and to develop stress charts for use by the practising engineer. The findings and comments are summarized as follows:

- Flexural stresses are calculated considering conventional bending theory.The results indicate that by increasing live loading by 50 percent , the bending stress increases by 11.6 percent at top flange and top web junction and end point of the cantilever and by 11.47 percent at bottom flange and web junction .The shear deformation were not considered.
- The statically determinate shear flows are plotted with incremental live loading at different locations of the section.The study shows that by increasing the live loading by 20 percent, the shear flow increases by 2.6 percent in all location of the cross-section.
- Statically determinate shear flows are plotted for varying spans. In this case, the results indicate that the shear flow increases non-uniformly at different locations of the cross-section. The results show that by increasing span length by 20 percent , the shear flow increases by 17.37 percent at A on AE, 7.9 percent at A on AC, 12.6 percent at the middle of AC and 17.37 percent at C.
- The study shows that by increasing the live loading by one percent, the increase in the shearing stresses are 0.26,0.27, 0.32, 0.27 and 0.27 percent at A on AE, at A on AC, at the middle of AB, at the middle of AC and at C, respectively.
- The results indicate that by increasing the torsional moment by one percent, the increases in the St. Venant's shearing stresses at A on AE, at C on AC, at C on CD and at E on DE are 0.99, 0.99, 1.06 and 0.99 percent ,respectively.
- The results indicate that by increasing the torsional moment by one percent, the torsional warping shear stresses increase in AB, AC, CD and AE by 0.97 ,0.99,1.01 and 1.01 percent, respectively.
- The study shows that by increasing the torsional moment by one percent at midspan, the distortional warping shear stresses increase at E on ED, at E on EA,

at the middle of EF, at the middle of DE, at D on CD, at the middle of AE and at the middle of CD by 0.98, 1.0, 0.99, 1.004, 0.99, 0.98 and 0.99 percent, respectively.

- The results indicate that by increasing the torsional moment at midspan by one percent, the torsional warping stress increases at A,C,D,E,B and F by 1.004, 1.001, 1.001, 1.004, 1.002 and 1.002 percent, respectively.
- The results indicate that by increasing the torsional moment at midspan by one percent, the distortional warping stresses increases at A,C,D,E,B and F by 0.97, 0.99, 0.99, 0.97, 0.99 and 0.99 percent, respectively.
- Considering the geometry and the loading studied , it is observed that for a one percentage increase in the top flange thickness, there will be an increase in the shear flow at A.B are 0.62, 0.6 percent, respectively and 0.38 percent at C and D. On the other hand, a one percent increase in the web thickness has very little effect on the shear flow at A and B that is 0.017 and 0.013 percent, respectively.However, the effect is slightly heigher at C , which is 0.47 percent.
- Considering the geometry studied Figure 1.2-1.14 and Figure 1.15-1.17 for eccentric loading of 1000 kN, it is noted that with an increase in the top flange thickness, the shearing stresses increase at A,B and E.Consequently, the shearing stresses decrease at C and D as these locations are on the bottom flange. The torsional warping stresses and the distortional warping stresses decrease at A,B,C ,D and E with an increase in the top flange thckness. Ratios of bottom flange thickness to top flange thick of 0.54 to 0.425 have been considered here.
- Considering the geometry described in Figure 1.2-1.14 and Figure1.18-1.20 with 1000kN eccentric loading, an increase of bottom flange thickness does not affect on the shearing stress at A,B and E. The shearing stress at C and D decrease with an increase in the bottom flange thickness. Ratios of the bottom flange thickness to the top flange thickness of 0.48 to 0.8 have been considered here.
- The study shows that for same L/B ratio, it is preferable to use the trapezoidal section instead of the rectangular section with the same depth for economic reasons; In addition, the different stresses at all locations with the similar loading conditions have nearly identical values.

- Only shear lag stresses due to live load along the width of the top flange are plotted in Figure 8.15. The study shows that for live load of 1000 kN at midspan, the shear lag stresses increase by about 2 percent of the combined(live load & dead load) stresses at the midspan section.

9.3: Limitations:

- It is an elastic analysis.
- Non-linearity of materials including cracking and prestressing of concrete is not considered here.
- Local buckling of steel sections is not considered here.

9.4: Recommendation for Future Research:

The program needs to be extended to enable evaluation of the various stresses for CHBDC live loads consisting of the truck and lane loads. In addition, the effect of dynamic loads need to be incorporated in the program.

REFERENCES:

Al-Raifaie, W.N.,and Evans, H.R.(1979). "An approximate method for the analysis of box girder bridges that are in curved in plan." Proceeding, International Association of Bridges and Structural Engineering, International Association for Bridges and Structural Engineering (IABSE), 1-21.

Abdullah, M.A., Abdul-Razzak, A.A.(1970)."Finite strip analysis of prestressed box-girders"Computational Structures, 36(5), 817-822.

Aneja, I.K.,and Roll, F.(1971). "A model analysis of curved box-beam highway bridges."Journal of the Structural Division,ASCE, 97(12) 2861-2878.

Arizumi, Y., Hamada, S and Oshiro, T. (1983)" Static behaviour of curved composite box girders." Japan Society for Civil Engineering, 15,212-216.

ASCE-AASHTO Subcommittee of Box Girder Bridges on the Committee of the flexural members.(1967) " Trend in the design of steel box-girder bridges."Journal of the Structural Division, ASCE, 93(30, 165-180.

ASCE-AASHTO Task Committee on curved box girders of the Committee on Metals of the ASCE (1978a), " Curved steel box girder bridges: a survey." Journal of the Structural Division, ASCE, 104(11), 1,697-1,718.

Aslam, M., and Godden, W.G. (1973). "Model studies of curved box girder bridges." Report No. UC/SESM 73-5, Department of Civil Engineering University of California, Berkely.

Aslam, M., and Godden, W.G. (1975) " Model studies of multicell curved box girder bridges."Journal of the Engineering Mechanics, ASCE, Vol. 101, No. (3),207-222,1975.

Benscoter, S.U. (1954) . " A theory of torsion bending for multicell beams." Journal of Applied Mechanics, 21(1),25-34.

Boswell, F., Zhang, S.H.(1984) "The effect of distortion in thin-walled box spine beams." Inst. Solids Struct.,20(9/10),845-862.

Buragohain,D.N., and Agrawal, B.L. (1973)." Analysis of curved box girder bridges," Journal of the Structural Division, ASCE, 99(5), 799-819.

Branco, F.A., and Green,R.(1984) "Bracing in completed composite box girder bridges.

Li,W.Y.,Tham,L.G., and Cheung,Y.K.(1988) "Curved box girder bridges".Journal of the Structural Division,ASCE, 114(6), 1324-1338

Bakht, B., Jaegor, L.G., and Cheung,M.S. (1981) 'State of art in analysis of cellular and voided slab bridges.'Canadian Journal of Civil Engineering, 8(3), 376-391.

Benscoter, S.U. A theory of torsion bending for multicell beams. Journal of applied mechanics.Vol.21,No.1.March 1954.pp.25-34.

Chang and Zheng (1987): "Negative shear lag in cantilever box girder with constant depth." Journal of Structural Engineering 116(9), 20-35

Cheung, M. S., and Jaeger,L.G.(1992) "Spline finite strip analysis of continious haunched box-girder bridges.''Canadian Journal of Civil Engineering,19, 724-728.

Cheung, M.S.,and Li, W.(1989)."Analysis of continious, haunched box girder bridges by finite strips." Journal of the Structural Division, ASCE, 115(5),1076-1087.

Chang,S.T., and Gang, J.Z. (1990): "Analysis of cantilever decks of thin walled box girder bridges." Journal of the Structural Division , ASCE, 116(9), 2410-2418.

Cheung, M.S., and Cheung,Y.K. (1971). "Analysis of curved box girder bridges by finite strip method."International Association for Bridges and Structural Engineering (IABSC) 31(I),1-8

Daniels,J.H., Abraham,D., and Yen, B.T. (1979)"Fatigue of curved steel bridge elements-effects of internal diaphragms on fatigue strength of curved box girders."Federal Highway Adminstration, Washington, D.C.Report. No. FHWA-RD-79-136

Dezi, L. (1995) " Aspect of the deformation of the cross-section in curved single cell box beam." Industria Italiana Del Cemento, 55(7-8)500-808.

Dilger,W., Ghoneim and Tadros,G., (1988): "Diaphragms in skew box girder bridges." . Candian Journal of Civil Engineering 15(5) 869-878.

Evans,H.R.(1984). Simplified methods for the analysis and design of bridges of cellularcross-section." Proceeding, NATO Advanced Study Institute on Analysis and Design of Bridges,Cesme,Izmir,Turkey,74,95-115.

Evans, H.R., and Shanmugam, N.E., (1984)."Simplified analysis for cellular structures." Journal of Structural Division, ASCE, 110(3),531-543.

Elbadry, M. M., and Ibrahim, A. M. (1996) "Temperature distributions in curved concrete box girder bridges." Proceeding, Ist Structural Speciality Conference, Canadian Society of Civil Engineering, Edmonton, Alberta, Canada, 1-12

Gambir, M.L., and Singla, K.G.(1988). "Optimization of concrete multi-cellular bridge decks."Ind.Concr.J.,62(1),21-26.

Heilig,R. A contribution to the theory of boxgirders of arbitrary cross-sectional shape-Der Stahlbau.Vol-30,No.11.November 1961,pp.333-349.Vol.31 No-2,February 1962,p64.No-4,April1962,p128.(C&CA Translation No.145,1971)

Heilig, R. :A contribution to the theory of box girders of arbitrary cross-sectional shape. Der Stahlbau. Vol. 30, No.11. November 1961, pp333-349,Vol. 31. No.2. February 1962, p. 64, No.4 April 1962,p. 128. (C & CA Translation No. 145, 1971)

Hambly, E.C. and Pennells, E. : Grillage analysis applied to cellular bridge decks. The Structural Engineer. Vol. 53, No.7. July 1975. pp. 267-275. Discussion: Vol.53, No. 1. January 1976. pp 39-40.

Ishac, I. I., and Smith, T. R. G. (1985): Approximations for moments in box girders." Journal of Structural Division, ASCE, 111(11), 2,333-2,342.

Kollbrunner, C. F.and Basler, K."Sektorielle Grossen und Spannungen bei offenen, dunnwandigen Querschnitten"Sectorial quantities and stresses in open thin walled cross-sections.)Zurich,Schweizer Stahlbau-Vereinigung,January 1964.Mitteilungen der Technischen Kommission,Heeft 28.50 pp+Table

Kollbrunner, C.F and Hajdin, N. Warping torsion of thinwalled beams of closed section.Zurich,Verlag Schweizer Stahlbau-Vereinigung1966.Mitteilungen der Technischen Kommission,Heft 32.175pp+ Tables.

Kollbrunner, C. F and Hajdin, N. "Warping torsion of thinwalled beams of open section". Zurich,Verlag Schweizer Stahlbau-Vereinigung,October1964.Mitteilungen der Technischen Kommission, Heft 29. 121pp+ Tables.

Kabir, A.F., and Scordelis, A.C.(1974) "Computer programs for curved bridges on flexible bents." Structural Engineering and Structural Mechanics Report. No. UC/SESM 74-10, University of California, Berkely.

Kelsey, S. "Lecture notes on analysis of thin walled,closed tubes".London, Department of Aeronautics, Imperial College,1961.

Kollbrunner,C.F. and Hajdin,N: Warping torsion of thin walled beams of open sections. May 1965.

Luoxi, Mingsheng and Lin (1993): "Time dependent analysis of non prismatic curved P.C. box girder bridges." 5th International Conference on Computing in Civil and Building Engineering." New York, 1703-1710.

Lim, P.T.K. and Moffatt, K.R.(1971) : Finite element analysis of curved slab bridges with special reference to local stresses. Development in bridge design and construction, London, U.K., 264-286.

Maisel, B.I. (1970): Review of Literature related to the analysis and design of thin walled beams. London, Cement and Concrete Association. July 1970.34 pp. Technical Report 440(publication 42.440)

Maisel,B.I.(1982). Analysis of concrete box beams using small computer capacity."Cement and Concrete Association, London.

Maisel,B.I.(1985). Analysis of concrete box beams using small computer capacity."Canadian Journal of Civil Engineering,12(2), 265-278.

Maisel,B.I.(1986). Shear lag analysis of concrete box beams using small computer capacity."Proc.2nd International Conference on Short and Medium Span Bridges, Canadian Scociety of Civil Engineering.Ottawa,Canada,1,125-137

Maisel, B.I., and Roll,F.(1974) Methods of analysis and design of concrete box beams with side cantilevers, Cement and Concrete Association London.

Mishra, P. K., Das, S., and Dey, S. S. (1992) "Discrete energy method for the analysis of right box girder bridges." Computational Structures, 43(2), 223-235.

Maffatt, K. R., and Lim, P. T. K. (1976) "Finite element analysis of composite box girder bridge having complete and incomplete interaction." Proceeding, Institute Civil Engineering Part 2, 63(3), 1-22.

Maisel, B.I. and Roll,F. Methods of analysis and design of concrete boxbeams with side cantilevers.London,Cement and Concrete Association,November 1974.176 pp.Technical Report 494 (publication 42.494)

Maisel, B.I., Rowe,R.E., and Swann,R.A.(1973) Concrete box girder bridges." Structural Engineering 51(10), 363-376.

Maleki, S.(1991) 'Compound strip method for box girders and folded plates." Computational Structures 40(3),527-538.

Mavadat, S., and Mirza,M.S.(1989) "Computer analysis of thin walled concrete box beams."Canadian Journal of Civil Engineering16(6),902-909.

Malcolm, D. J., and Redwood, R. G. (1970): "Shear lag in stiffened box girders." Journal of Structural Divisison, ASCE, 96(7)

Meyer C., and Scordelis, A.C.(1971) Analysis of curved folded plate structures."Journal of Structural Division, ASCE, 97(10),2459-2480.

Megson,T.H.G. Linear analysis of thin-walled elastic structures. Leighton Buzzard,Surrey University Press, Internet Publishing Ltd. 1974.232 pp.

Marsh,J.G.,and Taylor,P.(1990) "PC program for orthotropic plate box girder bridges."Australia Second National Structural Engineering Conference Institute of Engineers Australia, 224-235.

Moffat, K.R. and Dowling,P.J. Shear lag in steel box girder bridges.The Structural Engineer.Vol.53,No.10 October 1975.pp 439-448,Discussion: Vol.54,No.8.August 1976.pp. 258-298.

Moffat,K.R. and Dowling, P.J. The longitudinal bending behaviour of composite box girder bridges having incomplete interaction.The Structural Engineer. September 1978.Vol.56B, No.3. pp 53-60.

Richmond,B.Matrix difference analysis of box girders.Proceedings of the Institution of Civil Engineers.Vol. 43.August 1969. pp. 651-655. Full manuscript of Abstract paper in ICE Library.

Roik, K. and Sedlacek, G. : Extension of Engineers theory of bending and torsion, considering shear deformation. Die Bautechnik. Vol. 47, No. 1. January 1970. pp.20-32

Roik, K. and Sedlacek, G. Extension of engineers theory of bending and torsion, considering shear deformation. Die Bautechnik.Vol.47,No.1 January 1970. pp.20-32.

Steinle,A.: Torsion and cross-sectional distortion, (Technische Hochschule)Stuttgart,1967.

Sennah, K. M. and Kennedy, J. B. : Literature Review in Analysis of Box-Girder Bridges;Journal of Bridge Engineering, Vol 7, No.2, March 1, 2002, ASCE

Shanmugam, N. E., and Balendra, T.(1986) 'Free vibration of thin walled multicell structures." Thin walled structures, 4(6), 457-485.

Shimuzu, S.,and Yoshida,S.(1991) "Reaction allotment of continious curved box girders." Thin walled struct. 11(4),319-341.

Scordelis,A.C., and Larsen,P.K.(1997). Structural response of curved RC box girder bridge." Journal of Structural Division, ASCE, 103(8),1507-1524.

Sisodlya, R. G., Cheung, Y. K., and Ghali, A. (1970) Finite element analysis of skew curved box girder bridges." International Association of Bridges and Structural Engineering, (IABSE), 30(II), 191-199.

Soliman, M. I and Mirza, M. S (1985)" Design of box girder bridges" ACI Convention, Washinton ,D.C., 81-108.

Sung C. Lee;Chai H. Yoo, and Dong Y. Yoon:Analysis of Shear Lag Anomaly in Box Girders, Journal of Structural Engineering, Vol.128, No. 11 , November 1, 2002. ASCE

Swann, R.A. : A feature survey of concrete box spine- beam bridges. London. Cement and Concrete Association, June 1972. 76 pp. Technical Report (publication 42. 469)

Turner, J.G., Rawnsley, T.J. and Salter, J.B. : Shear lag in single cell concrete box sections with side cantilevers.Technical Report, Midland Road construction Unit.Warwickshire County Council Sub Unit, December 1977.

Sedlacek, G. Application of extended bending and torsion theory to the analysis of box beams of deformable cross-section. Strasse Brucke Tunnel.No. 9. September 1971.pp.241-244. No. 12. December 1971. pp. 329-335.

Templeman, A. B., and Winterbottom, S. K. (1979): " Optimum design of concrete cellular spine beam bridge decks." Proceeding of Institute Civil Engineering, London, 67(2), 389-409.

Venkatraman, B. and Patel, S.A. Structural mechanics with introductions to elasticity and plasticity. London, McGraw-Hill,1970. 648 pp.

Vlasov,V.Z. (1965) "Thin walled elastic beams." OTS61-11400, National science Foundation, Washington, D.C.

Wolfram Research, Inc. Mathematica, Version 5. Champaign, USA

APPENDIX-1

Program-A:

```
L1=2800;L2=3300;L3=2805;L4=2760;ee=34.5;A3=500;
I1=170^3/12;I2=310^3/12;I3=500^3/12;
kb=Table[0,{i,1,4},{j,1,4}];
kb[[1,1]]=(3*ee*I1/L1^3)+((A3*ee*(L4/L3)^2)/L3)+((12*ee*I3*(
(L2-L1)/L3)^2)/L3^3);
kb[[1,2]]=-((A3*ee*(L4/L3)^2)/L3)-((12*ee*I3*((L2-
L1)/L3)^2)/L3^3);
kb[[1,3]]=-(6*ee*I3*((L2-L1)/L3)/L3^2)+(3*ee*I1/L1^2);
kb[[1,4]]=-(6*ee*I3*((L2-L1)/L3)/L3^2);
kb[[2,1]]=kb[[1,2]];
kb [[2,2]]=(A3*ee*((L4/L3)^2)/L3)+((12*ee*I3*((L2-
L1)/L3)^2)/L3^3)+(3*ee*I2/L2^3);
kb[[2,3]]=(6*ee*I3*((L2-L1)/L3)/L3^2);
kb[[2,4]]=(6*ee*I3*((L2-L1)/L3)/L3^2)+(3*ee*I2/L2^2);
kb[[3,1]]=kb[[1,3]];
kb[[3,2]]=kb[[2,3]];
kb[[3,3]]=(4*ee*I3/L3)+(3*ee*I1/L1);
kb[[3,4]]=2*ee*I3/L3;
kb[[4,1]]=kb[[1,4]];
kb[[4,2]]=kb[[2,4]];
kb[[4,3]]=kb[[3,4]];
kb[[4,4]]=(4*ee*I3/L3)+(3*ee*I2/L2);
MatrixForm[kb]
hh=Inverse[kb]
R={10,0,0,0}
r=R.hh
MatrixForm[r]
```

Output program-A:

A1

$$\begin{pmatrix} 5.96214 & -5.96021 & -43.4457 & -48.8507 \\ -5.96021 & 5.96736 & 48.8507 & 72.4455 \\ -43.4457 & 48.8507 & 527612. & 256239. \\ -48.8507 & 72.4455 & 256239. & 590341. \end{pmatrix}$$

A2

$$\begin{pmatrix} 1237.97 \\ 1237.05 \\ 0.014418 \\ -0.055624 \end{pmatrix}$$

Program B

```
(*Program # B, this program evaluates necessary input data
for spreadsheet programming in excell for the analysis of
shear lag effect in simply-supported single cell box
section*)
 a11=8.283*10^6;a12=0;a13=0;a14=0;a15=-136400000;a16=-
165333333.3;a17=63466666.67;a22=109.037*10^12;
a23=0;a24=0;a25=a26=a27=0;a33=9.315*10^12;a34=0;a35=1.07074*
10^11;a36=1.29787*10^11;a37=1.25347*10^11;
a44=19.3915*10^18;a45=a46=a47=0;a55=10912000000;a56=a57=0;a6
6=13226666667;a67=0;a77=4918666667;
c11=0;c12=0;c13=0;c14=0;c15=0;c16=0;c17=0;c22=0;
c23=0;c24=0;c25=c26=c27=0;c33=0;c34=0;c35=0;c36=0;c37=0;
c44=0;c45=c46=c47=0;c55=2505;c56=c57=0;c66=2067;c67=0;c77=16
19;
u11=1;u12=0;u13=0;u14=0;u15=0;u16=0;u17=0;u21=0;u22=1;
u23=0;u24=0;u25=u26=u27=0;u31=u32=0;u33=1;u34=0;u35=0;u36=0;
u37=0;
u41=u42=u43=0;u44=1;u45=u46=u47=0;u51=16.46746348;u52=0;u53=
-
0.011495262;u54=0;u55=1;u56=u57=0;u61=19.96056179;u62=0;u63=
-0.013933651;u64=u65=0;u66=1;u67=0;u71=-7.662280;u72=0;u73=-
0.013456981;u74=u75=u76=0;u77=1;
v11=1;v12=0;v13=0;v14=0;v15=0;v16=0;v17=0;v21=0;v22=1;
v23=0;v24=0;v25=v26=v27=0;v31=v32=0;v33=1;v34=0;v35=0;v36=0;
v37=0;
v41=v42=v43=0;v44=1;v45=v46=v47=0;v51=0;v52=0;v53=0;v54=0;v5
5=1;v56=0.88;v57=1.21;v61=0;v62=0;v63=0;v64=0;v65=1.25;v66=1
;v67=-2.42;v71=0;v72=0;v73=0;v74=0;v75=20.55;v76=-
29.36;v77=1;
rv={0,0,1,0,0,0,0};
mul1=1.3298*10^6;
mul2=1.9036*10^6;
mul3=5.35916*10^6;
kb=Table[0,{i,1,7},{j,1,7}];
kb[[1,1]]=a11;
kb[[1,2]]=kb[[2,1]]=a12;
kb[[1,3]]=kb[[3,1]]=a13;
kb[[1,4]]=kb[[4,1]]=a14;
kb[[1,5]]=kb[[5,1]]=a15;
kb[[1,6]]=kb[[6,1]]=a16;
kb[[1,7]]=kb[[7,1]]=a17;
kb[[2,2]]=a22;
kb[[2,3]]=kb[[3,2]]=a23;
kb[[2,4]]=kb[[4,2]]=a24;
kb[[2,5]]=kb[[5,2]]=a25;
kb[[2,6]]=kb[[6,2]]=a26;
kb[[2,7]]=kb[[7,2]]=a27;
kb[[3,3]]=a33;
```

```
kb[[3,4]]=kb[[4,3]]=a34;
kb[[3,5]]=kb[[5,3]]=a35;
kb[[3,6]]=kb[[6,3]]=a36;
kb[[3,7]]=kb[[7,3]]=a37;
kb[[4,4]]=a44;
kb[[4,5]]=kb[[5,4]]=a45;
kb[[4,6]]=kb[[6,4]]=a46;
kb[[4,7]]=kb[[7,4]]=a47;
kb[[5,5]]=a55;
kb[[5,6]]=kb[[6,5]]=a56;
kb[[5,7]]=kb[[7,5]]=a57;
kb[[6,6]]=a66;
kb[[6,7]]=kb[[7,6]]=a67;
kb[[7,7]]=a77;
nn=MatrixForm[kb]
kd=Table[0,{i,1,7},{j,1,7}];
kd[[1,1]]=c11;
kd[[1,2]]=kd[[2,1]]=c12;
kd[[1,3]]=kd[[3,1]]=c13;
kd[[1,4]]=kd[[4,1]]=c14;
kd[[1,5]]=kd[[5,1]]=c15;
kd[[1,6]]=kd[[6,1]]=c16;
kd[[1,7]]=kd[[7,1]]=c17;
kd[[2,2]]=c22;
kd[[2,3]]=kd[[3,2]]=c23;
kd[[2,4]]=kd[[4,2]]=c24;
kd[[2,5]]=kd[[5,2]]=c25;
kd[[2,6]]=kd[[6,2]]=c26;
kd[[2,7]]=kd[[7,2]]=c27;
kd[[3,3]]=c33;
kd[[3,4]]=kd[[4,3]]=c34;
kd[[3,5]]=kd[[5,3]]=c35;
kd[[3,6]]=kd[[6,3]]=c36;
kd[[3,7]]=kd[[7,3]]=c37;
kd[[4,4]]=c44;
kd[[4,5]]=kd[[5,4]]=c45;
kd[[4,6]]=kd[[6,4]]=c46;
kd[[4,7]]=kd[[7,4]]=c47;
kd[[5,5]]=c55;
kd[[5,6]]=kd[[6,5]]=c56;
kd[[5,7]]=kd[[7,5]]=c57;
kd[[6,6]]=c66;
kd[[6,7]]=kd[[7,6]]=c67;
kd[[7,7]]=c77;
ff=MatrixForm[kd]
ky=Table[0,{i,1,7},{j,1,7}];
ky[[1,1]]=u11;
ky[[1,2]]=u12;
ky[[2,1]]=u21;
ky[[1,3]]=u13;
ky[[3,1]]=u31;
ky[[1,4]]=u14;
ky[[4,1]]=u41;
ky[[1,5]]=u15;
```

```
ky[[5,1]]=u51;
ky[[1,6]]=u16;
ky[[6,1]]=u61;
ky[[1,7]]=u17;
ky[[7,1]]=u71;
ky[[2,2]]=u22;
ky[[2,3]]=u23;
ky[[3,2]]=u32;
ky[[2,4]]=u24;
ky[[4,2]]=u42;
ky[[2,5]]=u25;
ky[[5,2]]=u52;
ky[[2,6]]=u26;
ky[[6,2]]=u62;
ky[[2,7]]=u27;
ky[[7,2]]=u72;
ky[[3,3]]=u33;
ky[[3,4]]=u34;
ky[[4,3]]=u43;
ky[[3,5]]=u35;
ky[[5,3]]=u53;
ky[[3,6]]=u36;
ky[[6,3]]=u63;
ky[[3,7]]=u37;
ky[[7,3]]=u73;
ky[[4,4]]=u44;
ky[[4,5]]=u45;
ky[[5,4]]=u54;
ky[[4,6]]=u46;
ky[[6,4]]=u64;
ky[[4,7]]=u47;
ky[[7,4]]=u74;
ky[[5,5]]=u55;
ky[[5,6]]=u56;
ky[[6,5]]=u65;
ky[[5,7]]=u57;
ky[[7,5]]=u75;
ky[[6,6]]=u66;
ky[[6,7]]=u67;
ky[[7,6]]=u76;
ky[[7,7]]=u77;
mm=MatrixForm[ky]
jj=Transpose[ky]
MatrixForm[jj]
K=ky.kb.jj
MatrixForm[K]
K1=ky.kd.jj
MatrixForm[K1]
K2a=Simplify[mul1*ky.kd.jj]
MatrixForm[K2a]
K3a=Simplify[K-K2a]
MatrixForm[K3a]
K2b=Simplify[mul2*ky.kd.jj]
MatrixForm[K2b]
```

```
K3b=Simplify[K-K2b]
MatrixForm[K3b]
K2c=Simplify[mul3*ky.kd.jj]
MatrixForm[K2c]
K3c=Simplify[K-K2c]
MatrixForm[K3c]
ke=Table[0,{i,1,7},{j,1,7}];
ke[[1,1]]=v11;
ke[[1,2]]=v12;
ke[[2,1]]=v21;
ke[[1,3]]=v13;
ke[[3,1]]=v31;
ke[[1,4]]=v14;
ke[[4,1]]=v41;
ke[[1,5]]=v15;
ke[[5,1]]=v51;
ke[[1,6]]=v16;
ke[[6,1]]=v61;
ke[[1,7]]=v17;
ke[[7,1]]=v71;
ke[[2,2]]=v22;
ke[[2,3]]=v23;
ke[[3,2]]=v32;
ke[[2,4]]=v24;
ke[[4,2]]=v42;
ke[[2,5]]=v25;
ke[[5,2]]=v52;
ke[[2,6]]=v26;
ke[[6,2]]=v62;
ke[[2,7]]=v27;
ke[[7,2]]=v72;
ke[[3,3]]=v33;
ke[[3,4]]=v34;
ke[[4,3]]=v43;
ke[[3,5]]=v35;
ke[[5,3]]=v53;
ke[[3,6]]=v36;
ke[[6,3]]=v63;
ke[[3,7]]=v37;
ke[[7,3]]=v73;
ke[[4,4]]=v44;
ke[[4,5]]=v45;
ke[[5,4]]=v54;
ke[[4,6]]=v46;
ke[[6,4]]=v64;
ke[[4,7]]=v47;
ke[[7,4]]=v74;
ke[[5,5]]=v55;
ke[[5,6]]=v56;
ke[[6,5]]=v65;
ke[[5,7]]=v57;
ke[[7,5]]=v75;
ke[[6,6]]=v66;
ke[[6,7]]=v67;
```

```
ke[[7,6]]=v76;
ke[[7,7]]=v77;
MatrixForm[ke]
K4=Simplify[ky.ke]
MatrixForm[K4]
hh=Transpose[ke]
K5=MatrixForm[hh]
K9=Simplify[ke.K.hh]
MatrixForm[K9]
K7=Simplify[ke.kd.hh]
MatrixForm[K7]
K8=Simplify[K4.rv]
MatrixForm[K8]
```

Output Program-B

B1 [$\underline{C}_v$ matrix]

$$\begin{pmatrix} 8.283\times10^{6} & 0 & 0 & 0 & -136400000 & -1.65333\times10^{8} & 6.34667\times10^{7} \\ 0 & 1.09037\times10^{14} & 0 & 0 & 0 & 0 & 0 \\ 0 & 0 & 9.315\times10^{12} & 0 & 1.07074\times10^{11} & 1.29787\times10^{11} & 1.25347\times10^{11} \\ 0 & 0 & 0 & 1.93915\times10^{19} & 0 & 0 & 0 \\ -136400000 & 0 & 1.07074\times10^{11} & 0 & 10912000000 & 0 & 0 \\ -1.65333\times10^{8} & 0 & 1.29787\times10^{11} & 0 & 0 & 13226666667 & 0 \\ 6.34667\times10^{7} & 0 & 1.25347\times10^{11} & 0 & 0 & 0 & 4918666667 \end{pmatrix}$$

B2

$$\begin{pmatrix} 0 & 0 & 0 & 0 & 0 & 0 & 0 \\ 0 & 0 & 0 & 0 & 0 & 0 & 0 \\ 0 & 0 & 0 & 0 & 0 & 0 & 0 \\ 0 & 0 & 0 & 0 & 0 & 0 & 0 \\ 0 & 0 & 0 & 0 & 2505 & 0 & 0 \\ 0 & 0 & 0 & 0 & 0 & 2067 & 0 \\ 0 & 0 & 0 & 0 & 0 & 0 & 1619 \end{pmatrix}$$

B3

$$\begin{pmatrix} 1 & 0 & 0 & 0 & 0 & 0 & 0 \\ 0 & 1 & 0 & 0 & 0 & 0 & 0 \\ 0 & 0 & 1 & 0 & 0 & 0 & 0 \\ 0 & 0 & 0 & 1 & 0 & 0 & 0 \\ 16.4675 & 0 & -0.0114953 & 0 & 1 & 0 & 0 \\ 19.9606 & 0 & -0.0139337 & 0 & 0 & 1 & 0 \\ -7.66228 & 0 & -0.013457 & 0 & 0 & 0 & 1 \end{pmatrix}$$

B4

$$\begin{pmatrix} 1 & 0 & 0 & 0 & 16.4675 & 19.9606 & -7.66228 \\ 0 & 1 & 0 & 0 & 0 & 0 & 0 \\ 0 & 0 & 1 & 0 & -0.0114953 & -0.0139337 & -0.013457 \\ 0 & 0 & 0 & 1 & 0 & 0 & 0 \\ 0 & 0 & 0 & 0 & 1 & 0 & 0 \\ 0 & 0 & 0 & 0 & 0 & 1 & 0 \\ 0 & 0 & 0 & 0 & 0 & 0 & 1 \end{pmatrix}$$

B5 [$\underline{\overline{C}}_v$ matrix]

$$\begin{pmatrix} 8.283\times10^{6} & 0. & 0. & 0. & 0.00483999 & 0.00656998 & 1.43 \\ 0. & 1.09037\times10^{14} & 0. & 0. & 0. & 0. & 0. \\ 0. & 0. & 9.315\times10^{12} & 0. & -4.36553\times10^{6} & -4.95906\times10^{6} & -4.77801\times10^{6} \\ 0. & 0. & 0. & 1.93915\times10^{19} & 0. & 0. & 0. \\ 0.00483999 & 0. & -4.36553\times10^{6} & 0. & 7.43504\times10^{9} & -4.2145\times10^{9} & -3.95703\times10^{8} \\ 0.00656998 & 0. & -4.95906\times10^{6} & 0. & -4.2145\times10^{9} & 8.11818\times10^{9} & -4.79644\times10^{8} \\ 1.43 & 0. & -4.77801\times10^{6} & 0. & -3.95703\times10^{8} & -4.79644\times10^{8} & 2.74564\times10^{9} \end{pmatrix}$$

B6

$$\begin{pmatrix} 0. & 0. & 0. & 0. & 0. & 0. & 0. \\ 0. & 0. & 0. & 0. & 0. & 0. & 0. \\ 0. & 0. & 0. & 0. & 0. & 0. & 0. \\ 0. & 0. & 0. & 0. & 0. & 0. & 0. \\ 0. & 0. & 0. & 0. & 2505. & 0. & 0. \\ 0. & 0. & 0. & 0. & 0. & 2067. & 0. \\ 0. & 0. & 0. & 0. & 0. & 0. & 1619. \end{pmatrix}$$

B7

$$\begin{pmatrix} 0. & 0. & 0. & 0. & 0. & 0. & 0. \\ 0. & 0. & 0. & 0. & 0. & 0. & 0. \\ 0. & 0. & 0. & 0. & 0. & 0. & 0. \\ 0. & 0. & 0. & 0. & 0. & 0. & 0. \\ 0. & 0. & 0. & 0. & 3.33115\times10^{9} & 0. & 0. \\ 0. & 0. & 0. & 0. & 0. & 2.7487\times10^{9} & 0. \\ 0. & 0. & 0. & 0. & 0. & 0. & 2.15295\times10^{9} \end{pmatrix}$$

B8 [for first eigenvector]

$$\begin{pmatrix} 8.283\times10^{6} & 0. & 0. & 0. & 0.00483999 & 0.00656998 & 1.43 \\ 0. & 1.09037\times10^{14} & 0. & 0. & 0. & 0. & 0. \\ 0. & 0. & 9.315\times10^{12} & 0. & -4.36553\times10^{6} & -4.95906\times10^{6} & -4.77801\times10^{6} \\ 0. & 0. & 0. & 1.93915\times10^{19} & 0. & 0. & 0. \\ 0.00483999 & 0. & -4.36553\times10^{6} & 0. & 4.1039\times10^{9} & -4.2145\times10^{9} & -3.95703\times10^{8} \\ 0.00656998 & 0. & -4.95906\times10^{6} & 0. & -4.2145\times10^{9} & 5.36949\times10^{9} & -4.79644\times10^{8} \\ 1.43 & 0. & -4.77801\times10^{6} & 0. & -3.95703\times10^{8} & -4.79644\times10^{8} & 5.92693\times10^{8} \end{pmatrix}$$

B9

$$\begin{pmatrix} 0. & 0. & 0. & 0. & 0. & 0. & 0. \\ 0. & 0. & 0. & 0. & 0. & 0. & 0. \\ 0. & 0. & 0. & 0. & 0. & 0. & 0. \\ 0. & 0. & 0. & 0. & 0. & 0. & 0. \\ 0. & 0. & 0. & 0. & 4.76852\times10^{9} & 0. & 0. \\ 0. & 0. & 0. & 0. & 0. & 3.93474\times10^{9} & 0. \\ 0. & 0. & 0. & 0. & 0. & 0. & 3.08193\times10^{9} \end{pmatrix}$$

B10 [for second eigenvector]

$$\begin{pmatrix} 8.283\times10^{6} & 0. & 0. & 0. & 0.00483999 & 0.00656998 & 1.43 \\ 0. & 1.09037\times10^{14} & 0. & 0. & 0. & 0. & 0. \\ 0. & 0. & 9.315\times10^{12} & 0. & -4.36553\times10^{6} & -4.95906\times10^{6} & -4.77801\times10^{6} \\ 0. & 0. & 0. & 1.93915\times10^{19} & 0. & 0. & 0. \\ 0.00483999 & 0. & -4.36553\times10^{6} & 0. & 2.66653\times10^{9} & -4.2145\times10^{9} & -3.95703\times10^{8} \\ 0.00656998 & 0. & -4.95906\times10^{6} & 0. & -4.2145\times10^{9} & 4.18344\times10^{9} & -4.79644\times10^{8} \\ 1.43 & 0. & -4.77801\times10^{6} & 0. & -3.95703\times10^{8} & -4.79644\times10^{8} & -3.36289\times10^{8} \end{pmatrix}$$

B11

$$\begin{pmatrix} 0. & 0. & 0. & 0. & 0. & 0. & 0. \\ 0. & 0. & 0. & 0. & 0. & 0. & 0. \\ 0. & 0. & 0. & 0. & 0. & 0. & 0. \\ 0. & 0. & 0. & 0. & 0. & 0. & 0. \\ 0. & 0. & 0. & 0. & 1.34247\times10^{10} & 0. & 0. \\ 0. & 0. & 0. & 0. & 0. & 1.10774\times10^{10} & 0. \\ 0. & 0. & 0. & 0. & 0. & 0. & 8.67648\times10^{9} \end{pmatrix}$$

B12 [for third eigenvector]

$$\begin{pmatrix} 8.283\times10^{6} & 0. & 0. & 0. & 0.00483999 & 0.00656998 & 1.43 \\ 0. & 1.09037\times10^{14} & 0. & 0. & 0. & 0. & 0. \\ 0. & 0. & 9.315\times10^{12} & 0. & -4.36553\times10^{6} & -4.95906\times10^{6} & -4.77801\times10^{6} \\ 0. & 0. & 0. & 1.93915\times10^{19} & 0. & 0. & 0. \\ 0.00483999 & 0. & -4.36553\times10^{6} & 0. & -5.98965\times10^{9} & -4.2145\times10^{9} & -3.95703\times10^{8} \\ 0.00656998 & 0. & -4.95906\times10^{6} & 0. & -4.2145\times10^{9} & -2.9592\times10^{9} & -4.79644\times10^{8} \\ 1.43 & 0. & -4.77801\times10^{6} & 0. & -3.95703\times10^{8} & -4.79644\times10^{8} & -5.93084\times10^{9} \end{pmatrix}$$

B13 [$\underline{K}_{bv}$ matrix]

$$\begin{pmatrix} 1 & 0 & 0 & 0 & 0 & 0 & 0 \\ 0 & 1 & 0 & 0 & 0 & 0 & 0 \\ 0 & 0 & 1 & 0 & 0 & 0 & 0 \\ 0 & 0 & 0 & 1 & 0 & 0 & 0 \\ 0 & 0 & 0 & 0 & 1 & 0.88 & 1.21 \\ 0 & 0 & 0 & 0 & 1.25 & 1 & -2.42 \\ 0 & 0 & 0 & 0 & 20.55 & -29.36 & 1 \end{pmatrix}$$

B14 [$\underline{K}_{v}$ matrix]

$$\begin{pmatrix} 1. & 0. & 0. & 0. & 0. & 0. & 0. \\ 0. & 1. & 0. & 0. & 0. & 0. & 0. \\ 0. & 0. & 1. & 0. & 0. & 0. & 0. \\ 0. & 0. & 0. & 1. & 0. & 0. & 0. \\ 16.4675 & 0. & -0.0114953 & 0. & 1. & 0.88 & 1.21 \\ 19.9606 & 0. & -0.0139337 & 0. & 1.25 & 1. & -2.42 \\ -7.66228 & 0. & -0.013457 & 0. & 20.55 & -29.36 & 1. \end{pmatrix}$$

B15

$$\begin{pmatrix} 1 & 0 & 0 & 0 & 0 & 0 & 0 \\ 0 & 1 & 0 & 0 & 0 & 0 & 0 \\ 0 & 0 & 1 & 0 & 0 & 0 & 0 \\ 0 & 0 & 0 & 1 & 0 & 0 & 0 \\ 0 & 0 & 0 & 0 & 1 & 1.25 & 20.55 \\ 0 & 0 & 0 & 0 & 0.88 & 1 & -29.36 \\ 0 & 0 & 0 & 0 & 1.21 & -2.42 & 1 \end{pmatrix}$$

B16 [$\underline{\tilde{C}}_v$ matrix]

$$\begin{pmatrix} 8.283\times10^{6} & 0. & 0. & 0. & 1.74092 & -3.44798 & 1.33657 \\ 0. & 1.09037\times10^{14} & 0. & 0. & 0. & 0. & 0. \\ 0. & 0. & 9.315\times10^{12} & 0. & -1.45109\times10^{7} & 1.14682\times10^{6} & 5.11085\times10^{7} \\ 0. & 0. & 0. & 1.93915\times10^{19} & 0. & 0. & 0. \\ 1.74092 & 0. & -1.45109\times10^{7} & 0. & 8.34509\times10^{9} & 3.47766\times10^{8} & 2.69685\times10^{8} \\ -3.44798 & 0. & 1.14682\times10^{6} & 0. & 3.47766\times10^{8} & 2.99942\times10^{10} & -1.31737\times10^{9} \\ 1.33657 & 0. & 5.11085\times10^{7} & 0. & 2.69685\times10^{8} & -1.31737\times10^{9} & 1.52381\times10^{13} \end{pmatrix}$$

B17 [$\underline{\tilde{S}}_v$ **matrix**]

$$\begin{pmatrix} 0. & 0. & 0. & 0. & 0. & 0. & 0. \\ 0. & 0. & 0. & 0. & 0. & 0. & 0. \\ 0. & 0. & 0. & 0. & 0. & 0. & 0. \\ 0. & 0. & 0. & 0. & 0. & 0. & 0. \\ 0. & 0. & 0. & 0. & 6476.06 & 209.454 & 32.0744 \\ 0. & 0. & 0. & 0. & 209.454 & 15462.6 & -257.912 \\ 0. & 0. & 0. & 0. & 32.0744 & -257.912 & 2.84126\times10^{6} \end{pmatrix}$$

B18 [$\underline{\tilde{r}}_v$ **matrix**]

$$\begin{pmatrix} 0. \\ 0. \\ 1. \\ 0. \\ -0.0114953 \\ -0.0139337 \\ -0.013457 \end{pmatrix}$$

Subroutine-C

```
u=(7.43509*10^9-2505*λ)*((2.74564*10^9-
1618*λ)*(8.11818*10^9-2067*λ)-
(4.79*10^8*4.79*10^8))+4.2145*10^9*(-
4.2145*10^9*(2.74564*10^9-1618*λ)-(4.79*10^8*3.95*10^8))-
.3957*10^9*((-4.2145*10^9)*(-0.479644*10^9))-(8.11818*10^9-
2067*λ)*(-0.395703*10^9);
sol=Solve[{u=0},{λ}]
```

Output Subroutine-C:

C1

$$\{\{\lambda \to 1.3298\times 10^6\},\ \{\lambda \to 1.9036\times 10^6\},\ \{\lambda \to 5.35916\times 10^6\}\}$$

Subroutine-D

```
(* Subroutine-D, evaluation of first eigenvectors*)
ke=Table[0,{i,1,3},{j,1,3}];
ke[[1,1]]=4.1039*10^9;
ke[[1,2]]=-4.21*10^9;
ke[[1,3]]=-3.95*10^8;
ke[[2,1]]=-4.21*10^9;
ke[[2,2]]=5.36*10^9;
ke[[2,3]]=-4.79*10^8;
ke[[3,1]]=-3.95*10^8;
ke[[3,2]]=-4.79*10^8;
ke[[3,3]]=5.92*10^8;
MatrixForm[ke]
Eigenvectors[ke]
```

Output Subroutine-D:

D1

$$\begin{pmatrix} 4.1039\times 10^9 & -4.21\times 10^9 & -3.95\times 10^8 \\ -4.21\times 10^9 & 5.36\times 10^9 & -4.79\times 10^8 \\ -3.95\times 10^8 & -4.79\times 10^8 & 5.92\times 10^8 \end{pmatrix}$$

D2

```
{{0.652124,-0.758008,0.0125623},{-0.516333,-
0.431953,0.739471},{-0.555099,-0.488713,-0.673071}}
```

Subroutine-E

```
(*Subroutine-E,evaluation of second eigen vectors*)
ke=Table[0,{i,1,3},{j,1,3}];
ke[[1,1]]=2.666*10^9;
ke[[1,2]]=-4.21*10^9;
ke[[1,3]]=-3.95*10^8;
ke[[2,1]]=-4.21*10^9;
ke[[2,2]]=4.183*10^9;
ke[[2,3]]=-4.79*10^8;
ke[[3,1]]=-3.95*10^8;
ke[[3,2]]=-4.79*10^8;
ke[[3,3]]=-3.36*10^8;
MatrixForm[ke]
Eigenvectors[ke]
```

Output Subroutine-E:

E1

$$\begin{pmatrix} 2.666\times10^{9} & -4.21\times10^{9} & -3.95\times10^{8} \\ -4.21\times10^{9} & 4.183\times10^{9} & -4.79\times10^{8} \\ -3.95\times10^{8} & -4.79\times10^{8} & -3.36\times10^{8} \end{pmatrix}$$

E2

```
{{0.640514,-0.767813,0.0142762},{-0.634925,-0.539933,-
0.552578},{-0.431985,-0.34487,0.833339}}
```

Subroutine-F

```
(*Subroutine-F, evaluation of third eigen vectors*)

ke=Table[0,{i,1,3},{j,1,3}];
ke[[1,1]]=-5.98*10^9;
ke[[1,2]]=-4.21*10^9;
ke[[1,3]]=-3.95*10^8;
ke[[2,1]]=-4.21*10^9;
ke[[2,2]]=-2.95*10^9;
ke[[2,3]]=-4.79*10^8;
ke[[3,1]]=-3.95*10^8;
ke[[3,2]]=-4.79*10^8;
ke[[3,3]]=-5.93*10^9;
MatrixForm[ke]
Eigenvectors[ke]
```

Output program-F:

F1

$$\begin{pmatrix} -5.98\times10^{9} & -4.21\times10^{9} & -3.95\times10^{8} \\ -4.21\times10^{9} & -2.95\times10^{9} & -4.79\times10^{8} \\ -3.95\times10^{8} & -4.79\times10^{8} & -5.93\times10^{9} \end{pmatrix}$$

F2

```
{{-0.80149,-0.567569,-0.188359},{-0.170069,-
0.0856356,0.981704},{0.573315,-0.81886,0.02789}}
```

Subroutine -G:

k=0.032;l=32000;t=310;μ=1/6;Dm=7.4*10^10;u=0.74;v=0.74;ξ=16000;η=3300;P=1000000;b=6600;
βn=n*3.14*b/l;
w1[x_,y_]=(l^2/(2*π^2*Dm))*(Sum[(1/n^2)*(En*(-(βn/(Sinh[βn])^2)*Sinh[n*π*y/l]-(n*π*y/l)*Sinh[n*π*y/l]+Coth[βn]*(n*π*y/l)*Cosh[n*π*y/l])+Fn*((βn*Cosh[βn]/Sinh[βn]^2)*Sinh[n*π*y/l]-(1/Sinh[βn])*(n*π*y/l)*Cosh[n*π*y/l]))*(Sin[n*π*x/l]),{n,1,40}])+(16*P/(π^6*u*v*Dm))*(Sum[((Sin[n*π*ξ/l]*Sin[m*π*η/b]*Sin[n*π*u/(2*l)]*Sin[m*π*v/(2*b)]))/(m*n*(n^2/l^2+m^2/b^2)^2)*Sin[n*π*x/l]*Sin[m*π*y/b],{n,1,40},{m,1,40}]);
w2[x_,y_]=w1[x,y];
rrp[x_,y_]=D[w2[x,y],y];
aa[x_,y_]=rrp[x,y];
rr1=aa[x,0];
rr2=aa[x,b];
K=k*Dm/b;
rr3=rr1*K;
rr4=rr2*K;
ttt=-Sum[En*Sin[n*π*x/l],{n,1,40}];
ttt2=Sum[Fn*Sin[n*π*x/l],{n,1,40}];
uu=rr3-ttt;
uu2=rr4-ttt2;
sol=Solve[{uu==0,uu2==0},{En,Fn}];
MM[x_,y_]=w1[x,y]/.sol;
hh1=D[MM[x,y],{x,2}];
hh2=D[MM[x,y],{y,2}];
MX[x_,y_]=-Dm*(hh1+μ*hh2);
MY[x_,y_]=-Dm*(hh2+μ*hh1);
VALX=MY[16000,3300];
VAY=MX[16000,3300]
Plot[MX[x,6600],{x,0,32000}];
Plot[MY[16000,y],{y,0,6600}];
qq=MX[x,3300];
qqq=MY[16000,y];
For[qqq=MY[16000,y];y=0,y<6600,y=y+1000,Print[qqq,y]];
For[qq=MX[x,6600];x=0,x<32000,x=x+8000,Print[qq,x]];

APPENDIX-2

PROGRAM-1
(Spread-sheet program)

Analysis of Simply-Supported Single Cell Prismatic Box Sections

INPUT SHEET

The box beam is idealized as being simply supported over a span given bellow, and has diaphragms only at the supports, where there is full torsional and distortional restraint, but no resistance to warping. At midspan there is a live point load at flange web junction (Figure 7.1) shows the geometry and loading.

Geometry data:

Span length	= 27.4 m
Top flange width	= 5640 mm
Bottom flange width	= 5640 mm
Cantilever width	= 2580 mm
Depth of web (vertical)	= 2760 mm
Depth of web (inclined)	= 2760 mm
Thickness of top slab	
With side cantilever	= 310 mm
Thickness of bottom flange	= 170 mm
Thickness of web	= 500 mm

Load data:

Live load at flange web junction:	= 1000 kN
Torsional moment	= 1650 kN.m

Material properties:

Density of concrete	= 25 kN/m^3
Poisson's ratio	= 0.15

Distortional analysis of frame representing cross-section: (Figure 7.13b)

IGC	= 409400 mm^4
ICA	= 10420000 mm^4
IAH	= 2483000 mm^4
Sidesway at level of load δ (for F=10 kN)	= 871.27 mm
E	= 34.5 kN/mm^2
Rotation at C from matrix analysis	= 0.01724
Rotation at A from matrix analysis	= -0.053342

APPENDIX-3

PROGRAM-2
(Spread-sheet program)

Analysis of Simply-Supported Single Cell Prismatic Box Sections

(Shear lag analysis)

INPUT SHEET

Since torsional and distortional effects are not being considered in the treatment of shear lag, the live loading of Figure 7.1 will be regarded as acting at the vertical centre line of cross-section.

Span length = 32 m

Geometric data:

Width:

Top flange	= 6600 mm
Cantilever	= 4000 mm
Bottom flange	= 5600 mm

Thickness:

Top flange	= 310 mm
Web	= 500 mm
Bottom flange	= 170 mm

Load data:

Live load at flange web junction = 3000 kN

(Appendix-1)

Material data:

G	= 15.0075
E	= 34.5

Ordinates of general parabolic function for shear lag:

y_o	= -100
y_1	= -75
y_2	= 0

Δx (Top flange)	= 1650 mm
Δx for w_{6v} (Cantilever)	= 2000 mm
Δx for w_{7v} (Bottom flange)	= 1400 mm

From Program B:

$\tilde{y}$ (From top flange)	= 785 mm
$\tilde{y}$ (From bottom flange)	= 1975 mm

Total dead load	= 6626 mm

For C_v matrix:

A	= 8283000 mm^2
I_x	= $9.31*10^{12}$ mm^4
I_y	= $1.093*10^{14}$ mm^4
C_{twr}	= $1.939*10^{19}$

From Mathematica analysis:

$\underline{\tilde{r}_{5v}}$	= -0.0114953

$\tilde{\underline{S}}_{55}$ = 6476.06

$\tilde{\underline{C}}_{55}$ = 8340000000

$\tilde{\underline{r}}_{6v}$ = -0.0139337

$\tilde{\underline{S}}_{66v}$ = 15462.6

$\tilde{\underline{C}}_{66}$ = 29994200000

$\tilde{\underline{r}}_{7v}$ = -0.013457

$\tilde{\underline{C}}_{77}$ = $1.5238 * 10^{13}$

$\tilde{\underline{S}}_{77v}$ = 2841260

For orthogonalization of basic warping functions:

From Figure 7.23(a)

$\tilde{w}_{5v}$ at,

A, E = 25.49
C, D = -6.23

B, F = -62.51

Between B and A &

Between E and F = -40.51

Between A and E = -74.51

Between C and D = -114.77

From Figure 7.24 (a)

$\tilde{w}_{6v}$ **at,**

A, E = 30.87

C, D = -7.55

B, F = -69.13

Between B and A &

Between E and F = -44.13

Between A and E	= -94.13
Between C and D	= -249.55

From Figure 7.25(a)

$\widetilde{w}_{7v}$ at,

A, E	= 2.85
C, D	= -34.12
B, F	= 2933.15
Between B and A & between E and F	=2199.15
Between A and E	= -2052.15
Between C and D	= 65.88